# Use of novel insertion sites for the development of polyvalent ORFV D1701-V vectored vaccines

**Dissertation**
der Mathematisch-Naturwissenschaftlichen Fakultät
der Eberhard Karls Universität Tübingen
zur Erlangung des Grades eines
Doktors der Naturwissenschaften
(Dr. rer. nat.)

vorgelegt von
Ferdinand Salomon
aus Hannover

Tübingen
2019

Gedruckt mit Genehmigung der Mathematisch-Naturwissenschaftlichen Fakultät der Eberhard Karls Universität Tübingen.

| | |
|---|---|
| Tag der mündlichen Qualifikation: | 11.12.2019 |
| Dekan: | Prof. Dr. Wolfgang Rosenstiel |
| 1. Berichterstatter: | Prof. Dr. Hans-Georg Rammensee |
| 2. Berichterstatter: | Prof. Dr. Stefan Stevanović |

# Table of Contents

# Zusammenfassung

Virale Vektoren stellen vielversprechende Impfstoffe zur Induktion sowohl starker zellulärer als auch humoraler Immunantworten dar. Innerhalb der Gattung *Parapoxvirus* der *Poxviridae* weist der Orf Virus (ORFV) Stamm D1701-V wünschenswerte Eigenschaften auf, die sich für die Entwicklung einer Vektor-Plattformtechnologie eignen und sich bereits in verschiedenen Vakzinierungsansätzen bewähren konnten. Um die Immunogenität von viralen Vektoren zu verbessern, setzen gegenwärtige Strategien u.a. auf die Insertion heterologer, und die gezielte Deletion viraler immunmodulatorischer Elemente in das Virusgenom. Um die Insertion mehrerer Transgene in einen einzelnen Vektor zu ermöglichen, untersucht die vorliegende Arbeit die Eignung von neun neuen Insertionsstellen für die Transgenexpression bei simultaner Deletion von ORFV D1701-V kodierten, für die Virusreplikation verzichtbaren Gene. Die neuen Deletionsmutanten des ORFV-D1701-V wurden einer detaillierten Charakterisierung der genetischen Stabilität von insertierten GFP-Reportergenen, ihres Wachstumsverhaltens und ihrer Fähigkeit zur Induktion der Transgenexpression in verschiedenen Zielzellen unterzogen. Zusätzlich wurde die Immunogenität der D1701-V Mutanten auf ihre Fähigkeit hin untersucht, pro-inflammatorische Stoffwechselwege, mononukleäre Zellen des peripheren Blutes und Antigenpräsentierende Zellen zu aktivieren oder antigenspezifische Immunantworten *in vitro* und *in vivo* zu induzieren. Zusammengenommen zeigen die durchgeführten Analysen ein hohes Potenzial für das Design polyvalenter Impfstoffe durch die Integration von jeweils einer von drei Gendeletionen in das Virusgenom. Der jeweilige Austausch der offenen Leseraster ORF112, ORF119 und ORF126 mit dem Reportergen GFP führte hierbei nicht nur zu einer effizienten Replikation stabiler Virusvektoren mit der gewünschten Transgen-Expression, sondern auch zu bemerkenswerten Immunogenitätseigenschaften der neu erzeugten Rekombinanten.

Außerdem zeigten „Proof-of-Concept“ Studien die Eignung von ORFV D1701-V Rekombinanten für die Expression der CTLA-4 und PD-L1 spezifischen Immun-Checkpoint-Inhibitoren (ICIs) Ipilumumab bzw. Avelumab. Die Ergebnisse belegen die korrekte Expression funktionaler Antikörper durch ORFV D1701-V und eröffnen somit weitere neue Möglichkeiten für das Design von polyvalenten, ICI oder stimulierende Antikörper exprimierenden ORFV D1701-V Impfstoffen für gesteigerte Immunantworten und somit für die erfolgreiche Behandlung von Infektionskrankheiten oder Krebs.

# Abstract

Viral vector-based vaccines are promising to elicit strong cellular and humoral immune responses. Within the genus *Parapoxvirus* of the *Poxviridae*, the Orf Virus (ORFV) strain D1701-V comprises various properties particularly favorable for the development of a vector platform technology and was shown to facilitate various vaccination approaches. To enhance viral vectors' immunogenicity, current strategies implement the use of immunomodulatory elements and the elimination of viral immunomodulatory genes still present in the viral genome. To allow the insertion of multiple transgenes into a single vector, the present work examines the suitability of nine novel insertion sites for transgene expression by simultaneous deletion of ORFV D1701-V encoded genes non-essential for viral replication. Novel D1701-V deletion mutants were subjected to detailed characterization of the genetic stability of inserted GFP reporter constructs, their growth behavior and capability to induce transgene expression in different target cells *in vitro*. Additionally, the D1701-V mutants' immunogenicity was analyzed by their ability to activate pro-inflammatory pathways, peripheral blood mononuclear and antigen presenting cells, or to induce antigen-specific immune responses *in vitro* and *in vivo*. Taken together, the analyses performed demonstrate a high potential for the design of polyvalent, single vectored vaccines by integrating at least three knockouts into the ORFV D1701-V genome. Thus, the exchange of either of the open reading frames (ORF) ORF112, ORF119 and ORF126 with the reporter gene GFP resulted not only in efficient replication of stable vectors expressing the desired transgenes, but also attributed remarkable immunogenicity properties to the newly generated recombinants.

Additionally, proof-of-concept studies were performed to evaluate the suitability of ORFV D1701-V recombinants for the expression of the CTLA-4 and PD-L1 targeting immune checkpoint inhibitors (ICIs) Ipilumumab and Avelumab, respectively. The correct expression of functional antibodies by ORFV D1701-V opens new possibilities for the design of polyvalent, single vectored ORFV D1701-V vaccines expressing ICIs or stimulatory antibodies for increased immune responses and thus, for the successful treatment of infectious diseases or cancer.

# List of Abbreviations

| | |
|---|---|
| °C | Celsius |
| α | anti |
| µl | Microliter |
| µM | Micromolar |
| ANK | Ankyrin repeat |
| APC | Antigen presenting cell |
| APC/C | Anaphase promoting complex |
| BCR | B cell receptor |
| bp | Basepairs |
| BPSV | Bovine papular stomatitis virus |
| BSA | Bovine serum albumin |
| BV | Brilliant violet |
| CAR | Chimeric antigen receptor |
| CD | Cluster of differentiation |
| CD40L | CD40 ligand |
| CBP | Chemokine binding protein |
| CLIP | Class II associated invariant chain peptide |
| $CO_2$ | Carbon dioxide |
| CPE | Cytopathic effect |
| CTL | Cytotoxic T lymphocyte |
| CTLA-4 | Cytotoxic T-lymphocyte-associated antigen 4 |
| Da | Dalton |
| DC | Dendritic cell |
| DIG | Digoxygenin |
| DMEM | Dulbecco's modified eagle medium |
| DMSO | Dimethyl sulfoxide |
| DNA | Deoxyribonucleic acid |
| EBV | Epstein-Barr Virus |
| EDTA | Ethylenediaminetetraacetic acid |
| ELISA | Enzyme-linked immunosorbent assay |
| EtOH | Ethanol |
| EV | Extracellular enveloped virion |
| FACS | Fluorescence activated cell sorting |
| FCS | Fetal calve serum |
| FIH | Factor inhibiting HIF |
| FSC | Forward scatter |
| g | Gram |
| GFP | Aequorea coerulescens Green fluorescent protein |
| GM-CSF | Granulocyte macrophage colony-stimulating factor |
| h | hour(s) |
| HCMV | Human cytomegalovirus |

| | |
|---|---|
| HCV | Hepatitis C virus |
| HIF | Hypoxia-inducible factor |
| HIV | Human immunodeficiency virus |
| HLA | Human Leukocyte Antigen |
| i.m. | Intramuscular |
| i.v. | Intravenous |
| ICI | Immune checkpoint inhibitor |
| ICS | Intracellular cytokine staining |
| IFNγ | Interferon γ |
| Ig | Immunoglobulin |
| IL | Interleukin |
| irAE | Immune-related adverse event |
| IRF | Interferon regulatory factor |
| ITR | Inverted terminal repeat |
| kbp | Kilo basepair(s) |
| kDa | Kilo Dalton |
| l | Liter |
| LPS | Lipopolysaccharide |
| M | Molar |
| MACS | Magnetic Cell Sorting |
| MAVS | Mitochondrial antiviral signalling proteins |
| MFI | Mean fluorescent intensity |
| mg | Milligram |
| MHC | Major histocompatibility complex |
| min | Minute |
| ml | Milliliter |
| moDC | Monocyte derived dendritic cell |
| MOI | Multiplicity of infection |
| mRNA | Messenger ribonucleic acid |
| MV | Mature virion |
| MVA | Modified-Vaccinia-Ankara-Virus |
| NF | Nucleofection |
| ng | Nanogram |
| NK cell | Natural killer cell |
| nm | Nanometer |
| ON | Over night |
| ORF | Open reading frame |
| ORFV | Orf virus |
| OVA | Ovalbumin |
| P | Promoter |
| PACR | Poxvirus anaphase promoting complex/cyclosome regulator |
| PAGE | Polyacrylamide gel electrophoresis |
| PBMC | Peripheral blood mononuclear cell |
| PCPV | Pseudocowpox virus |

| | |
|---|---|
| PCR | Polymerase chain reaction |
| PD-1 | Programmed cell death protein 1 |
| PD-L1 | Programmed cell death protein 1 ligand |
| PE | Phycoerythrin |
| PFU | Plaque forming unit |
| PRANC | Pox protein repeats of Ankyrin C-terminus |
| pRB | Retinoblastoma protein |
| PRR | Pattern recognition receptor |
| PVNZ | Parapoxvirus of red deer in New Zealand |
| RIG | Retinoic acid-inducible gene |
| RLU | Relative light units |
| RNA | Ribonucleic acid |
| rpm | Rounds per minute |
| RT | Room temperature |
| s | Second(s) |
| SCF | Skp1-cullin1-F-box protein |
| SEAP | Secreted embryonic alkaline phosphatase |
| SOC | Super Optimal Broth |
| SSC | Side scatter |
| TCR | T cell receptor |
| TIL | Tumor infiltrating lymphocyte |
| TLR | T cell receptor |
| TNF | Tumor necrosis factor |
| TNFR | Tumor necrosis factor receptor |
| TRAF | TNF receptor associated factor |
| TRICOM | Triad of co-stimulatory molecules |
| U | Unit |
| UV | Ultraviolet |
| UZ | Ultracentrifuge |
| VACV | Vaccinia virus |
| VEGF | Vascular endothelial growth factor |
| VT | Versen Trypsin |
| WB | Western blot |
| WV | Wrapped virion |
| x g | Relative gravitiy acceleration |

# List of Figures

# List of Tables

# 1 Introduction

## 1.1 The Adaptive Immune System

The immune system can be divided into the innate and the adaptive immune system. While the innate immune system provides crucial mechanisms to rapidly detect and remove microbial pathogens, adaptive immunity evolves upon a highly specific and regulated interplay between T and B lymphocytes and antigen presenting cells (APCs). This process provides the ability to discriminate between self- and non-self antigens, facilitates pathogen-specific cellular and humoral immune responses, generates immunologic memory and regulates the maintenance of immune homeostasis under normal physiological conditions [1].

### 1.1.1 Hematopoiesis

All blood cells arise from hematopoietic pluripotent stem cells in the bone marrow during the process of hematopoiesis. Here, pluripotent stem cells in the bone marrow divide into a common lymphoid or myeloid progenitor giving rise to white or red blood cells termed leukocytes and erythrocytes, respectively. Most of the leukocytes including natural killer (NK), T and B cells are derived from the lymphoid progenitor cell and can be distinguished by the possession or absence of antigen receptors (T cell receptor (TCR) or the B cell receptor (BCR)) or the site of differentiation (thymus or bone marrow). In contrast, the myeloid progenitors give rise to erythrocytes and megakaryocytes, as well as the remaining leukocytes comprising the neutrophil, eosinophil and basophil granulocytes, and monocytes that differentiate into macrophages upon tissue entry. Dendritic cells (DCs) represent a heterogeneous leukocyte population as they evolve both from the lymphoid and myeloid progenitors [2].

### 1.1.2 Antigen Presenting Cells

APCs play an important role in the innate, but also the initiation of the adaptive immune responses. Professional APCs such as macrophages and dendritic cells are able to take up pathogens by phago- and macropinocytosis [3] and to process both intra- and extracellular antigens to activate adaptive immune cells via their peptide/major histocompatibility complexes (MHC). Thus, intracellular antigens derived from viruses or tumors are processed into peptides by the proteasome. These peptides are transported to the endoplasmatic reticulum where they are loaded onto MHC class I molecules and presented on the surface of APCs to CD8+ T cells. In contrast, extracelluar antigens like bacteria are degraded and processsed by the activity of endolysosomal enzymes. Adjacently, they are loaded onto MHC class II molecules by displacing the class II associated invariant chain peptide (CLIP) and presented to CD4+ T cells on the surface [2, 3].

### 1.1.3 T cells

T cells undergo a complex developmental process during maturation from lymphoid progenitors to single-positive CD4+ or CD8+ T cells in the thymus. After TCR development, T cell differentiation is mediated by the process of positive and negative selection involving antigens and MHC class I and II molecules. Non-functional T cells and, to avoid autoreactivity, those that strongly bind MHC complexed with self-peptides are eliminated, while an engagement with low avidity leads to positive selection of T cells. Depending on the interaction with thymic epithelial MHC class I or II molecules, T cells mature to antigen-naive single positive CD8 (cytolytic T lymphocytes (CTL)) or CD4 T cells in the thymic medulla, respectively, from which they exit to circulate the lymph and blood. Despite the shared mechanisms of T cell maturation in the thymus, a large diversity of effector T cell subsets has been determined depending on the type of APC and cytokine milieu at the site of antigen encounter. The largest population constitutes the CD4+ T helper cells that can be categorized mainly into $T_H1$ and $T_H2$, which drive the activation of monocytic phagocytes, NK cells and CTLs, or enhances antibody production, respectively. Other T helper cell populations induce inflammatory responses ($T_H17$) or attenuate immune responses ($T_{reg}$) [1].

For activation, mature naive T cells migrate into the peripheral lymphoid organs such as the lymph nodes, in which TCRs interact with MHC/peptide complexes on APCs [1, 4], a mechanism termed priming. Besides this first signal, the co-stimulatory molecules CD80/CD86 ensure cell survival and proliferation in binding to their ligand CD28 in a second signal, while a third signal mediated by APCs and the secretion of cytokines stimulates the expansion and differentiation of T cells to different effector and long-lived memory T cell subsets [5, 6].

### 1.1.4 B cells

Following differentiation in the bone marrow, B cells migrate to the peripheral lymphoid organs and circulate the blood. Only those B cells recognizing cognate antigen via its BCR exhibit an immune response and differentiate into mature memory or effector B cells. The maturation pathway of B cells depends on the location of the response and type of antigen being processed. The T cell dependent pathway describes the B cell activation in the secondary lymphoid organs, in which specific antigen is bound by the respective BCR, processed and presented to CD4+ T cell on MHC class II molecules. Following TCR/peptide-MHC class II interaction, T cells activate B cells by the expression of the co-stimulatory molecule CD40L and cytokines such as IL-4 and IL-21 stimulating their proliferation and differentiation to antibody producing plasma cells. In contrast, some antigens like polysaccharides are T cell independent and induce rapid B cell responses by single BCR engagement. Those B cells can proliferate outside lymphoid follicles and tend to produce antibodies with lower antigen affinity [6].

## 1.2 Vaccines

The term vaccination describes the inoculation of healthy individuals with attenuated or dead biological material, or genetically engineered antigens consisting of peptides, protein, DNA or RNA. It is derived from Edward Jenner, who demonstrated that inoculation with cowpox provided cross-protection against the fatal smallpox infection in 1796. While the smallpox vaccine was the first, and so far, only vaccine leading to an eradication of a human disease in 1979, another major milestone in the control of infectious diseases comprises the eradication of rinderpest that caused a high mortality in cattle [7]. Recent successes account for a close eradication of guineaworm infections, while tremendous polio or measles vaccination campaigns significantly reduced infection caused deaths by 99.9% and 84% in 2013 and 2016, respectively [7, 8]. Thus, the principle of vaccination has been contributing enormously to global health, in the US alone preventing more than estimated 103 million selected contagious diseases since 1924 [9]. Despite the progress made over the past 200 years, infectious diseases including human immunodeficiency virus (HIV), tuberculosis, malaria, leishmania or hepatitis C (HCV) still account for more than 15 million deaths a year due to a lack of effective vaccine availability and distribution [10].

In general, vaccines can be divided into two main groups that include either live-attenuated or inactivated vaccines. Live-attenuated vaccines consist of attenuated versions of the pathogen and induce protective immunity by mimicking an infection without causing disease. This type of vaccination has been shown to be very powerful as it can confer long lasting cellular and humoral responses with only a single immunization [11], and includes prominent examples as those against smallpox, measles, mumps, rotavirus, chickenpox or yellow fever [12]. The group of inactivated vaccines comprises inactivated and subunit vaccines. Inactivated vaccines represent killed versions of a pathogen that show a high safety profile and induce immune responses against multiple antigens of the pathogen. Despite these favorable characteristics, immune responses are usually poor, require boost immunizations and are frequently linked to significant side effects [7], which paved the way for the development of subunit vaccines that employ only fractions of the pathogen like sugars or proteins. To enhance the magnitude and to modulate the immune response, such subunit vaccines are conjugated to proteins or combined with adjuvants consisting of aluminum salts, Toll like receptor (TLR) agonists, emulsions or combinations of immunopotentiators [13]. Additionally, an increasing number of technologies has become available that induces the expression of disease related proteins within APCs. Those DNA-expression or viral vectors have been shown to elicit potent cellular and humoral responses alone or in heterologous prime-boost combinations [14-16] and thus, represent promising technologies for effective vaccination campaigns.

While prophylactic vaccination is applied to induce a protective cellular and humoral immunity against diseases in healthy individuals, the design of therapeutic vaccines aims to elicit or suppress immune responses in order to alter the course of a disease upon its manifestation. In this context, especially the activation and modulation of the

immune system to treat various forms of cancer have come into focus creating the field of cancer immunotherapy.

### 1.2.1 Cancer Immunotherapy

Cancer describes a collection of diseases that are characterized by uncontrolled cell growth and division due to genetic inheritances or mutations. Those abnormalities can affect all types of body cells leading to the formation of malignant solid or non-solid tumors, which are able to spread into nearby tissues or travel via the blood or lymph system to distant regions in the body to form new tumors (metastases). Cancer is among the leading causes of deaths worldwide accounting for more than 18 million incidences and approximately 10 million deaths in 2018 [17]. In 2012, 57% of new cases and 65% of cancer caused deaths occurred in less developed regions of the world including Asia, Africa and Central America [18]. Despite the progress made in developing effective technologies to tackle cancer, the number of new cases is rising and expected to reach 23 million in 2030 [18].

Among all cancer treatments available, a combination or single use of radiotherapy, chemotherapy or surgical resection for solid tumors is most common. These conventional therapies have proven to be effective against many cancer types as they kill cancer cells by DNA damage or restrict their growth and division [19]. However, these treatments can cause serious side effects as they also damage healthy cells. In contrast, cancer immunotherapy aims to specifically activate frequently evaded natural mechanisms of the immune system to improve the antitumor immune responses and eventually kill cancer cells. Initially introduced by Wilhelm Busch, who observed tumor regression in a patient upon a bacterial infection in 1867 [20] and William Coley, who approached spontaneous sarcoma remissions using intratumoral injections of *Streptococcus pyogenes* and *Serratia marcescens* in 1891 [21, 22], only Hans-Jochem Kolb's donor lymphocyte transfusions for the treatment of leukemic relapse [23] and phase III trials performed within the past decade have shown cancer immunotherapy to significantly enhance the overall survival of patients with advanced-stage cancer [24-27].

In order to develop therapies to effectively treat cancers, it is mandatory to understand the underlying mechanisms of cancer-immunity interactions. In 1957, Burnet and Thomas proposed the theory of immunosurveillance predicting the immune system to recognize and eliminate transformed cells [28]. Decades passed until the concept of immunoediting was introduced by Schreiber and colleagues, which describes how the immune system not only protects against cancer development but also shapes the character of the emerging tumor in three phases: elimination, equilibrium and escape [29-32]. The elimination phase is determined by the joint action of the innate and adaptive immune system that detect and eliminate the tumor prior to clinical appearance and thus, resembles in principle the concept of immunosurveillance [33]. The equilibrium phase is characterized by the presence of rare tumor cell variants that survived the elimination phase, and an adaptive immune system shaping the

immunogenicity of the tumor cells. By preventing the outgrowth of the tumor cells, the adaptive immune system maintains the tumor in a functional state of dormancy before it eventually resumes its growth as recurrent tumor or distant metastases [33, 34]. In the escape phase, the tumor increases its immunosuppression functions or circumvents immunoediting by the immune system to gain the capacity to promote its outgrowth. The underlying tumor escape mechanisms are driven by Darwinian selection processes and include alterations leading to reduced immune recognition (e.g. loss of strong rejection antigen or MHC class I proteins) or resistance to cytotoxic effects of immunity [33].

The concept proposed by Schreiber and colleagues contributed strongly to understanding the underlying mechanisms in generating and regulating antitumor immunity and thus, enforce three sites of therapeutic intervention: (i) Promoting the antigen presenting functions of DCs, (ii) promoting the generation of protective T cell responses and (iii) conquering the immunosuppression by the tumor [22]. Several therapies have been developed to approach these sites of intervention, which can be classified into checkpoint inhibitors, lymphocyte promoting cytokines, engineered T cells such as chimeric antigen receptor (CAR) T and T cell receptor (TCR) T cells, agonistic antibodies against co-stimulatory receptors, and cancer vaccines [35]. The most thoroughly investigated class of immunotherapies is the class of immune checkpoint inhibitors (ICIs). These monoclonal antibodies dissolve immunosuppression by tumor cells by blocking the interaction of immune checkpoints and thus, maintain anti-tumor immune responses by T cells (see 1.5.2). Currently, five PD-1/PD-L1 ICIs and one CTLA-4 ICI have been approved by the US Food and Drug Administration (FDA), while >700 clinical trials are ongoing [35]. Cytokines and co-stimulatory receptor agonists resemble classes of molecules that stimulate the growth and the activation of immune cells including macrophages, NK cells, lymphocytes and DCs directly in order to sustain anti-tumor responses. Cytokines pursued for cancer immunotherapy cover interferons, interleukins and the granulocyte-macrophage colony-stimulating factor (GM-CSF), and with IFNα, comprise the first class of immunotherapies approved by the FDA in 1986 [36, 37]. On the other hand, agonistic antibodies target co-stimulatory receptors like CD28, OX40 and 4-1BB on T cells to trigger intracellular signaling that promotes T cell proliferation and anti-tumor activity [38-40]. While these classes of immunotherapy aim to tackle immunosuppression by the tumor, CAR T and TCR T cell therapies promote anti-tumor responses using the patients' own lymphocytes. Thus, T cells are collected from the patients' blood and genetically engineered to express either CARs or TCRs that specifically recognize a tumor antigen or tumor-associated intracellular antigens presented by MHC molecules, respectively. Upon readministration into the patient, these T cells find their targeted antigen on tumor cells, which induces their killing [35, 41]. Lastly, the class of cancer vaccines aims to train the immune system to recognize and destroy cancer cells. Therefore, cancer vaccines promote the antigen presentation by APCs and include e.g. DCs engineered to present tumor-associated antigens [25], peptides, as well as RNA-, DNA- and viral vector based vaccines that rely on the intracellular delivery of exogenous nucleic acids into the target cells. Vaccination

with tumor-associated antigen derived peptides is usually performed together with an adjuvant resulting in the activation of immune cells and consequently the optimal processing and presentation of peptides on MHC molecules [42]. For vaccines that utilize nucleic acids, the cancer vaccine-encoded DNA is expressed and presented on MHC proteins to activate T cells and to promote the antigen specific killing of the tumor [35].

## 1.3 Viral vectors

Viral vectors are presently widely used for gene delivery and regarded as promising tools for gene therapy and vaccines. The concept of using viral vectors for gene delivery was introduced in 1972 by Jackson et al. [43] and, by inducing immunity to sufficiently protect chimpanzees from hepatitis B infection, shown as potential vaccine for infectious diseases a decade later [44, 45]. Generally, viral vectors comprise the advantages of (i) highly efficient gene transduction, (ii) specific delivery of genes to targeted cells, (iii) the induction of strong and robust humoral and cellular immune responses and (iv) high immunogenicity by the stimulation of interferon and inflammatory cytokine production by the innate immune system without the need of an adjuvant [46, 47]. The most widely used vectors are based on adenoviruses, which are able to generate strong immune responses alongside with a short-term episomal transgene expression in a broad range of host cells. Nevertheless, the presence of pre-existing immunity against adenoviruses due to previous exposure represents a disadvantage [47]. In contrast, e.g. adeno-associated virus based vectors comprise a high safety profile and generate low immune responses and toxicity, but provide long-term expression through chromosomal integration of the transgene [48]. Many non-replicative and oncolytic viral vectors have been studied extensively and were developed for the use in animal studies and clinical trials [49]. Hereby, vectors are selected for application based on their properties and undergo constant optimization and careful assessment concerning their gene expression, safety, stability, replication efficiency, or their ability to evade pre-existing immunity and to induce tumorigenesis [47]. The high potential and growing interest in the application of viral vectors is reflected by their use in 70% of nearly 3000 conducted clinical trials that employed gene therapies by 2017 [50]. Notably, 65 % of these therapies related to cancer and highlight the significance of viral vectors for cancer immunotherapy. In fact, the first viral vector based gene therapy drug Gendicine™ delivering a *p53* gene has been successfully used in the clinics upon its approval by the Chinese National Medical Products Administration in 2003 for the treatment of head and neck squamous cancer [51, 52]. Since then, an oncolytic adenovirus based H101 vector for the treatment of head and neck cancer [53] and the Herpes Simplex Virus (HSV) type 1 based OncoVex$^{GM\text{-}CSF}$ for the treatment of melanoma have been approved [54], while many vectors including the JX-594 (Pexa-Vec) [55], the adenovirus based CG0070 [56] or a wild-type Reovirus (Reolysin®) [57, 58] are at late-stage development. In particular, the most widely used viral vectors alongside adenoviruses comprise Poxviruses. Due to their favorable properties such as high safety profiles and their ability to induce protective and significant immunogenicity against several different antigens, Poxviruses

are currently subjected at various stages of many clinical trials [10] and will thus be described separately in the following chapter.

### 1.3.1 Poxviruses

The family of *Poxviridae* consists of two subfamilies named *Entomopoxvirinae* and *Chordopoxvirinae*, whose members infect insects or vertebrates, respectively. Due to the medical and veterinary relevance in causing disease both, in humans and other animals, *Chordopoxvirinae* have been subject of extensive investigations [59]. They consist of eleven genera named *Avipoxvirus*, *Capripoxvirus*, *Centapoxvirus*, *Cervidpoxvirus*, *Crocodylidpoxvirus*, *Leporipoxvirus*, *Molluscipoxvirus*, *Orthopoxvirus*, *Parapoxvirus*, *Suipoxvirus*, *Yatapoxvirus* and two unclassified species [60]. Poxviruses are large and complex viruses, which replicate entirely in the cytoplasm of host cells [61] and consist of linear, double-stranded DNA.

The success of Poxviruses as viral vectors is mainly determined by several desirable characteristics, which generally include (i) the packing flexibility of the genome, (ii) the lack of tumorigenesis in target cells of the host due to cytoplasmic replication, (iii) the induction of long-lasting humoral and cellular responses against heterologous antigens, and (iii) thermostability and ease to manufacture [10]. Furthermore, Poxviruses spare the necessity of adjuvants as TLR and inflammasome mediated signaling elicits strong innate immune responses [62, 63], while attenuated vectors merge the safety of inactivated vaccines due to their impaired replication efficiency in the human host with the immunogenicity of live vaccines. Thus, their ability to induce the expression of foreign genes in target cells additionally leads to adaptive immune responses by CD8 and CD4 T cells upon antigen presentation on MHC class I and II proteins [10].

Among the Poxviruses, vaccinia virus (VACV) has been used to generate several attenuated replication-competent (LC16m8) and replication-deficient (NYVAC, ALVAC, TROVAC and MVA) strains, which are most promising in moving towards approval as they entered various prophylactic and therapeutic clinical trials. In this context, the cancer vaccine therapy PANVAC for the treatment of pancreatic cancer showed encouraging results in a phase I clinical trial as it was found safe and well tolerable eliciting antigen specific immune responses that correlated with overall survival [64]. The therapy is delivered as a heterologous prime/boost regimen and consists of a VACV and a fowlpox virus based vector encoding the carcinoembryonic antigen (CEA) and mucin-1, as well as a cassette of the co-stimulatory molecules B7.1, ICAM-1 and LFA-3 known as TRICOM (TRIad of CO-stimulatory Molecules) [65]. Although the therapy failed to meet its primary efficacy endpoint of improving overall survival compared with palliative chemotherapy or best supportive care in a phase III trial [66, 67], recent results suggest efficacy by direct injection into the tumor in the frame of a phase I trial [68]. Furthermore, an ALVAC-based vaccine was tested in a phase III trial demonstrating first evidence for modest protection against HIV-1 in a large-scale study [69], while an MVA-based vector against smallpox has been safely administered to 120.000 individuals with no reported adverse side effects [47, 70].

## 1.4 Orf virus (ORFV)

### 1.4.1 Classification

Within the family of Poxviridae, the genus *Parapoxvirus* and the species *Orf virus* (ORFV) belong to the *Chordopoxvirinae* subfamily. Currently, this genus encompasses four species including ORFV, the *Bovine papular stomatitis virus* (BPSV), *Parapoxvirus of red deer in New Zealand* (PVNZ), and the *Pseudocowpox virus* (PCPV) [60].

### 1.4.2 Morphology

The morphology of ORFV virions can be described as an approximately 260 nm long and 160 nm wide ovoid particle surrounded by a tubule-like structure in a spiral fashion [71, 72]. Analogous to all other poxviruses, the virus genome is located in the core, a protein nucleoid containing many enzymes and factors necessary for cytoplasmic replication. The core is enclosed by a lipoprotein double membrane, in whose outer membrane tubular protein filaments are embedded granting the ORFV the characteristic image of a "ball of wool" [71, 72]. Studies using electron microscopy and recombinants expressing FLAG-tagged envelope structural proteins revealed ORFV to undergo morphogenesis similar to VACV, the prototype for *orthopoxviruses*. Thus, the intracellular mature virion (MV) is wrapped by two additional membranes derived from the *trans*-Golgi network to form wrapped virions (WV). Eventually, the WVs fuse with the cell membrane essentially losing the outermost membrane to release MVs as extracellular enveloped virions (EV) [71, 73, 74].

### 1.4.3 The ORFV genome

As for all members of the *Parapoxvirus* genus, the ORFV genome consists of a double-stranded, linear DNA that comprises an unusually high average G + C content of 64 % and is linked terminally by approximately 60 bp long hairpin loops [75-78]. Currently, many ORFV strains have been isolated around the world including the USA, Germany, Korea, Japan, India, Argentina, Malaysia, Egypt and China, while only 10 genomes have been sequenced showing lengths between 132 – 158 kbp and sequence identity between 85 – 95 % [79]. The organization of the ORFV genome resembles a typical pattern observed in Poxviruses, in which the core region encodes for essential genes conserved in position, spacing and orientation, while genes dispensable for *in vitro* growth and responsible for virulence and pathogenesis are located at the highly variable genomic termini [80, 81]. These genomic termini contain inverted terminal repeats (ITR) and have been exposed to genetic recombination events even between non-homologous segments resulting in transposition or duplication of DNA sequences. In addition, the processes of non-essential gene deletion as well as the acquisition of host genes shape the variety of ORFV variants in the population [82, 83], while non-essential gene deletions have also been reported to be the result of attenuation by cell culture passaging [79, 84, 85].

### 1.4.4 Viral Replication

Although most DNA viruses make use of cellular proteins and replicate or express their genome in the nucleus, Poxviruses strictly replicate in the cytoplasm of vertebrate and invertebrate cells [61]. These enveloped viruses require the fusion of the viral membrane with the endosomal or plasma membrane in order to release their nucleoprotein core inside of the host cell [86]. This core not only consists of the double-stranded DNA but also includes virus-encoded enzymes and factors initiating early gene transcription and protein synthesis under the control of early promoters upon cell entry. Following DNA replication, the synthesized DNA matrices provide templates for the expression of temporarily regulated intermediate and late genes under the control of cellular transcription factors [87], which eventually results in the assembly of initial infectious MVs [74].

### 1.4.5 Medical Relevance

The ORFV is an epitheliotropic virus naturally infecting scarified or damaged skin of sheep and goats causing a disease commonly known as contagious pustular dermatitis, orf, scabby or sore mouth disease [88]. ORFV replicates in regenerating epithelial keratinocytes and does not spread systemically in the host, even after intravenous administration or in immunosuppressed animals [89-93]. Usually, lesions in the natural host are benign and resolve within 6-8 weeks by evolving through the stages of macule, papule, vesicle, pustule scab and resolution [88]. However, infections can become serious upon secondary infections with bacteria or fungi. ORFV infections are characterized by inflammatory proliferative lesions affecting the skin, nostrils and muzzle, while infection of the oral cavity is associated with papular and erosive lesions on the gums, palate and tongue [94]. The host immune response against ORFV infection is vigorous, however, infections can occur repeatedly despite reduced lesion sizes and resolution times of 3 weeks. Thus, ORFV infection is usually not fatal but most serious for lambs that have not been exposed to the virus [89]. Furthermore, ORFV is a zoonotic virus that has been reported to infect cats [95], Japanese serows [96] and camels [97] amongst others, and frequently causes acute localized infections in humans working close to animals in the sheep and goat industry that resolve within 4-8 weeks, or as vascularized tumor-like lesions of the skin in immunosuppressed individuals [98-100].

### 1.4.6 Immune Response against ORFV

Animals reinfected by ORFV induce a vigorous inflammatory and typical antiviral T helper type 1 adaptive immune response during the early stage of infection [98]. Thus, histological analyses on infected tissue showed an infiltration of neutrophils, T cells, B cells and DCs, with CD4+ T cells being predominant in the infected skin [89, 98]. These results were confirmed by investigations on afferent and efferent lymph draining the site of infection, while analyses on cultured lymph cells from the afferent lymph and ORFV infected tissue suggested production of GM-CSF, IL-1, IL-2, IL-8, IFNγ and TNFα [89, 101, 102]. The observed immune responses do not appear to impact the

immunologic memory due to a strong delayed-type hypersensitivity to ORFV, however, protective immunity against ORFV elicited by virus vaccines only lasts for approximately 6-8 months [103-105]. The ability to re-infect its host thus indicates potent intrinsic immune escape mechanisms mediated by ORFV encoded immunomodulators, which are partially described in detail in 1.5.1.

### 1.4.7 ORFV D1701-V

The ORFV strain D1701 was originally isolated from pustular material of a lamb prior to its attenuation and plaque-purification *in vitro* by 135 passages in secondary ovine and bovine cell cultures. The resulting strain showed strongly reduced pathogenicity leading to its registration as live vaccine against contagious pustular dermatitis [103]. Additionally, due to its ability to induce strong humoral and cellular immune responses, an inactivated form of ORFV D1701 has been used as non-specific prophylactic and therapeutic immunomodulator named Baypamun or Zylexis across different species in veterinary medicine [88, 106, 107]. Eventually, the strain D1701-V was obtained from an adaptation of the designated ORFV strain D1701-B [108] for growth in the African green monkey cell line Vero, and shown to result in asymptomatic disease progression even in immunosuppressed sheep [91]. Consecutive analyses on the genomic basis for the loss of virulence revealed remarkable rearrangements as a result of deletion, duplication and translocation of genes located at the genomic termini in comparison to the parental strain D1701-B [84, 93]. Thus, three major deletions designated A, AT and D were observed affecting complete or partial sequences of the open reading frame (ORF) ORF008 and ORF009, ORF102 and ORF103, or ORF114-ORF117, respectively. While most of these genes' functions are unknown or obscure, ORF008 has been predicted to stimulate the activity of the hypoxia-inducible factor activity involved in angiogenesis and apoptosis [109, 110] (see 1.5.1.5), and ORF117 to encode for the GM-CSF/IL-2 inhibiting factor (GIF) engaged in the recruitment of immune and antigen presenting cells [111]. In D1701-V, the entire ORF008 but only the N-terminus of ORF117 are deleted suggesting loss of virulence due to diminished ovine GM-CSF binding capability [84]. In addition, the major virulence factor vascular endothelial growth factor (*vegf-e*) mediating angiogenesis was artificially deleted and exchanged by a LacZ gene cassette from *Escherichia coli*, which not only further attenuated D1701-V but also allowed for blue/white selection in the screening for recombinant ORFV [112-115]. D1701-V vectors expressing antigens of diverse pathogens including Pseudorabies virus, Rabies virus, Borna disease virus, Influenza A virus and Classical swine fever virus have been shown to induce excellent, long-term protective immunity in many different hosts without the need of an adjuvant [16, 91, 116-123]. Recent analyses on the mode of action revealed D1701-V to target professional APCs for heterologous transgene expression and activation of distinct immune cells including T cells, B cells and NK cells [124]. Other outstanding properties of ORFV D1701-V are the absence of its systemic spread and very restricted host and skin tropism both, *in vivo* or *in vitro*, making the occurrence of pre-immunity against the viral backbone in humans unlikely [91, 93, 116, 125]. In this context, an exceptional feature of ORFV is the lack of neutralizing antibodies

in infected animals [94, 126]. Due to the highly specific virus/host interactions, immune responses against ORFV are only short-termed and weak, and thus, allow a repeated vector application [89, 117, 127]. Because of the favorable properties characteristic for D1701-V, the vector has been subjected for the development of a platform technology to deliver heterologous microbial antigens to the immune system. Recent optimizations on the vector aimed to improve the transgene expression strength by the utilization of the strong early promotors Pv and eP2, and demonstrated the suitability of the genomic locus D as insertion site allowing the production of polyvalent, single vectored vaccines. Furthermore, the adaptation to Vero cells now enables standardized production without antibiotics or the need of eggs, and, along with a substitution of the LacZ cassette by fluorescent reporter genes, facilitates the transfection and selection process significantly [84].

## 1.5 Optimization of Viral Vectors

Due to their manifold advantages described above, attenuated, replication-deficient [128-130] poxviral vectors developed from Canarypox virus, Fowlpox virus or VACV proved most suitable and are currently subject of many clinical trials [10, 131]. Nevertheless, these attractive viral vector platforms are thought to be less effective and lasting than their replication competent counterparts despite their favorable safety and immunogenicity properties. Thus, alternative poxviral vectors or the optimization of vectors triggering stronger, broader, polyfunctional and more durable immune responses are desirable [10, 132, 133]. Strategies to improve the vaccine's efficacy include heterologous prime-boost protocols, the use of co-stimulatory molecules, the deletion of immunomodulatory genes in the viral genome, the enhancement of virus promoter strengths or the optimization of transgene expression [10].

As shown over the past decades, one prominent strategy to increase the immunogenicity of viral vectors is to combine the vaccines in heterologous prime-boost immunization regimes. Using a poxvirus as booster component to enhance the antigen specific T cell responses, and as a priming component in combination with a protein and an adjuvant to trigger B cell responses, has been the lesson learned from preclinical and clinical trials [10]. These prime-boost regimes have been studied less extensively for ORFV D1701-V. However, investigations on the immunogenicity and protection capabilities of ORFV against challenge infection with Pseudorabies virus in pigs concluded that the priming with a DNA based vaccine and a boost with an ORFV based vaccine was most effective [16]. Notably, studies on the protection against Rabies virus (RABV) using an ORFV based vaccine encoding for the RABV glycoprotein in a homologous prime-boost regimen showed strong increases in antigen specific antibody titers after booster vaccinations in different animals [122].

Numerous studies further suggest a significantly enhanced immunogenicity and efficacy of viral vectors if the disease related antigen was simultaneously delivered with co-stimulatory molecules. This can be achieved by the insertion of genes encoding for immune stimulating factors into the viral genome or the exogenous inoculation of these molecules into the organism. The most prominent example is the TRICOM consisting of

B7–1, ICAM-1, and LFA-3 co-stimulatory molecules naturally expressed on APCs. Upon binding to their ligands, these molecules stimulate specific pathways resulting in an activation of T cells [134]. Expression of TRICOM induced by VACV, MVA or Fowlpox virus vectors has been studied comprehensively *in vitro* and *in vivo*, consistently resulting in enhanced activation and proliferation of antigen specific T cells as well as antitumor activity in clinical trials [135-142]. Beside the TRICOM coding vectors, other co-stimulatory molecules such as interleukin (IL)-12 [143-149], OX40/OX40L [137, 150, 151], a triad of CD80, CD83 and CD86 [152], IL-2 [153-155], IFNγ [143, 156], IL-15 [157-162], GM-CSF [148, 163-166] or CD40L [167-169] have been identified to further stimulate the antigen specific immune response and thus, improve the immunogenicity and efficacy of the viral vector used.

Furthermore, the quality, magnitude and type of immune responses was shown to correlate strongly with the level of transgenes expressed in the targeted host as observed in mice immunized with an MVA vectored HIV vaccine [170]. Moreover, also the timing of antigen expression influences the type of immune response as CD8+ T cells recognized early expressed transgenes, while intermediate or late transgenes elicited predominantly CD4+ T cell responses [171-173]. The timing and strength of expression is largely determined by the viral promoters located 5' of the transgene. Thus, bioinformatic analyses based on early and late promoter consensus sequences are performed to design strong synthetic promoters with favorable properties to enhance the transgene expression [171, 174, 175]. While codon optimization may also lead to better transgene expression levels, the design of immunogens could increase the breadth and depth of epitope recognition and therefore contribute to the efficacy of the vaccine. Thus, efforts targeting the rational design of proteins led to the construction of mosaic immunogens resembling all potential disease specific T cell epitopes as shown for HIV [176, 177], or string of beads harboring only few short immunogenic peptide sequences derived from antigens [178].

### 1.5.1 Insertion Sites

Many recombinant viral vector platforms have been described to deliver various heterologous microbial antigens to the immune system. Generation of such recombinants requires the insertion of transgenes into non-essential regions of the viral genome under the control of a virus specific promoter located 5' of the inserted sequence. Common strategies to identify suitable non-essential regions include the use of (i) deleted genomic regions as a result of adaptation to changing growth conditions, (ii) intergenic regions that circumvent alterations in vector backbones and prevent its instability [179], or (iii) the targeted deletion of potentially non-essential immunomodulatory genes.

The ORFV strain D1701-V was obtained from the bovine kidney cell line BK-KL3A adapted strain D1701-B and showed several genomic rearrangements after adaptation for growth in the African green monkey cell line Vero [180, 181]. These genomic rearrangements include the deletion of genes that are non-essential for the strain's

replication and were shown suitable for transgene expression such as the deleted region D (D locus) [84]. Furthermore, the angiogenic factor VEGF-E was predicted a major virulence determinant responsible for the induction of bloody lesions in sheep [181] and thus, used as insertion site to generate ORFV recombinants triggering long-lasting immunity with a high protective efficacy against several viral diseases in different hosts [182-189]. Besides these successfully used insertion sites, other genes potentially suited for transgene expression have been identified in the terminal ends of the D1701-V genome. As the central regions of poxviruses generally encode for essential genes conserved in position, spacing and orientation, these regions encode for factors influencing virulence, pathogenesis or host range and are considered dispensable for *in vitro* growth [115, 132, 190-192]. While these factors are predicted to interfere with the optimal induction of cellular and humoral immune responses triggered by the host, a deletion of these immunomodulatory genes may further enhance the immunogenicity of the D1701-V vector. Thus, the present work focuses strongly on the deletion of potentially non-essential genes of known or unknown function as listed in Table 1 and their use as insertion site for transgene expression.

**Table 1: Selected genes encoded in the ORFV D1701-V genome predicted to be non-essential and to interfere with the induction of immune responses triggered by the host.**

| Gene (open reading frame) | Function |
|---|---|
| **014** | Poxvirus APC/cyclosome regulator (PACR) |
| **024** | NF-κB Inhibitor |
| **112** | Chemokine Binding Protein (CBP) |
| **113** | Unknown function |
| **119** | NF-κB Inhibitor |
| **121** | NF-κB Inhibitor |
| **126** | ANK-1 |
| **127** | IL-10 ortholog |
| **128** | ANK-2 |

#### *1.5.1.1 Poxvirus APC/cyclosome regulator (PACR) - ORF014*

The anaphase promoting complex or cyclosome (APC/C) is a multicomponent ubiquitin ligase consisting of several subunits. Due to its activity from mid-mitosis to late G1 phase, in which it regulates cell division and transition into the S phase, it has been considered a dominant regulator of the cell cycle [193, 194]. APC/C consists of at least 12 subunits with a catalytic core comprising APC2 and the RING-H2 protein APC11. Using the adapter proteins Cdh1 and Cdc20, substrates subjected to proteasomal degradation are recruited to the complex, while ubiquitination by ubiquitin conjugating enzymes (E1 and E2) is facilitated by the APC11/2 catalytic core module [195]. The ORFV-expressed poxvirus APC/cyclosome regulator (PACR) protein mimics APC11 and

incorporates into the APC/C. Due to sequence differences, PACR lacks the ubiquitinase activity leading to an inhibition of the APC/C [196]. Eventually, ORFV infected cells transition into an S phase like state providing an increased abundance of nucleotides and metabolic enzymes for viral DNA replication and synthesis [195].

#### *1.5.1.2 NF-κB inhibitors - ORF024, ORF119 and ORF121*

The NF-κB transcription factor family consists of five members, which differ in their N-terminal Rel homology domain responsible for DNA sequence specific DNA binding and homo- or heterodimerization [197]. The translocation of those dimers into the nucleus leads to the transcription of genes involved in biological processes ranging from cell growth and survival, tissue and organ development to immune response and inflammation [198], and is dependent on the activation of two major signaling pathways, which respond to diverse stimuli including ligands of pattern recognition receptors (PRRs), TNF receptor (TNFR) superfamily members, as well as the TCR and BCR [199]. While translocation in the canonical pathway relies on the phosphorylation of IκBα by the multi-subunit IκB kinase (IKK) complex [200], the non-canonical pathway involves the processing of the NF-κB precursor protein p100 [201].

Since poxvirus infections, besides many others, are sensed by PRRs such as TLRs or retinoic acid-inducible gene (RIG-I)-like receptors [202], these viruses have evolved strategies to interfere with the NF-κB pathway. Thus, also ORFV has been described to encode for at least five NF-κB inhibitors. ORF002 and ORF121 both are known to bind to the NF-κB transcription factor NF-κB-p65, thereby inhibiting its acetylation by the co-activator p300 [203] or its phosphorylation [202], respectively. Thus, these inhibitors counteract the activation of the transcription factor and prevent its translocation into the nucleus. In contrast, the expression of ORF024 interferes with the phosphorylation of the IKK subunits IKKα and IKKβ [204], while ORF073 interacts with the regulatory subunit NEMO of the IKK complex [205]. These interactions strongly impact the activity of the IKK complex as the bottleneck for most NF-κB activating stimuli. Additionally, ORF119 was described to harbor a C-terminal LxCxE motif allowing a strong interaction with the retinoblastoma protein pRB, which is known for its tumor suppressor activity. By preventing the recruitment of the TNF receptor associated factor 2 (TRAF2), ORF119/pRB inhibits TNFα-induced IKK activation and NF-κB signaling [206]. Nevertheless and despite its function in NF-κB signaling, ORF119 has also been shown recently to inhibit cell proliferation and to induce apoptosis in order to facilitate the release of viral particles [207]. The interaction between the NF-κB and apoptosis regulation thus still needs further investigations.

#### *1.5.1.3 Chemokine Binding Protein (CBP) – ORF112*

The family of chemokines consists of secreted chemotactic proteins that activate and regulate the homeostatic migration and recruitment of leukocytes to sites of infection through the lymphoid organs [208, 209]. The classification into CC, CXC, C or $CX_3C$ chemokines relies on their N-terminal cysteine arrangement, which impacts the cell type

migrating along the chemokine gradient towards the site of inflammation. Hence, CC chemokines generally attract monocytes [210], while lymphocytes, NK and B cells as well as neutrophils sense CXC chemokines [211]. To attenuate inflammation of infected cells, the *Orthopoxvirus* and *Leporipoxvirus* genera produce the poxvirus type II CC-chemokine binding proteins (CBP-II) that share a 17% sequence identity to the CBP encoded by ORFV (ORF112). This CBP has been shown to be functionally similar to the poxviral CBP-II in its ability to bind lymphotactin or many human inflammatory and constitutive CC-chemokines such as CCL19 or CCL21 with high affinity [212-214] and thus, to play a critical role in virulence and pathogenesis [215].

#### *1.5.1.4 ORF113*

Only very little is known about ORF113. Genome analysis comparing the Parapoxviruses ORFV and BPSV identified 16 and 15 ORFs located at the right terminal end of the genome, respectively, with no significant homology to any known protein [80]. Predicting these genes to encode for putative virulence or host range genes, Ning et al. generated a recombinant ORFV lacking ORF113, which did not affect their ability to replicate *in vitro* and proved its suitability for transgene insertion using the ORFV strain IA82 [216].

#### *1.5.1.5 Ankyrin Repeat (ANK)-1 and -2 – ORF126 and ORF128*

Ankyrin repeats (ANK) are protein motifs ubiquitous throughout the kingdoms of life, however, absent in most viruses except the poxvirus family, specifically the *Chordopoxviruses* [217]. The motif consists of tandem repeated consensus domains that are crucial to facilitate protein-protein interactions and is found in four proteins encoded by ORFV D1701-V (ORF123, -126 (ANK-1), -128 (ANK-2) and -129 (ANK-3)) [84, 218]. While plenty of cellular ANK proteins are described to be involved in cell–cell signaling, cytoskeleton integrity, regulation of transcription and cell cycle, inflammatory response, or protein transport [219], only little is known about the function of poxviral ANK proteins. It has been demonstrated that these four proteins harbor F-box-like motifs that may recruit specific substrates to SCF1 ubiquitin ligases via a substrate-binding domain and thereby exploit the cell's ubiquitin-proteasome machinery [220]. One of these proteins, the ORF126 encoded ANK-1 protein, was shown to co-localize with the mitochondria via the essential ankyrin repeats 8 and 9. Nevertheless, the physiological consequences have not been demonstrated yet [221]. Furthermore, a recent study reported an influence of ORFV encoded ANK proteins on the Hypoxia-inducible factor (HIF) pathway [109]. While this pathway plays a crucial role in the regulation of cellular responses to hypoxia, downstream targets like angiogenesis- and anti-apoptotic programs favor viral pathogenesis [110]. In their study, Chen et al. could show that the factor inhibiting HIF (FIH) was sequestered by ANK proteins upon ORFV infection resulting in enhanced HIF activity [109].

#### *1.5.1.6 Interleukin (IL-)10 – ORF127*

The pleiotropic cytokine interleukin 10 (IL-10) is known to induce immunostimulatory or immunosuppressive effects in many cell types. ORFV encodes a polypeptide with remarkable homology to mammalian and viral IL-10 [222], whose role in virulence and viral immune evasion has been studied extensively. Thus, it was shown to influence the immune suppression in preventing the synthesis of cytokines, such as IFNγ in peripheral blood mononuclear cells (PBMCs) or TNFα, IL-1β and IL-8 in macrophages and keratinocytes [223, 224]. Additionally, studies on the maturation of DCs found that the up-regulation of CD80, CD83, CD86 and MHC class II was inhibited by the presence of ORFV IL-10, which indirectly suppresses the $T_H1$ activation by decreased antigen processing and presentation abilities of the DCs [79, 225, 226]. Further, ORFV IL-10 limited the recruitment of Langerhans cells, macrophages, DCs and mast cells into inflamed tissue [226, 227], while a recombinant ORFV lacking IL-10 showed attenuated properties in sheep [228].

### 1.5.2 Immune Checkpoint Inhibitors

One of the major advances in the field immune-oncology is the development of immune checkpoint inhibitor antibodies (ICIs). Immune checkpoints refer to a vast number of inhibitory pathways involved in the maintenance of self-tolerance mitigating collateral tissue damage and the modulation of immune responses, which are used by tumors as a crucial mechanism of immune resistance. Due to their ability to specifically recognize protein derived peptides, their capacity to kill antigen-expressing cells and to concert adaptive and innate immune responses, T cells have been a major focus to enhance antitumor immunity. Thus, immune checkpoints impacting the activation or inhibition of T cells have been targeted by agonists of co-stimulatory receptors, or antagonists of inhibitory receptors to amplify the antigen specific T cell responses. The most prominent examples studied in the context of clinical cancer immunotherapy are the inhibitory T cell receptors cytotoxic T-lymphocyte-associated antigen 4 (CTLA-4) and programmed cell death protein 1 (PD-1) [229], however, hundreds of phase I-IV clinical studies are currently carried out worldwide to evaluate the efficacy of several ICIs as a mono- or combination therapy [230].

CTLA-4 is exclusively expressed by T cells and shares the identical ligands CD80 and CD86 with the co-stimulatory molecule CD28, which is known to strongly amplify the T cell receptor (TCR) signaling in order to activate T cells. While CD28 affects T cell activation upon cognate antigen engagement by the TCR, CTLA-4 counteracts the T cell activation by outcompeting CD28 in binding the shared ligands CD80 and CD86 delivering inhibitory signals to the T cells [231-234]. Moreover and despite the expression of CTLA-4 by activated CD8+ T cells, its major physiological role appears to be the decrease of effector CD4+ T cell activity and stimulation of regulatory T cell dependent immunosuppression [235, 236]. Predicting a blockade of CTLA-4 to result in enhanced T cell responses, initial preclinical studies demonstrated a therapeutic window to induce significant immunity against an immunogenic tumor [237] despite the

lethal autoimmune and hyperimmune phenotype previously seen for *Ctla-4*-knockout mice [238, 239]. Eventually, encouraging findings from preclinical studies led to the development of the fully humanized antibody Ipilimumab showing a mean 3.5 month survival benefit of recipients with advanced melanoma and thus, to approval by the FDA in 2010 [240].

PD-1 is a co-stimulatory molecule expressed on T cells, but also on other activated non-T lymphocyte subsets including B cells or NK-cells [241, 242]. Engagement by its ligands PD-L1 and PD-L2 induces inhibitory pathways triggering the inactivation of T cells. While PD-1 expression is induced upon T cell activation, regulatory T cells highly express PD-1 enhancing the proliferation in the presence of ligand [243]. In contrast to CTLA-4, which regulates T cell activation, PD-1 predominantly regulates effector T cell activation within the tissue and tumor microenvironment at the time of an inflammatory response [244-246]. As studies on several tumors have shown, both, CD4+ and CD8+ tumor infiltrating lymphocytes (TILs) highly express PD-1 [247, 248], which may reflect an anergic or exhausted state of these cell populations, whereas PD-1 ligands are commonly expressed on the surface of different tumor cells as an immune escape mechanism [249]. Considering the mild phenotype in *PD-1*-knockout mice, blocking the interaction between PD-1 and its ligands therefore represented a promising approach to enhance the antitumor effector functions in the tumor microenvironment using mouse models of cancer [249-251]. This eventually resulted in the approval of some antibodies targeting the PD-1-pathway blockade including Pembrolizumab and Nivolumab, which elicited objective response rates of 40-45 % in melanoma and non-small cell lung cancer [252-254].

Despite the impressive and beneficial antitumor activity elicited in clinical applications of ICIs, cases report on the occurrence of severe or even fatal side effects due to an excessive immune activation referred to as immune-related adverse events (irAEs) [24, 255, 256]. These irAEs relate to the drug's normal tissue exposure by systemic application and potentially affect multiple organ systems leading to life threatening conditions of the patient. Thus, local production of ICIs was suggested to be beneficial both, for safety and efficacy of the drug and was thus initially tested using a tumor cell line simultaneously expressing GM-CSF and a full-length monoclonal anti-CTLA-4 antibody. Here, the lower systemic exposure of the host to the antibody therapy correlated with an enhanced therapeutic efficacy and reduced evidence of systemic autoimmunity [257]. Indeed, this principle could be proven in several preclinical studies by the delivery of genetic information of ICIs using oncolytic viral vectors or mRNA based platform technologies [258-262].

## 1.6 Objective of this Work

A desirable vaccine would induce a strong early expression of antigen leading to a well-balanced antigen specific humoral and cellular immune response. To accomplish this aim, the supplementation of viral vectors with immunomodulatory elements along with immunogenic antigens is inevitable and requires the space to be integrated stably into the viral genome. In this context, the development of a platform technology enabling the

quick insertion or exchange of antigen or immunomodulatory elements is desirable. Thus, the present work assesses the suitability of different genomic loci for the insertion of transgenes. For this, genes predicted to be non-essential for the replication of ORFV D1701-V were identified and replaced with the fluorescence marker AcGFP (GFP). Newly generated deletion site recombinants were characterized by growth efficiency, plaque physiology, genetic stability and their ability to express encoded transgenes. Further, the capability of those novel D1701-V recombinants to elicit immune responses was studied *in vitro* and *in vivo*.

Several preclinical studies using mRNA or viral vectored vaccines have shown the effective expression of monoclonal antibodies as a transgene in target cells, which lead to an increase of tumor-localized concentrations and antitumor efficacy while reducing irAEs. To this end, no study has shown ORFV D1701-V or other non-oncolytic viruses to be suitable for monoclonal antibody expression. Thus, a side project of the present work aimed to develop ORFV D1701-V based vectors capable of the expression of functional anti-CTLA-4 and anti-PD-L1 ICIs to further enhance the potency of ORFV D1701-V vectored vaccines.

# 2 Materials and Methods

## 2.1 Material

### 2.1.1 Devices

| | |
|---|---|
| Amaxa CLB Transfection Device | LONZA |
| BD FACSjazz | BD Biosciences |
| BD LSR Fortessa | BD Biosciences |
| BlotCycler Touch | Precision Biosystems |
| BLX-E254 UV Crosslinker | Vilber |
| Eclipse Ti2 | Nikon |
| FLUOstar Optima | BMG Labtech |
| Fresco 21 | Heraeus |
| Function Line BB16 | Heraeus |
| Fusion SL | Peqlab |
| Galaxy 170 S | Eppendorf |
| Gammacell® 1000 Elite | Nordion |
| Hybridization Oven TYP 30 | Bachofer |
| Infinite M200 Plate Reader | Tecan |
| Innova 44 | New Brunswick |
| Inverted Phase Contrast Microscope CK40 | Olympus |
| Luff-shaker WS 5 | Bühler |
| L80 Ultracentrifuge | Beckmann |
| Megafuge 1.0R | Heraeus |
| MidiMACS Separator | Miltenyi Biotec |
| MiniMACS Separator | Miltenyi Biotec |
| Neubauer counting chamber | Brand |
| Owl D2 Wide-Gel Electrophoresis System | ThermoFisher |
| Rotator | ThermoFisher |
| Rotilabo-Microlitercentrifuge Gusto | Roth |
| Sonopul GM mini20 | Bandelin |
| SuperCycler SC-200 | Kyratec |

| | |
|---|---|
| SW 41 Ti Swinging-Bucket Rotor | Beckmann |
| TFA-20.250 Rotor | Kontron |
| ThermoMixer 5437 | Eppendorf |
| Trans-Blot Turbo Transfer System | Bio-Rad |
| Transilluminator TI2 | Biometra |
| Water bath | Julabo |

### 2.1.2 Consumables

| | |
|---|---|
| 6-well cell culture plate | Greiner bio-one |
| 12-well cell culture plate | Corning Costar |
| 24-well cell culture plate | Greiner bio-one |
| 96-well cell culture plate (flat bottom) | Greiner bio-one |
| 96-well cell culture plate (round bottom) | Corning Costar |
| 96-well ELISA plate | Thermo Scientific |
| 384-well cell culture plate | Greiner bio-one |
| T25 cell culture flask | Greiner bio-one |
| T75 cell culture flask | Greiner bio-one |
| T175 cell culture flask | Greiner bio-one |
| Safe-Lock Tubes, 0.5 ml | Eppendorf |
| Safe-Lock Tubes, 1.5 ml | Eppendorf |
| Safe-Lock Tubes, 2 ml | Eppendorf |
| Safe-Lock Tubes, 5 ml | Eppendorf |
| 8-well PCR Tube Strips | Nippon |
| 15 ml Tubes | Corning Costar |
| 50 ml Tubes | Greiner bio-one |
| 5/10/25 ml serological pipets | Falcon |
| 50 ml serological pipets | Corning Costar |
| Cell strainer, 40 µm | Falcon |

| | |
|---|---|
| Chromatography Paper (3 MM) | Whatman |
| Cryo.S Tubes (2 ml) | Greiner bio-one |
| MACS-Column MS | Miltenyi Biotec |
| MACS-Column LS | Miltenyi Biotec |
| Nitrocellulose Membranes (0.45 µm) | GE Healthcare |
| Nylon Membranes, positively charged | Roche |
| Pasteurpipets | Roth |
| Polyallomer 200 ml ultracentrifuge buckets | Beranek Laborgeräte |
| Polyallomer centrifuge tubes open-top | Seton |
| Trifill multichannel pipette reservoir | Camlab |

### 2.1.3 Commercial Kits

| | |
|---|---|
| Amaxa CLB Transfection Kit | LONZA |
| CTLA-4 Blockade Assay | Promega |
| DIG Luminescent Detection Kit | Roche |
| GeneElute Gel Extraction Kit | Sigma Aldrich |
| GeneElute HP Plasmid Miniprep Kit | Sigma Aldrich |
| MasterPure DNA Purification Kit | Epicentre Biotechnologies |
| PCR DIG Probe Synthesis Kit | Roche |
| PD-L1 Blockade Assy | Promega |
| Plasmid Midi Kit 100 | Qiagen |
| Quick Ligation Kit | New England Biolabs |
| Zombie Aqua Fixable Viability Kit | BioLegend |

### 2.1.4 Chemicals and Reagents

| | |
|---|---|
| 2'-3'-cGAMP | Invivogen |
| ACK Lysis-Buffer | Gibco |
| Acrylamide Mix (30%) | Roth |
| Ammonium Persulfate (APS) | Thermo Scientific |
| Ampicillin (100 mg/ml) | Sigma-Aldrich |

| | |
|---|---|
| Blasticidin | Invivogen |
| BSA (Bovines Serum-Albumin) | Sigma-Aldrich |
| Biocoll | Biochrom |
| Brefeldin A | Sigma-Aldrich |
| CD4 MicroBeads | Miltenyi Biotec |
| CD14 MicroBeads | Miltenyi Biotec |
| CutSmart buffer (10 x) | New England Biolabs |
| Cytofix/Cytoperm | BD Biosciences |
| DIG Easy Hyb | Roche |
| DIG Wash and Block Buffer Set | Roche |
| DMEM (Dulbecco's Modified Eagle Medium) | Gibco by Life Technologies |
| DMSO (Dimethyl-Sulfoxid) | Biochrom |
| DNA Molecular Weight Marker II, DIG-labeled | Roche |
| HyperLadder 1 kb | Bioline |
| EDTA | Invitrogen |
| Ethanol (100 %) | VWR Chemicals |
| FastGene Agarose-Tabletten | Nippon Genetics |
| FCS (fetal calf serum) | Biochrom |
| Formaldehyde | Sigma-Aldrich |
| Gel Loading Dye Purple (6 x) | New England Biolabs |
| GM-CSF (Leukine, Sagramostim) | University pharmacy |
| Human TruStain FcX Fc BlocK | BioLegend |
| IL-2 | R&D Systems |
| IL-4 | Peprotech |
| IMDM (Iscove's Modified Dulbecco's Medium) | Lonza |
| Isopropanol | Sigma-Aldrich |
| LPS | Sigma-Aldrich |
| Methanol | Sigma-Aldrich |
| Mouse BD Fc Block | BD Biosciences |
| Midori-Green Advanced DNA Stain | Nippon Genetics |
| NEB Buffer 1.1 (10 x) | New England Biolabs |
| NEB Buffer 2.1 (10 x) | New England Biolabs |

| | |
|---|---|
| NEB buffer 3.1 (10 x) | New England Biolabs |
| Normocin | Invivogen |
| NuPAGE LDS Sample Buffer | Thermo Scientific |
| NuPAGE Sample Reducing Buffer | Thermo Scientific |
| NuPAGE Transfer Buffer | Thermo Scientific |
| PageRuler Prestained Protein Ladder | Thermo Scientific |
| PBS (Phosphate Buffered Saline) | Gibco by Life Technologies |
| Penicillin/Streptomycin | Sigma-Aldrich |
| Peroxidase Substrate | Sigma-Aldrich |
| Phosphoric acid | Sigma-Aldrich |
| Quick-Load® 1 kb DNA Ladder | New England Biolabs |
| Ready-To-Use 1 kb Ladder | Nippon Genetics |
| Restore Western Blot Stripping Buffer | Thermo Scientific |
| RPMI-Medium 1640 | Gibco by Life Technologies |
| SDS | Sigma-Aldrich |
| Skim Milk Powder | Sigma Aldrich |
| Sulforic acid | AppliChem |
| SOC (Super Optimal Broth) | New England Biolabs |
| Streptavidin-HRP | BD Biosciences |
| Tetramethylethylendiamin (TEMED) | Invitrogen |
| Trypanblau | Sigma-Aldrich |
| Trypsin | Lonza |
| Zeocin | Invivogen |

### 2.1.5 Buffers and Media

| | |
|---|---|
| Denaturation solution | 0.5 N NaOH<br>1.5 M NaCl |
| Depurination solution | 0.25 N HCL |
| ELISA Wash Solution (PBS-T) | PBS<br>0.05% Tween 20 |

| | |
|---|---|
| ELISA Block Solution | PBS<br>10% BSA |
| Freezing-Medium | 90% FCS<br>10% DMSO |
| HEK Cell Medium | 1x DMEM<br>10 % (v/v) heat-inactivated FCS<br>2 mM L-glutamine<br>100 U/ml Penicillin<br>100 µg/ml Streptomycin |
| IMDM Complete Medium | 1x IMDM<br>10 % (v/v) heat-inactivated FCS<br>100 U/ml Penicillin<br>100 µg/ml Streptomycin |
| LB Amp/Kan Medium (liquid) | 10 g Bacto-Trypton<br>5 g Bacto-yeast extract<br>5 g NaCl<br>2 ml 2 N NaOH (pH 7.0-7.2)<br>1 l ddH2O<br>100 µg/ml Ampicillin or<br>50 µg/ml Kanamycin |
| LB Amp/Kan Medium (solid) | 10 g Bacto-Trypton<br>5 g Bacto-yeast extract<br>5 g NaCl<br>2 ml 2 N NaOH (pH 7.0-7.2)<br>1 l ddH2O<br>15 g agar<br>100 µg/ml Ampicillin or<br>50 µg/ml Kanamycin |
| NF Stop Solution | PBS<br>3% FCS |
| PBE | PBS<br>0.5% (v/v) FCS<br>5 mM EDTA |
| Permwash | PBS<br>0.1 % Saponin<br>0.02 % Sodium azide<br>0.5 % FCS |

| | |
|---|---|
| PFEA | 1 x PBS<br>2 mM EDTA<br>2 % FCS<br>0.02 % Sodium azide |
| Resolving gel (15%) | 2.3 ml $H_2O$<br>5 ml 30% acrylamide mix<br>2.5 ml 1.5 M Tris (pH = 8.8)<br>0.1 ml 10% SDS<br>0.1 ml 10% APS<br>4 µl TEMED |
| Ripa buffer | 50 mM Tris-HCl<br>150 mM NaCl<br>1 mM EDTA<br>1% (v/v) Triton X-100<br>0.5% (v/v) Sodium deoyxcholate<br>0.1% (v/v) SDS<br>5% (v/v) Glycerol |
| RPMI Complete Medium | 1x RPMI Medium 1640<br>10 % (v/v) heat-inactivated FCS<br>100 U/ml Penicillin<br>100 µg/ml Streptomycin |
| RPMI Dual Medium | 1x RPMI Medium 1640<br>10 % (v/v) heat-inactivated FCS<br>100 U/ml Penicillin<br>100 µg/ml Streptomycin<br>100 µg/ml Normocin<br>100 µg/ml Blasticidin<br>100 µg/ml Zeocin |
| SB Stripping Buffer | 0.2 N NaOH<br>0.1% (v/v) SDS |
| SB Transfer Solution | 0.25 N NaOH<br>1.5 M NaCl |
| SSC | 0.15 M NaCl<br>0.015 M Na-citrate, pH = 7.0-7.4 |

| | |
|---|---|
| Stacking Gel | 1.75 ml $H_2O$<br>425 µl 30% Acrylamide mix<br>325 µl 1 M Tris (pH = 6.8)<br>25 µl 10% SDS<br>25 µl 10% APS<br>2.5 µl TEMED |
| TAE 50x | 2 M Tris-Aminomethane<br>0.5 M EDTA<br>1 M Acetic acid |
| Tetramer-Buffer | 50% FCS<br>50%PBS<br>2 mM EDTA |
| T Cell Medium | 1x RPMI Medium 1640<br>5 % (v/v) heat-inactivated human serum<br>100 U/ml Penicillin<br>100 µg/ml Streptomycin |
| Vero Cell Medium | 1x DMEM<br>5 % (v/v) heat-inactivated FCS<br>100 U/ml Penicillin<br>100 µg/ml Streptomycin |
| Versen Trypsin | 50 ml Trypsin (10x)<br>50 ml PBS (10x)<br>6 mM EDTA<br>1 l ddH2O |
| WB Blocking Buffer 1 | 1 x TBS-T<br>5% (w/v) BSA |
| WB Blocking Buffer 2 | 1 x TBS-T<br>5% (w/v) Skim milk powder |
| WB Running Buffer | 1 x SDS<br>$H_2O$ |
| WB Washing Buffer | 1 x Tris-buffered Saline<br>0.1% Tween20<br>dd$H_2O$ |

### 2.1.6 Enzymes

| | |
|---|---|
| AmpliTaq Gold Polymerase | ThermoFisher Scientific |
| BamH*I*-HF | New England Biolabs |
| Bgl*II* | New England Biolabs |
| DNAse I (stock: 10 mg/ml in PBS) | Roche |
| Dra*III* | New England Biolabs |
| EcoR*I*-HF | New England Biolabs |
| Hind*III*-HF | New England Biolabs |
| Kpn*I*-HF | New England Biolabs |
| Mlu*I* | New England Biolabs |
| OptiTaq Polymerase | Roboklon |
| Spe*I* | New England Biolabs |
| Streptavidin HRP | BD Biosciences |

### 2.1.7 Oligonucleotides

All synthesized oligonucleotides (primer) were generated by Metabion.

**Table 2: Forward and reverse primer used in this work, their nucleotide sequence in 5'-3', amplicon sizes of primer pairs if applicable and PCR in which primers were used.**

| Primer | Nucleotidesequence | Amplicon [bp] | PCR |
|---|---|---|---|
| **014-F** | CGA AGC ACA CTT CCG TGT TA | | |
| **014-R** | GCC CGT TAA GGT TAA GCA GT | 200 | 014 |
| **024-F** | TGG AGG AAA CTT CGG TCT CA | | |
| **024-R** | CTC TAG CAC GCG CTT TCG | 299 | 024 |
| **112-F** | AAG TTA CAT AGG CCT CGG ATT C | | |
| **112-R** | GTT GGG TAG TTG TGG GTT CT | 209 | 112 |
| **113-F** | CCT CCT TAT TGA ACT CGG CTT AG | | |
| **113-R** | AGT GGT ATC CAG GGT CGT T | 329 | 113 |
| **119-F** | CTC GCC AGCATG ACA CAG | | |
| **119-R** | GGG CTC ATG CCG AAG AAC | 407 | 119 |
| **121-F** | CTG AAC CGC GAC CTG ATG | | |
| **121-R** | GGG TCT CGT AGT GAT GTT TGG | 316 | 121 |
| **126-F** | CGT ACG TGA ACG CCA AAG A | | |
| **126-R** | TGA AGG ACT CGC AGT GGT A | 273 | 126 |
| **128-F** | AAC ACT CCT CCT GCA AAC AC | | |
| **128-R** | ACT ACG TAC GCC ACA CAG A | 334 | 128 |

| | | | |
|---|---|---|---|
| **374** | GGT GCT CAG CGT GGT GGC GGT TTC | | |
| **pdV-R** | ACC ACA AGG CCG CCC AGA AGA CGC CGC TAG | Insert specific | *vegf*-locus |
| **CD4-F3** | GAT CGC GCT GAC TCA AGA A | | |
| **CD4-R3** | AGG TCA AAG GTG ATC CAA GAC | 536 | CD4 |
| **d014-F** | TAC AGA GGA GGA GTT CGA CAA | | |
| **d014-R** | AAG AAC CGT TGA CGG CAT AA | 1238 with GFP | d014 |
| **d024-F2** | TTC CTC ATG GAG AAG CTA T | | |
| **d024-R2** | GCT GGA CAA TAA GGC TAT G | 1154 with GFP | d024 |
| **d112-F** | GCT GGA CGT GGC CAT ATA A | | |
| **d112-R** | GCC GTT CCA GTT AAG CAT ATT AC | 1138 | d112 |
| **d113-F** | CGT GGG AAA GGA TCA CAA TAT G | | |
| **d113-R** | AAG TCC AGA GTC AGA CAT TCC | 1202 | d113 |
| **d119-F** | CTC TCG TAG GCT CGC TCT C | | |
| **d119-R** | CAG TGA AAT GTG GGA CTC CTT C | 1155 | d119 |
| **d121-F** | TGA AAT TCA AAC ACG CTT TGG G | | |
| **d121-R** | GCG AAT CTT TGT GAA GAC ACA TTT | 1222 | d121 |
| **d126-F2** | GAC TTC ATG CGG CTC GTG TA | | |
| **d126-R2** | GCA CCA TTA CTA CCG CAC TGT T | 1360 | d126 |
| **d127-F** | ACC GTG GAG GAA CTC TCT T | | |
| **d127-R2** | TCG GCA ACG TAG TCG TGA A | 1117 | d127 |
| **d128-F** | CGT TCA GAT TCT CGT ATC GTC TG | | |
| **d128-R** | CGC GTT CAG GAT GAA GTA GTC | 1157 | d128 |
| **Del2-F** | GCA ACA AGG TCT GCG TGC CTG CCG ACC | | |
| **Del2-R2** | CGG CGA TCT GGA TGG TTG GAG CCA TGC C | Insert specific | Del2 locus |
| **DIL-10-F** | CGC TCA TGG CCT TGT AAA CAC C | | |
| **DIL-10-R** | CAC ATG CTC AGA GAA CTC AGG G | 364 | 127 |
| **HC-F** | CTG GGA ACC CAG ACC TAC AT | | |
| **LC-R** | CTC TGG GTC AGC ACG ATT TC | 1061 | Ipilimumab |
| **OVA-F** | CAG TGC GTG AAA GAG CTG TA | | |
| **OVA-R** | GGG CAG GTA CAC TTT GAT CTT | 495 | OVA |
| **PDL1-F** | CTC TGA TCG TGT ACT GGG AGA T | | |
| **PDL1-R** | CTG TTT GTG GTG GTG GTC TT | 1671 | Avelumab |
| **Recall-F** | ATG AAC CTG GTG CCC AT | | |
| **Recall-R** | CAG GGT GAA CAC GAA GC | 220 | Recall |

### 2.1.8 Antibodies

Antibodies used in this work for FACS, western blot or ELISA analyses are listed in Table 3 - Table 6.

**Table 3: Specificity, antibody-clone, fluorochrome, dilution and manufacturer of applied antibodies in FACS analyses.**

| Specificity | Clone | Fluorochrome | Dilution | Manufacturer |
|---|---|---|---|---|
| **α-human CD4** | RPA-T4 | Pacific Blue | 1:400 | BioLegend |
| **α-human CD8** | SK1 | APC/CY7 | 1:150 | BioLegend |
| **α-mouse CD8** | 53-6.7 | PerCP/Cy5.5 | 1:900 | eBioscience |
| **α-human CD14** | HCD14 | Alexa Fluor 700 | 1:200 | BioLegend |
| **α-human CD19** | HIB19 | PerCP | 1:160 | BioLegend |
| **α-mouse CD19** | 6D5 | FITC | 1:200 | BioLegend |
| **α-human CD56** | HCD56 | BV605 | 1:50 | BioLegend |
| **α-human CD69** | FN50 | PE | 1:50 | BioLegend |
| **α-human CD80** | 2D10 | FITC | 1:50 | BioLegend |
| **α-human CD83** | HB15E | APC | 1:100 | BioLegend |
| **α-human CD86** | IT2.2 | BV605 | 1:100 | BioLegend |
| **α-mouse CD90.2** | 53-2.1 | APC | 1:1500 | eBioscience |
| **α-mouse CD127** | SB/199 | eFluor 450 | 1:100 | eBioscience |
| **α-human CD154** | 24-31 | APC | 1:50 | BioLegend |
| **α-human HLA-DR** | L243 | BV711 | 1:200 | BioLegend |
| **α-human IFNγ** | B27 | APC | 1:400 | BioLegend |
| **α-mouse KLRG1** | 2F1 | PE/Cy7 | 1:200 | BioLegend |
| **α-human TNFα** | MAb11 | PE/Cy7 | 1:400 | BioLegend |

**Table 4: Isotype, clones, fluorochromes and manufacturer of used controls in FACS analyses.**

| Isotype | Clone | Fluorochrome | Manufacturer |
|---|---|---|---|
| **IgG1κ** | MOPC-21 | FITC | BioLegend |
| **IgG1κ** | MOPC-21 | PE | BioLegend |
| **IgG1κ** | MOPC-21 | APC | BioLegend |
| **IgG1κ** | MOPC-21 | PE/Cy7 | BioLegend |
| **IgG2bκ** | MPC-11 | BV605 | BioLegend |
| **IgG2bκ** | MPC-11 | BV711 | BioLegend |

**Table 5: Specificity, trade name, dilution and manufacturer of applied antibodies used in western blot analyses.**

| Specificity | Trade Name | Dilution/Conc. | Manufacturer |
|---|---|---|---|
| **α-human CTLA-4** | Ipilumumab | 100 ng | Bristol-Meyers Squibb |
| **α-human PD-L1** | Avelumab | 100 ng | Merck KGaA |
| **Mouse α-human IgG (H+L)** | | 1:33333 | Jackson |
| **α-mouse IgG (H+L), HRP conjugate** | | 1:10000 | Promega |

**Table 6: Specificity, trade name, dilution and manufacturer of applied antibodies used in ELISA or blockade bioassay analyses.**

| Specificity | Trade Name | Dilution/Conc. | Manufacturer |
|---|---|---|---|
| **α-human CTLA-4** | Ipilumumab | 3 µg/ml | Bristol-Meyers Squibb |
| **α-human PD-L1** | Avelumab | 3 µg/ml | Merck KGaA |
| **α-human CD20** | Rituximab | 3 µg/ml | Roche |
| **α-human IgG, F(ab')$_2$** | | 1:200 | Jackson |
| **α-mouse IgG2a[b]** | | 1:300 | BD Biosciences |
| **α-mouse IgG1** | | 1:600 | BD Biosciences |
| **α-Endoglin human IgG1** | | 5 µg/ml | In-house |

### 2.1.9 Recombinant Proteins

**Table 7: Recombinant proteins used in ELISA experiments.**

| Protein | Concentration | Manufacturer |
|---|---|---|
| **Human CTLA-4-Fc fusion** | 1 µg/ml | In-house |
| **Human PD-L1-Fc fusion** | 1 µg/ml | In-house |
| **Ovalbumin (OVA)** | 20 µg/ml | Sigma |

### 2.1.10 Viruses and Transfer Plasmids

Table 8 and Table 9 list ORFV recombinants and transfer plasmids generated and already described in the Amann group, as well as newly generated ORFV recombinants. DNA fragments were synthesized by Invitrogen, while cloning of new transfer plasmids is described in 2.2.1 - 2.2.7.

**Table 8: ORFV recombinants and their abbreviation used in this work.**

| Virus recombinant | Abbreviation |
|---|---|
| **D12-Cherry** | n.d. |
| **V12-Cherry-Del014-7-2-GFP** | VCh014GFP |
| **V-Cherry-Del024-9-2-GFP** | VCh024GFP |
| **V12-Cherry-Del112-10-2-GFP** | VCh112GFP |
| **V12-Cherry-Del113-11-2-GFP** | VCh113GFP |
| **V12-Cherry-Del121-1-2-GFP** | VCh121GFP |
| **V12-Cherry-Del126-4-2-GFP** | VCh126GFP |
| **V12-Cherry-Del127-3-2-GFP** | VCh127GFP |
| **V12-Cherry** | V12-Ch |
| **V12-Cherry-D12-GFP** | VChD12GFP |
| **V12-OVA** | n.d. |
| **V-GFP-D12-Cherry** | V-GFP-D12-Ch |
| **V-CD4-D12-Cherry** | V-CD4-D12-Ch |

**Table 9: ORFV recombinants generated in this work, their abbreviation, transfer plasmid and parental ORFV recombinant. Italic type indicates transfer plasmids generated in this study as described in 2.2.1 - 2.2.7.**

| Virus recombinant | Abbreviation | Transfer plasmid | Parental virus |
|---|---|---|---|
| **V12-Cherry-Del119-1-2-GFP** | VCh119GFP | *pDel119-1-2-GFP* | V12-Cherry |
| **V12-Cherry-Del128-5-2-GFP** | VCh128GFP | pV12-Cherry | VOVA128GFP |
| **V12-OVA-Del014-7-2-GFP** | VOVA014GFP | *pDel014-7-2-GFP* | V12-OVA |
| **V12-OVA-Del024-9-2-GFP** | VOVA024GFP | *pDel024-9-2-GFP* | V12-OVA |
| **V12-OVA-Del112-10-2-GFP** | VOVA112GFP | *pDel112-10-2-GFP* | V12-OVA |
| **V12-OVA-Del113-11-2-GFP** | VOVA113GFP | pV12-OVA | VCh113GFP |
| **V12-OVA-Del119-1-2-GFP** | VOVA119GFP | *pDel119-1-2-GFP* | V12-OVA |
| **V12-OVA-Del121-1-2-GFP** | VOVA121GFP | *pDel121-1-2-GFP* | V12-OVA |
| **V12-OVA-Del126-4-2-GFP** | VOVA126GFP | *pDel126-4-2-GFP* | V12-OVA |
| **V12-OVA-Del127-3-2-GFP** | VOVA127GFP | pV12-OVA | VCh127GFP |
| **V12-OVA-Del128-5-2-GFP** | VOVA128GFP | *pDel128-5-2-GFP* | V12-OVA |
| **V-HLAA02-Mini-Del024-9-2-GFP** | VHLA024GFP | *pV-HLAA02-Mini* | VCh024GFP |
| **V-HLAA02-Mini-Del112-10-2-GFP** | VHLA112GFP | *pV-HLAA02-Mini* | VCh112GFP |
| **V-HLAA02-Mini-Del119-1-2-GFP** | VHLA119GFP | *pV-HLAA02-Mini* | VCh119GFP |
| **V-HLAA02-Mini-Del121-1-2-GFP** | VHLA121GFP | *pV-HLAA02-Mini* | VCh121GFP |
| **V-HLAA02-Mini-Del126-4-2-GFP** | VHLA126GFP | *pV-HLAA02-Mini* | VCh126GFP |
| **V-HLAA02-Mini-Del128-5-2-GFP** | VHLA128GFP | *pV-HLAA02-Mini* | VCh128GFP |
| **V-HLAA02-Mini-D12-GFP** | VHLAD12GFP | *pV-HLAA02-Mini* | VChD12GFP |
| **V-IpiHC-2-IpiLC-D12-Cherry** | Ipi-Ch | *pV-IpiHC-2-IpiLC* | V-CD4-D12-Ch |
| **V-AveHC-2-AveLC-D12-Cherry** | Ave-Ch | pV-AveHC-2-AveLC* | V-GFP-D12-Ch |

*Transfer plasmid was generated and kindly provided by BI.

### 2.1.11 Bacteria

Transformations were performed using *E. coli DH5α* (high efficiency) from New England Biolabs, while subcloning was carried out using the *E. coli DH5α* derived strain NEB 5-alpha competent (subcloning efficiency) from New England Biolabs according to manufacturers' instructions.

### 2.1.12 Peptides

**Table 10: Peptides used in this work, their source and manufacturer.**

| Peptide | Source | Manufacturer |
|---|---|---|
| **NLVPMVATV** | HCMV $pp65_{495-503}$ | In-house |
| **GLCTLVAML** | EBV $BMLF1_{280-288}$ | In-house |
| **GILGFVFTL** | Influenza A $MP_{58-66}$ | In-house |

### 2.1.13 Multimeres

**Table 11: Multimeres used in this work, their epitope, fluorochrome and manufacturer.**

| Multimere | Epitope | Fluorochrome | Manufacturer |
|---|---|---|---|
| **Tetramer** | NLVPMVATV | PE | In-house |
| **Tetramer** | GLCTLVAML | PE | In-house |
| **Tetramer** | GILGFVFTL | PE | In-house |
| **Dextramer** | SIINFEKL | PE | Immudex |

### 2.1.14 Cell Lines

The ORFV-permissive monkey kidney cell line Vero (ATCC, CCL-81) was used for the generation, propagation and culture of ORFV D1701-V. The monocytic ORFV non-permissive suspension cell line THP-1 (ATCC TIB-202) was used for expression kinetics of the new Del Site recombinants, as well as for the ORFV induced production of antibodies Ipilimimab and Avelumab. HEK 293 T (ATCC, CRL-3216) and ExpiCHO-S cells (Thermo Fisher) were utilized to study the ORFV induced production of Ipilimumab and Avelumab. The human THP-1 derived THP-1 Dual cell line (Invivogen) was used to investigate the ORFV induced activation of the NF-κB- and IRF-pathway.

### 2.1.15 Human Primary Cells

Blood samples from healthy donors were received from the Blood Donation Center Tübingen and used for the isolation of PBMCs (Peripheral Blood Mononuclear Cells) as described in 2.4.4. The use of PBMCs from donor blood was approved by the Tübingen Ethics Committee ("Influence of Orf Virus Vectors on Cells of the Immune System", Ethics Application Number: 156 / 2012BO1).

### 2.1.16 Mice

*In vivo* experiments were performed using mice of the C57BL/6 strain C57BL/6NTac from Taconic.

### 2.1.17 Software

| | |
|---|---|
| BD FACSDiva | BD Biosciences |
| FlowJo V10 | Tree Star |
| Fusion-Capt | Peqlab |
| ImageJ | NIH |
| MS Office 2010 | Microsoft |
| NanoDrop 1000 3.7.1 | Peqlab |
| NIS-Elements | Nikon |
| Optima | BMG Labtech |
| Prism 5 | GraphPad |
| Serial Cloner 2.5 | Serial Basics |
| SnapGene | GSL Biotech LLC |

## 2.2 Molecular Biological Methods

### 2.2.1 DNA Cleavage using Restriction Endonucleases

The cloning and subsequent control cleavage of new transfer plasmids was performed using restriction endonucleases from New England Biolabs and followed manufacturers' instructions. Thus, inserts and vectors were cleaved with the same restriction endonucleases resulting in complementary ends allowing ligation of cleaved DNA fragments. Restriction digest was carried out in supplied recommended restriction buffers for 1 h at 37°C in a total volume of 20 µl.

### 2.2.2 Agarose Gel Electrophoresis

Restriction digests or PCR products were applied onto agarose gels and separated by size via horizontal gel electrophoresis. DNA size markers allowed the size determination of DNA fragments. Preparation of 1% agarose gels was conducted for the analysis of DNA fragments of estimated 0.5-10 kbp, whereas DNA fragments of estimated >10 kbp were run on 0.8% agarose gels. The preparation of gels used agarose tablets, which were boiled according to the manufacturers' instructions in 1 x TAE buffer and supplemented with 4 µl Midori Green Advanced DNA Stain for each 100 ml agarose solution. If necessary, the samples were complemented with 1 x Gel Loading Dye Purple. Electrophoresis was carried out at about 100 V in 1 x TAE running buffer and subsequently visualized under UV light (Fusion SL, Peqlab).

### 2.2.3 Isolation of DNA Fragments from Agarose Gels

If necessary, DNA fragments were isolated from agarose gels using the Gene Elute Gel Extraction Kit (Sigma Aldrich) according to manufacturers' instructions.

### 2.2.4 Ligation of DNA Fragments

Using the Quick Ligation Kit by New England Biolabs, ligation of linearized DNA fragments was carried out in a vector:insert ratio of 1:5 with 50 ng vector according to manufacturers' instructions.

### *2.2.5* Transformation of Bacteria

Transformation of freshly ligated transfer plasmids was carried out using *E. coli DH5α* (High Efficiency) from New England Biolabs according to manufacturers' instructions. Pre-existing plasmids were subcloned using the *E. coli DH5α* derived strain NEB 5-alpha competent (subcloning efficiency) from New England Biolabs according to manufacturers' instructions. Next, bacteria were plated on LB/Amp- or LB/Kan-plates ON at 37°C prior to selection of grown colonies.

### 2.2.6 Plasmid Isolation from transformed Bacteria

For validation, plasmids of transformed bacteria were isolated using the GeneElute HP Plasmid Miniprep Kit (Sigma Aldrich) for small scale, and the Plasmid Midi Kit (Qiagen) for large scale according to manufacturers' instructions.

### 2.2.7 Sequencing

Sequencing was performed by GATC Biotech. For this purpose, 50-80 ng DNA were mixed with 5 µM primers and filled up with $H_2O$ to a volume of 10 µl.

### 2.2.8 Isolation of viral DNA from infected Vero Cells

For the isolation of viral DNA from cell culture, the Master Pure DNA Purification Kit (Epicenter Biotechnologies, Biozym) was used. Depending on the volume of cell culture, 200 µl (12/24 well plates), 75 µl (48/96 well plates) or 50 µl (384 well plates) of harvested cell lysates were re-suspended in 1 ml PBS and centrifuged for 3 min at 5000 x g. The cell pellet was dissolved in Tissue and Cell Lysis Solution (200 µl, 100 µl or 50 µl, respectively), supplemented with Proteinase K (0.6 µl, 0.3 µl or 0.15 µl, respectively) and vortexed for 10 s. After an incubation for 15 min at 65°C on a shaker, samples were put on ice for 2 min and supplemented with 50 µl precipitation reagent (MPC solution). Following centrifugation at 21000 x g for 10 min at 4°C, the supernatant was mixed with 170 µl isopropanol by inversion and centrifuged for 2 min at 21000 x g. The pellet was washed with 170 µl 70% EtOH (v/v) and centrifuged for 2 min at 21000 x g. Finally, the dry DNA pellet was re-suspended in 25 µl $H_2O$.

### 2.2.9 Polymerase Chain Reaction

The correct insertion of genes in newly generated ORFV recombinants was validated by primer-mediated amplification of specific sequences using the polymerase chain reaction (PCR). Thus, insert-specific as well as parental gene specific PCRs were performed and complemented using genomic locus specific PCRs. For each reaction, 5 µl of polymerase mix (2 x OptiTaq Polymerase Master Mix or 2 x AmpliTaq Gold Polymerase Master Mix), 1-2 µl of a 30 ng primer mix and 1 µl DNA were supplemented

with $H_2O$ to a total volume of 10 µl. The PCR was carried out in the Supercycler (Kyratec). An initial denaturation step (98°C, 2 min) was followed by 35-40 cycles of denaturation (96°C, 15 s), primer hybridization (primer-specific temperature) and elongation (72°C, 30-150 s, respectively). After a final elongation (72°C, 2 min), the samples were stored at 4°C until analysis. The corresponding temperature profiles of cycles used to amplify specific DNA fragments in this work are summarized in Table 12.

**Table 12: Temperature profiles of cycles in polymerase chain reactions.**

| PCR | Initial Denaturation | Denaturation | Annealing | Elongation | Final Elongation |
|---|---|---|---|---|---|
| **014** | | | 57°C, 30 s | 72°C, 30 s | |
| **024** | | | 57°C, 30 s | 72°C, 30 s | |
| **112** | | | 57°C, 30 s | 72°C, 30 s | |
| **113** | | | 57°C, 30 s | 72°C, 30 s | |
| **119** | | | 57°C, 30 s | 72°C, 30 s | |
| **121** | | | 57°C, 30 s | 72°C, 30 s | |
| **126** | | | 57°C, 30 s | 72°C, 30 s | |
| **127** | | | 65°C, 30 s | 72°C, 30 s | |
| **128** | | | 57°C, 30 s | 72°C, 30 s | |
| **Avelumab** | | | 57°C, 30 s | 57°C, 30 s | |
| **CD4** | | | 62°C, 30 s | 72°C, 30 s | |
| **d014** | | | 57°C, 30 s | 72°C, 30 s | |
| **d024** | 98°C, 2 min | 98°C, 15 s | 55°C, 30 s | 72°C, 30 s | 72°C, 2 min |
| **d112** | | | 57°C, 30 s | 72°C, 30 s | |
| **d113** | | | 57°C, 30 s | 72°C, 30 s | |
| **d119** | | | 57°C, 30 s | 72°C, 30 s | |
| **d121** | | | 57°C, 30 s | 72°C, 30 s | |
| **d126** | | | 58°C, 30 s | 72°C, 2 min | |
| **d127** | | | 57°C, 30 s | 72°C, 30 s | |
| **d128** | | | 57°C, 30 s | 72°C, 30 s | |
| **Del2 locus** | | | 65°C, 30 s | 72°C, 90 s | |
| **Ipilimumab** | | | 59°C, 30 s | 72°C, 30 s | |
| **OVA** | | | 60°C, 30 s | 72°C, 30 s | |
| **Recall** | | | 60°C, 30 s | 72°C, 30 s | |
| ***vegf*-locus** | | | 72°C, 30 s | 72°C, 150 s | |

### 2.2.10 Western Blot

Western blotting is an analytical method in molecular biology used to detect specific proteins in samples of tissue homogenate or extract. In this work, western blots were used to detect full-length antibodies, as well as their light and heavy chains, generated by the ORFV recombinant induced expression of antibodies in Vero and THP-1 cells upon infection. For this purpose, 5 x $10^5$ cells were seeded in 3 ml medium and infected with Ipilimumab and Avelumab encoding ORFV recombinants for 72 h at 37°C and 5% $CO_2$. Supernatants were centrifuged for 5 min at 500 x g at RT and frozen at -20°C, while attached cells were treated with 60 µl Ripa buffer for 15 min at 4°C. The lysate was transferred to a fresh 1.5 ml Eppendorf cup, centrifuged for 5 min at 21.000 x g and frozen at -20°C. For analyses, samples were supplemented with 1 x NuPAGE LDS sample buffer and 1 x NuPAGE sample reducing agent for denaturing conditions, vortexed and cooked for 5 min at 95°C. Polyacrylamide gels were prepared by overlaying 10 ml resolving gel with 2.5 ml stacking gel, 15 µl of samples were loaded and electrophoresis was performed in WB running buffer at 150 V for approximately 90 min. Subsequently, the western blot was assembled as shown in Figure 1 and samples were blotted onto nitrocellulose membranes at 25 V and 1 A for 35 min in 1 x NuPAGE transfer buffer containing 20% methanol.

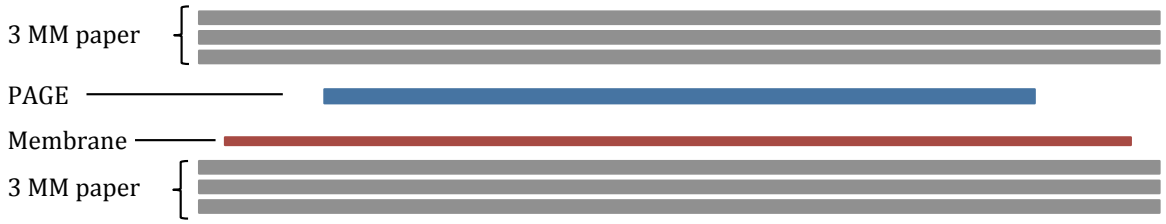


**Figure 1: Western blot assembly. The western blot was assembled by placing the polyacrylamide gel and nitrocellulose membrane between three wet 3 MM chromatography papers on each site.**

During staining procedures, each of the following steps was linked by three consecutive washing steps using 10 ml WB washing buffer at RT for 5 min on a roller. First, non-specific antibody binding was prevented by incubating the membrane with WB blocking buffer 1 for 30 min at RT on a roller. Next, the primary antibody was applied in WB blocking buffer 1 ON at 4°C prior to incubation with the secondary antibody in WB blocking buffer 2 at RT for 2 h. After a final washing step, the membrane was developed according to manufacturers' instructions using the AceGlow chemiluminescence substrate. If necessary, membranes were stripped and stained with other antibodies using the Restore western blot Stripping Buffer according to manufacturers' instructions.

### 2.2.11 Southern Blot

Southern blotting is a molecular biological method that combines the transfer of DNA separated by agarose gel electrophoresis to a filter membrane for the detection of specific DNA fragments by probe hybridization. Hence, this method was used to study the genomic location of genes encoded by ORFV recombinants. In order to generate

sufficient amounts of purified viral DNA, 3.3 x $10^6$ Vero cells were seeded in T75 cultivation flasks containing 25 ml Vero cell medium, infected (MOI 0.5) and incubated at 37°C and 5% $CO_2$. Virus purification was performed as described in 2.3.3. Next, DNA was isolated as described in 2.2.8, whereas all centrifugation steps were carried out at 21.000 x g and 4°C. Subsequently, 3 µg viral and 0.5 µg plasmid DNA were digested using restriction enzymes (100 U EcoR*I*, 200 U Kpn*I*, 100 U Hind*III*) for 6 h at 37°C in a total volume of 20 µl according to manufacturers' instructions. Samples were supplemented with loading buffer and electrophoresis was carried out at 75 V for 6 h using a 0.8% agarose gel. Adjacently, the gel was agitated twice in depurination solution at RT for 10 min, washed three times in $H_2O$ and agitated in denaturation solution for 30 min at RT. Afterwards, samples were transferred onto a positively charged nylon membrane in transfer solution ON at RT by alkaline blotting as shown in Figure 2.

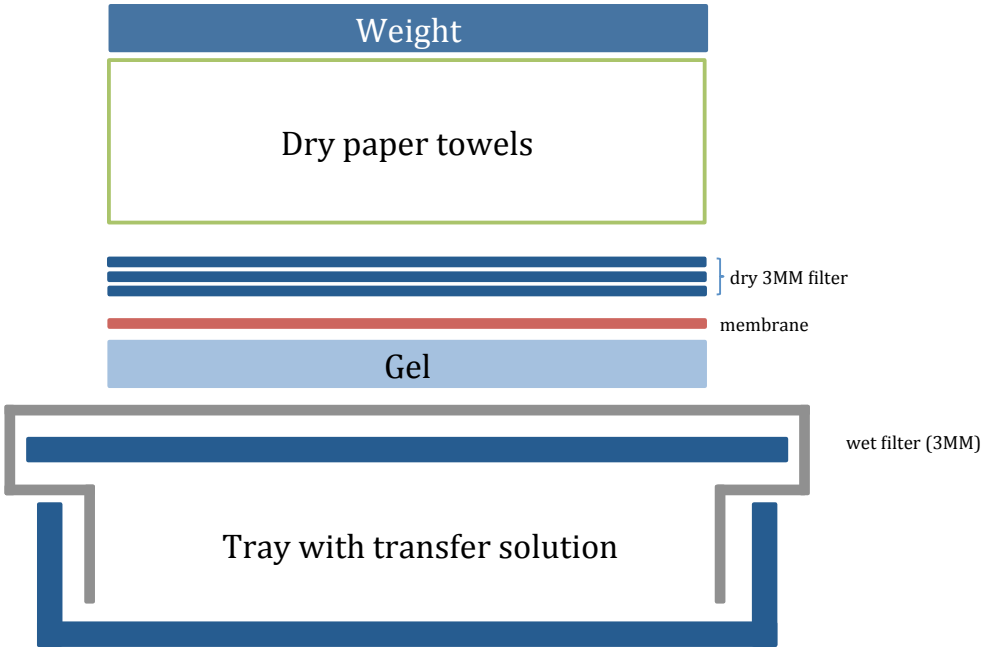


**Figure 2: Assembly of DNA sample transfer onto a nylon membrane via alkaline blotting.**

After the transfer, the membrane was rinsed three times in SSC and DNA was constantly fixed to the membrane by UV crosslinking for 3 min. In the next step, non-radioactive southern blot hybridization was performed, which uses the steroid hapten digoxigenin (DIG) coupled to dUTP, UTP or ddUTP to label DNA for hybridization and subsequent luminescent detection. For this, DNA probes were synthesized with the PCR DIG probe synthesis kit and hybridized using the DIG Easy Hyb hybridization solution according to manufacturers' instructions at 50°C or 56°C for DIG probes corresponding to GC-contents of 59% or 68%, respectively. The membrane was washed and blocked, and chemiluminescent detection was performed using the DIG Wash and Block Buffer Set and DIG luminescent detection kit according to manufacturers' instructions. If desired, the membrane was washed briefly in $H_2O$ and subsequently stripped twice for 15 min in SB stripping buffer at 37°C under constant agitation. Prior to pre-hybridization, the membrane was equilibrated using 2 x SSC.

## 2.3 Virological Methods

### 2.3.1 Transfection of ORFV infected Vero Cells

The generation of recombinant ORFVs followed two steps, in which Vero cells were transfected with transfer plasmids prior to infection with ORFV. Transfection was performed by an electroporation-based transfection method called nucleofection. Due to homologous sequences on the transfer plasmid and the ORFV genome, the inserts could be integrated into the ORFV genome via homologous recombination. For this purpose, Vero cells were detached as described in 2.4.1, re-suspended in 5 ml NF stop solution and counted. For each transfection batch, 2.5 x $10^6$ cells were transferred into a 1.5 ml Eppendorf cup and centrifuged at 63 rcf for 10 min. The cell pellet was re-suspended in 100 µl transfection solution (transfection supplement and CLB transfection buffer of the Amaxa transfection kit mixed in a ratio of 1:4.5), supplemented with 2 µg plasmid DNA and transferred into a transfection cuvette. For transfection, the CLB Transfection Device was used. Subsequently, nucleofected cells were re-suspended in NF stop solution and transferred into a T25 cell culture flask containing 6 ml pre-warmed Vero cell medium using a Pasteur pipette. Cells were immediately infected with parental virus (MOI 1) for 4 hours at 37°C and 5% $CO_2$, washed using 6 ml pre-warmed PBS and incubated in fresh Vero cell medium for 72 h at 37°C and 5% $CO_2$. When virus plaques or a cytopathic effect (CPE) could be observed, cells were frozen and thawed three times at -80°C and 37°C in a water bath, respectively, to disrupt the cells and release viral progeny.

### 2.3.2 Selection of ORFV Recombinants

Homologous recombination is an event occurring in a ratio of approximately 1:10000 between the insert of the transfer plasmid and the target region in the ORFV genome. To select for this rare event and to separate the recombinant ORFVs from parental viruses, different selection methods can be used.

#### *2.3.2.1 FACS based Selection of ORFV Recombinants*

Selection by fluorescence activated cell sorting (FACS) is based on the loss or gain of a fluorescent label such as GFP or mCherry. For this purpose, 3 x $10^5$ Vero cells were seeded in a 6-well plate containing 3 ml Vero cell medium. Transfection lysate was used for infection in serial dilutions and took place for 20-24 h at 37°C and 5% $CO_2$. To ensure an optimal selection process, cells with a low infection rate of approximately 1-5% were harvested and centrifuged for 5 min at 400 rcf. Subsequently, cells were washed thrice with 1 ml PBE and eventually re-suspended in 500 µl PBE. Single cell FACS sorting was performed into a 96-well plate containing $10^4$ Vero cells per well in 150 µl Vero cell medium using the BD FACSjazz (Biosciences). After 72 h of incubation at 37°C and 5% $CO_2$, wells showing single virus plaques of recombinant ORFV could be picked for further propagations and analyses.

#### *2.3.2.2 MACS based Selection of ORFV Recombinants*

Selection by MACS (Magnetic Cell Sorting) is based on the surface expression of CD4 on Vero cells infected with parental, CD4-encoding ORFV recombinants. For this, 80% confluent Vero cells in a T175 flask were washed with 10 ml PBS and infected with 1/3 of the transfection lysate in a total volume of 8 ml including Vero cell medium for 2 h on a tilt shaker at RT. Subsequently, the adherent cells were washed with 10 ml of PBS and incubated with 30 ml fresh Vero cell medium at 37°C and 5% $CO_2$ for 20-24 h. Next, the cells were washed once with 10 ml PBS and 5 ml of VT, and eventually detached with 2.5 ml of VT to be taken up in 9 ml of Vero cell medium in a 50 ml tube. Cells were centrifuged for 5 min at 500 x g and re-suspended in 300 µl PBE. The suspension was mixed with 50 µl α-CD4 MicroBeads in a 2 ml Eppendorf cup and incubated for 30 min at RT on a rotator. The MS column was equilibrated using 1 ml PBE and the cell suspension was loaded onto the column and washed three times with 1 ml of PBE. Due to the binding of magnetic α-CD4 MicroBeads to the Vero cells infected with CD4-encoding parental virus, the negative fraction of this selection process contains enriched recombinant virus infected Vero cells. Afterwards, $5 \times 10^6$ Vero cells were seeded together with $5 \times 10^6$ viable cells of the negative fraction in a T175 containing 30 ml fresh Vero cell medium and incubated at 37°C and 5% $CO_2$ for 20-24 h. To enrich as much recombinant ORFV as possible, CD4-negative MACS selection was performed on four consecutive days.

#### *2.3.2.3 Selection of ORFV Recombinants by Limiting Dilutions*

Further selection and purification of recombinant viruses after FACS based sorting or MACS selection was carried out by limiting dilutions. For this purpose, $2 \times 10^6$ Vero cells in 25 ml of Vero cell medium were split into a 12-well pipetting reservoir, in which the first and the rest of wells contained either 3 ml or 2 ml of the cell solution, respectively. The first well was supplemented with either $3 \times 10^5$ cells of the MACS selection or 50-100 µl of virus lysate and diluted 1:3 each from the first to the last well. 150 µl of each dilution were transferred into the corresponding wells of a 96-well plate and incubated at 37°C and 5% $CO_2$ for 72 h. After 72 h, wells containing single virus plaques could be selected for further processing by (fluorescence-) microscopy.

### 2.3.3 Propagation and Purification of ORFV Recombinants

For the propagation of ORFV recombinants, confluent Vero cells from a T175 cell culture flask were harvested and split into six T175 cell culture flasks. The cells were supplemented with 40 ml of Vero cell medium and incubated for 24 h at 37°C and 5% $CO_2$. Next, Vero cells were infected with ORFV recombinants (MOI 0.3) and incubated at 37°C and 5% $CO_2$. When cells showed a CPE of approximately 80% after 72 h, cells were frozen at -80°C, thawed to release the virus by disruption and merged in ultracentrifugation cups. After a centrifugation for 2 h at 25000 x g and 4°C, the pellet was overlaid with 1 ml PBS and re-suspended after an incubation ON at 4°C. Adjacently, the virus lysate was treated with DNAse I (10 µg/ml) and shaken for 10 min at RT. For the purification of Orf viruses, residual cell debris was removed by centrifugation at 500 x g for 10 min and the supernatant treated with ultrasound. For this purpose, the

virus lysate was sonicated on ice three times for 20 s with an ultrasonic rod (Sonopuls, Bandelin). Afterwards, 3 ml of 36% sucrose in an UZ tube were overlaid with the virus lysate and centrifuged on a swinging rotor at 49000 x g and 4°C for 30 min. The pellet was re-suspended and washed three times in 1 ml of PBS by centrifugation at 21000 x g and 4°C for 10 min, and finally taken up in 1 ml PBS.

### 2.3.4 Titration of ORFV Recombinants

Determination of ORFV recombinant titers was performed by plaque titration. For this purpose, 8 x $10^4$ Vero cells in 1 ml Vero cell medium were seeded in each well of a 24-well plate and infected with different dilutions of virus lysate. 1:10 dilution series were performed in 1.5 ml Eppendorf cups containing 450 µl of Vero cell medium up to a dilution of $10^{-9}$. 100 µl of the dilutions were pipetted into the wells of the 24-well plate according to the scheme shown in Figure 3.

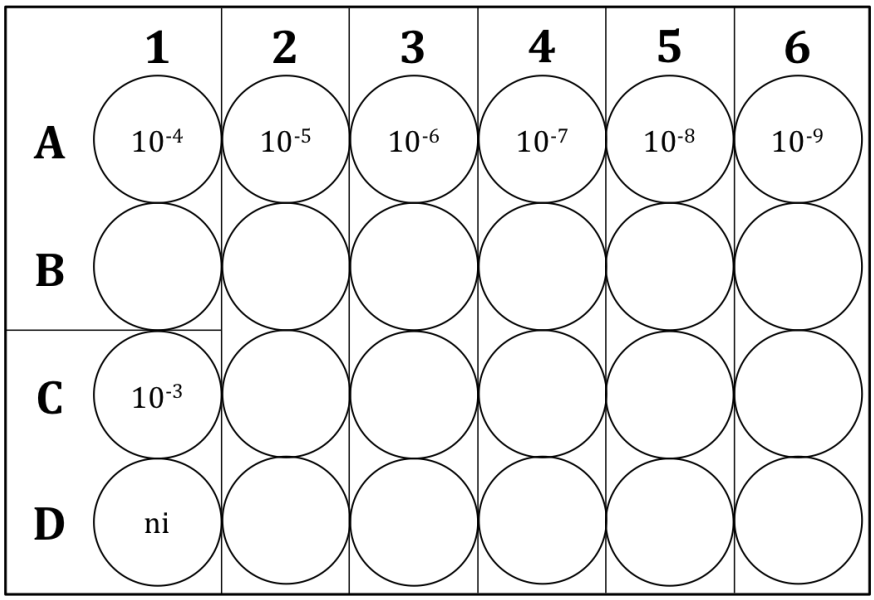


**Figure 3: Plaque titration scheme for ORFV recombinant titer determination in a 24-well plate. 8x$10^4$ Vero cells/well were infected with 100 µl of the indicated dilution. Non-infected (ni) cells served as a control.**

After a four day incubation at 37°C and 5% $CO_2$, single plaques were counted in each well and mean values of the replicates were determined for the respective dilution. The following formula was used to calculate the virus titer in plaque forming units (PFU) per ml:

$$\text{Virustiter } \left(\frac{PFU}{ml}\right) = \text{n} \times 10^{x+1}$$

n = mean plaque count per dilution

x = dilution

### 2.3.5 Infection with ORFV recombinants

If not stated otherwise, cells were infected using corresponding volumes of virus lysates resulting in an infection rate of 20-25% after 24 h. Infection rates were determined by FACS as described in 2.7.3.

### 2.3.6 Growth curves

To validate the capability of ORFV recombinants to replicate despite of genomic changes, single-step growth curve experiments were performed. For this, $10^5$ Vero cells were seeded in 24-well plates containing 500 µl Vero cell medium per well and infected for 2 h at 37°C and 5% $CO_2$. Cells were washed twice with PBS and incubated for 6 h, 24 h, 48 h, 72 h, 96 h and 120 h. Cells were harvested using 100 µl VT and pooled with the supernatant to be titrated as described in 2.3.4. In parallel, 200 µl cell suspension was used to determine the infection rates as described in 2.7.3.

### 2.3.7 Determination of Plaque Sizes

To study plaque phenotypes after ORFV infection, titrations of respective recombinants were performed as described in 2.3.4 and plaque areas were determined using the NIS-Elements software after 48 h, 72 h, 96 h and 120 h. Plaque diameters were deduced from the following formula:

$$Diameter = 2 \times \sqrt{\frac{A}{\pi}}$$

### 2.3.8 Determination of Genetic Stability by Serial Passages

To investigate the genetic stability of fluorophore coding sites, ten serial passages of respective ORFV recombinants were performed. For this, 5 x $10^5$ Vero cells were seeded in 6-well plates containing 3 ml Vero cell medium. At first, virus lysates showing one single plaque in a limiting dilution as described in 2.3.2.3 were used for infection in serial dilutions and took place for 2 h at 37°C and 5% $CO_2$. Cells were washed twice with PBS and were subsequently incubated in 3 ml Vero cell medium for 72 h at 37°C and 5% $CO_2$. Fluorescent plaque counts were determined for wells showing 100-200 plaques using the Eclipse Ti2 microscope (Nikon). Next, cells were frozen at -80°C, thawed at RT and 50 µl of virus lysates were used to infect freshly seeded Vero cells as described above.

## 2.4 Cell Biological Methods

### 2.4.1 Cultivation of Cell Lines

The monkey kidney cell line Vero was cultured in T175 cultivation flasks containing 35 ml Vero cell medium at 37°C and 5% $CO_2$. When cells became confluent, the medium was discarded and the cell lawn was washed with 5 ml VT. Adherent cells were incubated with 2.5 ml VT at 37°C and 5% $CO_2$ for 3 min, detached by vigorous tapping and eventually re-suspended in 7.5 ml Vero cell medium. Viable cell counting was performed as described in 2.4.2 and desired cell quantities were seeded.

THP-1 and THP-1 Dual cell cultures were maintained in T75 cultivation flasks at 37°C and 5% $CO_2$ up to a maximal cell density of $10^6$ cells/ml. Viable cell count was performed as described in 2.4.2 and cells were split as required by the addition or replacement of fresh RPMI complete medium or RPMI Dual medium, respectively.

HEK 293 T cells were maintained in T75 cultivation flasks containing at 37°C and 5% $CO_2$. ExpiCHO-S cells were maintained according to manufacturer's instructions.

### 2.4.2 Cell Counting

Viable cell counting was performed by staining 20 µl of the cell suspension with 20 µl trypan blue, which is taken up by dead cells enabling differentiation between living and dead cells. The suspension was applied to a Neubauer counting chamber, cells in four corner quadrants were counted and the cell number was determined using the following formula:

$$\frac{cells}{ml} = \frac{n}{2} \times 10^4$$

### 2.4.3 Isolation of PBMCs from donated Blood

PBMCs could be isolated from blood donations obtained from the blood donation center Tübingen. First, the blood was diluted with PBS to a total volume of 100 ml. Next, 4 x 15 ml Ficoll in 50 ml tubes were overlaid with 25 ml of diluted blood each and centrifuged at 700 x g and RT for 20 min. Leukocytes, which could be identified by the formation of a white layer after density gradient centrifugation, were transferred into two 50 ml tubes and each were supplemented with PBS up to a volume of 50 ml. After centrifugation at 400 x g and RT for 10 min, the cell pellets were re-suspended in 50 ml PBS and centrifuged at 300 x g and RT for 10 min. PBMCs were merged and supplemented with PBS up to a volume of 50 ml, and the cell number was determined as described in 2.4.2.

### 2.4.4 Isolation of Monocytes from PBMCs

The principle of isolating monocytes from PBMCs relies on the expression of CD14 by monocytes. Hence, PBMCs were centrifuged at 300 x g and RT for 10 min and the pellet

was re-suspended in 4 ml PBE and 100 µl of α-CD14 MicroBeads. The suspension was incubated at 4°C for 15 min and loaded onto a LS column equilibrated with PBE. The column was washed three times with 3 ml PBE before the CD14+ monocytes could be eluted from the column with 5 ml PBE and counted as described in 2.4.2.

### 2.4.5 Cultivation of Monocytes and PBMCs

Monocytes and PBMCs were cultivated in IMDM complete medium at 37°C and 5% $CO_2$. For experimental procedures, $3 \times 10^5$ monocytes and $5 \times 10^5$ PBMCs were seeded in 200 µl per well in 96-well round bottom plates, while $10^5$ monocytes were seeded to be differentiated into dendritic cells.

### 2.4.6 Differentiation of Monocytes to moDCs

Monocytes were cultured as described in 2.4.5. The differentiation of purified monocytes to dendritic cells (moDCs) was carried out for five days by the stimulation with 86 ng/ml GM-CSF and 10 ng/ml IL-4 at 37°C and 5% $CO_2$.

## *2.5* Functional Methods *in vitro*

### 2.5.1 Expansion of Human Antigen-specific Memory CD8+ T cells (12 day stimulation)

The expansion of antigen-specific memory CD8+ T cells is based on their stimulation by monocytes presenting HLA-A*02 restricted Epstein-Barr Virus (EBV) $BMLF1_{280\text{-}288}$ GLCTLVAML, Influenza A $MP_{58\text{-}66}$ GILGFVFTL and Human Cytomegalovirus (HCMV) $pp65_{495\text{-}503}$ NLVPMVATV epitopes over a time period of 12 days. Thus, blood from HLA*A02 positive donors was processed as described in 2.4.3 and 2.4.4, and monocytes were cultivated as described in 2.4.5 to be infected with various dilutions of different ORFV recombinants or stimulated with 1 µM synthetic peptide, respectively. Additionally, viable cell counting was performed for the CD14- fraction, $5 \times 10^5$ cells were seeded in 100 µl T cell medium per well in a 96-well round bottom plate and incubated at 37°C and 5% $CO_2$. After 20-24h, 20 µl of each infected monocyte group was transferred into a new 96-well plate and washed three times with PFEA by centrifugation at 700 x g and RT. FACS analysis was performed to determine the infection rates, while monocytes showing an infection rate of approximately 20% were co-cultured with CD14- fractions in a total volume of 200 µl T cell medium. Every 2-3 days, 50 µl of medium was replaced by fresh T cell medium containing 20 U/ml IL-2. After 12 days of stimulation, expansion of CD8+ T cells was analyzed by tetramer staining and functionality of the antigen-specific CD8+ T cells was evaluated by intracellular cytokine staining as described in 2.7.3.5.

### 2.5.2 NF-κB and IRF pathway activation

THP-1 Dual cells were used to analyze the NF-κB- and IRF-pathway activation after infection with ORFV recombinants. THP-1 Dual cells were derived from the human THP-

1 cells by stably integrating two inducible reporter constructs, NF-κB-SEAP and IRF-lucia. Thus, this cell line allows to simultaneously monitor the activity of SEAP and secreted luciferase. For this, $10^5$ THP-1 Dual cells were seeded each in a well of a 96-well plate in a total volume of 230 µl RPMI Dual medium and infected with ORFV recombinants or stimulated with LPS (10 ng/µl) or 2'-3'-cGAMP (10 ng/µl) for 20 h or 48 h in triplicates at 37°C and 5% $CO_2$. 100 µl of each supernatant was transferred to a new 96-well for determination of NF-κB- and IRF-pathway activation according to manufacturers' instructions, while the remaining cells were used to determine the infection rates as described in 2.7.3.

### 2.5.3 PD-L1 Blockade Bioassay

To analyze the functionality of ORFV encoded Avelumab, a PD-L1 blockade assay was used. For this, 5 x $10^5$ Vero cells were seeded in a 6-well plate in 3 ml Vero cell medium and infected with ORFV recombinants (MOI 1) for 72 h at 37°C and 5% $CO_2$. Supernatants were stored at -20°C for analyses. Blockade assays were performed using 200 µl of the supernatants according to manufacturers' instructions.

## *2.6* Functional Methods *in vivo*

### 2.6.1 Immunization of Mice

*In vivo* studies were performed using female, 7-8 week old C57BL/6NTac mice. Immunization was carried out by injecting ORFV recombinants at a dose of $10^6$ PFU or equal volumes of 100 µl PBS intravenously on day 0 and day 14.

### 2.6.2 Blood Sample Collection

Mice were anesthetized with isoflurane and approximately 25 ml of blood was taken retroorbitally using disposable capillary pipettes. Whole blood was collected in a Microvette® with EDTA and used for the determination of antigen-specific T cell responses by Dextramer staining.

### 2.6.3 Blood Serum Sample Collection

For the analysis of the antigen-specific antibody concentrations in the blood serum, blood was collected after retroorbital sampling in a Microvette® with serum-gel. Blood serum could be gathered after centrifugation at 10000 x g for 5 min and stored at -20°C for analysis.

### 2.6.4 Isolation of Splenocytes

Functionality of antigen-specific T cells was examined by intracellular cytokine staining (ICS) of splenocytes. For this purpose, the spleens of immunized mice were removed and washed with cold RPMI complete medium. Next, spleens were forced through a wet cell strainer into a 50 ml tube using a syringe stamp. The stamp and cell strainer were washed and the tube was filled up to 30 ml with RPMI complete medium. After

centrifugation for 7 min at 500 x g, the pellet was re-suspended in 10 ml ACK lysis buffer and incubated for 4 min at RT. The lysis of erythrocytes was stopped using 10 ml PBS + 10% FCS and the suspension was centrifuged at 500 x g for 5 min. The pellet was re-suspended in 20 ml PBS + 10% FCS and cell counting was performed. Finally, splenocytes were centrifuged at 500 x g for 5 min, re-suspended in freezing medium and stored at -80°C for further analyses.

## 2.7 Analytic Methods

### 2.7.1 Ipilimumab and Avelumab specific ELISA

Enzyme-linked immunosorbent assays (ELISA) were performed to analyze the presence of ORFV induced Ipilimumab and Avelumab expression, as well as to determine their concentration. First, 96-well Nunc plates were coated with 100 µl recombinant human CTLA4-Fc or PD-1-Fc fusion proteins in PBS for 1 h at 37°C or ON at RT. Supernatants were discarded and non-specific antibody binding was blocked using 100 µl ELISA block solution for 1 h at RT. All of the following steps were linked by two thorough washing steps with PBS-T and two washing steps with PBS. 100 µl of sample supernatants, as well as standards and controls were added into the wells for 1 h at RT. Next, wells were incubated with 100 µl biotinylated α-human IgG $F(ab')_2$ in PBS for 1 h at RT to allow non-covalent interaction with streptavidin-HRP, which was added 1:1000 in 100 µl PBS per well for 30 min at RT in the dark. After two final washing steps using PBS-T and PBS, Ipilimumab and Avelumab could be detected using 50 µl peroxidase substrate. The reaction was stopped by adding 100 µl phosphoric acid and absorbance was photometrically measured at 450 nm.

### 2.7.2 Ovalbumin specific IgG1 and IgG2 ELISA

To determine the concentration of OVA-specific IgG1 and IgG2a[b] antibodies in the blood serum of mice, an ELISA was performed. All of the following steps were linked by three thorough consecutive washing steps of the respective wells using PBS-T. First, the ELISA plate was coated ON at 4°C with 20 µg/ml OVA. Adjacently, non-specific bonds were blocked with 100 µl ELISA block solution for 3-4h on the shaker at 450 rpm and RT, while 50 µl of the serum samples or standards (IgG2a[b]: pooled mouse serum from animal trial (BI), IgG1: α-OVA, Sigma A6075) were added to be incubated at 4°C ON to allow IgG1 and IgG2a[b] antibody binding to coated OVA. Next, 50 µl of biotinylated α-mouse IgG1 or α-mouse IgG2 in ELISA block solution were applied for 2 h at 450 rpm and RT on a shaker to allow non-covalent interaction with streptavidin-HRP, which was added 1:1000 in 50 µl ELISA block solution per well for 30 min at RT in the dark. After four final washing steps using PBS-T, IgG1 and IgG2a[b] antibodies could be detected using 100 µl peroxidase substrate. The reaction was stopped by the addition of 50 µl 2 M sulfuric acid and absorbance was photometrically measured at 450 nm.

### 2.7.3 Flow Cytometry

The viability and infection rates, as well as the expression of surface and intracellular molecules was analyzed using the BD LSRFortessa flow cytometry system (BD Biosciences). The preparation of samples and staining of cells with fluorescence-labeled antibodies was carried out in 96-well U-bottom plates, while centrifugation occurred at 4°C and 400 x g for 5 min. For the determination of infection rates, cells were washed twice in 200 µl PFEA, and were re-suspended in 50 µl PFEA or optionally fixed for FACS analyses as described in 2.7.3.6.

#### *2.7.3.1 Inhibition of Fc Receptors*

To prevent non-specific antibody binding, cells expressing Fc receptors were treated with Fc-Block according to manufacturers' instructions prior to staining procedures.

#### *2.7.3.2 Staining with Multimeres*

Multimeres are frequently used to identify and quantify antigen-specific T cells. Tetramers consist of four recombinant MHC molecules conjugated to a fluorescently labeled streptavidin complex. In contrast, dextramers consist of a dextran backbone that carries several fluorophores and MHC molecules. Multimeres can be loaded with peptides of interest to form peptide-MHC complexes recognized by specific T cells, and thus, be detected by flow cytometry. For this, cells were washed twice with 200 µl of PBS and re-suspended in 50 µl of tetramer solution or PBS, respectively. Prior to staining with 50 µl of tetramer solution, PE-conjugated HLA tetramers were mixed 1:50 with tetramer buffer and centrifuged at 13.000 x g for 10 min. Staining with dextramers followed the same procedure by mixing dextramers in a ratio of 1:10 with PBS. The incubation was carried out at RT for 30 min in the dark.

#### *2.7.3.3 Determination of Cell Viability*

Cell viability was determined by Zombie Aqua staining. Zombie Aqua is an amine-reactive fluorescent dye that cannot penetrate live cells but enters cells with compromised membranes. Therefore, it can be used to differentiate between live and dead mammalian cells. For Zombie Aqua staining, cells were washed twice with 200 µl PBS and re-suspended in 50 µl of Zombie Aqua diluted 1:400 in PBS for 30 min at 4°C in the dark.

#### *2.7.3.4 Extracellular Antibody Staining*

For the analysis of surface molecule expression, cells were washed twice with 200 µl PFEA, re-suspended in 50 µl of freshly prepared antibody mix in PFEA according to Table 3, and incubated for 30 min at 4°C in the dark.

#### *2.7.3.5 Intracellular Cytokine Staining*

For the detection of intracellular cytokines, the cells were treated with 10 µg/ml Brefeldin A to prevent secretion of proteins and stimulated with respective synthetic peptides for 12-14 h. Prior to intracellular cytokine staining, cells were washed twice with 200 µl PFEA and permeabilized by incubation with 50 µl Cytofix/Cytoperm for 30 min at 4°C in the dark. Next, cells were re-suspended and washed twice with 200 µl

Permwash and subsequently stained with 50 µl antibody mix in Permwash for 30 min at 4°C in the dark. Respective dilutions of antibodies are listed in Table 3.

#### *2.7.3.6 Fixation of Cells*

For storage exceeding 4 h, cells were fixed. For this, cells were washed twice with 200 µl PFEA, re-suspended in 50 µl PFEA + 1% formaldehyde and stored at 4°C in the dark. Analysis of samples was carried out within 10 days.

### 2.7.4 Gating Strategies

Figure 4 illustrates the gating strategy used for the analyses on expression strengths by Vero cells, THP-1 cells and monocyte derived dendritic cells (moDCs) infected with new Del-site recombinants as presented in 4.1.2. Cells were first identified by FSC-A and SSC-A and subsequently gated for singlets using SSC-A and SSC-H. Infection rates were determined using the mCherry marker in Q2 of the GFP vs. mCherry gating, while mean fluorescence intensities of GFP and mCherry were calculated for cells expressing both fluorescence markers in gate Q2.

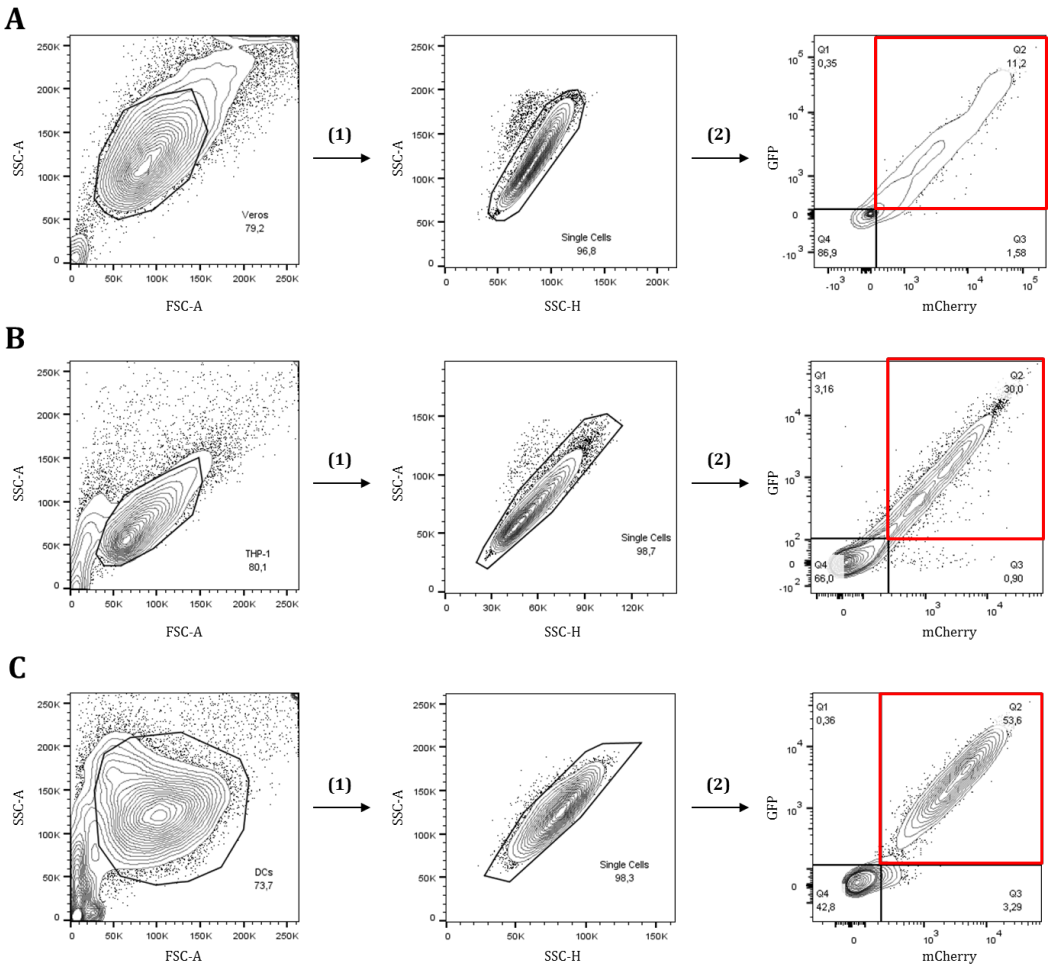


**Figure 4: Gating strategy for the analyses on expression strengths using new Del-sites. A) Gating for Vero cells. B) Gating for THP-1 cells. C) Gating for moDCs. 1) Identification of single cells. 2) Identification of infected, GFP and mCherry expressing cells for the determination of geometric mean fluorescence intensities (red).**

For the analyses on moDC activation markers, viable cells were identified by gating for Zombia Aqua negative cells in the Zombie Aqua vs. FSC-A gate. Singlets were determined by SSC-A and SSC-H, while infected cells could be measured using the marker mCherry (Figure 5). Geometric mean fluorescence intensities of CD40, CD80, CD83, CD86 and HLA-DR were calculated for infected moDCs.

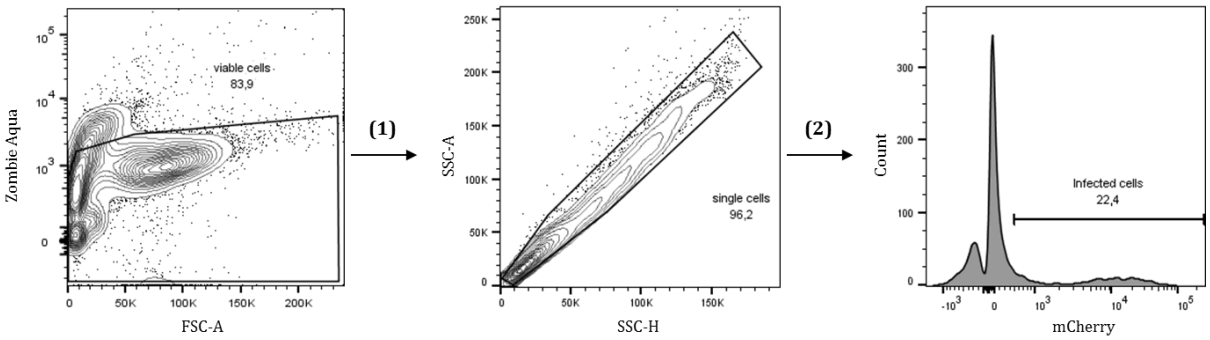


**Figure 5: Gating strategy for the analyses on moDC activation markers using new Del-site recombinants. 1) Identification of viable cells. 2) Identification of single cells. This population served to determine the geometric mean fluorescence intensity of expressed CD40, CD80, CD83, CD86 and HLA-DR in not infected cells. 3) Identification of infected, mCherry expressing cells. This population served to determine the geometric mean fluorescence intensity of expressed CD40, CD80, CD83, CD86 and HLA-DR in infected cells.**

To study the expansion of HLA-A*02 restricted EBV ($BMLF1_{280-288}$ GLCTLVAML), Influenza A ($MP_{58-66}$ GILGFVFTL) and HCMV ($pp65_{495-503}$ NLVPMVATV) epitope specific CD8+ T cells, viable cells were identified using a Zombie Aqua vs. FSC-A gate. Lymphocytes were determined using SSC-A and FSC-A, and singlets were detected in the SSC-A vs SSC-H gate. Next, CD4 and CD8 specific antibody staining allowed discrimination of CD8+ T cells, whose epitope specificity was revealed by tetramer staining (Figure 6).

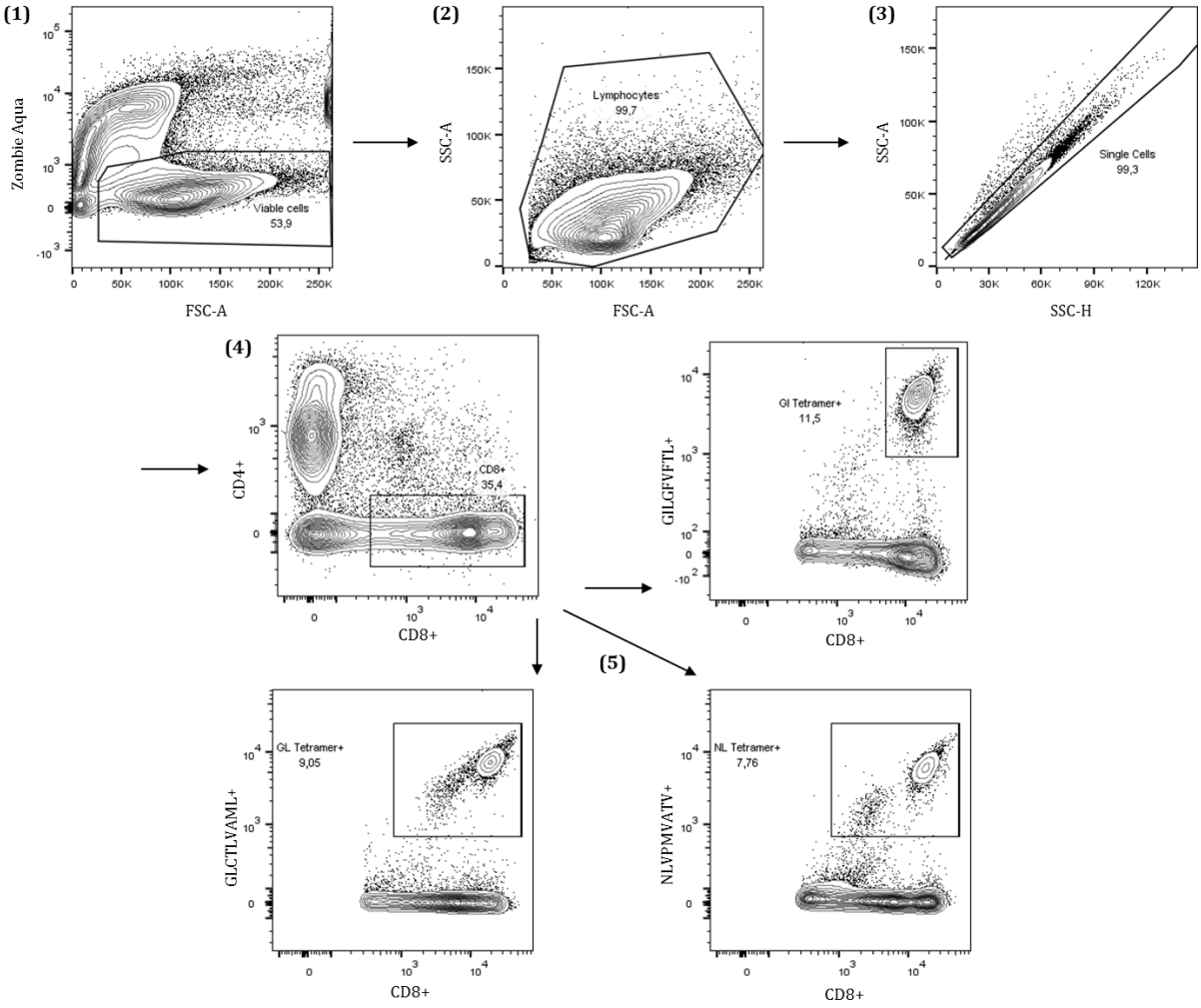


**Figure 6: Gating strategy for the expansion of CD8+ T cells. 1) Identification of viable cells. 2) Identification of lymphocytes. 3) Identification of single cells. 4) Identification of CD8+ T cells. 5) Identification of GLCTLVAML, GILGFVFTL and NLVPMVATV peptide specific CD8+ T cells.**

To analyze the functionality of CD8+ T cells, viable cells were identified using Zombie Aqua vs. FSC-A gating. Lymphocytes and single cells were determined in SSC-A vs. FSC-A and SSC-A vs. SSC-H gates, respectively. CD4 and CD8 specific antibody staining allowed discrimination of CD8+ T cells, whose TNFα and IFNγ production could be determined using intracellular cytokine staining as shown in Figure 7.

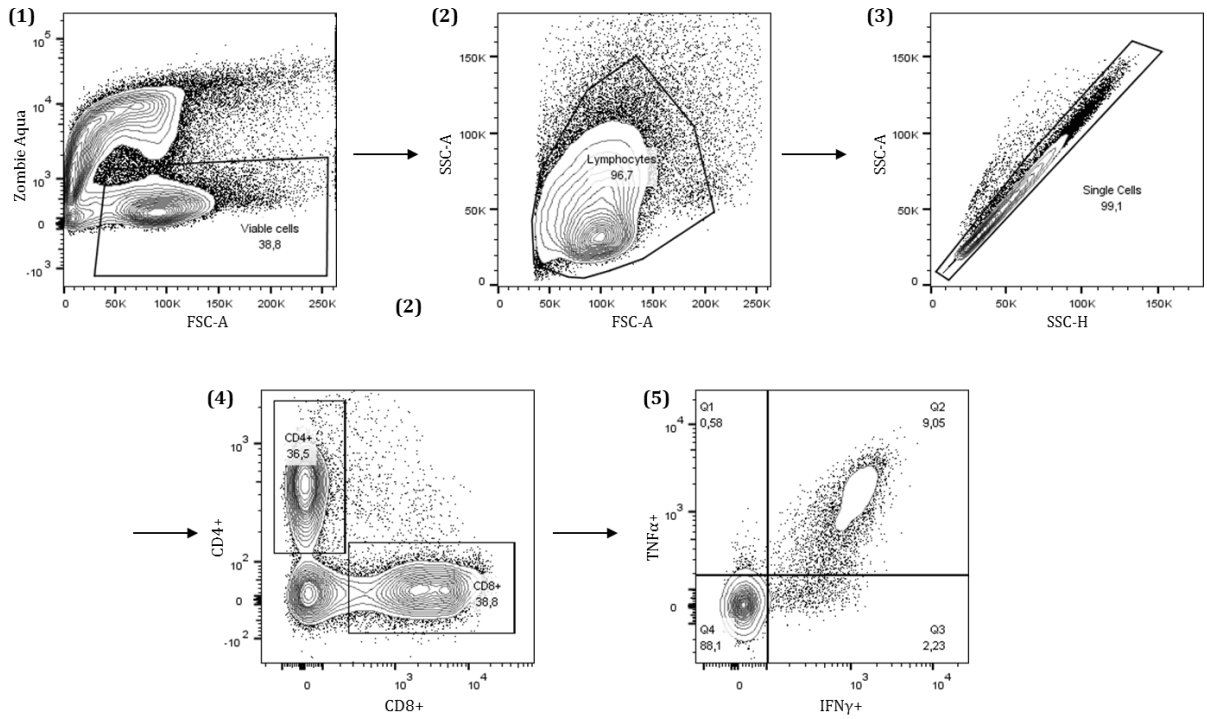


**Figure 7: Gating strategy for the functionality of CD8+ T cells. 1) Identification of viable cells. 2) Identification of lymphocytes. 3) Identification of single cells. 4) Identification of CD8+ T cells. 5) Identification of TNFα+ and IFNγ+ CD8+ T cells.**

# 3 Results

## 3.1 Generation and Characterization of new Del-Site recombinants

In order to generate the ORFV recombinants used in this work, transgenes synthesized and obtained from Invitrogen were cloned into transfer plasmids. Stable integration of transgenes into the ORFV genome was accomplished by homologous recombination between the transfer plasmid and the genomic DNA of the parental virus following transfection by nucleofection and subsequent infection of Vero cells as described in 2.3.1 and 2.3.2.

### 3.1.1 Generation of Transfer Plasmids

The generation of transfer plasmids followed the protocol described in 2.2.1 - 2.2.7. In short, DNA inserts as well as vectors were digested using the same restriction enzymes, fragments of interest were purified and ligated. Subsequently, bacteria were transformed with ligated plasmids and colonies selected for the production of the transfer plasmids. For validation, control digests using restriction enzymes was followed by agarose gel electrophoreses, while DNA sequencing using insert specific primers listed in 2.1.7 confirmed correct insertion of the transgenes into the vector. Table 13 summarizes the transfer plasmids generated in this work, while plasmid charts are shown in the supplementary information Figure S38 - Figure S47.

**Table 13: Transfer plasmids generated in this work, their insert and parental vector as well as the used restriction enzymes and resulting fragment sizes.**

| Transfer Plasmid | Insert Vector | Parental Vector | Restriction digest |
|---|---|---|---|
| **pDel014-7-2-GFP** | pD12-GFP | pDel014-P7 | Mlu*I* / Spe*I* (937+3416 bp) |
| **pDel024-9-2-GFP** | pD12-GFP | pDel024-P9 | Mlu*I* / Spe*I* (937+3317 bp) |
| **pDel112-10-2-GFP** | pD12-GFP | pDel112-P10 | Mlu*I* / Spe*I* (937+3512 bp) |
| **pDel113-11-2-GFP** | pD12-GFP | pDel113-P11 | Mlu*I* / Spe*I* (937+3362 bp) |
| **pDel119-1-2-GFP** | pD12-GFP | pDel119-P1 | Mlu*I* / Spe*I* (937+3315 bp) |
| **pDel121-1-2-GFP** | pD12-GFP | pDel121-P1 | Mlu*I* / Spe*I* (937+3321 bp) |
| **pDel126-4-2-GFP** | pD12-GFP | pDel126-P4 | Mlu*I* / Spe*I* (937+3411 bp) |
| **pDel127-3-2-GFP** | pD12-GFP | pDel127-P3 | Mlu*I* / Spe*I* (937+3369 bp) |
| **pDel128-5-2-GFP** | pD12-GFP | pDel128-P5 | Mlu*I* / Spe*I* (937+3432 bp) |
| **pV-HLAA02-Mini** | Recall_Mini_HLA-A02 | pV-GFP | EcoR*I* / Hind*III* (272+6094 bp) |

To demonstrate the process in detail, the generation of pDel014-7-2-GFP is described exemplarily. First, the parental vector pDel014-P7 was linearized by Mlu*I* and Spe*I* digestion resulting in a vector backbone of 3.4 kb, while the GFP insert of 0.9 kb was obtained from the insert vector pD12-GFP using the same restriction enzymes and

conditions. Complementary ends in both, insert and vector backbone, allowed these purified DNA fragments shown in Figure 8A and B to be ligated next. Upon ligation and transfer into competent *E. coli*, the plasmids were isolated from bacterial cultures. Validation of pDel014-7-2-GFP was performed by sequencing as well as control digestion using the restriction enzymes Dra*III* and BamH*I*, resulting in correctly sized DNA fragments of 3.7 kb and 0.66 kb as shown in Figure 8C.

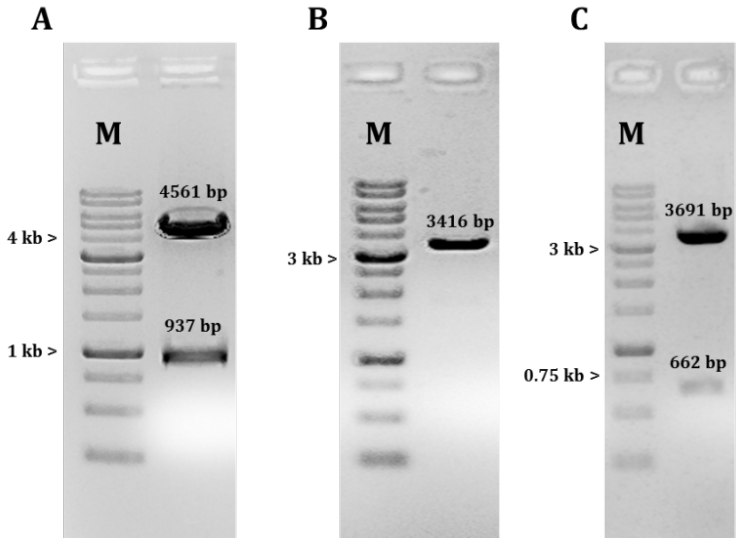


**Figure 8: Restriction digest of pD12-GFP, pDel014-P7 and pDel014-7-2-GFP. The 0.94 kb GFP insert was obtained from a Mlu*I* and Spe*I* digest of pD12-GFP (A) and ligated to the 3.4 kb vector backbone of Mlu*I* and Spe*I* digested pDel014-P7 (B). Control digestion of pDel014-7-2-GFP using Dra*III* and BamH*I* resulted in correctly sized fragments of 3.7 kb and 0.66 kb (C). 1% agarose gel; M = Ready-To-Use 1 kb Ladder, Nippon Genetics.**

### 3.1.2 Generation of new Del-Site Recombinants

After the successful generation of transfer plasmids, new ORFV recombinants were generated as exemplarily shown here for VHLA024GFP following the methods described in 2.3.1 and 2.3.2. Thus, the plasmid pV-HLAA02-Mini was transferred into Vero cells by nucleofection, which were subsequently infected with the parental virus VCh024GFP. Due to homologous sequences in the ORFV genome and the insert flanking regions of the transfer plasmid, homologous recombination led to stable integration of the HLAA02 Minigene and loss of mCherry in the *vegf*-locus of the ORFV D1701-V genome. Next, new ORFV recombinants could be isolated from infected GFP, but not mCherry expressing Vero cells selected by FACS sorting and limiting dilutions. DNA isolation followed by insert and locus specific PCR typing allowed monitoring of the genetic homogeneity of the purified ORFV recombinants as shown in Figure 9. Here, 024, d024, Recall and *vegf*-locus PCR proved both, the integration of the HLAA02 Minigene and lack of mCherry in the *vegf*-locus as well as the integration of GFP and lack of ORF024 in the Del024-locus. Subsequently, the new ORFV recombinants were propagated in large scale as described in 2.3.3.

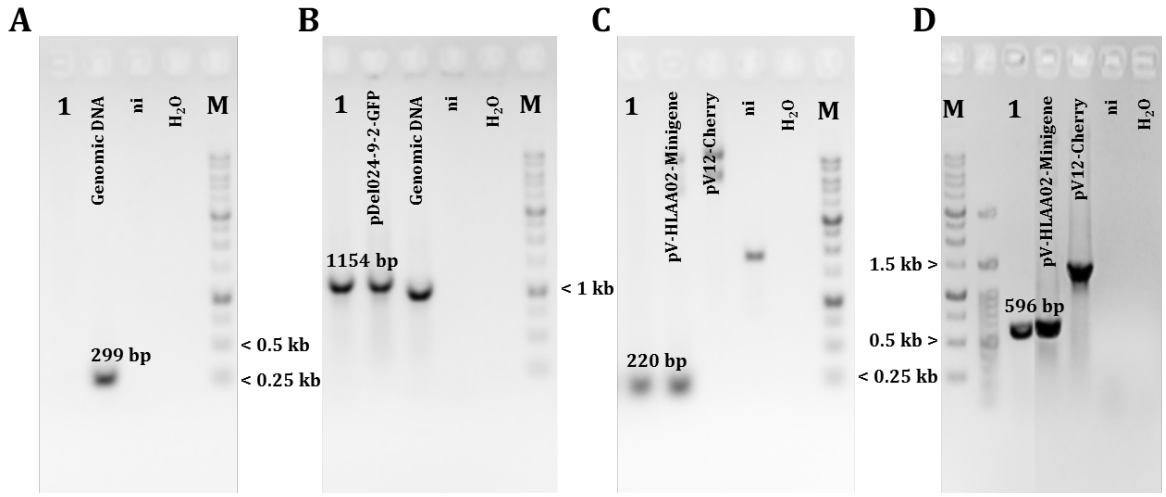


**Figure 9: PCR typing of purified Del-site recombinant VHLA024GFP. Genetic homogeneity of the Del024-locus was verified by PCRs 024 showing a loss of the ORF024 specific 299 bp fragment (A) and d024 showing the integration of GFP by detection of a specific 1154 bp fragment (B). Further, the Recall PCR detected the HLAA02 Minigene specific 220 bp fragment (C), while a *vegf*-locus PCR could confirm the Minigene integration by detection of a specific 596 bp fragment (D). 1% agarose gel; 1 = DNA from VHLA024GFP recombinant; ni = DNA from not infected Vero cells; M = Ready-To-Use 1 kb Ladder, Nippon Genetics.**

All new Del-site recombinants generated in this work are listed in 2.1.10 and respective PCR typing for the verification of genetic homogeneity are shown in Figure S50 - Figure S66 of the supplementary information. The used primer combinations and temperature profiles of the cycles in PCRs can be found in 2.1.7 and 2.2.9.

### 3.1.3 *In vitro* Characterization of new Del-Site Recombinants

After the purification and propagation of new Del-site recombinants, several experiments were performed to investigate the impact of gene deletions on the genetic stability, the growth efficiency, plaque phenotype, expression kinetics and immunogenicity *in vitro.*

#### *3.1.3.1 GFP is stably inserted into the new Del-Sites*

To investigate the stability of inserted GFP into the new Del-sites, Vero cells were infected with the new Del-site recombinants VCh014GFP, VCh024GFP, VCh112GFP, VCh113GFP, VCh119GFP, VCh121GFP, VCh126GFP, VCh127GFP and VCh128GFP, and 20 serial passages were performed as described in 2.3.8. Both, GFP and mCherry fluorescence could be observed by fluorescence microscopy in single plaques resulting from Vero cell infection with all new Del-site recombinants throughout this experiment as shown in Figure 10.

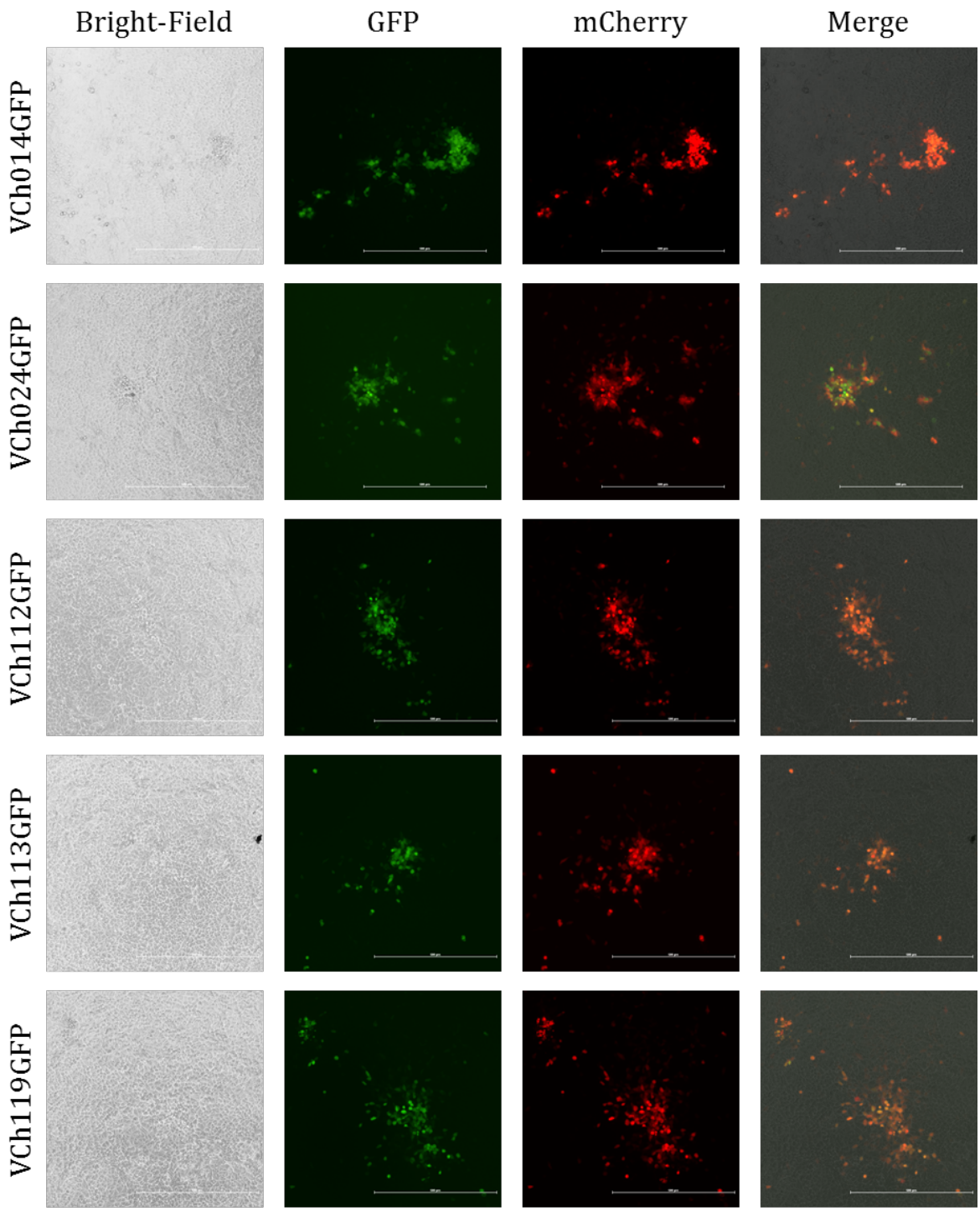
Bright-Field
GFP
mCherry
Merge
VCh014GFP
VCh024GFP
VCh112GFP
VCh113GFP
VCh119GFP

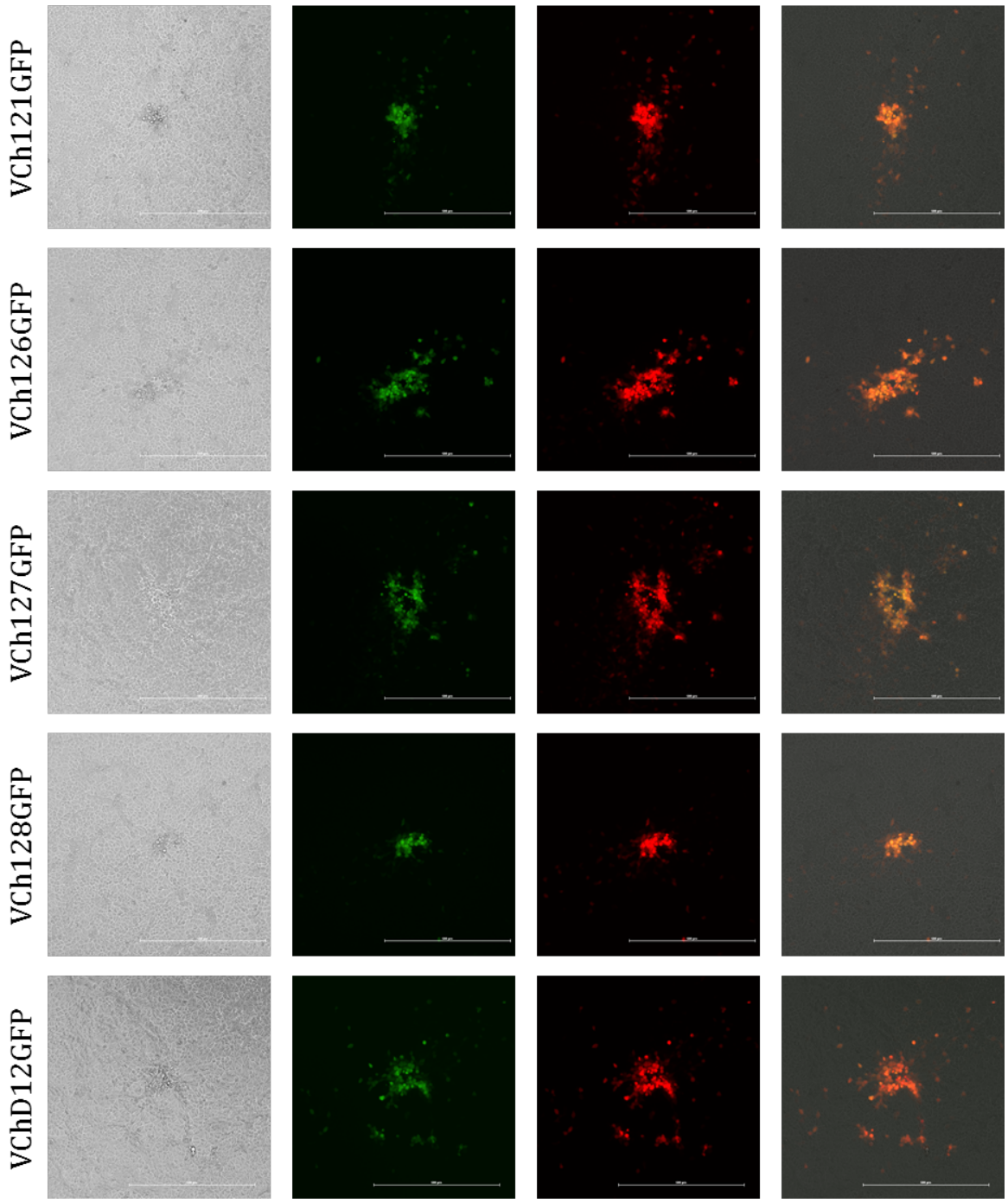


**Figure 10: New Del-site recombinants induce the expression of GFP and mCherry in Vero cells. Fluorescence microscopy of single plaques was performed five days after infection with the new Del-site recombinants and the reference virus VChD12GFP. Pictures obtained from bright field microscopy, single GFP and mCherry channels as well as merged pictures are shown, while scale bars represent 500 µm.**

Additionally, viral DNA was isolated from infected Vero cells after Passage 1, 5, 10, 15 and 20, and deleted gene-specific as well as locus-specific PCRs were performed to examine the Del-locus' integrity. As exemplarily shown for VCh119GFP, no ORF119 specific 407 bp fragments could be detected in 119 PCRs during 20 passages (Figure

11A), while the deletion site showed 1155 bp fragments specific for GFP inserted into the Del119 locus using the d119 PCR (Figure 11B).

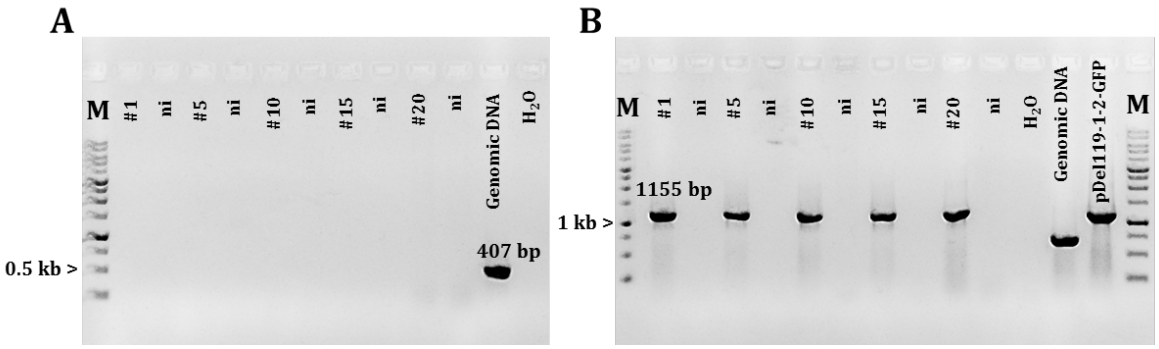


**Figure 11: GFP is stably integrated into Del119. 119 PCR after passage 1, 5, 10, 15 and 20 of VCh119GFP in Vero cells indicates a constant deletion of gene 119 (A), while d119 PCRs result in 1155 bp fragments specific for GFP inserted into the Del119 locus (B). 1% agarose gel; ni = DNA from not infected Vero cells; M = Ready-To-Use 1 kb Ladder, Nippon Genetics.**

Equivalent results could be obtained for the remaining recombinants. Here, deleted gene specific and locus specific PCRs conducted after serial passages resulted in PCR products or DNA fragments of expected sizes, respectively. The results are shown in Figure S69-Figure S76 of the supplementary information.

Next, viral DNA was isolated from the Del-site recombinants VCh014GFP, VCh024GFP, VCh112GFP, VCh113GFP, VCh119GFP, VCh121GFP, VCh126GFP, VCh127GFP and VCh128GFP to verify the genomic location of inserted transgenes after passage 1 and 20 by comparative restriction enzyme analyses as described in 2.2.1. DNA fragment sizes resulting from viral DNA digests were predicted on the basis of the ORFV D1701-V genome sequence (Rziha, unpublished) including deleted regions designated A, AT and D [84]. Figure 12 exemplarily shows the results for VCh014GFP after Eco*R*I and Kpn*I* digest and Southern blot hybridization with digoxygenin (DIG) labelled GFP, mCherry and ORF020 probes. While GFP probes identified the predicted 14 kb fragment in passage 20 after Eco*R*I digest, hybridization in passage 1 detected a larger fragment of approximately 23 kb. Furthermore, weak bands could be observed after hybridization at approximately 23 kb and 14 kb in passage 20 using both, Eco*R*I and Kpn*I* digested viral DNA, respectively, while the GFP probe strongly hybridized to a fragment of predicted 2.8 kb after Kpn*I* digest. ORF020 probes were used to examine the genomic neighborhood of the Del-site 014. Hybridization detected ORF020 in a fragment of approximately 23 kb and an expected 10.3 kb fragment after Eco*R*I and Kpn*I* digest, respectively. Integrity of the *vegf*-locus was demonstrated as mCherry probes hybridized to the predicted 12.5 kb and 11.5 kb fragments in passage 1 and 20 after Eco*R*I and Kpn*I* digest, respectively (Table 14).

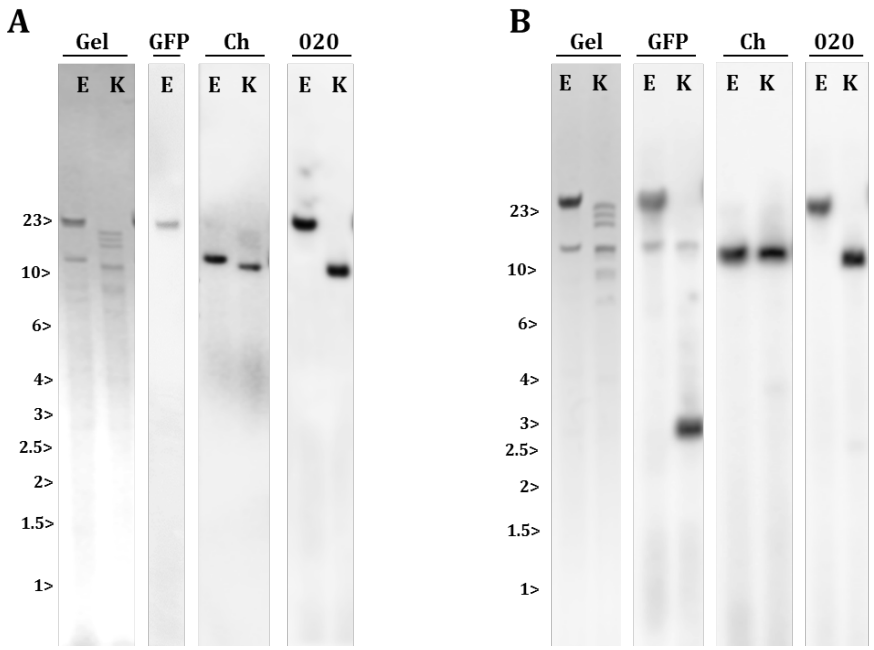


**Figure 12: Detection of GFP, mCherry and ORF020 in VCh014GFP DNA obtained after passage 1 (A) and 20 (B). Genomic viral DNA was digested with EcoR*I* (E) and Kpn*I* (K) prior to separation in a horizontal 0.8% agarose gel for 8 h. After alkaline blotting of the viral DNA onto nylon membranes, the digested DNAs (lanes Gel) were hybridized using DIG labelled GFP, mCherry and ORF020 probes to determine the corresponding genomic location.**

Equivalent results were obtained for hybridization analyses with DNA from VCh112GFP, VCh113GFP, VCh119GFP, VCh121GFP, VCh126GFP, VCh127GFP and VCh128GFP taking into account their specifically predicted genomic location. To analyze the genomic neighborhood of Del-sites located at the right terminal end of the ORFV D1701-V genome, DIG labelled ORF129 probes were used for hybridization purposes. The results are illustrated in Figure S77 - Figure S83 of the supplementary information, while a summary of diagnostic restriction fragments is shown in Table 14.

**Table 14: Summary of diagnostic restriction fragments of the new Del-site recombinants by the indicated DIG labelled hybridization probes. Restriction endonucleases and fragment sizes are indicated in kbp.**

| Probe | GFP | | mCherry | | | 020 | | 129 | | |
|---|---|---|---|---|---|---|---|---|---|---|
| Virus | EcoR*I* | Kpn*I* | EcoR*I* | Kpn*I* | Hind*III* | EcoR*I* | Kpn*I* | EcoR*I* | Kpn*I* | Hind*III* |
| **VCh014GFP** | 14 | 2.8 | 12.5 | 11.5 | - | 14.6 | 10.7 | - | - | - |
| **VCh024GFP** | 15 | 18.7 | 12.3 | 3.6 | 2.6 | 15 | 12.4 | - | - | 3.4 |
| **VCh112GFP** | 4.1 | 7.7 | 12.5 | 11.5 | - | - | - | 12.5 | 11.5 | - |
| **VCh113GFP** | 4.55 | 7 | 12.5 | 11.5 | - | - | - | 12.5 | 11.5 | - |
| **VCh119GFP** | 2.3 | 4.3 | 12.5 | 11.5 | - | - | - | 12.5 | 11.5 | - |
| **VCh121GFP** | 2.95 | 2.2 | 12.5 | 11.5 | - | - | - | 12.5 | 11.5 | - |
| **VCh126GFP** | 11.9 | 11 | 11.9 | 11 | - | - | - | 11.9 | 11 | - |
| **VCh127GFP** | 12.8 | 9.3 | 12.8 | 9.3 | - | - | - | 12.8 | 9.3 | - |
| **VCh128GFP** | 11.9 | 8.6 | 11.9 | 8.6 | - | - | - | 11.9 | 8.6 | - |

For VCh024GFP, fragments detected after EcoR*I* digest using a GFP or ORF020 probe resembled the results described above for VCh014GFP (Table 14). However, mCherry was diagnosed in a Kpn*I* fragment of 10.5 kb but detected at approximately 3.6 kb. Therefore, viral DNA of VCh024GFP was digested with Hind*III* and hybridized with DIG labelled mCherry and ORF129 probes to elucidate the genomic neighborhood of the mCherry insert. Hybridization of ORF129 probes resulted in the detection of the expected 3.4 kb fragment, while mCherry probe hybridization sensed a shortened Hind*III* fragment of approximately 2.6 kb instead of 2.8 kb. Since the genomic neighborhood appeared to be unaffected, a *vegf*-locus PCR of VCh024GFP DNA was performed and amplicons were sequenced. The results demonstrate mCherry to be controlled by P*vegf* and to lack promotor P1 and P2.

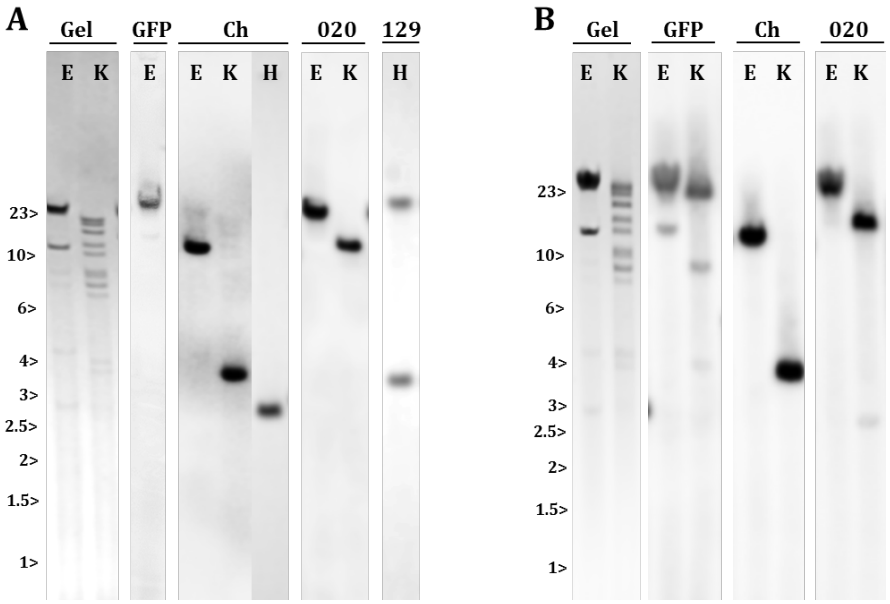


**Figure 13: Detection of GFP, mCherry and ORF020 in VCh024GFP DNA obtained after passage 1 (A) and 20 (B). Genomic viral DNA was digested with EcoR*I* (E), Kpn*I* (K) and Hind*III* prior to separation in a horizontal 0.8% agarose gel for 8 h. After alkaline blotting of the viral DNA onto nylon membranes, the digested DNA (lanes Gel) was hybridized using DIG labelled GFP, mCherry, ORF020 and ORF129 probes to determine the corresponding genomic location. GFP was detected in predicted 15 kb and 18.7 kb, and ORF020 in 15 kb and 12.4 kb fragments after EcoR*I* and Kpn*I* digest, respectively. Hybridization of mCherry probes showed an expected 12.3 kb fragment after EcoR*I* digest, and a 3.6 kb Kpn*I* and a 2.6 kb Hind*III* fragment. The ORF129-specific probe detected the expected 3.4 kb fragment.**

The results from southern blot analyses suggest transgenes inserted into the *vegf*-locus and the respective Del-site to be at the correct genomic location and remained stable both, after passage 1 and passage 20.

Finally, the stability of transgenes inserted into new Del-sites was examined during ten serial passages of three biological replicates (virus clones) of the ORFV D1701-V recombinants VCh014GFP, VCh024GFP, VCh112GFP, VCh113GFP, VCh119GFP, VCh121GFP, VCh126GFP, VCh127GFP, VCh128GFP and the reference virus VChD12GFP as described in 2.3.8. After 72 h of infection, wells containing 100-200 plaques were

used to determine the amount of single plaques expressing both, GFP and mCherry fluorophores, or either GFP or mCherry by fluorescence microscopy. The percentages of plaques expressing only one fluorophore during ten serial passages are shown in Figure 14.

The results demonstrate that frequencies of more than 1% single GFP expressing plaques only occurred for one viral VCh127GFP clone. By passage 5, this clone induced the expression of only GFP in more than 1% of all counted single plaques, while this frequency was increased continuously up to 3% by passage 10 as shown in Figure 14A. On the other hand, Figure 14B demonstrates that more than 1% of single mCherry expressing plaques were observed frequently for Del-site recombinants VCh014GFP at passage 1, 2 and 3, for VCh119GFP at passage 4 and 7, and VCh113GFP at passage 7. The frequencies did, however, not increase over time and were measured for most replicates below 1%. Notably, the reference virus VChD12GFP induced the expression of single mCherry fluorescence in up to 5% of all counted plaques in passage 2. Nevertheless, the frequencies of all three biological replicates did not increase for this recombinant over time either. Passage 9 showed a final peak percentage of 3% single mCherry expressing plaques for one viral VChD12GFP replicate, while at passage 10 only plaques expressing both GFP and mCherry could be counted. To demonstrate the overall genetic stability of transgenes inserted in either, the *vegf*-locus or the new Del-sites, single GFP and single mCherry frequencies were combined as shown in Figure 14C. The mean values plotted in Figure 14D indicate that only the reference virus VChD12GFP constantly elicited frequencies of more than 1% single fluorophore expressing plaques.

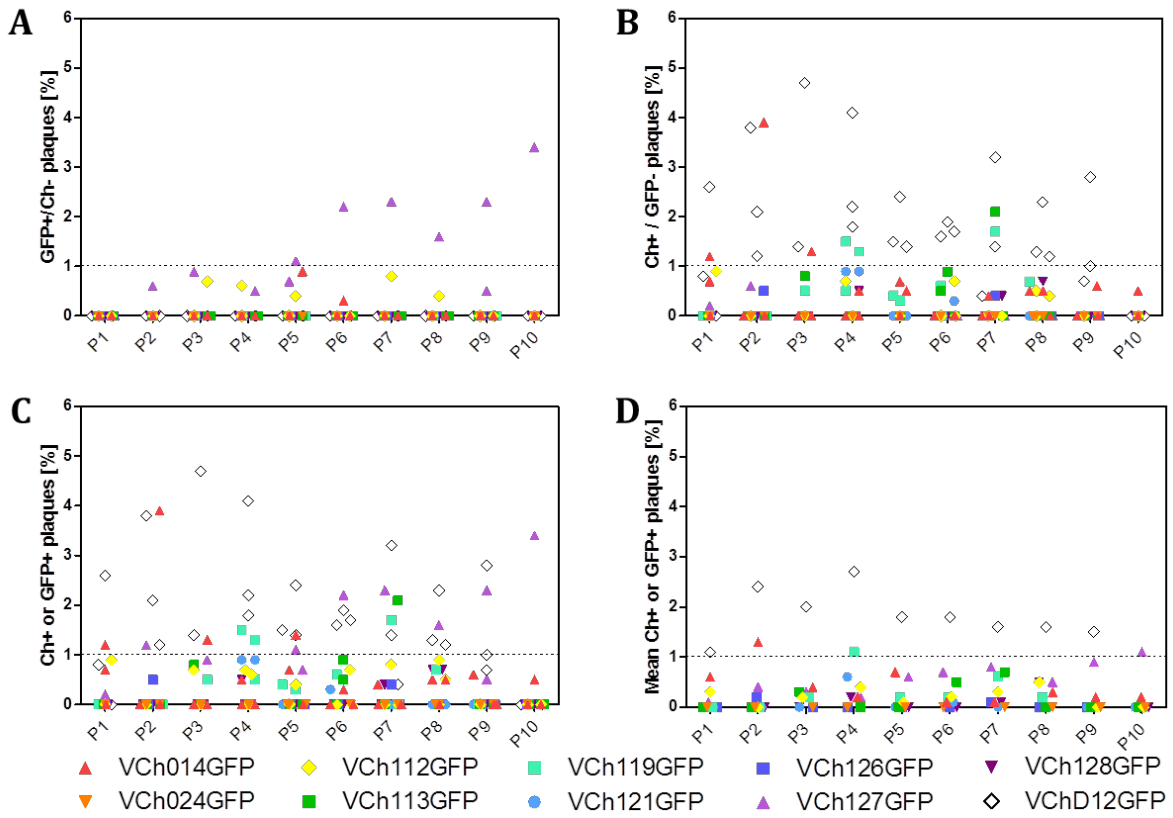


**Figure 14: Genetic stability of transgenes *gfp* and *mcherry* in Del-site recombinants. During ten serial passages (P1-P10), the expression of fluorophores by infected Vero cells was determined by single plaque counting after 72 h post infection. Frequencies of single GFP (A) and single mCherry (B) expressing plaques, as well as the overall frequency of plaques showing single fluorescence (C) are shown for three viral clones per Del-site recombinant obtained from 96-well limiting dilutions. The mean overall frequency of single fluorescent plaques was calculated and plotted in (D).**

Taken together, the results presented suggest that GFP is stably expressed in Vero cells infected with the new Del-site recombinants and can be detected throughout 20 passages in the predicted genomic locus. Furthermore, the genetic stability of both, GFP and mCherry in the new Del-site or the *vegf*-locus, respectively, was validated in ten serial passages studying the fluorescence of infected Vero cells. Since at least 99 % of all counted lytic plaques infected with each new Del-site recombinant, except of VCh127GFP, expressed GFP and mCherry simultaneously after ten passages, these results indicate genetic stability of the examined genomic loci.

### *3.1.3.2 Characterization of new Del-site recombinants' growth behavior*

To investigate, whether the deletion of genes introduced into the new Del-site recombinants alters the *in vitro* growth characteristics in the ORFV permissive Vero cells compared to the reference virus VChD12GFP, single-step growth curve experiments were performed. For this, Vero cells were infected with the new Del-site recombinants VCh014GFP, VCh024GFP, VCh112GFP, VCh113GFP, VCh119GFP, VCh121GFP, VCh126GFP, VCh127GFP and VCh128GFP leading to infection rates of approximately 20-25% after 24 h. Infected cells were washed and harvested 2 h after adsorption

(designated 0h) or 6 h, 24 h, 48 h, 72 h, 96 h and 120 h post infection. Virus lysates were titrated on Vero cells to determine the number of infectious particles measured in plaque forming units per ml (PFU/ml). The experiment was performed three times for each recombinant and the results are shown in Figure 15A-I.

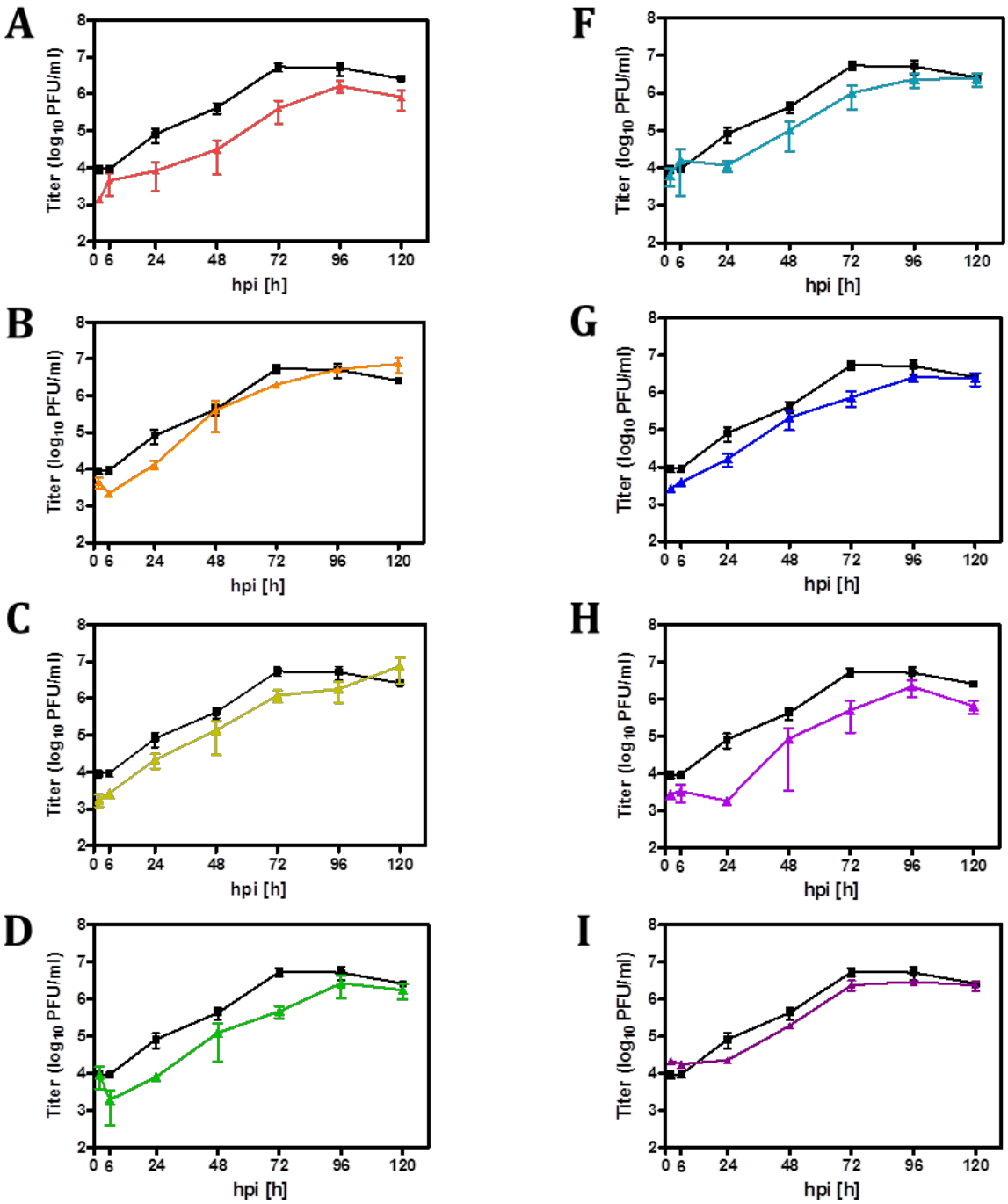

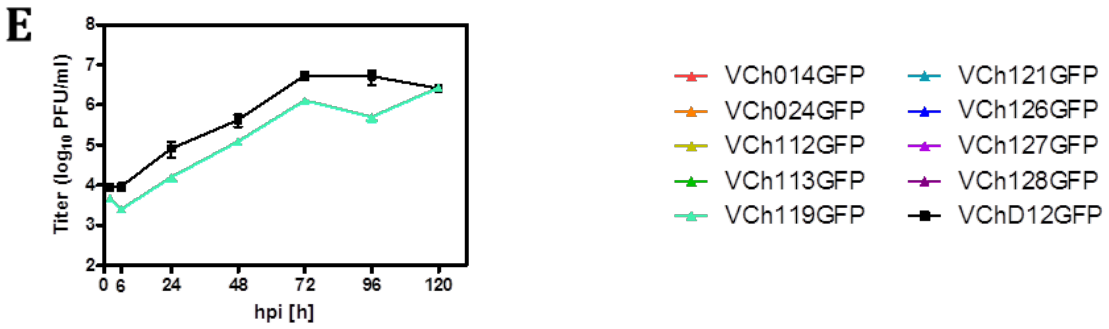


**Figure 15: Single step growth curves of Del-site recombinants. Infected cells (MOI 1) were washed and harvested 2 h after adsorption (0 hpi) and at the indicated hours post infection (hpi), while total cell lysates were titrated on Vero cells to determine the virus titer (PFU/ml). The virus growth curves of the recombinants VCh024GFP (B), VCh112GFP (C), VCh113GFP (D), VCh119GFP (E), VCh121GFP (F), VCh126GFP (G) and VCh128GFP (I) reach comparable virus titers than the control VChD12GFP, while VCh014GFP (A) and VCh127GFP (H) show diminished growth throughout the experiment.**

The growth characteristics of most new Del-site recombinants resemble the ones obtained for the reference virus VChD12GFP and reached comparable final titers of approximately 1-4 x $10^6$ PFU/ml after 120 hpi. This applied especially to VCh024GFP, VCh112GFP, VCh126GFP and VCh128GFP showing only slightly diminished final virus titers compared to the control throughout the experiment (Figure 15B, C, G and I). A delayed virus growth could be observed for VCh113GFP, VCh119GFP and VCh121GFP as titers comparable to VChD12GFP were achieved only 24 h later (Figure 15D, E and F). In contrast, VCh014GFP and VCh127GFP showed stronger growth retardation compared to VChD12GFP and did not accomplish equal titers after 120 h. Notably, none of the Del-site recombinants seemed to replicate as efficient as VChD12GFP, whose titers peaked at approximately $10^7$ PFU/ml after 72 h and 96 h. Additionally, growth curves of VCh014GFP, VCh112GFP, VCh126GFP and VCh127GFP indicate lower virus input as used for the growth curves of VChD12GFP. Nevertheless, these results suggest all new Del-site recombinants to be replication efficient as they were able to produce infectious progeny in the permissive cell line Vero.

Next, the correlation between plaque phenotype and virus growth was examined by the determination of plaque sizes. For this, titrations of Del-site recombinants and the reference virus VChD12GFP were performed to achieve single plaque formations 2, 3, 4 and 5 days after infection. Plaque sizes were determined using the NIS-Elements software from Nikon and the results are summarized in Figure 16.

Significantly smaller plaques were formed upon infection with VCh113GFP on day 2 and 3, for VCh119GFP on day 2, and for VCh121GFP and VCh128GFP throughout the experiment compared to those obtained from VChD12GFP infection. VCh014GFP formed significantly smaller plaques from day 4 on, while similar results were obtained for VCh126GFP and VCh127GFP on day 3 and 4. On the other hand, plaques resulting from VCh119GFP infection developed into significantly larger plaques on day 4 and 5, whereas VCh024GFP induced plaque formations were measured the largest between

day 2 and 4. VCh112GFP elicited plaques of similar phenotype compared to the control VChD12GFP. The results therefore indicate an influence of some gene deletions present in the new Del-site recombinants on the plaque phenotype.

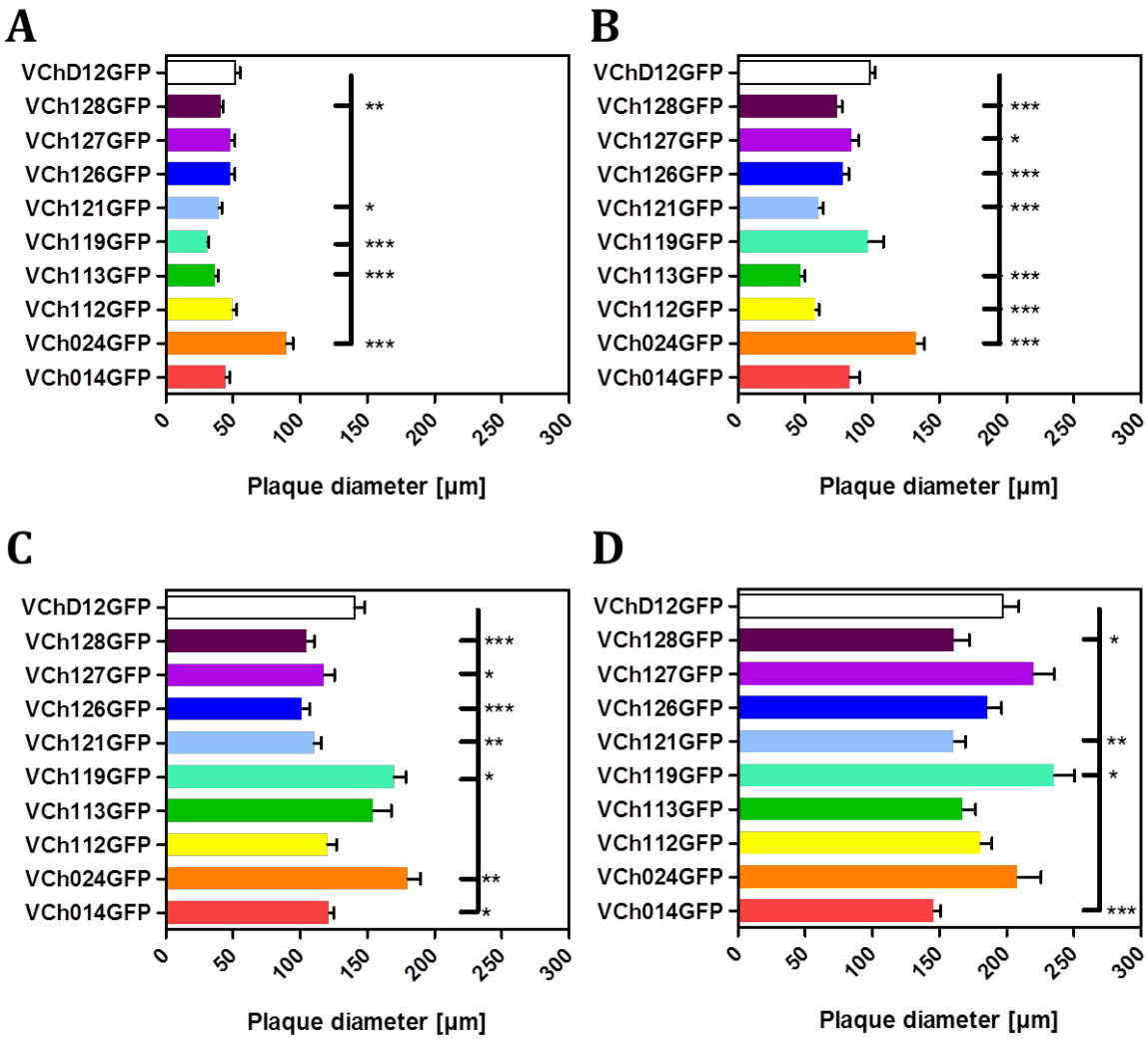


**Figure 16: Determination of plaque sizes. New Del-site recombinants and control VChD12GFP were titrated on 24-well plates and the size of >45 single plaques was determined by fluorescence microscopy on day 2 (A), 3 (B), 4 (C) and 5 (D). Shown are the mean values and standard errors of the mean of three independent experiments. Statistical analysis was performed using an unpaired t-test with a confidence interval of 95%: ns = $p \geq 0.05$, * = $p < 0.05$, ** = $p < 0.01$, *** = $p < 0.001$.**

### *3.1.3.3 Analyses on expression strengths using new Del-Sites*

To investigate the potential of transgene expression by the new Del-site recombinants, the reporter gene GFP integrated into the new Del-sites and mCherry inserted into the *vegf*-locus were used to compare their expression strength after ORFV infection of Vero cells, the monocytic cell line THP-1 and of human primary monocyte derived dendritic cells (moDCs). For this, cells were seeded as described in 2.3.5 and infected with VCh014GFP, VCh024GFP, VCh112GFP, VCh113GFP, VCh119GFP, VCh121GFP, VCh126GFP, VCh127GFP, VCh128GFP and the reference virus VChD12GFP for 24 h or

48 h. Subsequently, FACS analysis was performed and geometric mean fluorescent intensities (MFI) of GFP and mCherry expressed in the cells were determined. For the analysis of moDCs, experiments were performed with cells from several donors to estimate the differences between individuals. MFIs identified from new Del-site recombinants' infections were normalized to the mean of VChD12GFP derived MFIs of the same experiment. Results obtained from Vero cells, THP-1 cells and moDCs are shown in Figure 17, Figure 18 and Figure 19, respectively.

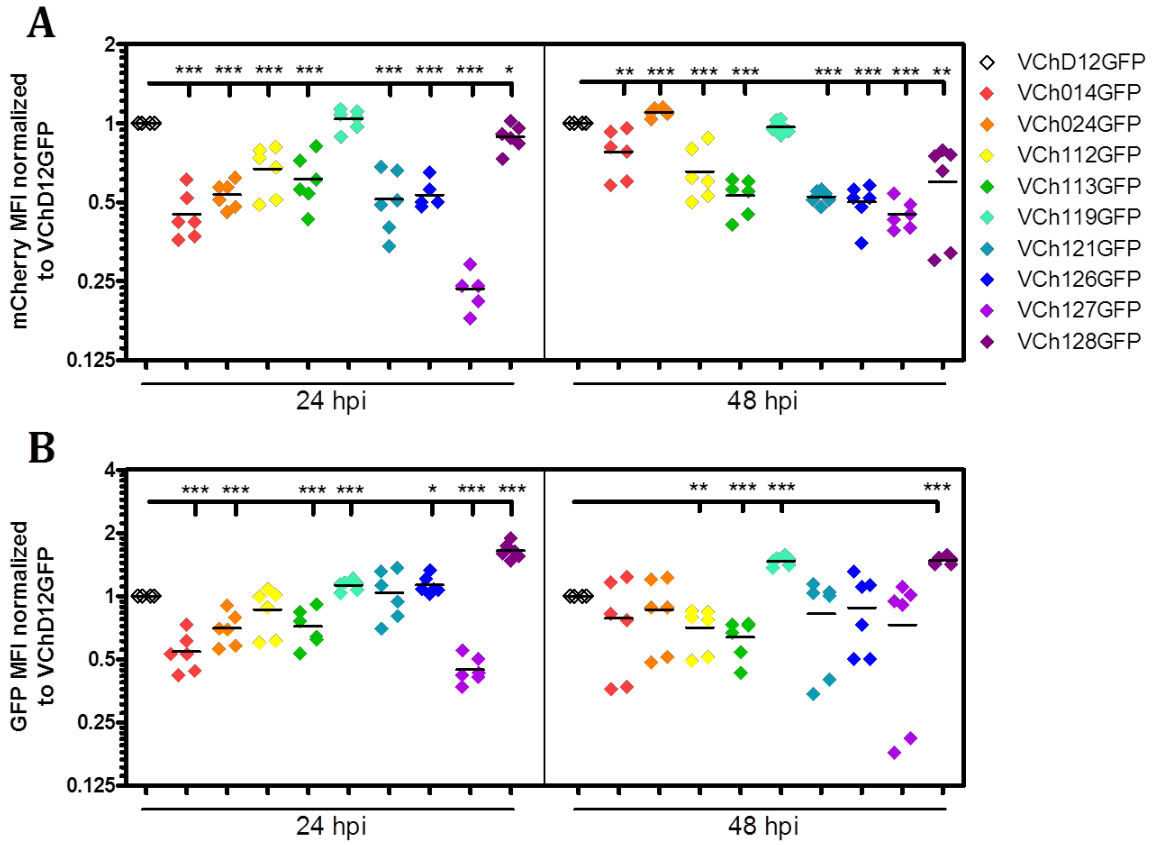


**Figure 17: Comparison of GFP and mCherry expression in Vero cells. Vero cells were infected with new Del-site recombinants and the reference virus VChD12GFP, and harvested 24 hpi and 48 hpi. mCherry (A) and GFP (B) geometric mean fluorescence intensities (MFI) were determined by FACS analysis and normalized to that of VChD12GFP. Shown are duplicates of three independent experiments. Statistical analysis was performed using an unpaired t-test with a confidence interval of 95%: ns = p ≥ 0.05, * = p < 0.05, ** = p < 0.01, *** = p < 0.001.**

For Vero cells, three independent experiments were performed in duplicates. The mCherry expression was comparable to VChD12GFP only after VCh119GFP infection at 24 hpi and 48 hpi, while VCh024GFP induced moderate but significantly, 1.1-fold higher mCherry levels after 48 h. For the remaining recombinants, significantly lower MFIs were detected (Figure 17A), which also aligns with most of the results obtained for GFP MFIs. Here, VCh112GFP and VCh121GFP resembled MFIs seen for VChD12GFP 24 hpi, while VCh126GFP and VCh128GFP induced GFP levels were significantly enhanced after 24 h and both, 24 h and 48 h regarding VCh128GFP (Figure 17B). Notably, also

VCh119GFP infection led to 1.1- to 1.5-fold enhanced GFP levels at both time points suggesting a positive impact of ORF119 deletion on transgene expression from the *vegf*- and Del-119 locus in Vero cells compared to VChD12GFP.

The expression strength of GFP and mCherry in monocytic THP-1 cells was analyzed in four independent experiments including three to six replicates 24 h after infection, and in two independent experiments including triplicates 48 h after infection, respectively. Here, mean mCherry levels resembled VChD12GFP induced levels after 24 h, while 1.4-fold stronger MFIs were obtained from THP-1 cells infected with VCh024-GFP and VCh119GFP (Table S20). Significant differences between VChD12GFP and most Del-site recombinants except of VCh127GFP and VCh128GFP could be detected after 48 h, in which mCherry expression was increased 1.2- to1.7-fold as shown in Figure 18A and Table S21. Additionally, the GFP expression was significantly accelerated for the Del-site recombinants VCh126GFP and VCh128GFP compared to VChD12GFP after 24 h, while elevated GFP levels could be detected in THP-1 cells treated with all new Del-site recombinants except of VCh014GFP and VCh024GFP. Those differences were significant for all Del-site recombinants except VCh119GFP 48 h after infection as demonstrated in Figure 18B (Table S22 and Table S23 of the supplementary information). Considering these elevated transgene levels in comparison to VChD12GFP, the deletion of all ORFs except 127 and 128 seem to facilitate the expression of transgenes integrated into the *vegf*-locus, whereas transgenes inserted into any new Del-site are expressed stronger than those encoded by the D-locus in THP-1 cells.

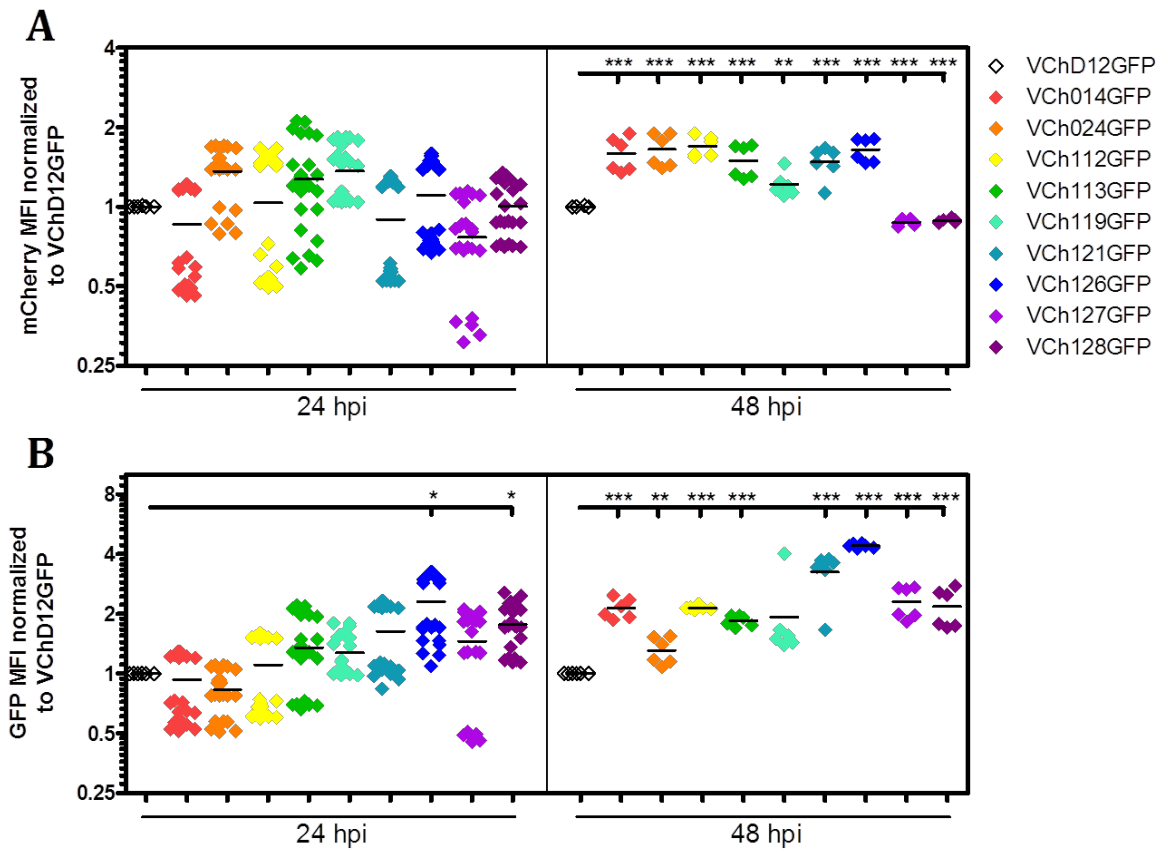


**Figure 18: Comparison of GFP and mCherry expression in monocytic THP-1 cells. THP-1 cells were infected with new Del-site recombinants and the reference virus VChD12GFP, and harvested 24 hpi and 48 hpi. mCherry (A) and GFP (B) geometric mean fluorescence intensities (MFI) were determined by FACS analysis and normalized to that of VChD12GFP. Mean values of each independent experiment were calculated to perform statistical analysis using an unpaired t-test with a confidence interval of 95%: ns = $p \geq 0.05$, * = $p < 0.05$, ** = $p < 0.01$, *** = $p < 0.001$.**

To study the expression of transgenes compared to the reference virus VChD12GFP in primary cells, moDCs were generated and infected. For each of the three donors, the GFP and mCherry MFIs of six technical replicates were evaluated by FACS 24 h and 48 h after infection. As demonstrated in Figure 19A, the expression of mCherry was increased 1.3-fold for VCh024GFP, whereas VCh112GFP, VCh121GFP and VCh126GFP leveled with VChD12GFP after 24 h. While the remaining recombinants showed strongly reduced mCherry levels here, this eventually applied to all Del-site recombinants after 48 h except for VCh024GFP and VCh126GFP (Table S24 and Table S25). In contrast, comparison of MFIs shown in Figure 19B revealed significantly enhanced GFP expression in moDCs infected with VCh112GFP, VCh121GFP, VCh126GFP and VCh128GFP after 24 h that leveled with VChD12GFP after 48 h. Comparable levels were observed for VCh024GFP and VCh127GFP, whereas the remaining recombinant's GFP expression was found in equal or significantly lower ranges than VChD12GFP's. Remarkably, the Del-site recombinant VCh119GFP was not able to induce expression profiles seen in Vero and THP-1 cells, but instead led to GFP and mCherry levels reduced by the factor 0.5 at most compared to the reference virus. Furthermore, the deletion of

ORF126 seemed not to affect transgene expression from the *vegf*-locus, while integration of a transgene into Del-site 126 appeared to enhance expression levels compared to those resulting from the D-locus in moDCs.

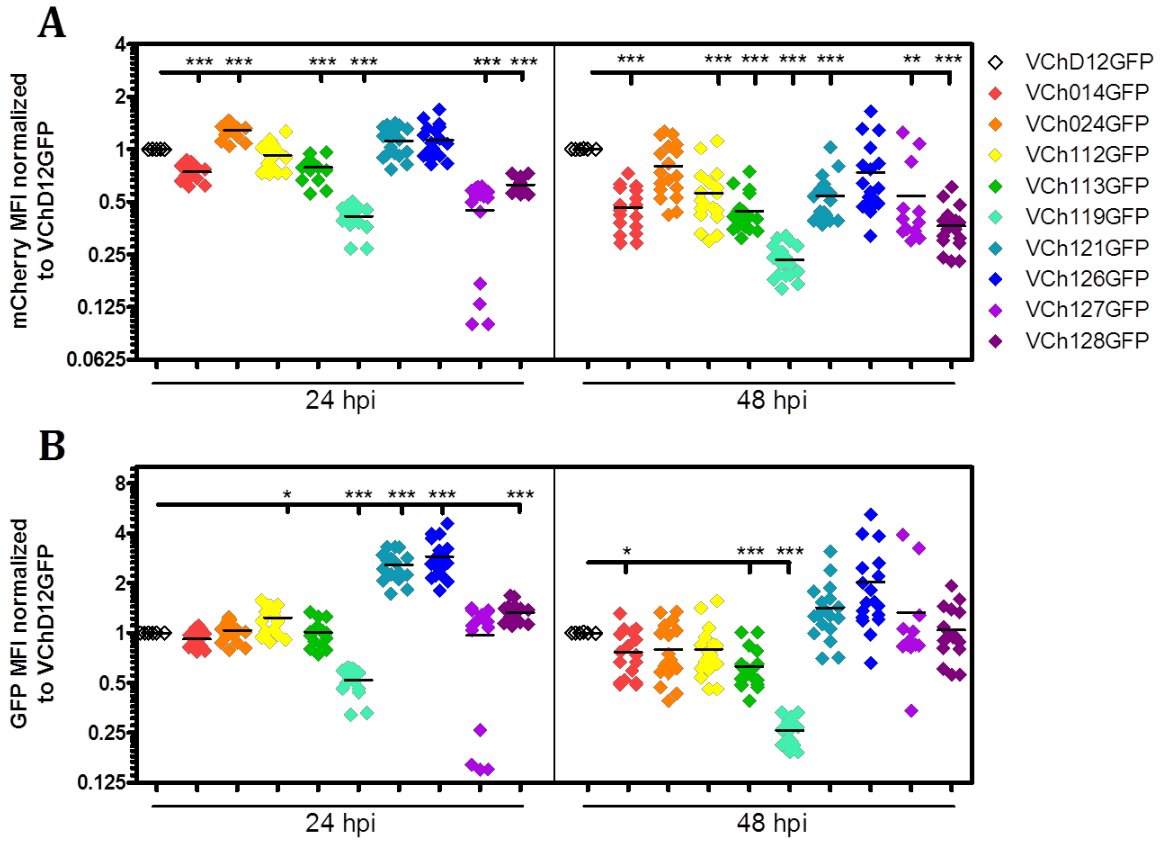


**Figure 19: Comparison of GFP and mCherry expression in moDCs. moDCs were infected with new Del-site recombinants and the reference virus VChD12GFP, and harvested 24 hpi and 48 hpi. mCherry (A) and GFP (B) geometric mean fluorescence intensities (MFI) were determined by FACS analysis and normalized to that of VChD12GFP. The ratio of GFP to mCherry MFI was calculated to compare the relative GFP expression (C). Statistical analysis was performed using an unpaired t-test with a confidence interval of 95%: ns = $p \geq 0.05$, * = $p < 0.05$, ** = $p < 0.01$, *** = $p < 0.001$.**

In conclusion, the analyses on expression strengths show that the deletion of selected ORFs encoded by ORFV D1701-V and their replacement with *gfp* causes alterations in the expression of transgenes inserted into the *vegf*-locus. Especially the deletion of ORF119 and ORF126, which encode an NF-κB-inhibitor and ANK-1, respectively, seemed to affect the expression kinetics of inserted transgenes. While the expression of the fluorescent reporters GFP and mCherry induced by most of the new Del-site recombinants appeared to be decreased, comparable or higher expression levels could be achieved in Vero and THP-1 cells upon VCh119GFP, and in THP-1 and moDCs upon VCh126GFP infection.

#### *3.1.3.4 Gene deletions in new Del-site Recombinants alter the activation of IFN and NF-κB pathways in vitro*

Both, the interferon regulatory factor (IRF) and the NF-κB transcription factor families are fundamental effectors in the innate immune response and act as key regulators in inflammation and antiviral response. Hence, these pathways were used to examine the *in vitro* immunogenicity of the new Del-site recombinants in THP-1 Dual cells. These human monocytic THP-1 cell line derived cells encode for two inducible reporter constructs, a secreted luciferase reporter gene (Lucia) and a secreted embryonic alkaline phosphatase (SEAP), allowing the simultaneous study of IRF- and NF-κB-pathway activation upon stimulation with certain type I IFNs, RIG-I-like receptors (RLRs) and cytosolic DNA sensors (CDSs), or TLR agonists, respectively.

Hence, THP-1 Dual cells were seeded and infected with VCh014GFP, VCh024GFP, VCh112GFP, VCh113GFP, VCh119GFP, VCh121GFP, VCh126GFP, VCh127GFP, VCh128GFP and the reference virus VChD12GFP for 24 h and 48 h in three independent experiments including three replicates for each group. The NF-κB pathway activation was monitored by secretion of SEAP, while the IRF-pathway activation was assessed by the determination of secreted Lucia luciferase as illustrated in Figure 20 and Figure 21. Absolute values of samples showing infection rates of approximately 30% (see supplementary information Figure S84) were normalized to the PBS control and are shown in relative light units (RLU) and normalized absorbance at 650 nm. 2'-3'-cGAMP and LPS were used as positive controls for the activation of IFN- and NF-κB-pathways, respectively.

As illustrated in Figure 20, the IRF-pathway activation observed in THP-1 cells was lower for those infected with the new Del-site recombinants compared to the reference virus VChD12GFP. While less IRF-pathway activation was induced by an infection of THP-1 Dual cells with the new Del-site recombinants VCh014GFP, VCh024GFP and VCh127GFP after 24 h, a significant reduction could be detected for the remaining recombinants 24 h (Figure 20A) and for all new Del-site recombinants 48 h after infection (Figure 20B). The least activation was detected in VCh119GFP infected cells showing approximately five times less activity than VChD12GFP after 24 h and only half the activation after 48 h.

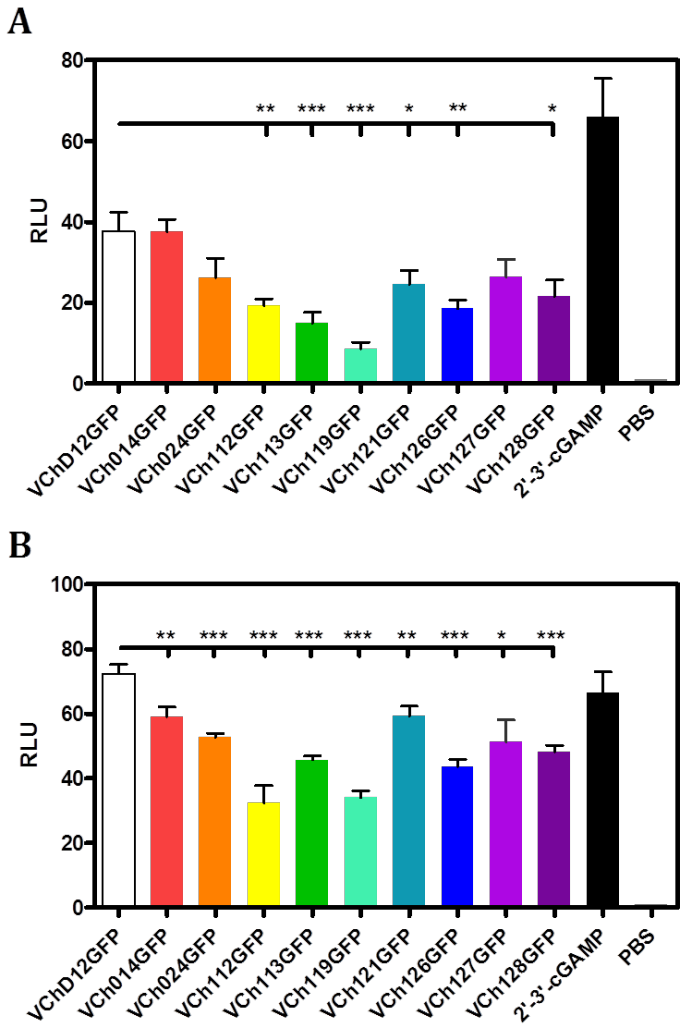


**Figure 20: IRF-pathway activation induced by new Del-site recombinants. THP-1 Dual cells were harvested 24 h (A) and 48 h (B) after infection, secreted Lucia luciferase was measured by luminescence and normalized to the PBS control. The strength of IRF-pathway activation induced by ORFV infection is depicted in relative light units (RLU). Shown are the mean values and standard errors of the mean of three independent experiments. Statistical analysis was performed using an unpaired t-test with a confidence interval of 95%: ns = $p \geq 0.05$, * = $p < 0.05$, ** = $p < 0.01$, *** = $p < 0.001$.**

Similar results were obtained for the activation of the NF-κB-pathway, which was decreased significantly using all new Del-site recombinants compared to VChD12GFP after 24 h (Figure 21A). Here, detected SEAP levels were comparable within the group of the new Del-site recombinants with VCh024GFp inducing most SEAP secretion, and revealed approximately half of the levels detected for VChD12GFP. These differences were also significant for most of the new Del-site recombinants after 48 h, while NF-κB-pathway activation using VCh014GFP and VCh024GFP revealed only 1.5 times less SEAP levels. Notably, VCh127GFP and VCh128GFP induced comparable NF-κB-pathway activities after 48 h (Figure 21B).

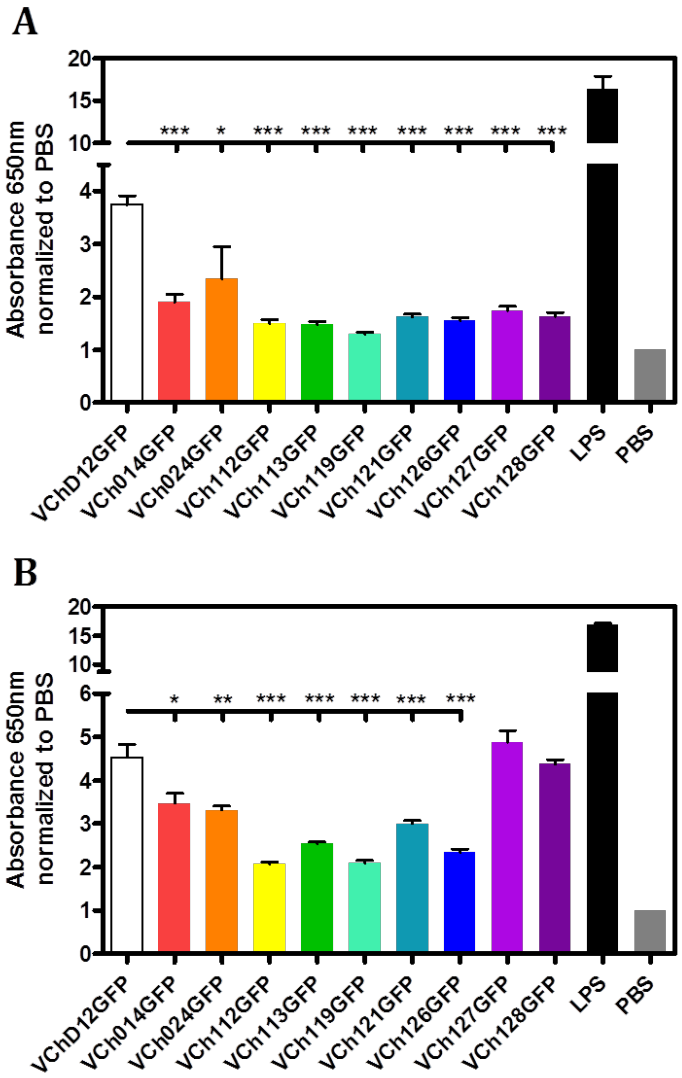


**Figure 21: NF-κB -pathway activation induced by new Del-site recombinants. THP-1 Dual cells were harvested 24 h (A) and 48 h (B) after infection and SEAP was measured by absorbance. The strength of NF-κB-pathway activation induced by ORFV infection is depicted in absorbance at 650 nm normalized to the PBS control. Shown are the mean values and standard errors of the mean of three independent experiments. Statistical analysis was performed using an unpaired t-test with a confidence interval of 95%: ns = p ≥ 0.05, * = p < 0.05, ** = p < 0.01, *** = p < 0.001.**

In conclusion, these results might indicate that deletions of selected ORFs impact the ability of new ORFV D1701-V recombinants to activate the IRF- and NF-κB-pathway. However, the negative effects on the IRF-pathway were not as strong after 24 h if PACR (ORF014), an NF-κB inhibitor (ORF024) and the IL-10 ortholog (ORF127) were deleted in the corresponding recombinants, while the NF-κB-pathway activation was not significantly affected after 48 h upon deletion of the IL-10 ortholog (ORF127) and ANK-2 (ORF128).

### *3.1.3.5 Activation of Dendritic Cells by Infection with new Del-site Recombinants*

Previously, Müller et al. (2019, in preparation) could show that the uptake of D1701-V ORFV recombinants encoding different transgenes can alter the activation of APCs such as dendritic cells or PBMCs. To elucidate the impact of selected ORF deletions introduced into the D1701-V genome, moDCs were infected with VCh014GFP, VCh024GFP, VCh112GFP, VCh113GFP, VCh119GFP, VCh121GFP, VCh126GFP, VCh127GFP, VCh128GFP and the reference virus VChD12GFP, while not infected cells served as negative control. After 24 h, cells were harvested to determine the expression of the activation markers CD40, CD80, CD83, CD86 and HLA-DR of mCherry expressing cells that showed most comparable infection rates within one donor by FACS analysis. LPS treated and not infected cells served as controls, whereas their activation marker expression was measured in mCherry negative cells (see 2.7.4).

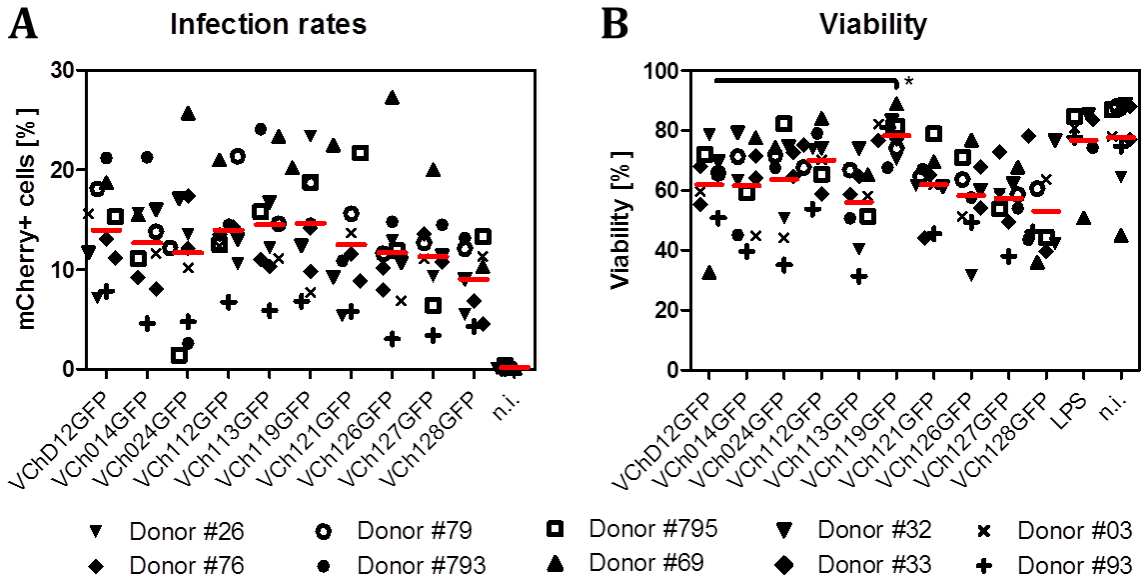


**Figure 22: Infection rates and viability of human moDCs. moDCs of ten different donors were infected with VCh014GFP, VCh024GFP, VCh112GFP, VCh113GFP, VCh119GFP, VCh121GFP, VCh126GFP, VCh127GFP, VCh128GFP and the reference recombinant VChD12GFP. Shown are the percentages of infected and viable cells determined by mCherry expression (A) and Zombie Aqua staining (B) for each of the five independently performed experiments and means, respectively. Statistical analysis was performed using a paired t-test with a confidence interval of 95%: ns = $p \geq 0.05$, * = $p < 0.05$, ** = $p < 0.01$, *** = $p < 0.001$.**

In total, the activation marker expression was determined in infected moDCs derived from ten healthy donors. High variations could be observed for infection rates of moDCs from different donors ranging from 5% - 20%, which in mean leveled between 10% to 15% (Figure 22A). The mean viability of moDCs infected with most new Del-site recombinants did not correlate with infection rates and leveled at approximately 60%. Interestingly, moDCs infected with VCh119GFP showed significantly increased mean viabilities of 80% (Figure 22B). To compare these data, the expression of activation markers was normalized to the geometric mean fluorescence intensity obtained from not infected cells. The results shown in Figure 23A and B indicate that the relative

expression of the activation markers CD40 and CD80 did not differ significantly upon infection with the reference virus VChD12GFP or any of the new Del-site recombinants. The expression of CD83, however, was significantly increased 1.7-fold after infection of moDCs with VCh126GFP as illustrated in Figure 23D. Strong differences were obtained for the expression of CD86 comparing VChD12GFP with VCh014GFP, VCh126GFP and VCh127GFP. Here, mean CD86 expression was accelerated 1.5-, 2.4- and 2.8-fold in moDCs treated with the new Del-site recombinants, respectively, whereas the remaining recombinants induced the surface expression of comparable CD86 levels (Figure 23E). Similarly, HLA-DR expression was elevated 1.5-2 fold compared to VChD12GFP in moDCs infected with VCh126GFP or VCh127GFP, while infection with VCh119GFP led to significantly reduced HLA-DR expression (Figure 23F).

In summary, the deletion of ORF014, 119, 126 and 127 in ORFV D1701-V recombinants impacts the surface expression of analyzed activation markers. With the exception of deleted ORF119 leading to decreased HLA-DR expression, deletion of ORF014, 126 and 127 seem to positively impact expression levels of CD83, CD86 and HLA-DR. Since high or low infection rates did not generally result in either high or low levels of activation markers, no correlation between these two parameters could be observed.

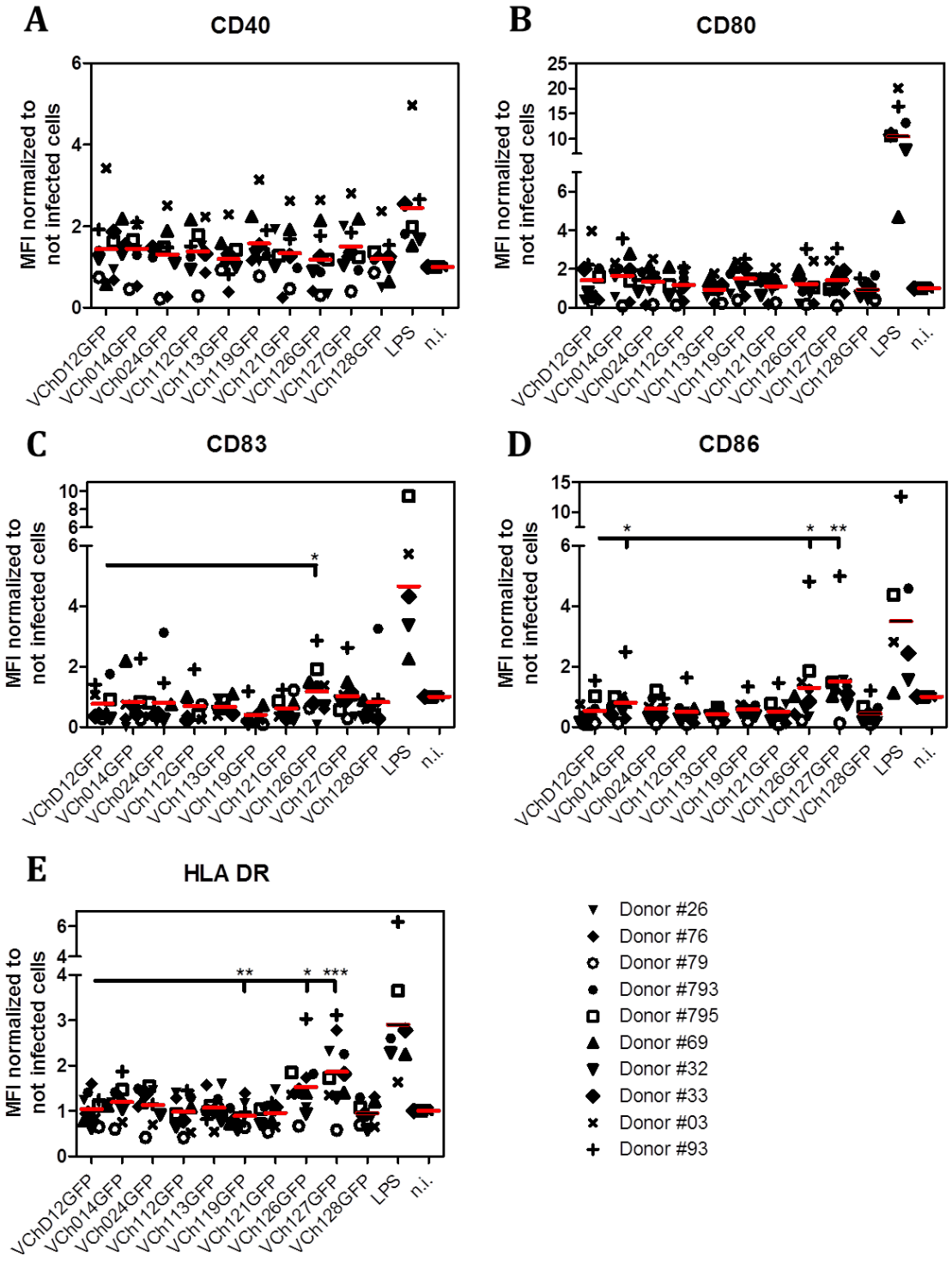


**Figure 23: Activation of human moDCs by new Del-site recombinants. moDCs of five different donors were infected with VCh014GFP, VCh024GFP, VCh112GFP, VCh113GFP, VCh119GFP, VCh121GFP, 126–Ch, VCh127GFP, VCh128GFP and the reference recombinant VChD12GFP. The percentage of infected cells was determined by mCherry expression (A), while normalization to not infected cells allowed analyses of the relative activation of moDCs by CD40 (B), CD80 (C), CD83 (D), CD86 (E) and HLA-DR (F) expression via flow cytometry. Shown are the changes in expression strengths for each of the five independently performed experiments and means. Statistical analysis was performed using a paired t-test with a confidence interval of 95%: ns = $p \geq 0.05$, * = $p < 0.05$, ** = $p < 0.01$, *** = $p < 0.001$.**

#### *3.1.3.6 Activation of human PBMCs by Infection with new Del-site Recombinants*

As mentioned above, the activation of moDCs could be altered upon infection with new Del-site recombinants. To study the impact of increased CD83, CD86 and HLA-DR surface expression by APCs on the activation of PBMCs, these cells were isolated from blood of eight healthy donors and *in vitro* infected for 24 h with the new Del-site recombinants VCh014GFP, VCh024GFP, VCh112GFP, VCh113GFP, VCh119GFP, VCh121GFP, VCh126GFP, VCh127GFP, VCh128GFP and the reference virus VChD12GFP. As monocytes are the only cell population within PBMCs to take up ORFV D1701-V, infection rates were determined by the mCherry expression in the CD14+ PBMC population. Similar to the infection of moDCs, samples showing most comparably infected monocytes within one donor were analyzed. After 24 h, PBMCs were harvested and the expression of the activation marker CD69 was determined on CD4+ and CD8+ T cells, CD14+ monocytes, CD19+ B cells and CD56+ NK cells by flow cytometry using surface marker specific antibodies.

Analyses on PBMC activation upon infection using the new Del-site recombinants and VChD12GFP as a reference are shown in Figure 24. Mean infection rates illustrated in Figure 24A ranged from approximately 22% - 32%, while high variations could be observed between different donors ranging from 10% - 40%. The activation of CD19+ B-cells was comparable between any of the new Del-site recombinants and VChD12GFP, while the largest mean CD69+ population was observed in PBMCs infected with VCh119GFP. In contrast, significant differences for the activation of CD4+, CD8+ and CD56+ were found comparing PBMCs infected with VChD12GFP and the new Del-site recombinants. Hence, significantly more CD8+ cells showed CD69 expression upon infection with VCh113GFP and VCh128GFP, while almost two times the amount of cells expressed CD69 in the group infected with VCh119GFP compared to VChD12GFP (Figure 24C). Very similar results were observed for the expression of CD69 in CD4+ cells depicted in Figure 24B. Here, significantly larger populations were activated in PBMCs infected with VCh024GFP, VCh112GFP, VCh113GFP, VCh127GFP and VCh128GFP compared to the group infected with VChD12GFP. The largest population of CD4+ and CD69+ cells was found in PBMCs treated with VCh119GFP. Here, the population increased five-fold in comparison to PBMCs treated with VChD12GFP. Lastly, also the CD56+ NK-cell population revealed significantly stronger activation upon infection with new Del-site recombinants in comparison to the PBMCs infected with VChD12GFP. Whereas only infection of PBMCs using VCh014GFP and VCh126GFP resulted in the activation of NK-cells comparable to the reference virus, significantly stronger CD69 expression on NK cells could be detected upon infection with the remaining recombinants compared to VChD12GFP as shown in Figure 24E. Notably and similar to all other analyzed PBMC populations, the strongest CD69 expression was seen for VCh119GFP.

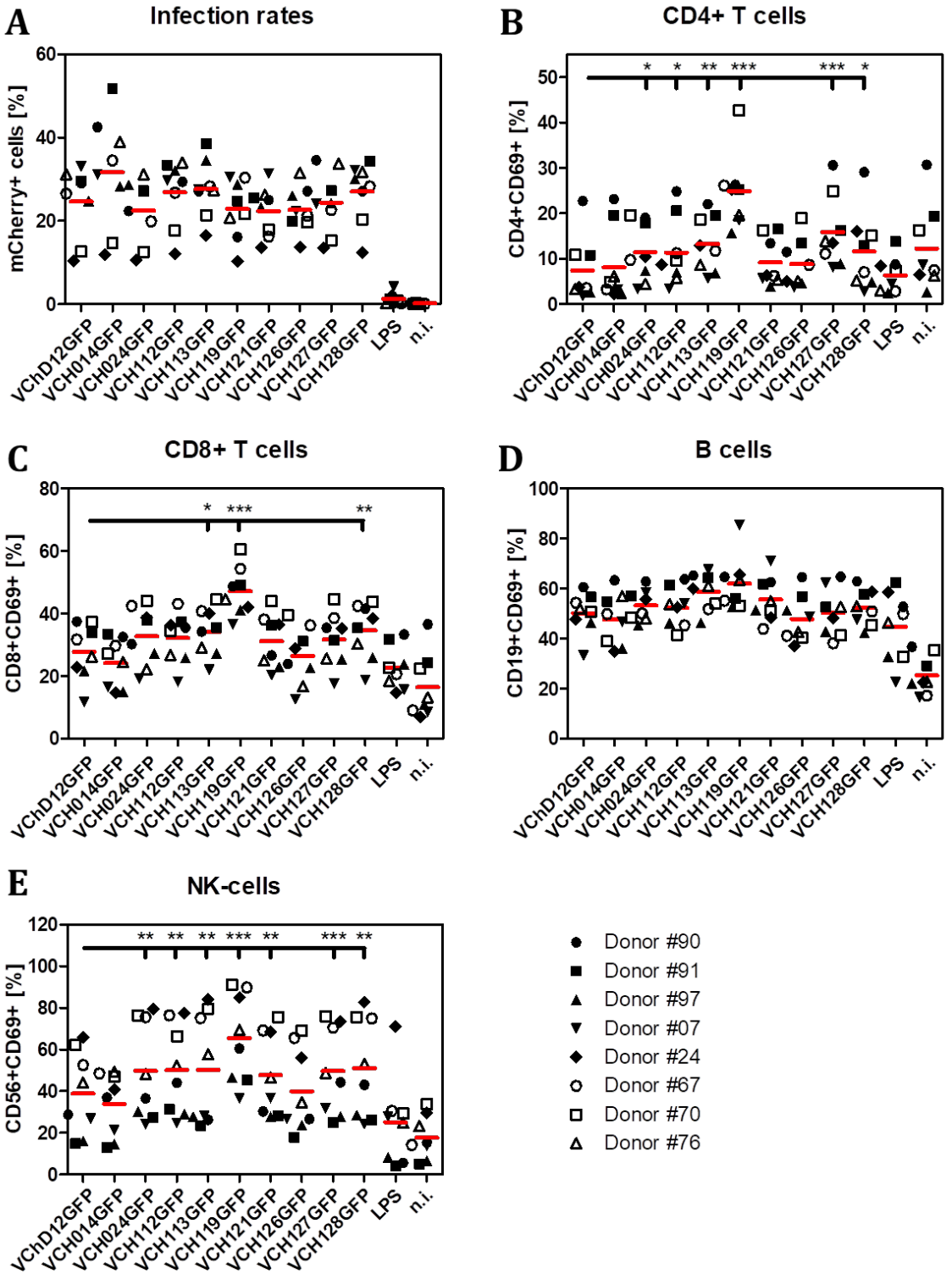


**Figure 24: Activation of human PBMCs by new Del-site recombinants. PBMCs of eight different donors were infected for 24 h with VCh014GFP, VCh024GFP, VCh112GFP, VCh113GFP, VCh119GFP, VCh121GFP, VCh126GFP, VCh127GFP, VCh128GFP and the reference virus VChD12GFP. The percentage of infected cells was determined by mCherry expression of the CD14+ cell population (A), while the activation of CD4+ (B) and CD8+ (C) T cell, CD19+ B cell (D) and CD56+ NK-cell (E) populations was determined using CD69 as activation marker. Shown are the CD69+ fractions of different PBMC populations for each of the eight independently performed experiments and their means. Statistical analysis was performed using a paired t-test with a confidence interval of 95%: ns = $p \geq 0.05$, * = $p < 0.05$, ** = $p < 0.01$, *** = $p < 0.001$.**

Analyses performed on the activation on PBMCs by infection with the new Del-site recombinants revealed enlarged CD4+ and CD8+ T cell as well as CD56+ NK-cell populations expressing the activation marker CD69 compared to the reference virus VChD12GFP. As described for the activation of moDCs, the variations in the infection rates seemed not to impact the PBMC activation. Recombinants harboring deletions of ORF113, 119 and 128 encoding for an unknown protein, a NF-κB inhibitor and ANK-2, respectively, showed the highest capacities to activate the mentioned PBMC populations. Nevertheless, CD19 expressing B-cells showed a comparable activation status upon infection with each of the different ORFV D1701-V recombinants.

#### *3.1.3.7 In vitro expansion of human antigen-specific memory CD8+ T cells*

To further study the immunogenicity of new Del-site recombinants *in vitro*, their capacity to induce antigen-specific immune responses was analyzed. Therefore, new Del-site recombinants encoding for the HLA-A*02 restricted EBV ($BMLF1_{280-288}$ GLCTLVAML), Influenza A ($MP_{58-66}$ GILGFVFTL) and HCMV ($pp65_{495-503}$ NLVPMVATV) epitopes were generated as illustrated in Figure S61 - Figure S66 of the supplementary information. Subsequently, CD14+ fractions isolated from human PBMCs were infected with the newly generated recombinants VHLA024GFP, VHLA112GFP, VHLA119GFP, VHLA121GFP, VHLA126GFP, VHLA128GFP and the reference virus VHLAD12GFP or stimulated with a mix of corresponding synthetic peptides (Pepmix). Infection rates were determined by the mCherry or GFP expression using FACS, and monocytes showing comparable percentages within one donor were co-cultured with the CD14- fractions of PBMCs after 24 hpi. The expansion of antigen-specific CD8+ T cells as well as their functionality was determined 12 days after infection via tetramer staining and intracellular cytokine staining (ICS), respectively. Unstimulated CD14- fractions served as negative controls, while stimulation using a mixture of synthetic GLCTLVAML, GILGFVFTL and NLVPMVATV peptides represented the positive control. Additionally, CD14- fractions were stimulated with D12-Cherry infected CD14+ cells to study the influence of ORFV D1701-V without antigen on the expansion and functionality of T cells.

24 h after infection, monocytes showed mean infection rates of approximately 10% - 15% for most virus recombinants used, however, high variations were seen between donors resulting in percentages ranging from 5% - 25%. Notably, infection rates obtained from VHLA128GFP infection were in mean much lower than those resulting from other virus recombinants and varied between 4% -10% (Figure 25A). After 12 days, the expansion of T cells was measured by tetramer staining and their functionality was analyzed by ICS. Tetramer staining revealed that ORFV D1701-V recombinants encoding the HLA-A*02 restricted EBV, Influenza A and HCMV peptides, or the stimulation with Pepmix elicited antigen-specific CD8+ T cell proliferation. Interestingly, the expansion of CD8+ T cells could be induced against all peptides that the donors possessed memory T cells against. The mean frequencies of CD8+ T cells specific for any of the peptides as well as those obtained for each donor after 12 days of expansion are shown in Figure 25B. A high variation in T cell responses from different donors could be

detected. Thus, donor #186 showed antigen-specific CD8+ T cell frequencies of approximately 55% after stimulation, while only 10% CD8+ T cells could be expanded for donor #016. Nevertheless, most of the new Del-site recombinants as well as the Pepmix induced comparable mean memory T cell responses of approximately 25% than the reference virus VHLAD12GFP, while no antigen specific T cell expansion was detected in the unstimulated or D12-Cherry infected groups. Strikingly, the responses elicited by the deletion mutant VHLA119GFP were in mean increased 1.4-fold compared to the reference virus VHLAD12GFP showing approximately 35% of CD8+ T cells specific for any of the peptides.

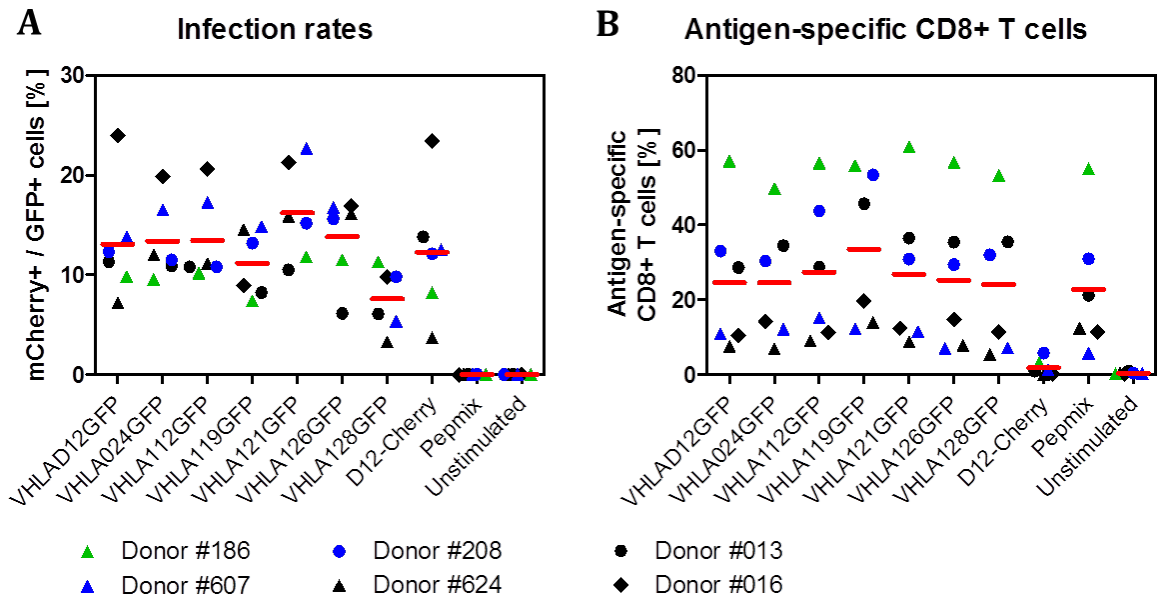


**Figure 25: Infection rates and expansion of memory T cells of 6 different donors after infection with the new Del-site recombinants. CD14- PBMC populations were stimulated with Pepmix or CD14+ monocytes infected with VHLA024GFP, VHLA112GFP, VHLA119GFP, VHLA121GFP, VHLA126GFP, VHLA128GFP and the reference virus VHLAD12GFP. D12-Cherry infected as well as unstimulated cells served as controls. A) Infection rates were determined 24 hpi by the expression of mCherry or GFP in CD14+ monocytes using FACS. B) After 12 days, the expansion of memory T cells was determined by the proportion of tetramer+ CD8+ T cells (antigen-specific CD8+ T cells). Colors indicate memory T cell specificities possessed by the different donors: Black: GLCTLVAML and GILGFVFTL; Blue: GILGFVFTL and NLVPMVATV; Green: GLCTLVAML, GILGFVFTL and NLVPMVATV. Shown are the results of 6 independent experiments and the calculated mean values. The statistical analysis was performed using a paired t-test with a confidence interval of 95%: ns = $p \geq 0.05$, * = $p < 0.05$, ** = $p < 0.01$, *** = $p < 0.001$.**

On the other hand, analyses undertaken on the expansion of memory T cells specific for each of the peptides showed mean frequencies of approximately 10% after stimulation with monocytes infected with most of the new Del-site recombinants, the reference virus VHLAD12GFP and Pepmix (Figure 26A). Divergently, mean frequencies of peptide specific CD8+ T cells could be significantly elevated 1.3-fold by the stimulation with VHLA119GFP infected monocytes compared to the stimulation with the reference virus VHLAD12GFP. The proportions of CD8+ T cells specific for each of the peptides are shown in the supplementary information for donors possessing memory T cells against

either the GLCTLVAML and GILGFVFTL, the GILGFVFTL and NLVPMVATV, or the GLCTLVAML, GILGFVFTL and NLVPMVATV peptide, respectively (Figure S85 - Figure S87).

Analyses on the functionality of memory T cells after re-stimulation with GLCTLVAML, GILGFVFTL or NLVPMVATV indicate the production of the pro-inflammatory cytokines TNFα and IFNγ in approximately 5% of the CD8+ T cells stimulated with Pepmix (Figure 26B). Here, the functionality of CD8+ T cells was significantly reduced 2-fold compared to those stimulated by monocytes infected with the reference virus VHLAD12GFP, which showed a mean polyfunctional CD8+ T cell proportion of 10%. Comparable frequencies were obtained in the VHLA024GFP, VHLA121GFP, VHLA126GFP and VHLA128GFP groups. Remarkably, the functionality of T cells stimulated with VHLA112GFP and VHLA119GFP infected monocytes was significantly enhanced with T cells of the VHLA119GFP group showing 1.4 times higher functionality than T cells in the reference group.

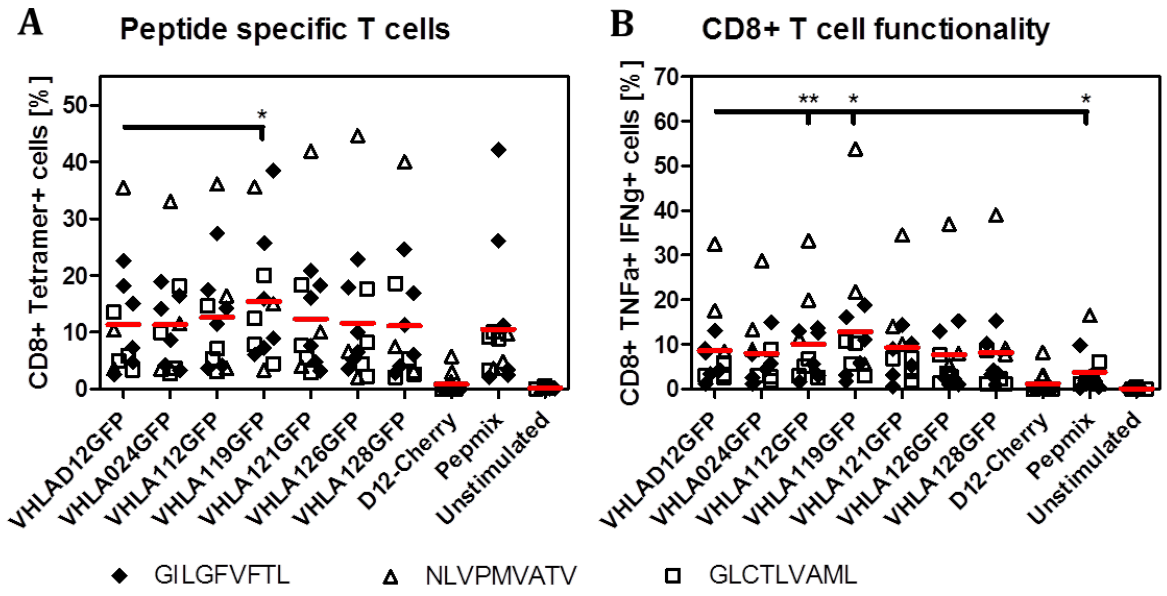


**Figure 26: Expansion and functionality of memory T cells of 6 different donors after infection with new Del-site recombinants. CD14- PBMC populations were stimulated with Pepmix or CD14+ monocytes infected with VHLA024GFP, VHLA112GFP, VHLA119GFP, VHLA121GFP, VHLA126GFP, VHLA128GFP and the reference virus VHLAD12GFP. D12-Cherry infected as well as unstimulated cells served as controls. A) After 12 days, the expansion of memory T cells was determined by the proportion of GILGFVFTL, GLCTLVAML or NLVPMVATV tetramer+ CD8+ T cells, which is indicated by different symbols. B) The functionality of the expanded CD8+ T cells was analyzed after re-stimulation with GILGFVFTL, GLCTLVAML or NLVPMVATV by intracellular staining of TNFα and IFNγ, and the proportion of TNFα+ IFNγ+ CD8+ T cells was determined. Shown are the results of 6 independent experiments and the calculated mean values. The statistical analysis was performed using a paired t-test with a confidence interval of 95%: ns = $p \geq 0.05$, * = $p < 0.05$, ** = $p < 0.01$, *** = $p < 0.001$.**

In conclusion, the immunogenicity of selected new Del-site recombinants encoding for HLA-A*02 restricted EBV, Influenza A and HCMV epitopes was analyzed *in vitro* by their

capacity to induce the expansion of functional CD8+ memory T cells after 12 days. Taken together the results presented above, frequencies of antigen-specific CD8+ T cells could be raised by the stimulation of T cells with monocytes previously infected with the Del-site recombinant VHLA119GFP. Consistently, also the functionality of these T cells in mean showed the highest polyfunctionality measured by the simultaneous expression of the pro-inflammatory cytokines TNFα and IFNγ. Thus, the deletion of ORF119 might indicate a positive influence on the strength of antigen-specific cellular immune responses elicited by ORFV D1701-V recombinants.

### 3.1.4 Characterization of new Del-Site recombinants *in vivo*

Analyses performed on the characteristics of the new Del-site recombinants *in vitro* demonstrate growth efficiency, stability and the ability to induce transgene expression in several cell lines as well as human primary cells. Experiments undertaken to examine their immunogenicity showed diminished potencies to activate the IRF- and NF-κB-pathway in comparison to a reference virus recombinant, however, also to elevate the activation of PBMCs and the capability to enhance the surface expression of activation markers in APCs.

To study the immunogenicity of the new Del-site recombinants *in vivo*, C57BL/6NTac mice were immunized intravenously (i.v.) with the selected Del-site recombinants VOVA024GFP, VOVA112GFP, VOVA121GFP, VOVA126GFP and VOVA128GFP encoding for Ovalbumin (OVA) in a homologous prime-boost dosis on study day 0 and 14. The VOVAD12GFP coding for OVA in the *vegf*-locus and GFP in the Del2-locus was used as a reference. Percentages of OVA-specific CD8+ T cells were determined seven days after the prime, and five days after the boost immunization via a SIINFEKL-Dextramer staining as illustrated in Figure 27. The functionality of splenocytes was analyzed five days after boost by intracellular IFNγ, TNFα and CD107α staining (Figure 29). To study the humoral responses, OVA specific IgG1 and IgG2c serum antibody titers were determined by ELISA five days after the boost immunization (Figure 30). Both, the performance of the animal experiments and the analyses of the generated data was carried out by Boehringer Ingelheim, while recombinants used in these experiments were generated in the frame of this work.

Seven days after the prime immunization, the SIINFEKL-Dextramer staining revealed approximately 14 % SIINFEKL-specific CD8+ T cells in mice immunized with the reference virus VOVAD12GFP. The fractions of SIINFEKL-specific CD8+ T cells stimulated with any of the examined Del-site recombinants were lower. While mice immunized with VOVA024GFP, VOVA112GFP and VOVA126GFP showed fractions of approximately 8-11 % OVA specific CD8+ T cells, the differences between the groups treated with VOVAD12GFP and VOVA121GFP or VOVA128GFP were significant (Figure 27A). The boost immunization led to an increase of SIINFEKL-specific CD8+ T cells in all groups resulting in comparable fractions of 70-80 %. Only mice immunized with VOVA121GFP revealed a significantly smaller SIINFEKL-specific CD8+ T cell fraction of

approximately 20 % compared to VOVAD12GFP, whereas this fraction was reduced 1.6 fold in mice immunized with VOVA024GFP.

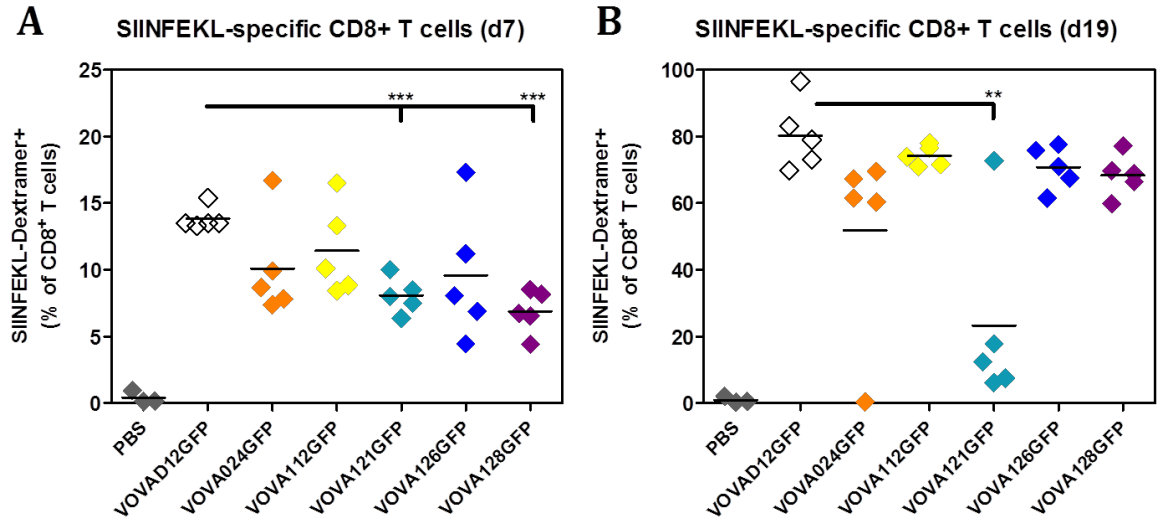


**Figure 27: SIINFEKL-specific CD8+ T cell response after immunization with new Del-site recombinants encoding for Ovalbumin. Immunization of five mice per group was carried out by injecting selected Del-site recombinants and the reference virus VOVAD12GFP at a dose of $10^6$ PFU or equal volumes of 100 µl PBS intravenously on day 0 and day 14. The percentage of OVA-specific CD8+ T cells was determined seven days after the prime- (A), and five days after the boost-immunization (B) via SIINFEKL-Dextramer staining. Shown are the SIINFEKL-specific CD8+ T cell fractions of single mice as well as the mean. Statistical analysis was performed using an unpaired t-test with a confidence interval of 95%: ns = $p \geq 0.05$, * = $p < 0.05$, ** = $p < 0.01$, *** = $p < 0.001$.**

The results from this experiment clearly show that the new Del-site recombinants were able to elicit strong cellular immune responses mainly comparable to those elicited with the reference virus VOVAD12GFP. While VOVA112GFP, VOVA126GFP and VOVA128GFP showed the highest SIINFEKL-specific CD8+ T cell fractions after the boost immunization, the fractions specific for OVA in VOVA121GFP treated mice seemed to stay at levels obtained after the prime immunization.

Next, the functionality of the SIINFEKL-specific CD8+ T cells was evaluated by ICS five days after the boost immunization. Boolean gating revealed highest frequencies of functional T cells in mice immunized with VOVA112GFP, while frequencies ranged from 45%-58.8% for most viruses used and T cells producing 1-2 cytokines were most prevalent (Figure 28A-C, E, F). In contrast, only 17.3% of functional T cells could be detected in mice treated with VOVA121GFP that mostly produced one cytokine (Figure 28D).

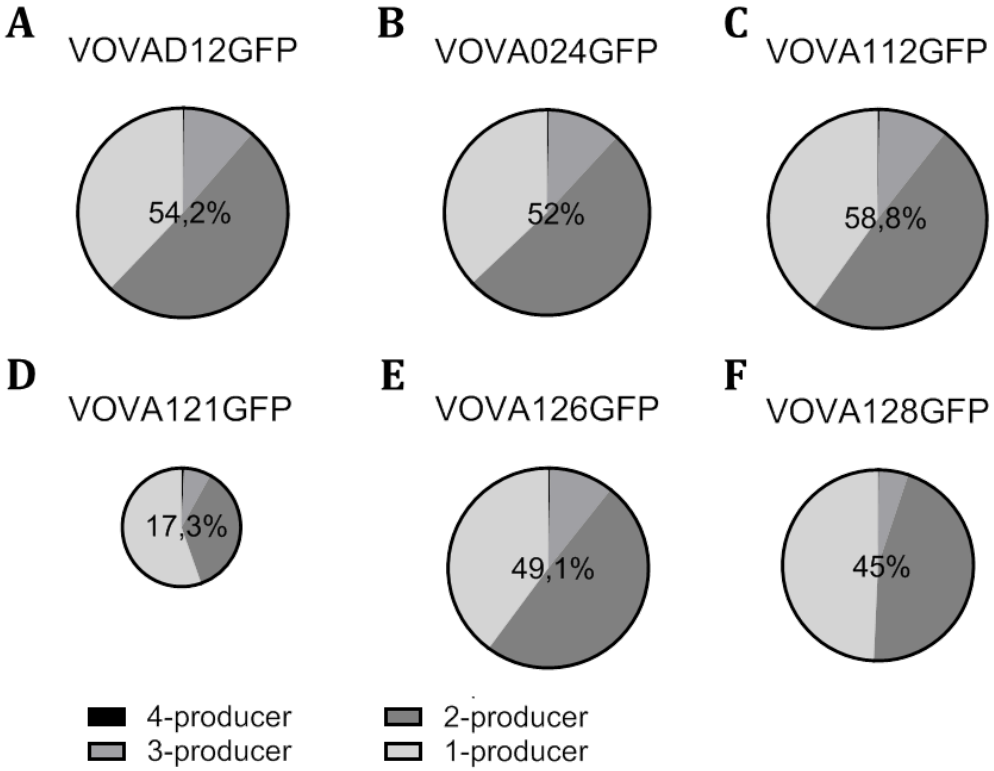


**Figure 28: Functionality of SIINFEKL-specific CD8+ T cells after immunization with new Del-site recombinants encoding for OVA. Immunization of five mice per group was carried out by injecting selected Del-site recombinants and the reference virus VOVAD12GFP at a dose of $10^6$ PFU or equal volumes of 100 µl PBS intravenously on day 0 and day 14. Intracellular staining of IFNγ, TNFα, IL-2 and CD107α was performed in splenocytes restimulated with SIINFEKL five days after the boost-immunization. Boolean gating revealed mean functional T cell populations as well as their fractions producing 1-4 cytokines simultaneously and is shown for each new Del-site recombinant (A-F).**

The largest IFNγ producing T cell fractions could be detected in mice infected with the reference virus VOVAD12GFP and the new Del-site recombinants VOVA024GFP or VOVA112GFP. Here, 35 % of OVA-specific T cells produced IFNγ, whereas this fraction was significantly smaller in the groups treated with VOVA126GFP, VOVA128GFP and especially VOVA121GFP showing IFNγ production in less than 10 % of all OVA-specific T cells (Figure 29A). Similar results were obtained from intracellular staining of TNFα, IFNγ and TNFα, or IFNγ and CD107α. Here, SIINFEKL-specific CD8+ T cell fractions of mice immunized with VOVA024GFP and VOVA112GFP leveled with VOVAD12GFP, while significant differences between the reference virus and the treatment with the new Del-site recombinants VOVA121GFP, VOVA126GFP and VOVA128GFP could be detected as shown in Figure 29B, D and E. Interestingly, CD107α staining revealed the expression in comparable OVA-specific CD8+ T cell fractions of mice immunized with all ORFV D1701-V recombinants except of VOVA121GFP. Here, the amount of CD107α expressing T cells was reduced two-fold compared to the other groups (Figure 29C).

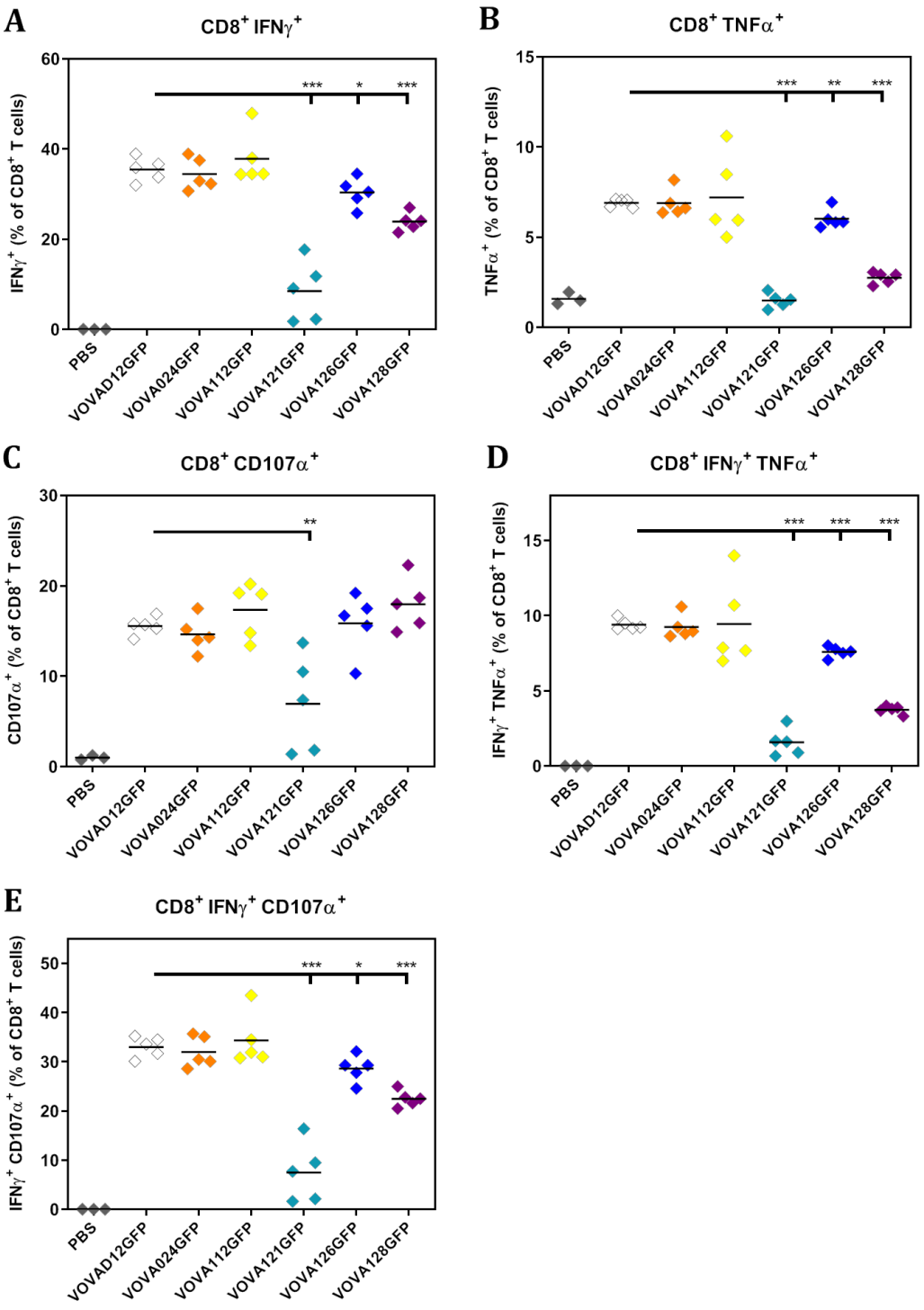


**Figure 29: Functionality of SIINFEKL-specific CD8+ T cells after immunization with new Del-site recombinants encoding for OVA. Immunization of five mice per group was carried out by injecting selected Del-site recombinants and the reference virus VOVAD12GFP at a dose of $10^6$ PFU or equal volumes of 100 µl PBS intravenously on day 0 and day 14. Intracellular staining of IFNγ, TNFα and CD107α was performed in splenocytes restimulated with SIINFEKL five days after the boost-immunization. Shown are fractions of IFNγ+ CD8+ T cells (A), TNFα+ CD8+ T cells (B), CD107α+ CD8+ T cells (C), IFNγ+ TNFα+ CD8+ T cells (D) and IFNγ+ CD107α+ CD8+ T cells (E) for single mice and the mean. Statistical analysis was performed using an unpaired t-test with a confidence interval of 95%: ns = $p \geq 0.05$, * = $p < 0.05$, ** = $p < 0.01$, *** = $p < 0.001$.**

Analyses on the humoral immune responses in mice infected with the new Del-site recombinants were performed five days after the boost immunization. For this, OVA-specific IgG1 and IgG2c titers in blood serum were measured by ELISA. As illustrated in Figure 30A, IgG1 could not be detected in blood serum of mice treated with VOVAD12GFP, VOVA024GFP and VOVA121GFP as titers leveled with those present in PBS infected mice. Nevertheless, elevated but not significantly increased IgG1 levels could be quantified in 60 % of VOVA112GFP and VOVA128GFP, as well as 20 % of VOVA126GFP immunized mice. In contrast, the OVA-specific IgG2c immune responses in the VOVA112GFP, VOVA126GFP and VOVA128GFP groups increased significantly in comparison to VOVAD12GFP treated mice. Additionally, elevated IgG2c levels could also be observed in the mice immunized with VOVA024GFP and VOVA121GFP (Figure 30B).

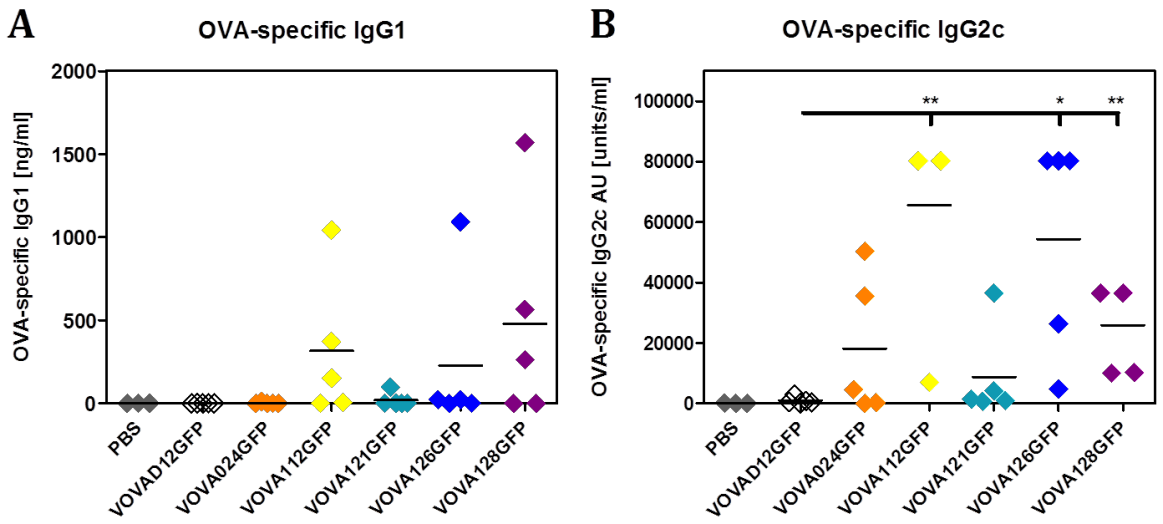


**Figure 30: OVA-specific IgG1 and IgG2c serum antibody titers after immunization with selected Del-site recombinants. Immunization of five mice per group was carried out by injecting selected Del-site recombinants and the reference virus VOVAD12GFP at a dose of $10^6$ PFU or equal volumes of 100 µl PBS intravenously on day 0 and day 14. OVA-specific IgG1 (A) and IgG2c (B) ELISAs were performed five days after the boost immunization. Shown are the IgG1 or IgG2c serum antibody titers in ng/µl and absolute units (AU)/ml for single mice as well as the mean. Statistical analysis was performed using an unpaired t-test with a confidence interval of 95%: ns = $p \geq 0.05$, * = $p < 0.05$, ** = $p < 0.01$, *** = $p < 0.001$.**

In summary, the results obtained from analyses performed on the humoral responses show elevated IgG1 and significantly increased IgG2c titers against OVA in three out of five groups that were immunized with VOVA112GFP, VOVA126GFP and VOVA128GFP. Thus, deletion of the ORFs 112, 126 and 128 seems to favor the formation of antigen specific antibodies in the performed prime-boost regimens.

In the frame of this work, the Del-site recombinants VOVA014GFP, VOVA113GFP, VOVA119GFP and VOVA127GFP were also generated as shown in Figure S52, Figure S55, Figure S56 and Figure S59 of the supplementary information. Due to deadlines within Boehringer Ingelheim, those recombinants could not be tested *in vivo*.

## 3.2 Generation and Characterization of Ipilimumab and Avelumab expressing ORFV recombinant

### 3.2.1 Generation of Transfer Plasmids

The generation of the transfer plasmid pV-IpiHC-2-Cherry followed five steps listed in Table 15, in which intermediate plasmids had to be cloned. As described in 3.1.1, cloning of the plasmids included restriction digests of insert and vector as well as their ligation, transformation of bacteria, purification of selected plasmids and their validation via sequencing and control digests as shown in Figure 31. Plasmid charts of both, pV-IpiHC-2-IpiLC and pV-AveHC-2-AveLC, are depicted in Figure S48 and Figure S49 of the supplementary information.

**Table 15: Generation of pV-IpiHC-2-IpiLC and its intermediate plasmids, their insert and parental vector as well as the restriction enzymes used.**

| Plasmid | Insert Vector | Parental Vector | Restriction Enzymes |
|---|---|---|---|
| **pV-IpiHC-2-Cherry** | Ipi_heavy_Chain | pV12-Cherry | Hind*III* / Spe*I* |
| **pV-IpiHC+SS-2-Cherry** | newPepTrio-Ipi-HC-SS | pV-IpiHC-12-Cherry | BamH*I* / Dra*III* |
| **pV12-IpiLC+SS** | Ipilimumab_LC-SigSeq | pV12-Cherry | Bgl*II* / EcoR*I* |
| **pV2-IpiLC+SS** | pV12-IpiLC+SS | pV-IpiHC+SS-2-Cherry | Bgl*II* / EcoR*I* |
| **pV-IpiHC-2-IpiLC** | Ipilimumab_LC-SigSeq | pV-SS-IpiLC | Bgl*II* |

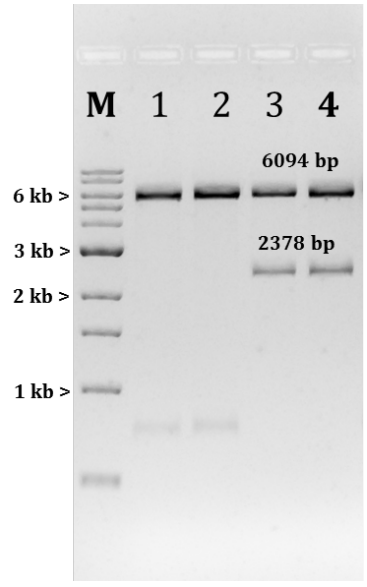


**Figure 31: Control digests of pV-IpiHC-2-IpiLC. After ligation, competent *E. coli* were transformed and plasmids produced by four different clones were digested using Hind*III* and EcoR*I*. Correctly sized fragments of 6.1 kb and 2.4 kb were observed for clone 3 and 4, but not for clone 1 and 2, while clone 4 was used to produce final pVIpiHC-2-IpiLC transfer plasmid. 1% agarose gel; M = Quick-Load® 1 kb DNA Ladder, NEB.**

### 3.2.2 Generation of Ipilimumab and Avelumab expressing ORFV Recombinants

The generation of Ipi-Ch and Ave-Ch followed the methods described in 2.2.1 - 2.2.7 and 2.3.1 - 2.3.2. Both, recombinants including their parental virus and transfer plasmids, are listed in 2.1.10 and respective PCR typings for the verification of genetic homogeneity are shown in Figure S67 and Figure S68 of the supplementary information. The used primer combinations and temperature profiles of the cycles in PCRs can be found in 2.1.7 and 2.2.9.

### 3.2.3 Characterization of Ipilimumab and Avelumab expressing Recombinants

ORFV D1701-V recombinants encoding for Ipilimumab and Avelumab were characterized by ELISA to demonstrate their capabilities to induce the expression of antibodies in several cell lines and human primary cells. Western blots served to validate the expression of predicted heavy and light chains, as well as the expression of native antibody constructs. Finally, the functionality of expressed antibodies was confirmed by an artificial blockade bioassay.

#### *3.2.3.1 ORFV Recombinants induce the Expression of functional Ipilimumab and Avelumab*

For a proof of concept, $5 \times 10^6$ Vero, HEK, CHO and THP-1 cells, as well as human primary monocytes, monocyte derived macrophages and moDCs were infected with Ipi-Ch (MOI 1) for five days in a T75 flask. Next, supernatants were collected to determine the Ipilimumab concentration in a CTLA-4 targeted, indirect ELISA as described in 2.7.1. As illustrated in Figure 32, both, cell lines and human primary cells, induce the expression of Ipilimumab as mean titers ranging from 0.11 µg/ml in monocytes to 3.4 µg/ml in HEK cells could be detected. Ipilimumab concentrations produced by infected macrophages or moDCs increased approximately two fold compared to concentrations determined for monocytes, while Vero cells showed mean Ipilimumab titers of 1.8 µg/ml.

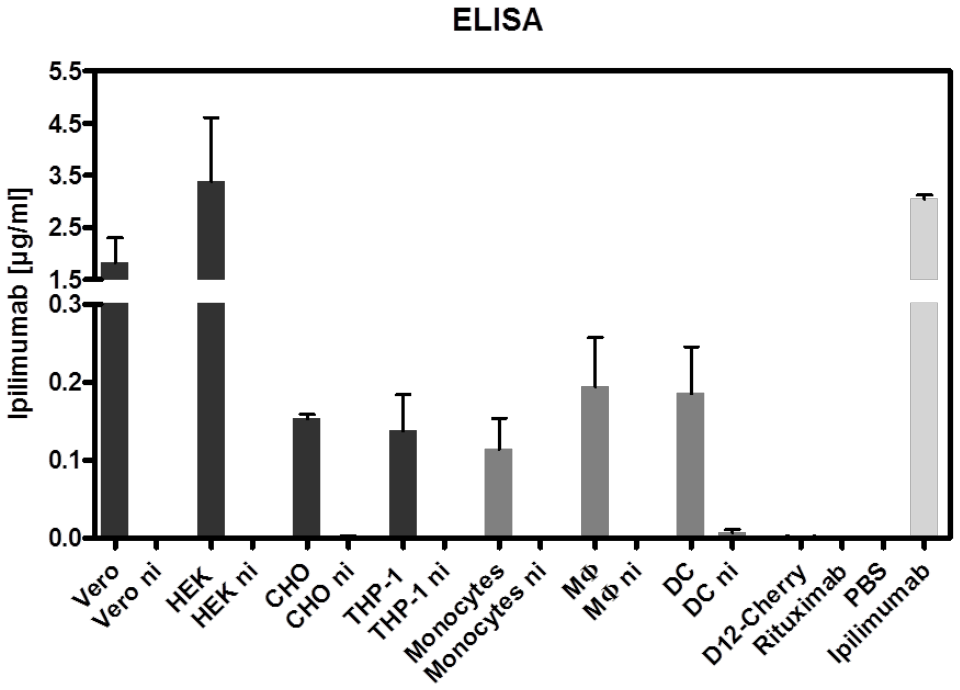


**Figure 32: Ipilimumab expression induced by Ipi-Ch infection. Vero, HEK, CHO and THP-1 cells, as well as human monocytes, macrophages (MΦ) and moDCs were infected with Ipi-Ch for five days in T75 flasks (MOI 1). Ipilimumab concentrations were determined in the supernatants using a CTLA4-Fc targeted indirect ELISA. Not infected cells (ni), D12-Cherry infected Vero cells (MOI 1), 3 µg/ml Rituximab in PBS, 3 µg/ml Ipilumumab in PBS, and PBS served as controls.**

Similarly, the expression of Avelumab was examined in Vero cells infected with Ave-Ch as described in 2.3.5. Supernatants were collected and Avelumab concentrations determined in an indirect ELISA targeting coated PD-L1-Fc fusion protein, which revealed titers of approximately 0.8 µg/ml Avelumab in Vero cell supernatants infected with Ave-Ch (Figure 33).

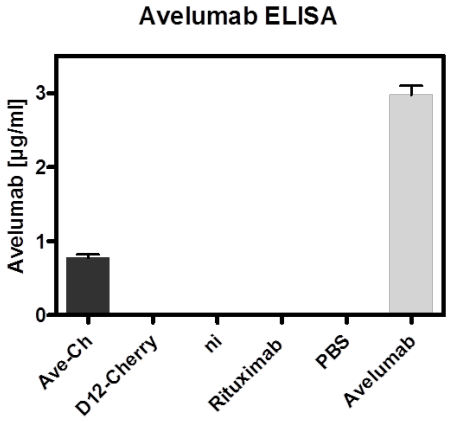


**Figure 33: Avelumab expression induced by Ave-Ch infection. 3 x $10^5$ Vero cells were seeded in a 6-well plate and infected with Ave-Ch for 72 h (MOI 1). Avelumab concentrations were determined in the supernatant using a PD-L1-Fc targeted indirect ELISA. Not infected cells (ni), D12-Cherry infected Vero cells (MOI 1), 3 µg/ml Rituximab in PBS, 3 µg/ml Avelumab, and PBS served as controls.**

In conclusion, these experiments demonstrate that several cell lines as well as human primary cells such as monocytes, moDCs or macrophages are susceptible to ORFV D1701-V Ipi-Ch or Ave-Ch that induce the production of functional, encoded checkpoint inhibitor antibodies binding their target antigen.

In the next step, the expression of Ipilumumab and Avelumab antibodies was validated by western blot analyses as described in 2.2.10. The results shown in Figure 34 not only support the results from ELISA experiments, in which Ipilimumab produced by Vero cells could be measured in much higher concentrations than in THP-1 cells, but also demonstrate correct heavy and light chain expression of both antibodies at approximately 50 kDa and 25 kDa obtained under reducing conditions, respectively. Nevertheless, the expression ratio of light to heavy chains was elevated compared to the commercial Ipilumumab, especially in Vero cells infected with Ave-Ch. Here, only weak bands could be detected in the supernatant, while no heavy chain signal was seen in denatured samples derived from the cell lysate. Interestingly, Ipilimumab and Avelumab were both detected at approximately 240 kDa in its native forms under non reducing conditions.

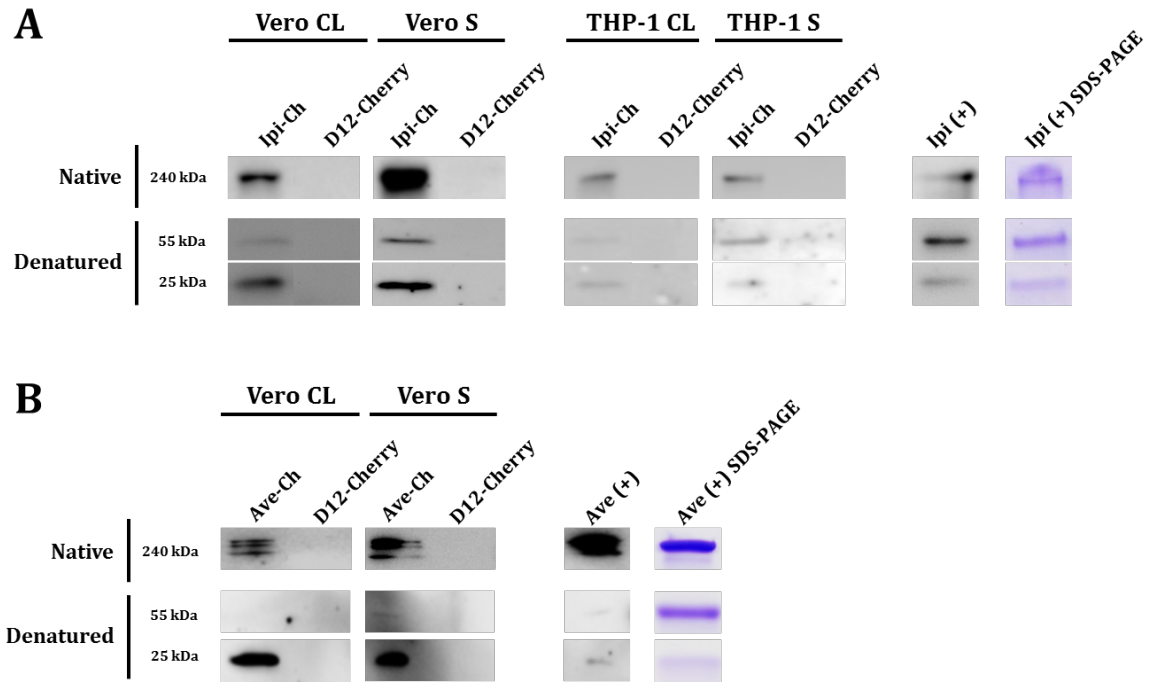


**Figure 34: Evaluation of Ipi-Ch- and Ave-Ch-produced Ipilimumab and Avelumab expression. A) Supernatants and cell lysates (CL) of Ipi-Ch infected Vero and THP-1 cells (A), and Ave-Ch infected Vero cells (B) were analyzed by IgG1 heavy and light chain specific western blotting under native and denaturing conditions. D12-Cherry infected cells and 12 ng/ml commercial Ipilimumab or Avelumab (Ipi(+)/Ave(+)) were used as controls.**

To study the expression kinetics of antibodies, whose expression is induced by ORFV recombinants, 3 x $10^5$ cells of the ORFV permissive cell line Vero and the monocytic cell line THP-1 were seeded in 6-well plates and infected with Ipi-Ch and D12-Cherry as a control. Supernatants were collected 24 h, 48 h, 72 h, 96 h and 168 h after infection and

used in an indirect ELISA targeting coated CTLA4-Fc fusion protein. The results are presented in Figure 35.

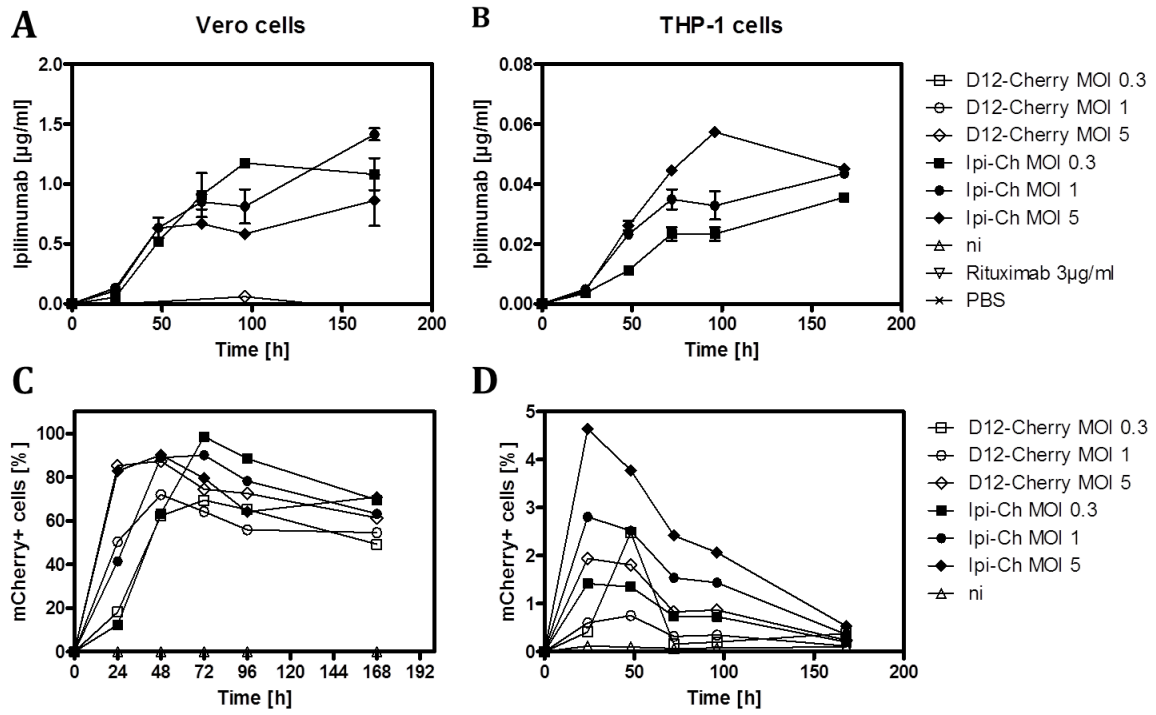


**Figure 35: Expression kinetics of Ipilimumab by Vero and THP-1 cells infected with Ipi-Ch. Vero and THP-1 cells were infected with different viral loads and supernatants collected after 24 h, 48 h, 72 h, 96 h and 168 h. Ipilimumab produced by Vero (A) and THP-1 cells (B) was measured by ELISA, while the infection rates in Vero (C) and THP-1 cells (D) were determined using the marker mCherry in flow cytometry. D12-Cherry and not infected (ni) cells, the isotype control Rituximab and PBS served as negative controls.**

Kinetics on the expression of Ipilimumab in Vero and THP-1 cells clearly show differences in the titers achieved. While none of the controls elicited Ipilimumab related signals in the ELISA experiments, the antibody could be detected in the supernatants of Ipi-Ch infected cells 24 h after infection. The highest concentration measured for THP-1 cell was approximately 60 ng/ml after 96 h using Ipi-Ch at a MOI 5 (Figure 35B), while Ipilimumab levels obtained in Vero cells peaked at 1.4 µg/ml after 168 h using Ipi-Ch at a MOI 5 as illustrated in Figure 35A. Nevertheless, titration curves strongly suggest an entry into the stationary phase after 72-96 h. Notably, the infection rates achieved in THP-1 cells using equal viral loads peaked at under 5 % and were much lower than those in Vero cells partially showing more than 90 % of infected cells (Figure 35B and D).

Next, the stability of antibodies produced by Vero cells after infection was analyzed. Therefore, supernatants of Ipi-Ch infected cells (MOI 1) were collected after 72 h as described above and incubated for 16 days at 37°C and 5 % $CO_2$. The concentration of Ipilimumab was determined prior (0 d) or 2 d, 4 d, 8 d and 16 d after the start of incubation by ELISA.

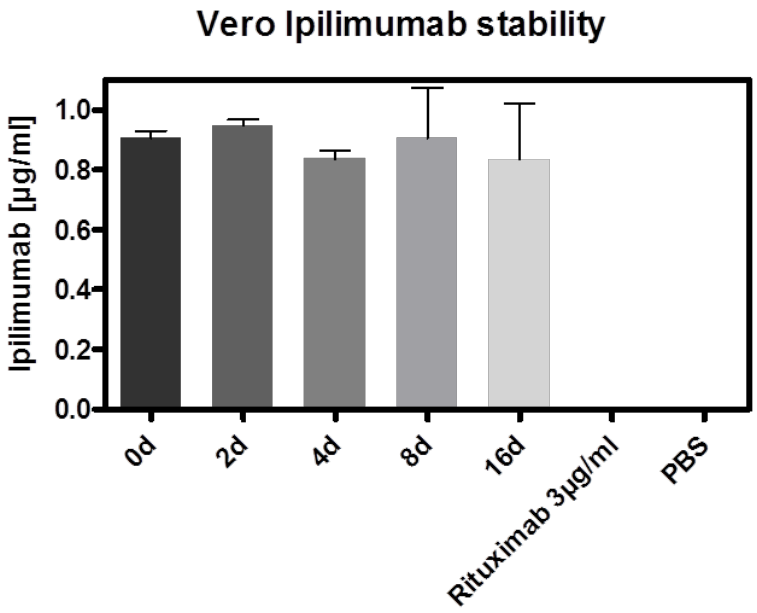


**Figure 36: Stability of Ipilimumab produced by Vero cells infected with Ipi-Ch. Supernatants were collected 72 h after infection and incubated for two to 16 days at 37°C and 5 % $CO_2$. Shown are Ipilimumab concentrations determined by ELISA, while 3 µg/ml Rituximab and PBS served as controls.**

As shown in Figure 36, supernatants incubated for two to 16 days resulted in comparable antibody titers as the one measured immediately prior to incubation. These results indicate protein stability under cell culture conditions at least for the investigated time period.

Finally, the functionality of antibodies expressed by Ave-Ch infected Vero cells was validated using a PD-1/PD-L1 blockade bioassay (Promega). This assay consists of two cell lines, Jurkat T cells expressing PD-1 and a NFAT-induced luciferase, and CHO-K1 cells stably expressing human PD-L1 and cell surface protein leading to an antigen independent activation of cognate T cell receptors. Since interaction between PD-1 and PD-L1 inhibits T cell receptor signaling, addition of an anti-PD-L1 antibody such as Avelumab should release the inhibitory signal, which can be detected by NFAT-mediated luciferase expression. Therefore, this assay was performed in supernatants of Ave-Ch and D12-Cherry infected Vero cells used in ELISA experiments (see Figure 33), while a chimeric α-Endoglin with a human IgG1 constant region in DMEM was used as negative control.

Results illustrated in Figure 37 suggest that Avelumab produced by Vero cells infected with Ave-Ch inhibits the interaction between PD-1 and PD-L1, since significantly elevated luciferase levels could be detected in samples containing Ave-Ch supernatants as a result of NFAT-mediated luciferase activity.

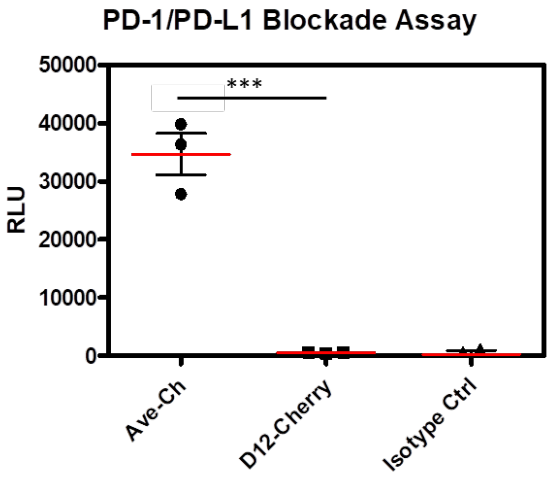


**Figure 37: PD-1/PD-L1 blockade bioassay using Avelumab produced by Ave-Ch infected Vero cells. 3 x $10^5$ Vero cells were seeded in a 6-well plate and infected with Ave-Ch or D12-Cherry for 72 h (MOI 1). The Promega blockade bioassay was performed using the supernatants of infected Vero cell cultures, while a chimeric α-Endoglin with a human IgG1 constant region in DMEM was used as isotype control. Shown is the relative NFAT-mediated luciferase activity in relative light units (RLU). Statistical analysis was performed using an unpaired t-test with a confidence interval of 95%: ns = $p \geq 0.05$, * = $p < 0.05$, ** = $p < 0.01$, *** = $p < 0.001$.**

In summary, characterization of Ipilimumab and Avelumab encoding ORFV D1701-V recombinants suggest their capacity to induce accurate expression of functional and stable antibodies in several different cell lines and human primary cells.

# 4 Discussion

Viral vectors represent promising tools for vaccination due to their capability to induce potent humoral and cellular immune responses, mostly without the need of an adjuvant. The advantages, especially of poxviral vectors, further include high safety profiles and large capacities to deliver several large sequences coding for antigens or immunomodulatory elements to the targeted host [46, 47]. Thus, viral vectors have shown prophylactic efficacy against infectious diseases [16, 91, 116, 118, 130, 182, 184, 185, 187-189] and are presently widely evaluated in clinical trials as immunotherapeutic agents to treat cancers [64-66, 68, 129, 263, 264]. Within the genus of *Parapoxvirus*, the ORFV derived strain D1701-V comprises several immuno-modulatory properties particularly favorable for the development of a platform technology facilitating such approaches [84, 91]. However, in view of highly attenuated, replication-restricted viral vectors triggering limited efficacy in clinical trials [10, 67, 69], improvements on ORFV D1701-V should be pursued to exploit the whole potential of this promising viral vector technology in the treatment of infectious diseases or cancer.

The use of immunomodulatory elements and the elimination of viral immuno-modulatory genes still present in the poxviral genome represent strategies currently implemented to enhance viral vectors' immunogenicity [10]. Therefore, the present study aimed to examine the suitability of nine novel, different insertion sites for transgene expression (Del-sites) by simultaneous deletion of ORFV D1701-V encoded genes predicted to be non-essential for viral replication in cell culture. Newly generated Del-site recombinants were subjected to detailed characterization of the genetic stability of inserted GFP reporter constructs, their growth behavior and capability to induce transgene expression in different target cells *in vitro*. Additionally, the D1701-V mutants' immunogenicity was analyzed by their ability to activate pro-inflammatory pathways, PBMCs and APCs, or to induce antigen-specific immune responses *in vitro* and *in vivo*. Furthermore, proof-of-concept studies were performed to evaluate the suitability of ORFV D1701-V recombinants for the expression of immunomodulatory immune checkpoint inhibitors (ICIs) in a side project.

## 4.1 Characterization of new Del-Site Recombinants

As typical for Poxviruses, ORFV D1701-V encodes genes essential for *in vitro* growth in the core region of its genome, while genes contributing to virulence and pathogenesis can be found in the terminal ends [98, 265, 266]. Analyses on the mechanism of action revealed that many of those ORFV encoded factors modulate the host innate and pro-inflammatory responses to infection by e.g. interaction with interferon [267], the NF-κB pathway [203, 204, 268] or the induction or inhibition of apoptosis [207, 269]. Given the presence of proteins in the ORFV D1701-V genome suspected to be involved in immune modulation, it was hypothesized that deletion of selected genes would enhance the immunogenicity of this attractive vector for vaccine delivery and simultaneously

generate potential additional sites for transgene insertion. In general, the deletion of the open reading frames (ORF) ORF014, ORF024, ORF112, ORF113, ORF119, ORF121, ORF126, ORF127 and ORF128, and replacement with the fluorescent reporter GFP resulted in genetically stable ORFV D1701-V mutants able to replicate in the African monkey kidney cell line Vero inducing the expression of encoded transgenes. In view on their immunogenicity, differences in the mutants' capability to activate PBMCs and moDCs, or to induce antigen-specific immune responses could be observed. Thus, a special focus is laid on recombinants harboring deletions of ORF112, ORF119 and ORF126 as the results indicate enhanced immunogenicity of the respective mutants.

### 4.1.1 Characterization of new Del-site recombinants' stability and growth behavior

Genetic stability of the newly generated Del-site recombinants was assessed by three different experimental approaches. Fluorescence microscopy confirmed transgene expression during 20 serial passages and parallel PCR typing of each deletion mutant revealed the Del-locus' integrity as no deleted ORF could be detected, while locus-spanning primers demonstrated specific GFP insertion. Further, Southern blot analyses using DIG labeled mCherry, GFP, ORF020 and ORF129 probes identified the corresponding targets at the predicted genomic location. Probe hybridization with fragments exceeding predicted sizes especially after utilizing the restriction endonuclease EcoR*I* could be explained by incomplete restriction digests or cross-hybridization. Finally, the genetic stability of transgenes encoded by the new Del-site recombinants was monitored by plaque counting during 10 serial passages using fluorescence microscopy. This technique allowed detection of the encoded reporter proteins mCherry and GFP in single plaques after Vero cell infection and thus, the examination of fluorescence loss as a result of genetic instability. Interestingly, with the exception of one clone of the mutant lacking ORF127, all remaining Del-site recombinants showed less than 1% of plaques expressing only GFP or mCherry after 10 passages.

The adaptation of D1701 to growth in Vero cells resulted in the strain D1701-V showing genomic rearrangements including the loss of genetic sequences in the regions designated A, AT and D [84, 181]. Remarkably, additional 20 passages of D1701-V on either Vero or BK cells did not result in further genomic changes despite the high variability of the left terminus of the *Parapoxvirus* genome [82-84, 270, 271]. Similarly, MVA was attenuated by hundreds of passages on chicken embryo fibroblasts and is considered stable as identical genome sequences were reported for three independent plaque isolates [272]. Nevertheless, a tendency for recombinant MVA to lose the ability of transgene expression after cell culture passages was reported [273-275], which resulted in the overgrowth of the parental MVA recombinant indicating a strong selection pressure. Although little systematic investigations have been conducted on the cause of genetic instabilities in MVA, harmful or toxic effects of the inserted transgenes as well as their expression strength are suggested to play a role in the selective advantage of non-expressing mutants. Furthermore, it was shown that frameshift or

viable deletion mutants could be eliminated or reduced by codon alterations to interrupt homonucleotide runs, transgene design and the insertion of transgenes into conserved intergenic regions within the genome [179]. In view on the production of large seed stocks of ORFV D1701-V vectored vaccines, the findings of the performed analyses are highly important as they suggest genetic stability of the inserted transgenes both in the *vegf*-locus and the analyzed Del-sites in most knockout mutants. Thus, ORFV D1701-V appears to possess highly reliable and robust mechanisms avoiding deletion, substitution or frameshift mutations during the event of viral replication. In contrast, the results also demonstrate that once a non-expressing mutant established within the population, it might overgrow the parental ORFV-recombinant as seen for one clone lacking ORF127. To ensure purity of ORFV D1701-V based vaccines, suggested improvements should be envisaged for future vaccine designs, while the generation of new recombinants must include detailed analysis of the genetic stability.

In this line, analyses on the growth behavior contribute strongly to understanding the biology of the subjected knockout mutants and are important for the feasibility of large-scale productions of viral vectors. Single step growth curves performed to study the viral yields obtained from infected Vero cells, as well as the determination of plaque morphologies revealed that not only all genes deleted in any of the knockout mutants were non-essential for D1701-V replication on the permissive cell line Vero, but also that most deletion mutants showed comparable growth kinetics compared to the reference virus. These results confirm previous findings using distinct ORFV strain deletion mutants lacking ORF024 [204], ORF112 [215], ORF113 [216], ORF119 [206, 276], ORF121 [203] and ORF127 [228], in which knockout recombinants and wild-type ORFV exhibited comparable growth characteristics. Notably, marked growth retardation and reduced plaque sizes were seen for mutants lacking ORF014, which coincides with literature highlighting the significant role of the coding protein PACR in viral replication. Although shown to be non-essential for ORFV replication, PACR disrupts the APC/C and is hypothesized to stimulate infected cells to enter an S phase-like state, in which cellular factors and nucleotides are provided to support viral genome replication [277]. Considering the up-scaling of vaccine candidates, ORF014 appears crucial for obtaining high viral yields and should thus be retained in future ORFV D1701-V vectored vaccine designs.

In conclusion, the present study encompasses the first detailed description of ORF014, ORF024, ORF112, ORF113, ORF119, ORF121, ORF126, ORF127 and ORF128 knockout mutants using the attenuated ORFV strain D1701-V. The results strongly suggest stability of the Del-sites 014, 024, 112, 113, 119, 121, 126 and 128 for transgene insertion, while analyses on their growth behavior affirm all Del-sites, except Del-site 014, the potential suitability for large-scale production of ORFV D1701-V vectored vaccines.

### 4.1.2 Analyses on transgene expression strengths using new Del-Sites

To understand the expression kinetics of transgenes inserted into different genomic loci of the new Del-site recombinants, the expression of the encoded fluorescent reporter proteins mCherry and GFP was studied using flow cytometry. Insertion of mCherry into the *vegf*-locus of each new Del site recombinant under the control of the synthetic promoter eP2 allowed comparison of total transgene expression induced by any recombinant, whereas GFP inserted into each new Del site under the control of eP2 was used to compare the locus specific transgene expression strengths. As promoter performances are known to vary in regard to relative expression strengths in different cell lines [278], this approach also aimed to draw general conclusions on the suitability of the new Del-sites for transgene expression by analyzing the kinetics in the permissive cell line Vero, the non-permissive monocytic cell line THP-1 and moDCs. Compared to the reference virus in Vero and THP-1 cells, the deletion of ORF119 caused enhanced or comparable mCherry expression driven by the promoter eP2 in the *vegf*-locus, while GFP expression controlled by eP2 in the Del 119 locus was elevated. In THP-1 cells and moDCs, this effect could especially be observed for the ORF126 knockout mutant. Despite the marked differences of GFP or mCherry levels induced by the various new Del-site recombinants in the distinct cell lines or primary cells (3.1.3.3), the results demonstrate that deletion of, and transgene integration into either Del-site 119 or 126 does not negatively influence the *vegf*-locus encoded transgene expression and simultaneously enhances the transgene expression compared to the reference D-locus (5.5). Notably, the comparison of GFP levels in THP-1 cells and moDCs infected with mutants lacking ORF126 displayed an up to 7.9-fold stronger expression than achieved with mutants lacking ORF119, which emphasizes the utilization of Del-site 126 for strong transgene expression, irrespective of the promoter used.

Several studies have stressed that the antigen expression can strongly influence the type, quality and magnitude of immune responses. Here, DNA vaccines induced stronger CD8+ T cell responses with increasing levels of antigen expression and dose [279, 280], while a positive correlation between dose and immunogenicity could be observed using recombinant Canarypox virus and MVA vectors [170, 281, 282]. Thus, the present findings might contribute significantly to the optimization of ORFV D1701-V vectored vaccines. On one hand, a strong expression of immunomodulatory elements encoded by recombinant ORFV vectors such as ICIs, cytokines or co-stimulatory molecules might enhance their immunogenicity and therapeutic efficacy when delivered with disease related and simultaneously expressed antigen. As shown for viral vectors encoding the TRICOM [134], the co-stimulatory molecules CD40L and CD80 encoded by recombinant D1701-V vectors improved their immunogenicity significantly compared to vectors solely expressing the antigen [124]. Using these novel insertion sites may thus constitute a promising strategy to optimize future D1701-V based vaccine designs.

Nevertheless, not only the strength but also the timing of transgene expression considerably shapes the quality of the immune response. For recombinant MVA vectors it was shown that CD8+ T cell responses to multiple immune dominant peptides

presented by DCs remained unaffected by utilization of different promoters, whereas those directed against subdominant peptides significantly increased as a result of strong expression during the early phase of infection [171, 283]. While cross-presentation of exogenously acquired antigens on MHC class I molecules remains the main pathway for presentation [284], strong early expression was hypothesized to favor the direct presentation of rapidly degraded proteins [283] and thus, shape the immune dominance hierarchy. Using the same strong early promoter eP2 [84] in each of the new Del-site recombinants, the marked differences in the locus-specific expression strengths emphasize future analyses on the early transgene expression to exploit the potential of the new insertion sites for the induction of potent antigen-specific immune responses. Furthermore, various synthetic early promoters were designed as described by Rziha et al. [84] and introduced into the new Del Site recombinants. Preliminary experiments (data not shown) on transgene expression distinguish some of these new promoters as strong inducers of early transcription and thus suggest detailed analyses in the near future.

In summary, analyses on the expression strengths of new Del-site recombinants highlight the potential utilization of Del-site 119 and 126 as the transgene expression using the respective knockout mutants was positively affected.

### 4.1.3 Immunogenicity of new Del-site recombinants

Optimizing the immunogenicity of D1701-V recombinants was sought by the deletion of potentially non-essential genes encoded by ORFV. Shown to be dispensable for *in vitro* growth, the impact of selected ORF deletions was studied *in vitro* and *in vivo* using mice. First, the activation of the IRF- and NF-κB pathways was examined upon infection with the new Del-site recombinants. In conclusion, the results suggest the deletions to negatively impact the activation of IRF- and NF-κB responses and were surprising, as the deletion of selected ORFs presumably encoding for virulence factors was hypothesized to increase inflammation and antiviral responses mediated by the two transcription factor families. Especially the deletion of ORF024, ORF119 and ORF121 was expected to trigger enhanced NF-κB pathway activation as literature reports these genes to encode for NF-κB inhibitors. Accordingly, the inhibitors block the phosphorylation of the IKK subunits IKKα and IKKβ [204], the phosphorylation of the transcription factor NF-κB-p65 [202] or interact with the retinoblastoma protein pRB eventually reducing the IKK activation [206]. Possibly, the distinct targets of the NF-κB inhibitors allow compensation of the NF-κB pathway inhibition, while generally, deletion of any selected ORF might disturb the highly complex virus/host interaction in regard to innate immune responses. As this hypothesis remains speculative, detecting phosphorylated NF-κB-p65 using western blotting or real time PCR of IRF and NF-κB targets must validate the suitability of the applied model. Additionally, mutants lacking either or all putative NF-κB inhibitors encoded by ORFV D1701-V would allow analyses on the compensation of NF-κB pathway inhibition.

As the activation of APCs correlates with their ability to present antigen and thus, to activate T cells, the expression of the activation markers CD80, CD83, CD86, CD40 and HLA-DR was studied in infected moDCs. Comprehensive analyses revealing the activation markers CD80, CD83 and the MHC class II molecule HLA-DR to be up-regulated in moDCs upon infection with recombinant ORFV D1701-V vectors were discussed recently [124]. Therefore, a special focus was laid on the differences between a reference recombinant ORFV D1701-V vector and the new Del-site recombinants each harboring an additional gene knockout. The deletion of ORF014 (PACR), 126 (ANK-1) and 127 (IL-10 ortholog) significantly increased the surface expression of some activation markers including CD83, CD86 and HLA-DR, while a ORF119 (NF-κB inhibitor) knockout resulted in significantly reduced HLA-DR expression. Notably, the deletion of ORF126 increased the surface expression of the three activation markers CD83, CD86 and HLA-DR significantly, which is in line with the positive correlation between CD83, CD86 and MHC class II expression reported in DCs of CD83(-/-) mice [285] and indicates a possible influence of the ORFV encoded protein ANK-1 on the activation of moDCs. Previously, ANK-1 was described to harbor a Pox protein Repeats of Ankyrin C-terminal (PRANC) domain representing a recognition module shown to interact with the Skp1-cullin1-F-box protein (SCF1)-type ubiquitin ligase [286-288], which generally results in the substrates' polyubiquitination and subsequent degradation via the proteasome [289-291]. Subsequent studies revealed ANK-1 to co-localize with the mitochondria [221], however, the importance or role mediated by the ankyrin repeat domain remains elusive. Mitochondria are known to play a fundamental role in the induction of innate immune responses against both RNA and DNA viruses, in which the activation of mitochondrial antiviral signalling proteins (MAVS) eventually leads to the stimulation of the IRF- and NF-κB pathway and thus, the expression of type I interferons and pro-inflammatory cytokines [292, 293]. Considering the up-regulation of CD83, CD86 and HLA-DR in moDCs infected with ORF126 knockout mutants, a potential influence of ANK-1 on the activation of MAVS should therefore be emphasized in future experiments.

As CD83 is involved in the regulation of T and B cell maturation, while HLA-DR and CD86 participate in delivering the first and second signal for T cell activation, respectively, deletion of ORF126 was expected to markedly influence the activation of PBMCs. However, studying the physiological effects of the ORF deletions on PBMCs revealed contradictory results. By measuring the expression of the activation marker CD69, almost all new Del-site recombinants except the mutant lacking ORF126 induced significantly elevated CD4, CD8 and NK cell populations expressing the activation marker. In fact, the ORF119 knockout mutant increased the CD4 T cell activation levels approximately 3-fold, while comparable effects could be detected for CD8 and NK cells. Thus, the up-regulation of moDC activation markers appears not to correlate with the activation of PBMCs. Accordingly, other approaches must be considered to explain these relationships. Potentially, the deletion of ORFs might also affect the expression of activating cytokines that impact the expression of CD69 [294, 295] and might thus explain the present results. Recently, analyses on the cytokine expression profiles of

ORFV D1701-V infected cells [124] revealed significantly enhanced concentrations of IL-6 and CXCL10 in the supernatants of infected moDCs, while also little amounts of IL-8 (CXCL8), CCL3 (MIP-1α) and CCL5 (RANTES) could be detected. In contrast, infection of PBMCs resulted in the production of CCL2 (MCP-1), MIP-1α, RANTES and CXCL10. These pro-inflammatory cytokines are involved in the formation of cellular adaptive immune responses and may thus be influenced by any of the deletions carried out in the new Del-site recombinants. For example, the CBP encoded by ORF112 binds many inflammatory and constitutive cytokines including the MCP-1, MIP-1α or RANTES with high affinity [214], while ORF119 is believed to impact the activation of NF-κB [206] as a key factor in the regulation of pro-inflammatory responses. A broad analysis on soluble and intracellular cytokine and chemokine expression profiles would thus be constructive to study the physiological effects of ORF deletions after infection *in vitro* and *in vivo* and might contribute significantly to explaining the present findings.

In addition, the immunogenicity of the new Del-site recombinants was examined by studying their capacity to induce antigen-specific immune responses. Therefore, new Del-site recombinants expressing either three distinct EBV, HCMV and Influenza A epitopes *in vitro*, or OVA *in vivo* were used. The results obtained from six donors harboring memory T cells specific for different combinations of the HCMV, Influenza A or EBV epitopes show high donor dependent variations in the amount of tetramer positive T cells following expansion, or functionality after re-stimulation with the respective synthetic peptides. Possibly, the activation and maturation status of isolated cells, or physiological factors like hormone levels known to influence the composition of immune cells might have influenced their ability to stimulate the T cells and could thus explain the high variance [124, 296]. Nevertheless, analyses on the expansion of antigen-specific memory CD8+ T cells depict in mean significantly increased populations of polyfunctional and antigen-specific T cells, which were induced by monocytes infected with ORFV D1701-V recombinants lacking ORF119. Therefore, the results generally allow two major conclusions: (i) ORFV D1701-V based recombinants are well suited as vectors for the simultaneous induction of immune responses against at least three distinct immunogenic antigens (EBV $BMLF1_{280-288}$, Influenza A $MP_{58-66}$ and HCMV $pp65_{495-503}$) and (ii) that the deletion of ORF119 significantly enhances the quantitative and polyfunctional antigen-specific cellular responses. To validate the results obtained *in vitro*, the immunogenicity of selected new Del-site recombinants expressing OVA was investigated *in vivo* using inbred mice. After the prime and boost immunizations administered i.v., the proportions of SIINFEKL-specific CD8+ T cells in mice immunized with recombinant ORFV D1701-V mutants lacking ORF024, 112, 126 and 128 were comparable to those immunized with the reference virus. Interestingly, mice immunized with the mutants lacking ORF112 and ORF126 showed the highest response with up to 75% antigen-specific CD8+ T cells. In concordance, especially T cells isolated from mice immunized with ORF112 knockout mutants revealed a high functionality represented by IFNγ, TNFα and CD107α production levels similar to the reference control. While the functionality of CD8+ T cells in mice immunized with the ORF126 knockout mutant was reduced, both, the mutants lacking ORF112 and ORF 126 were capable of eliciting

elevated amounts of OVA-specific IgG1 and significantly increased IgG2c antibody titers indicating seroconversion.

## 4.2 Characterization of Ipilimumab and Avelumab expressing ORFV recombinants

ICIs have been proven to elicit impressive and beneficial antitumor activity in clinical trials and have thus been considered the "breakthrough of the year" in 2013 as they mark a turning point in unleashing the immune system against tumors [297]. To this end however, cases of immune-related adverse events (irAEs) have been reported that relate to the drug's normal tissue exposure by systemic application [240, 255, 256] emphasizing the local production of ICIs using gene therapy approaches [258-262]. In this way, ICIs produced at the tumor site can efficiently block checkpoint interactions leading to T cell activation and priming, which reduces the risk of irAEs associated with systemically applied ICIs. To tie in with the recent successes following this strategy, ORFV D1701-V was subjected to insertion of Ipilimumab and Avelumab coding sequences and subsequent proof of principle studies. Western blot analyses demonstrated the correct expression of both, heavy and light chains, as well as full length antibodies, while an indirect ELISA developed to study the expression kinetics and functionality of ORFV-D1701-V expressed ICIs indicated the formation of stable antibodies whose titers peaked 72-96 h after infection. To exemplarily validate the functionality of an ORFV D1701-V expressed antibody, a commercially available bioassay was used that demonstrated efficient blockade of PD-1/PD-L1 by Avelumab produced by infected Vero cells. Therefore it is concluded that ORFV D1701-V based recombinants are suitable for the expression of antibodies.

## 4.3 Conclusion and Outlook

Taken together, the analyses on the new Del-site recombinants performed *in vitro* and *in vivo* demonstrate a high potential for the design of polyvalent, single vectored vaccines by integrating at least three knockouts into the ORFV D1701-V genome. The deletion of ORF112, ORF119 and ORF126 and simultaneous integration of the reporter construct GFP into the respective Del-site resulted not only in efficient replication of stable vectors expressing the desired transgenes, but also attributed remarkable immunogenicity properties to the newly generated recombinants. Accordingly, the deletion of ORF112 is abolishing the ORFV induced expression of a CBP, which was shown to bind several inflammatory CC-chemokines such as MCP-1, MIP-1α or RANTES [214] and found to be expressed by moDCs and PBMCs infected with recombinant ORFV D1701-V [124]. Furthermore, its deletion was shown to strongly reduce the virulence and pathogenesis of ORFV in sheep [215], which contributes significantly to safety aspects of the viral vector, and to favor the influx of NK cells, monocytes/macrophages and granulocytes to the site of infection [298]. In addition to binding CC-chemokines, the interaction of CBP with the C-chemokine lymphotactin involved in the chemotaxis of T cells, neutrophils and B cells was reported [299-301]. Therefore, the lack of CBP might constitute an important factor driving especially the B cell responses displayed as increased OVA-specific antibody titers in the *in vivo* experiments. ORF119 has been reported to interact

with the retinoblastoma protein pRB and thus to inhibit the TNFα-induced IKK activation and NF-κB signaling [206], while a more recent report proclaims its involvement in cell proliferation and apoptosis in order to facilitate the release of viral particles [207]. Although a positive effect on the activation of the NF-κB pathway upon deletion of ORF119 could not be shown and needs to be validated, this study revealed elevated CD4 and CD8 T cell, as well as NK cell activation levels and the induction of enhanced antigen-specific CD8+ T cell responses and poly-functionality *in vitro*. Interestingly, proportions of viable cells in groups infected with the ORF119 knockout mutant were raised compared to other groups supporting the involvement of ORF119 in the induction of apoptosis [207]. *In vivo* investigations on the immunogenicity of this promising mutant thus needs to be stressed in the future. Finally, the deletion mutant lacking ORF126 encoding for ANK-1 was shown to stimulate an enhanced expression of moDC activation markers *in vitro* and elicited similar cellular and superior humoral responses compared to the reference mutant *in vivo*. Moreover, expression kinetics on GFP inserted into the Del-site 126 led to the strongest reporter levels indicating its suitability for strong transgene expression. Thus, the findings of the present study may pave the way for the generation of ORFV D1701-V vectored vaccines with favorable properties, in which recombinants harboring ORF112, ORF119 and ORF126 deletions, or combinations thereof, simultaneously expressing several antigens and immunomodulatory elements from the *vegf*-locus and Del-site 126 lead to the induction of strong, long-lasting and efficient cellular as well as humoral immune responses. In order to ensure feasibility for virus up-scaling during production, vectors based on the suggested combinations are highly recommended to be tested for genetic stability and replication efficiency.

In the frame of the characterization of Ipilimumab and Avelumab expressing ORFV recombinants, western blot analyses indicate stronger light than heavy chain expression. Therefore, an expression of heavy chains under the control of the strong promoter eP2 and an expression of light chains under the control of Pv might result in optimized functional full-length antibody production titers [84]. An exchange of the present heavy and light chains would thus be constructive, while fine-tuning may also be achieved using several different synthetic ORFV promoters currently under investigation. Further, the therapeutic gain and efficacy of this immunovirotherapy needs to be assessed in the future by *in vivo* experiments, e.g by using C57BL/6 mice with subcutaneous B16-CD20 tumors as described by Engeland et al. [259]. Nevertheless, the findings presented in this work open further new possibilities for the generation of polyvalent, single vectored ORFV D1701-V vaccines combining disease related antigens with a plethora of immunomodulatory elements like ICIs, but also stimulatory antibodies for increased immune responses and the treatment of cancers.

# 5 Supplementary Information

## 5.1 Plasmid Charts of generated Transfer plasmids

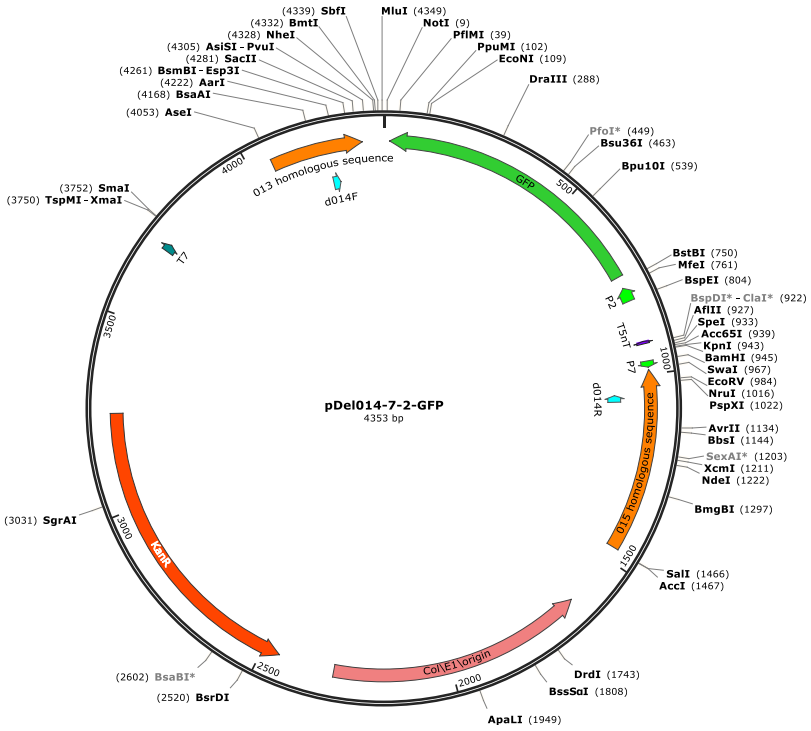


**Figure S38: Plasmid chart of pDel014-7-2-GFP.**

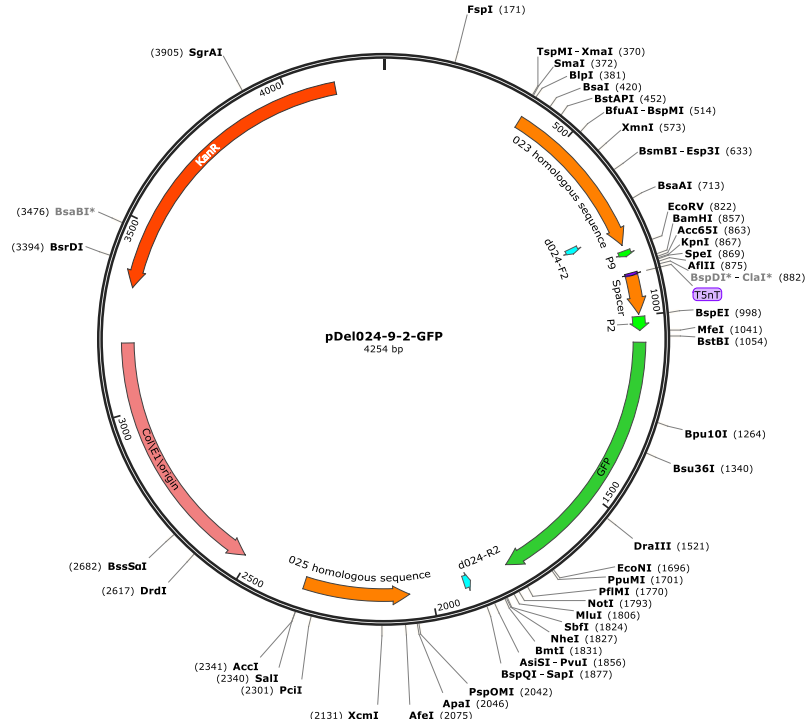


**Figure S39: Plasmid chart of pDel024-9-2-GFP.**

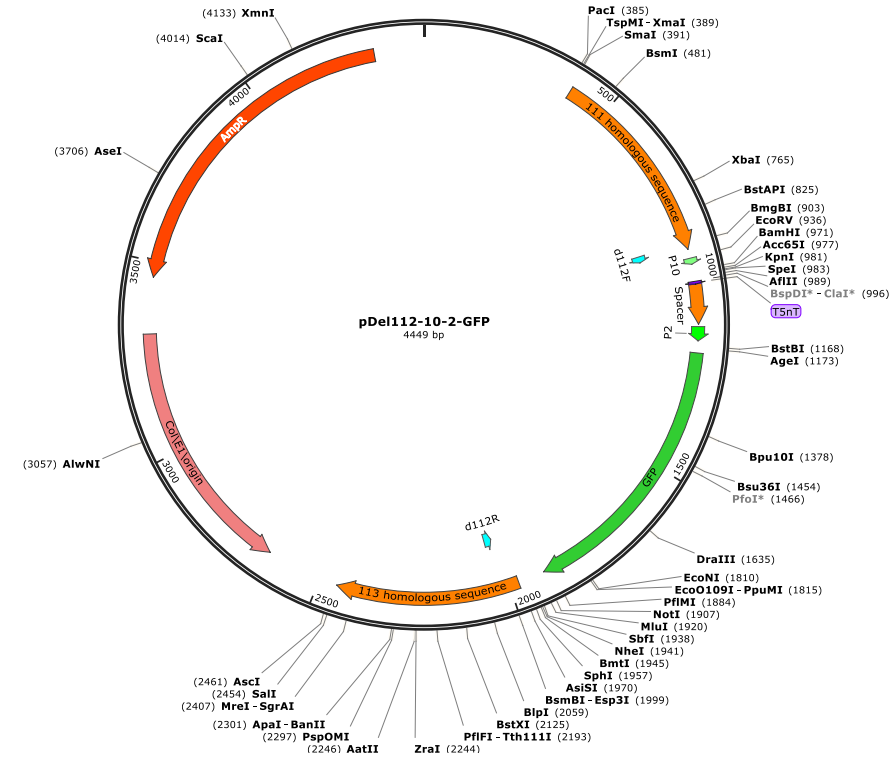


**Figure S40: Plasmid chart of pDel112-10-2-GFP.**

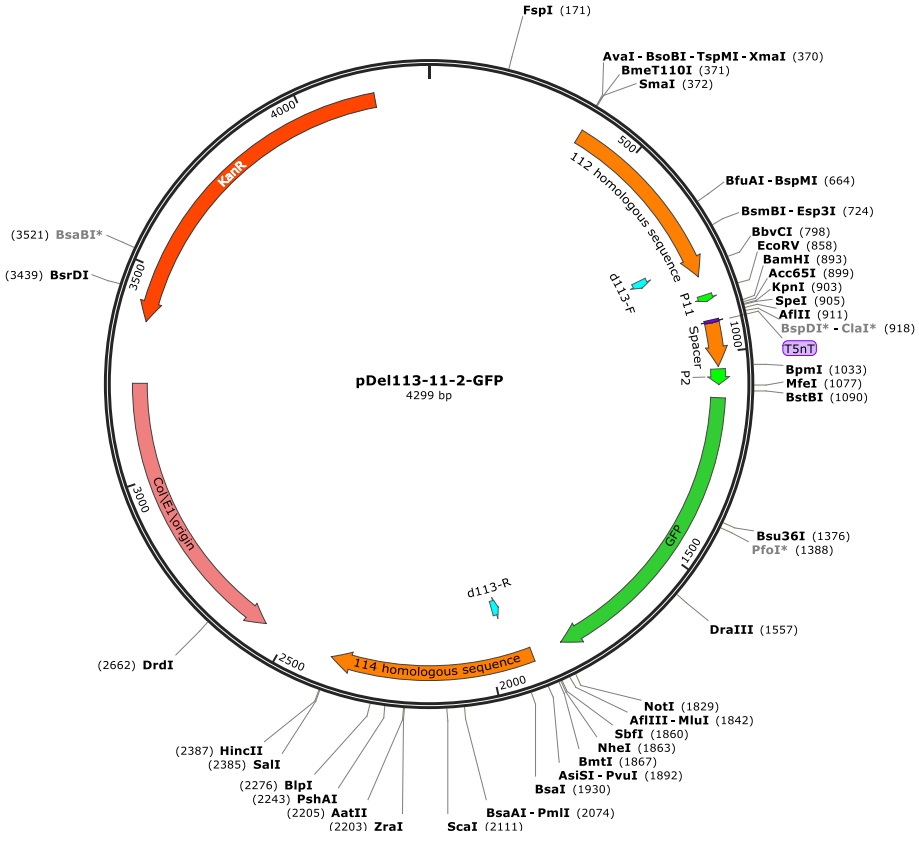


**Figure S41: Plasmid chart of pDel113-11-2-GFP.**

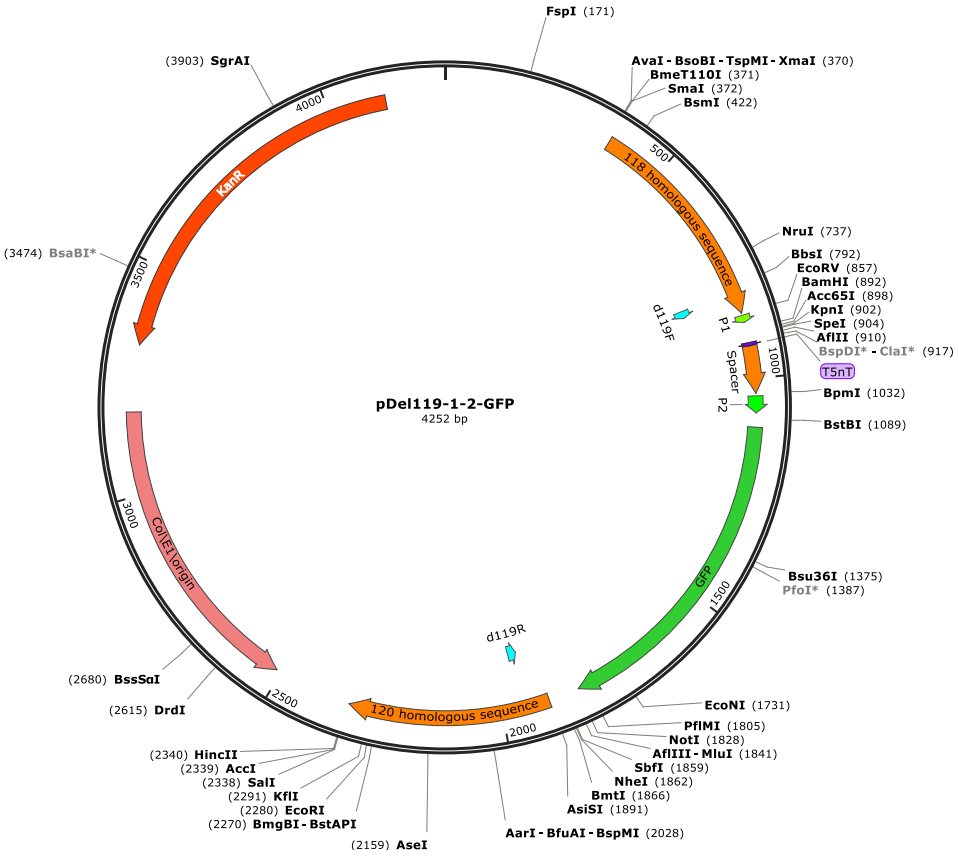


**Figure S42: Plasmid chart of pDel119-1-2-GFP.**

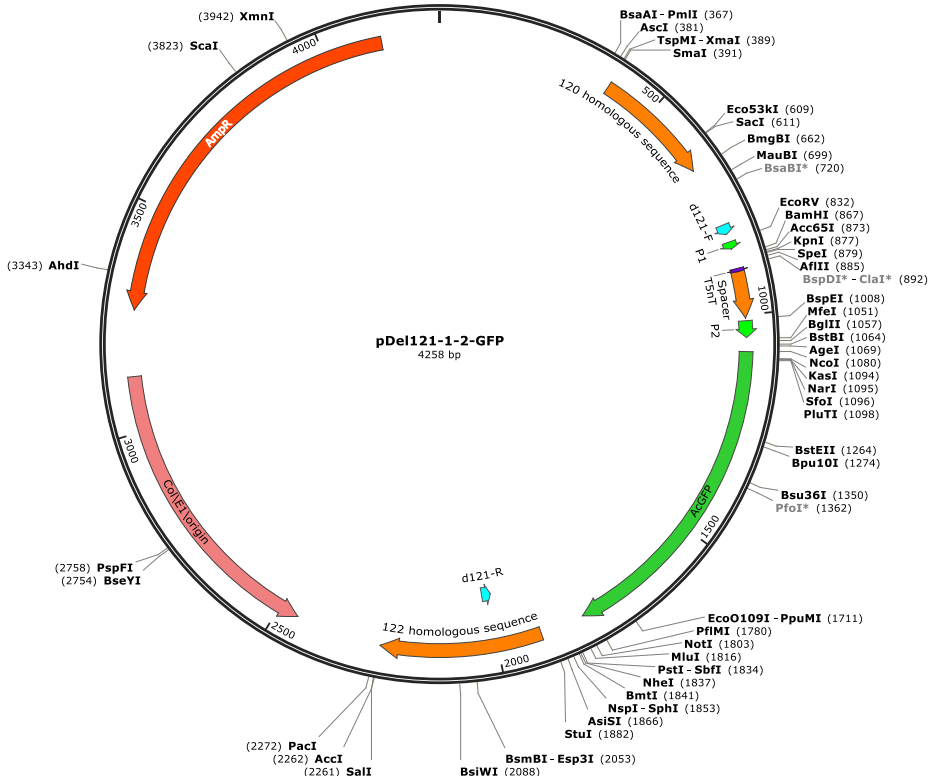


**Figure S43: Plasmid chart of pDel121-2-GFP.**

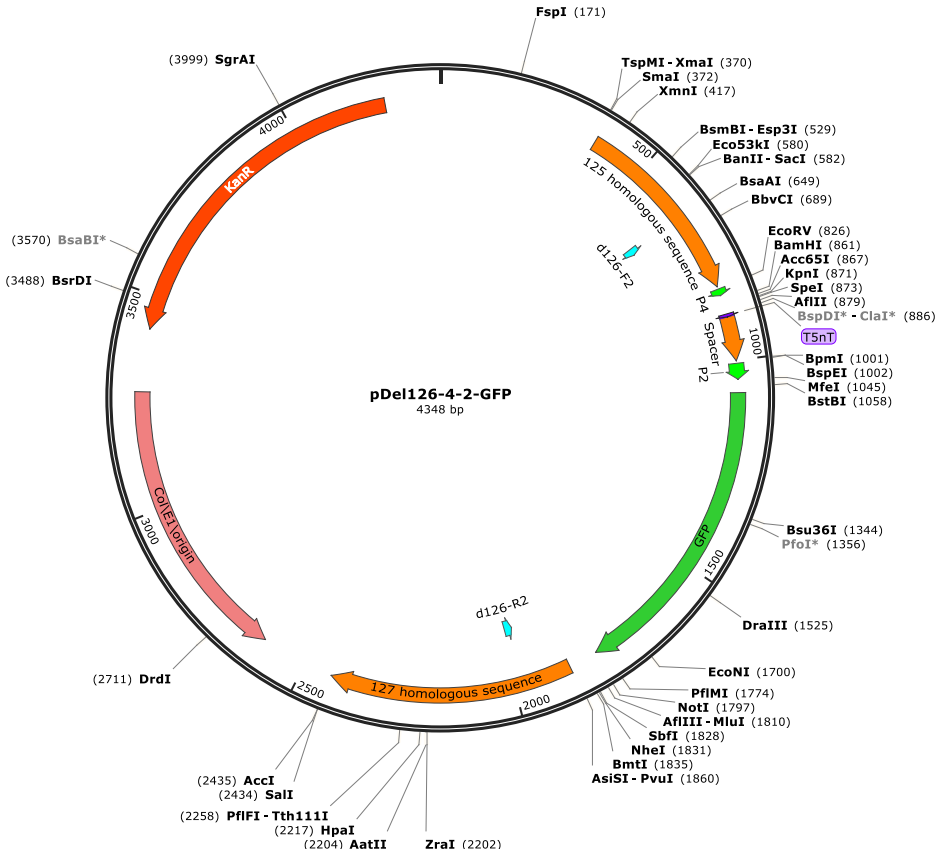


**Figure S44: Plasmid chart of pDel126-4-2-GFP.**

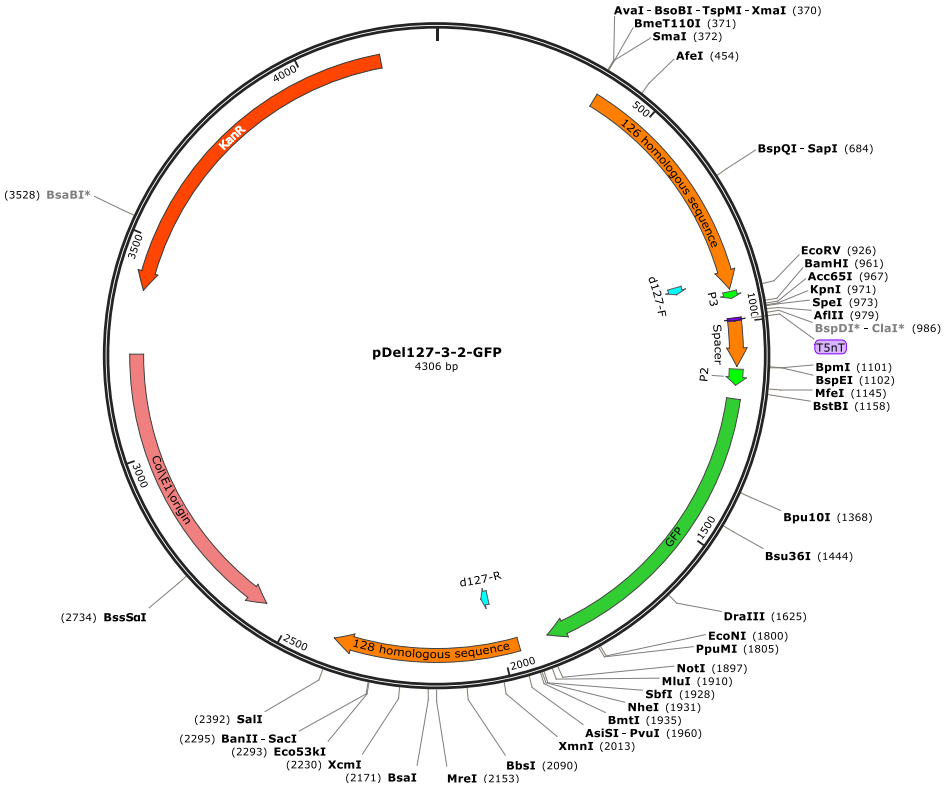


**Figure S45: Plasmid chart of pDel127-3-2-GFP.**

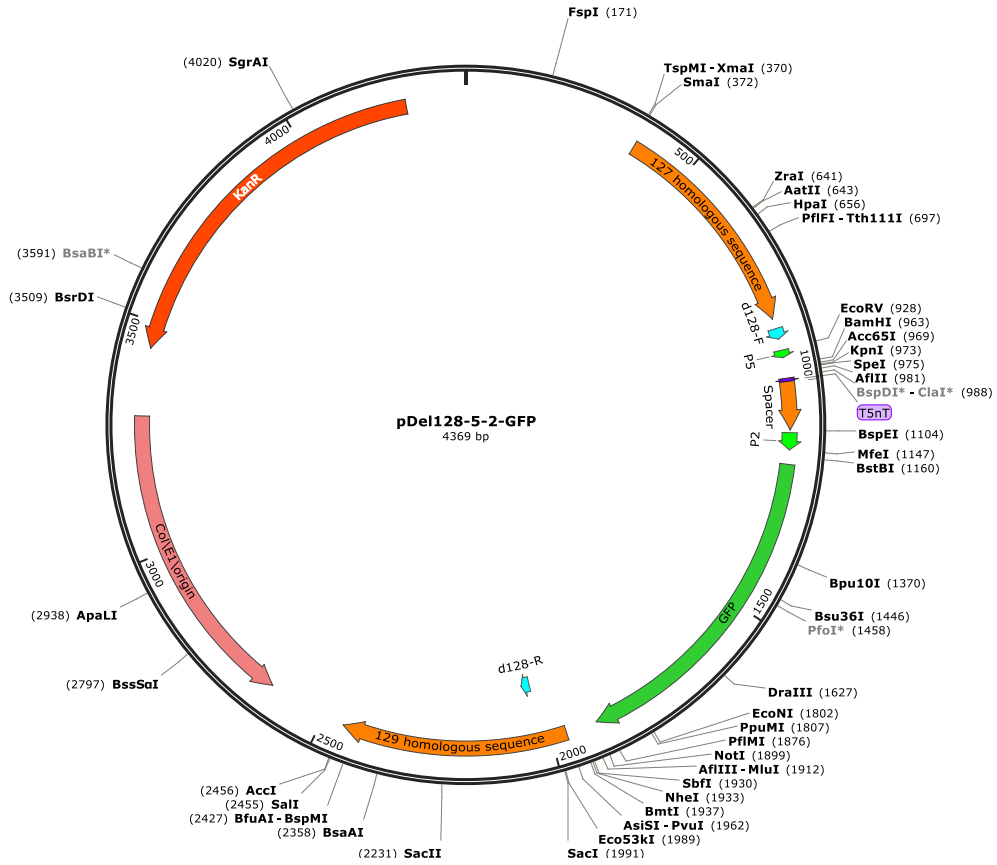


**Figure S46: Plasmid chart of pDel128-5-2-GFP.**

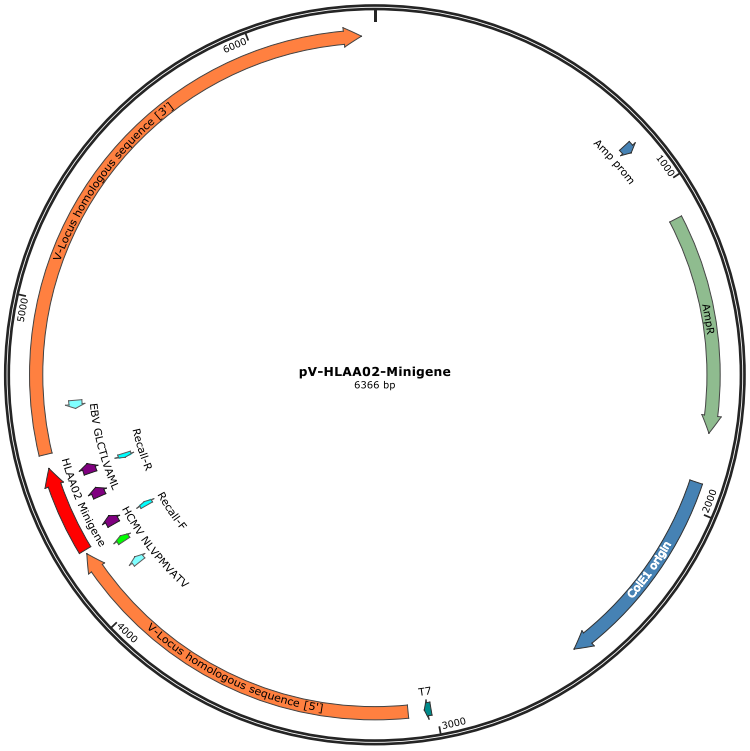


**Figure S47: Plasmid chart of pV-HLAA02-Minigene.**

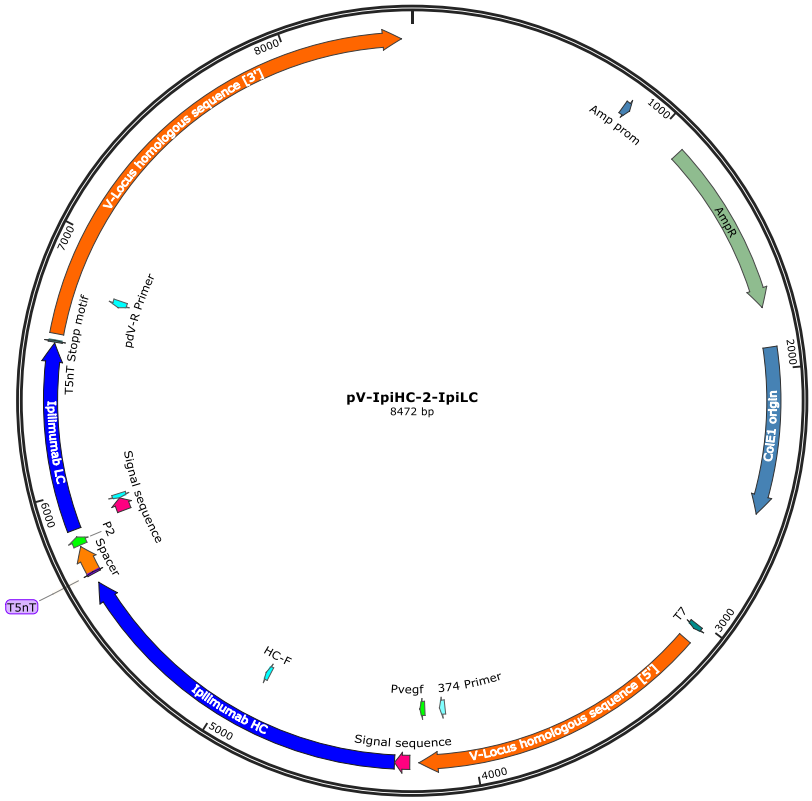


**Figure S48: Plasmid chart of pV-IpiHC-2-IpiLC.**

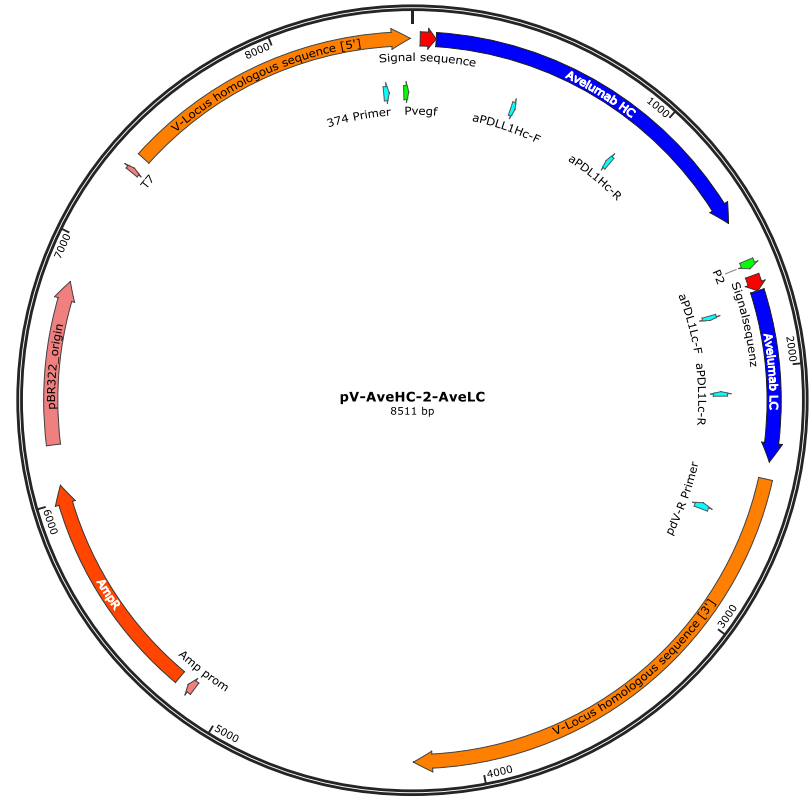


**Figure S49: Plasmid chart of pV-AveHC-2-AveLC.**

## 5.2 Generation of ORFV recombinants

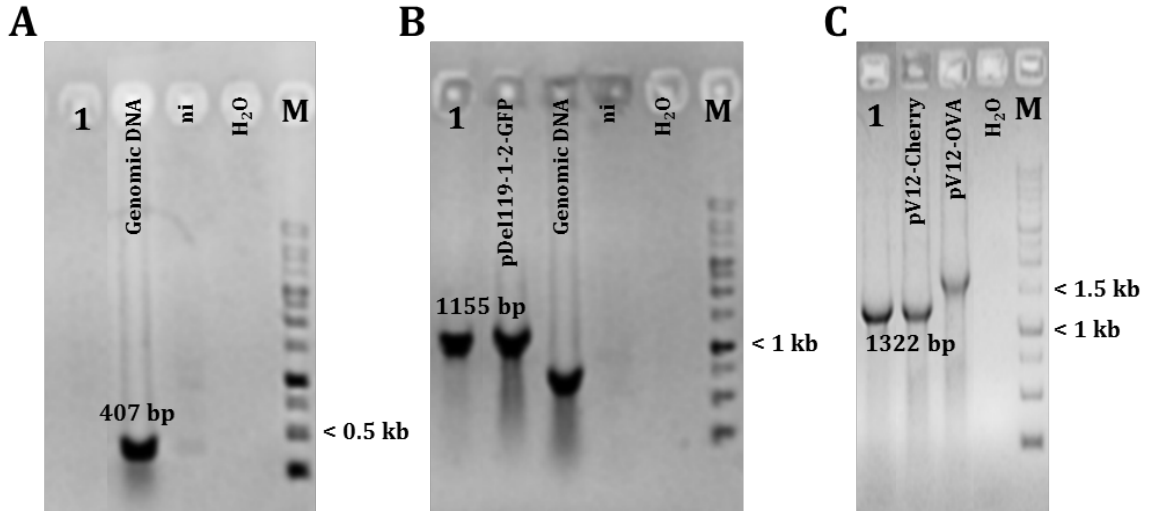


**Figure S50: PCR typing of purified Del-site recombinant VCh119GFP. Genetic homogeneity of the Del119-locus was verified by PCRs 119 showing a loss of the ORF119 specific 407 bp fragment (A) and d119 showing the integration of GFP by detection of a specific 1155 bp fragment (B). Further, a *vegf*-locus PCR could confirm the mCherry integration by detection of a specific 1322 bp fragment (C). 1% agarose gel; 1 = DNA from VCh119GFP recombinant; ni = DNA from not infected Vero cells; M = Ready-To-Use 1 kb Ladder, Nippon Genetics.**

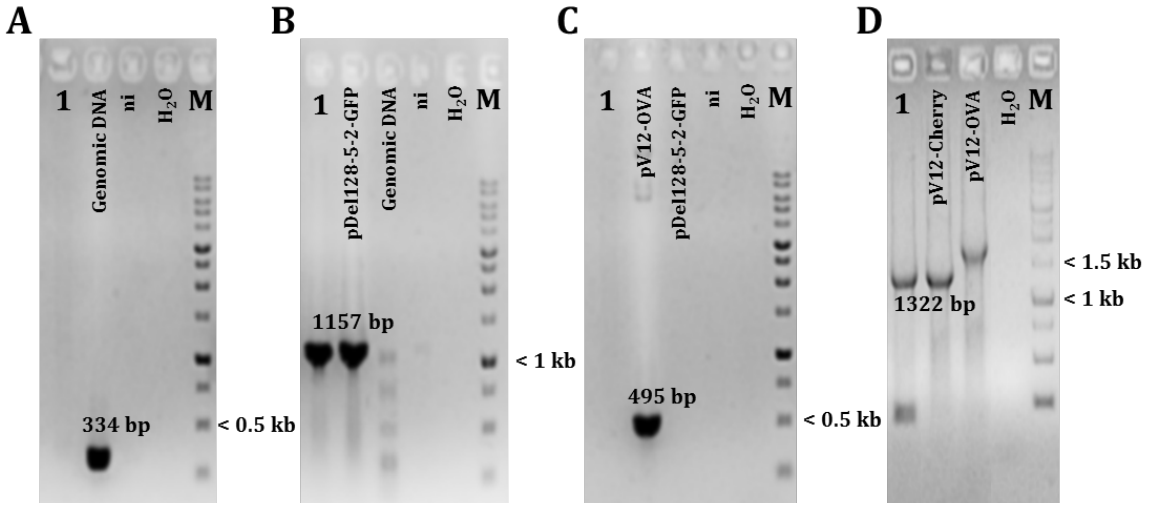


**Figure S51: PCR typing of purified Del-site recombinant VCh128GFP. Genetic homogeneity of the Del128-locus was verified by PCRs 128 showing a loss of the ORF128 specific 334 bp fragment (A) and d128 showing the integration of GFP by detection of a specific 1157 bp fragment (B). Further, the OVA PCR detected the OVA specific 495 bp fragment (C), while a *vegf*-locus PCR could confirm the mCherry integration by detection of a specific 1322 bp fragment (D). 1% agarose gel; 1 = DNA from VCh128GFP recombinant; ni = DNA from not infected Vero cells; M = Ready-To-Use 1 kb Ladder, Nippon Genetics.**

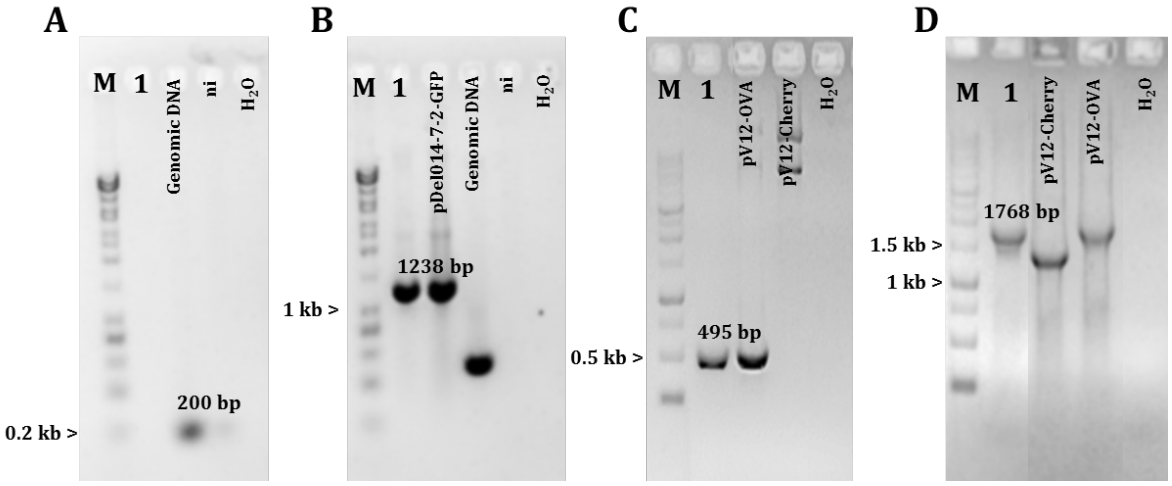


**Figure S52: PCR typing of purified Del-site recombinant VOVA014GFP. Genetic homogeneity of the Del014-locus was verified by PCRs 014 showing a loss of the ORF014 specific 200 bp fragment (A) and d014 showing the integration of GFP by detection of a specific 1238 bp fragment (B). Further, the OVA PCR detected the OVA specific 495 bp fragment (C), while a *vegf*-locus PCR could confirm the OVA integration by detection of a specific 1768 bp fragment (D). 1% agarose gel; 1 = DNA from VOVA014GFP recombinant; ni = DNA from not infected Vero cells; M = HyperLadder I, Bioline (A, B) or Ready-To-Use 1 kb Ladder, Nippon Genetics (C, D).**

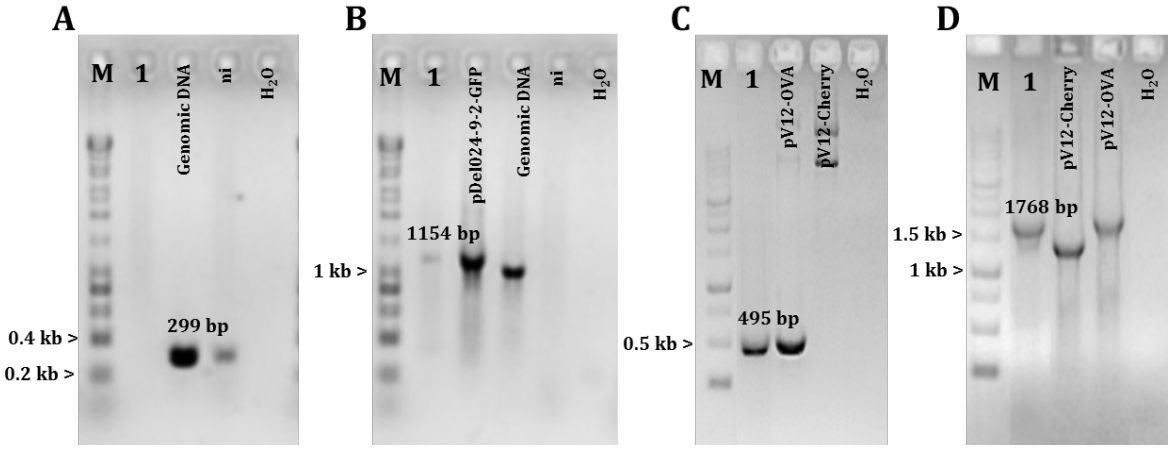


**Figure S53: PCR typing of purified Del-site recombinant VOVA024GFP. Genetic homogeneity of the Del024-locus was verified by PCRs 024 showing a loss of the ORF024 specific 299 bp fragment (A) and d024 showing the integration of GFP by detection of a specific 1154 bp fragment (B). Further, the OVA PCR detected the OVA specific 495 bp fragment (C), while a *vegf*-locus PCR could confirm the OVA integration by detection of a specific 1768 bp fragment (D). 1% agarose gel; 1 = DNA from VOVA024GFP recombinant; ni = DNA from not infected Vero cells; M = HyperLadder I, Bioline (A, B) or Ready-To-Use 1 kb Ladder, Nippon Genetics (C, D).**

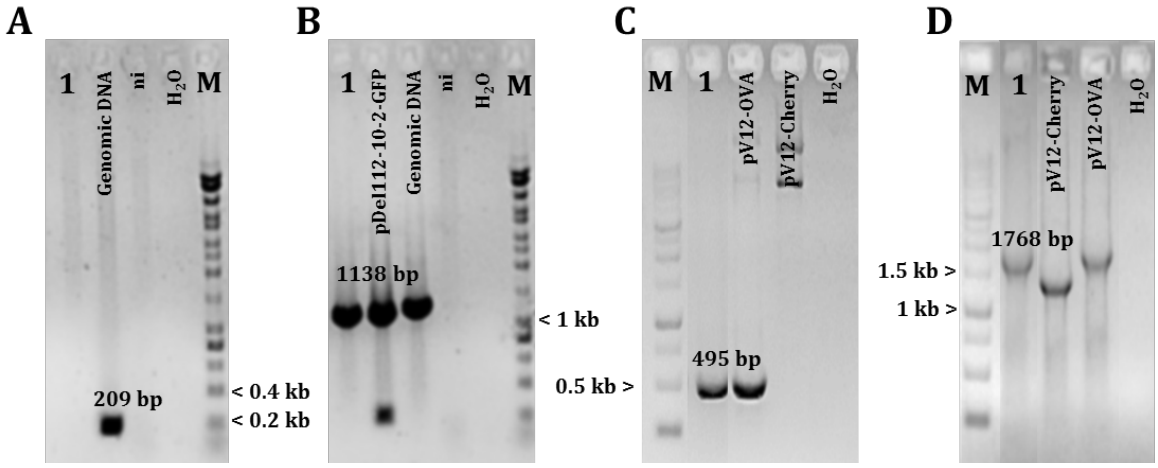


**Figure S54: PCR typing of purified Del-site recombinant VOVA112GFP. Genetic homogeneity of the Del112-locus was verified by PCRs 112 showing a loss of the ORF112 specific 209 bp fragment (A) and d112 showing the integration of GFP by detection of a specific 1138 bp fragment (B). Further, the OVA PCR detected the OVA specific 495 bp fragment (C), while a *vegf*-locus PCR could confirm the OVA integration by detection of a specific 1768 bp fragment (D). 1% agarose gel; 1 = DNA from VOVA112GFP recombinant; ni = DNA from not infected Vero cells; M = HyperLadder I, Bioline (A, B) or Ready-To-Use 1 kb Ladder, Nippon Genetics (C, D).**

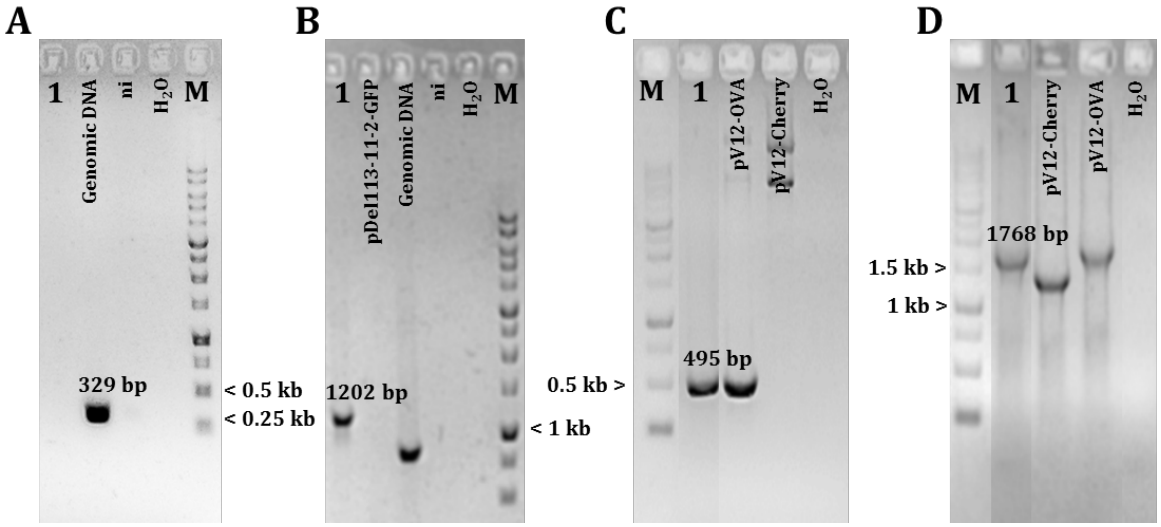


**Figure S55: PCR typing of purified Del-site recombinant VOVA113GFP. Genetic homogeneity of the Del113-locus was verified by PCRs 113 showing a loss of the ORF113 specific 329 bp fragment (A) and d113 showing the integration of GFP by detection of a specific 1202 bp fragment (B). Further, the OVA PCR detected the OVA specific 495 bp fragment (C), while a *vegf*-locus PCR could confirm the OVA integration by detection of a specific 1768 bp fragment (D). 1% agarose gel; 1 = DNA from VOVA113GFP recombinant; ni = DNA from not infected Vero cells; M = Ready-To-Use 1 kb Ladder, Nippon Genetics.**

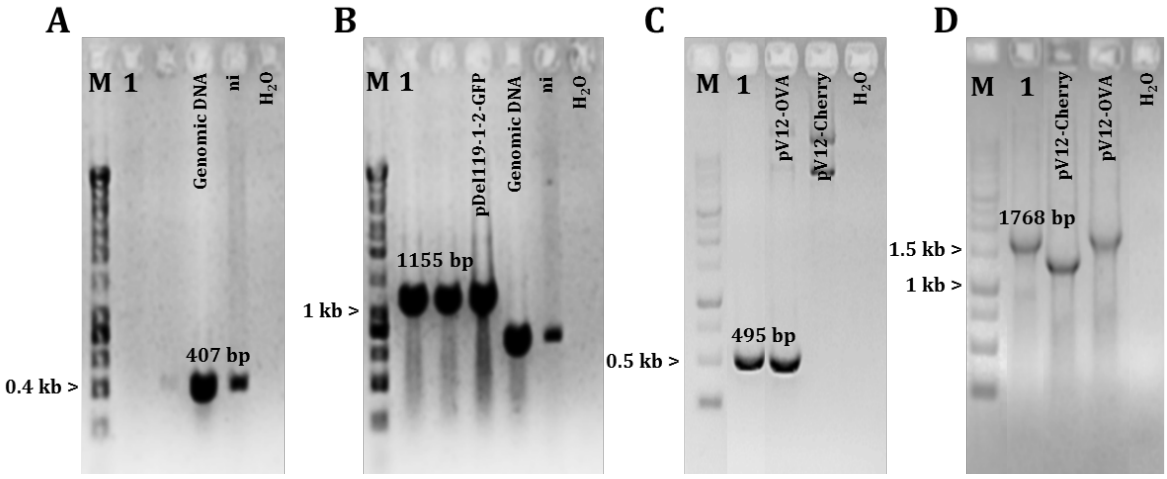


**Figure S56: PCR typing of purified Del-site recombinant VOVA119GFP. Genetic homogeneity of the Del119-locus was verified by PCRs 119 showing a loss of the ORF119 specific 407 bp fragment (A) and d119 showing the integration of GFP by detection of a specific 1155 bp fragment (B). Further, the OVA PCR detected the OVA specific 495 bp fragment (C), while a *vegf*-locus PCR could confirm the OVA integration by detection of a specific 1768 bp fragment (D). 1% agarose gel; 1 = DNA from VOVA119GFP recombinant; ni = DNA from not infected Vero cells; M = HyperLadder I, Bioline (A, B) or Ready-To-Use 1 kb Ladder, Nippon Genetics (C, D).**

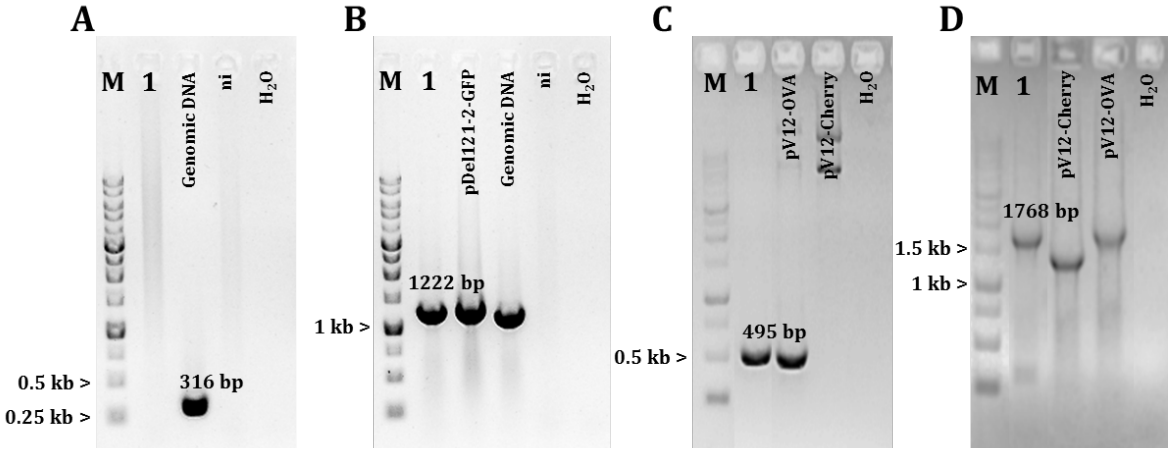


**Figure S57: PCR typing of purified Del-site recombinant VOVA121GFP. Genetic homogeneity of the Del121-locus was verified by PCRs 121 showing a loss of the ORF121 specific 316 bp fragment (A) and d121 showing the integration of GFP by detection of a specific 1222 bp fragment (B). Further, the OVA PCR detected the OVA specific 495 bp fragment (C), while a *vegf*-locus PCR could confirm the OVA integration by detection of a specific 1768 bp fragment (D). 1% agarose gel; 1 = DNA from VOVA121GFP recombinant; ni = DNA from not infected Vero cells; M = Ready-To-Use 1 kb Ladder, Nippon Genetics.**

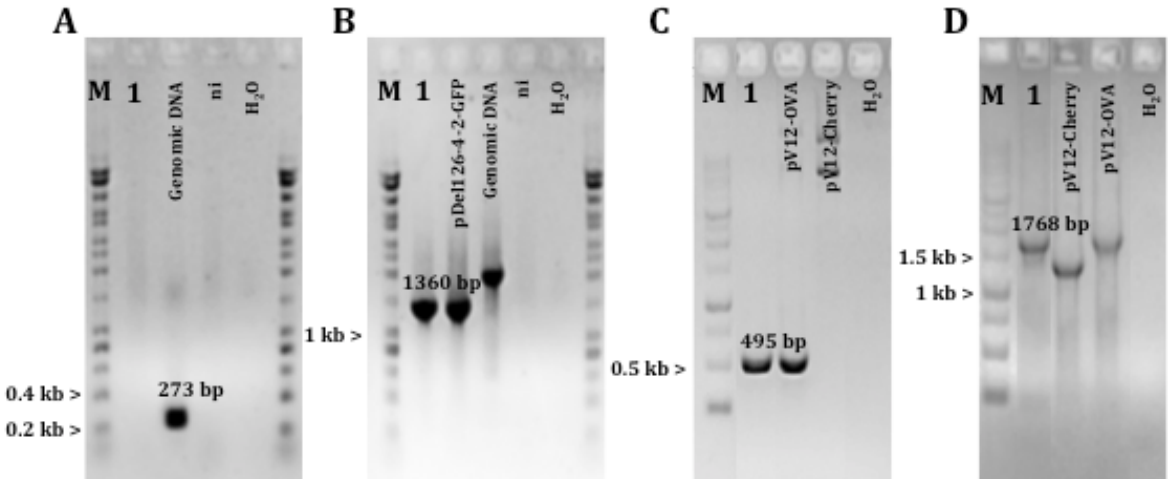


**Figure S58: PCR typing of purified Del-site recombinant VOVA126GFP. Genetic homogeneity of the Del126-locus was verified by PCRs 126 showing a loss of the ORF126 specific 273 bp fragment (A) and d126 showing the integration of GFP by detection of a specific 1360 bp fragment (B). Further, the OVA PCR detected the OVA specific 495 bp fragment (C), while a *vegf*-locus PCR could confirm the OVA integration by detection of a specific 1768 bp fragment (D). 1% agarose gel; 1 = DNA from VOVA126GFP recombinant; ni = DNA from not infected Vero cells; M = HyperLadder I, Bioline (A, B) or Ready-To-Use 1 kb Ladder, Nippon Genetics (C, D).**

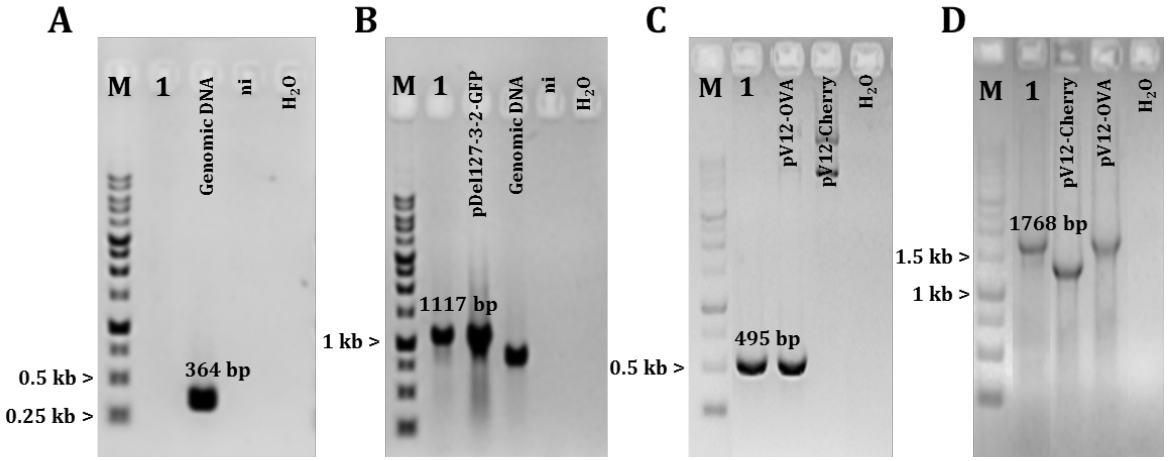


**Figure S59: PCR typing of purified Del-site recombinant VOVA127GFP. Genetic homogeneity of the Del127-locus was verified by PCRs 127 showing a loss of the ORF127 specific 364 bp fragment (A) and d127 showing the integration of GFP by detection of a specific 1117 bp fragment (B). Further, the OVA PCR detected the OVA specific 495 bp fragment (C), while a *vegf*-locus PCR could confirm the OVA integration by detection of a specific 1768 bp fragment (D). 1% agarose gel; 1 = DNA from VOVA127GFP recombinant; ni = DNA from not infected Vero cells; M = Ready-To-Use 1 kb Ladder, Nippon Genetics.**

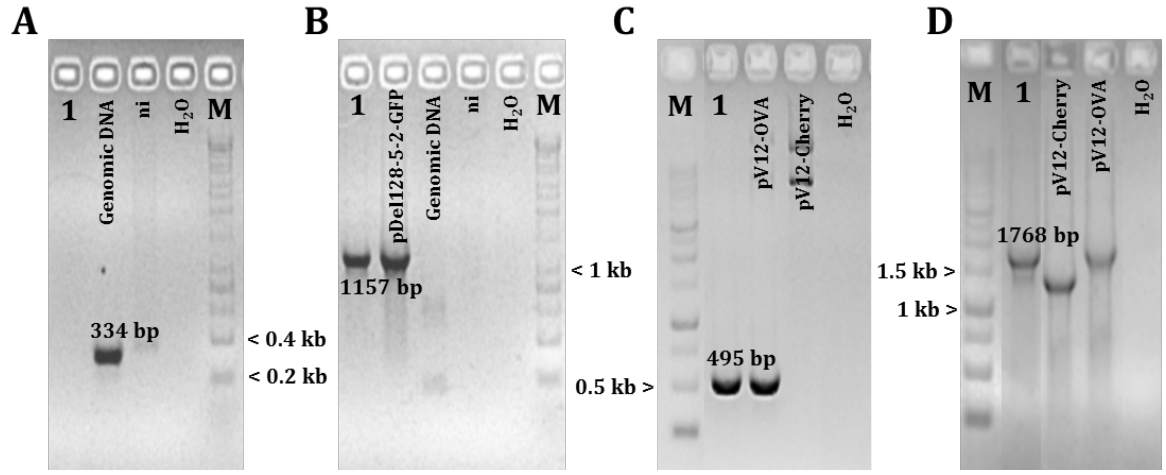


**Figure S60: PCR typing of purified Del-site recombinant VOVA128GFP. Genetic homogeneity of the Del128-locus was verified by PCRs 128 showing a loss of the ORF128 specific 334 bp fragment (A) and d128 showing the integration of GFP by detection of a specific 1157 bp fragment (B). Further, the OVA PCR detected the OVA specific 495 bp fragment (C), while a *vegf*-locus PCR could confirm the OVA integration by detection of a specific 1768 bp fragment (D). 1% agarose gel; 1 = DNA from VOVA128GFP recombinant; ni = DNA from not infected Vero cells; M = HyperLadder I, Bioline (A, B) or Ready-To-Use 1 kb Ladder, Nippon Genetics (C, D).**

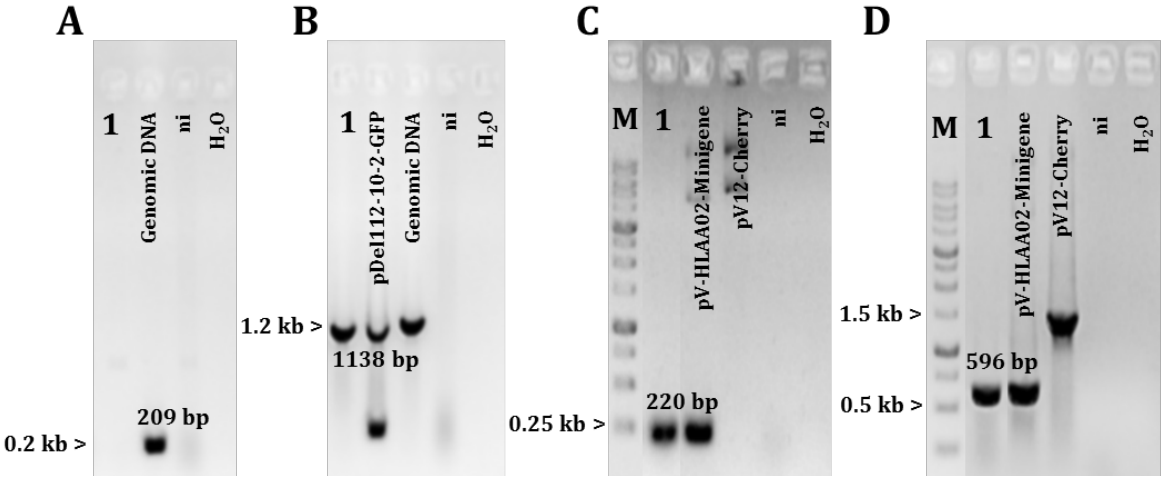


**Figure S61: PCR typing of purified Del-site recombinant VHLA112GFP. Genetic homogeneity of the Del112-locus was verified by PCRs 112 showing a loss of the ORF112 specific 209 bp fragment (A) and d112 showing the integration of GFP by detection of a specific 1138 bp fragment (B). Further, the Recall PCR detected the HLAA02 Minigene specific 220 bp fragment (C), while a *vegf*-locus PCR could confirm the Minigene integration by detection of a specific 596 bp fragment (D). 1% agarose gel; 1 = DNA from VHLA112GFP recombinant; ni = DNA from not infected Vero cells; M = Ready-To-Use 1 kb Ladder, Nippon Genetics.**

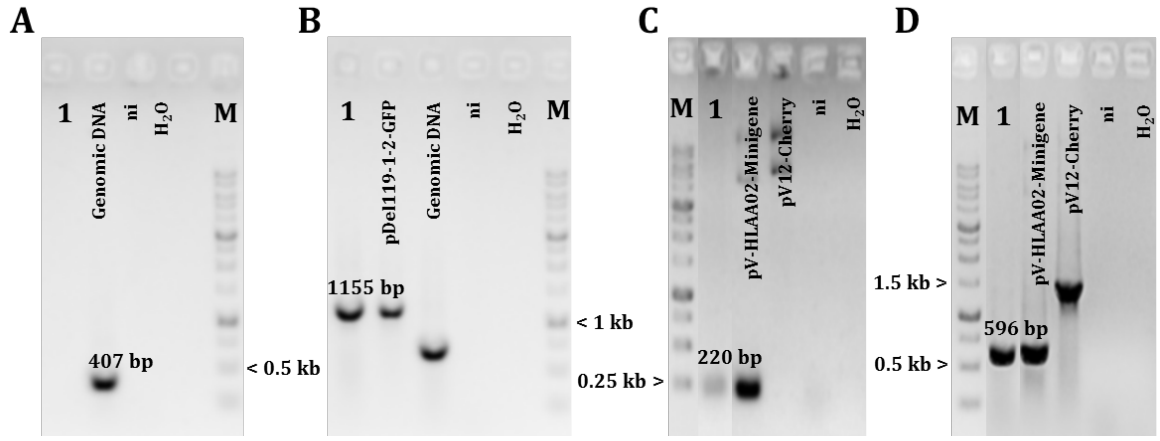


**Figure S62: PCR typing of purified Del-site recombinant VHLA119GFP. Genetic homogeneity of the Del119-locus was verified by PCRs 119 showing a loss of the ORF119 specific 407 bp fragment (A) and d119 showing the integration of GFP by detection of a specific 1155 bp fragment (B). Further, the Recall PCR detected the HLAA02 Minigene specific 220 bp fragment (C), while a *vegf*-locus PCR could confirm the Minigene integration by detection of a specific 596 bp fragment (D). 1% agarose gel; 1 = DNA from VHLA119GFP recombinant; ni = DNA from not infected Vero cells; M = Ready-To-Use 1 kb Ladder, Nippon Genetics.**

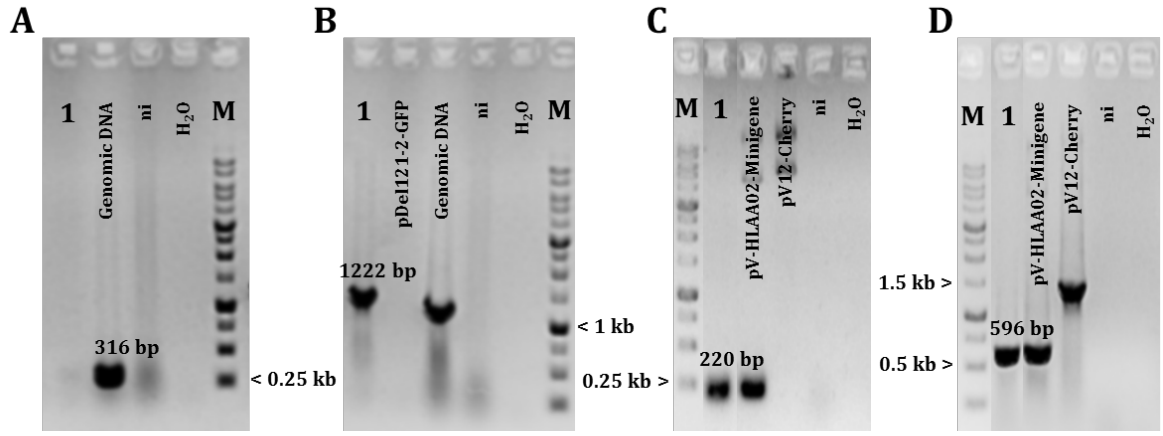


**Figure S63: PCR typing of purified Del-site recombinant VHLA121GFP. Genetic homogeneity of the Del121-locus was verified by PCRs 121 showing a loss of the ORF121 specific 316 bp fragment (A) and d121 showing the integration of GFP by detection of a specific 1222 bp fragment (B). Further, the Recall PCR detected the HLAA02 Minigene specific 220 bp fragment (C), while a *vegf*-locus PCR could confirm the Minigene integration by detection of a specific 596 bp fragment (D). 1% agarose gel; 1 = DNA from VHLA121GFP recombinant; ni = DNA from not infected Vero cells; M = Ready-To-Use 1 kb Ladder, Nippon Genetics.**

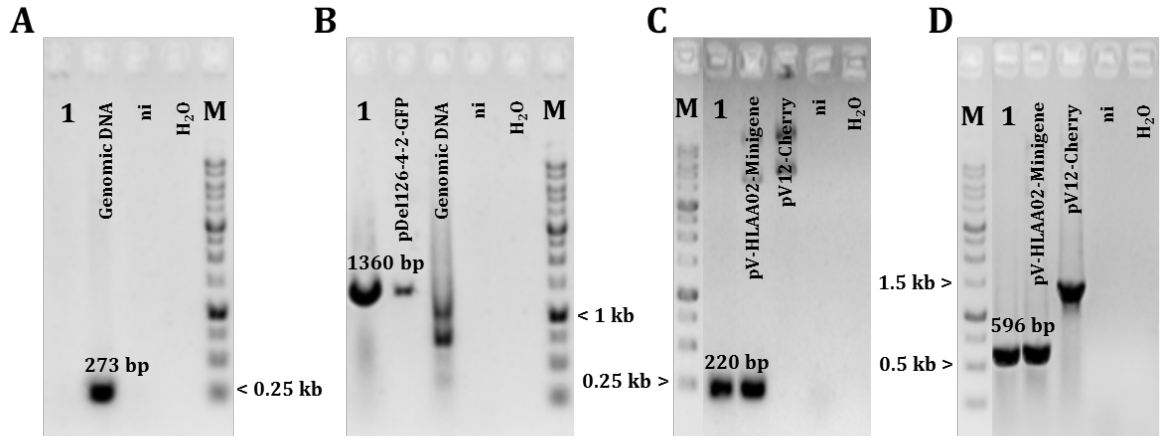


**Figure S64: PCR typing of purified Del-site recombinant VHLA126GFP. Genetic homogeneity of the Del126-locus was verified by PCRs 126 showing a loss of the ORF126 specific 273 bp fragment (A) and d126 showing the integration of GFP by detection of a specific 1360 bp fragment (B). Further, the Recall PCR detected the HLAA02 Minigene specific 220 bp fragment (C), while a *vegf*-locus PCR could confirm the Minigene integration by detection of a specific 596 bp fragment (D). 1% agarose gel; 1 = DNA from VHLA126GFP recombinant; ni = DNA from not infected Vero cells; M = Ready-To-Use 1 kb Ladder, Nippon Genetics.**

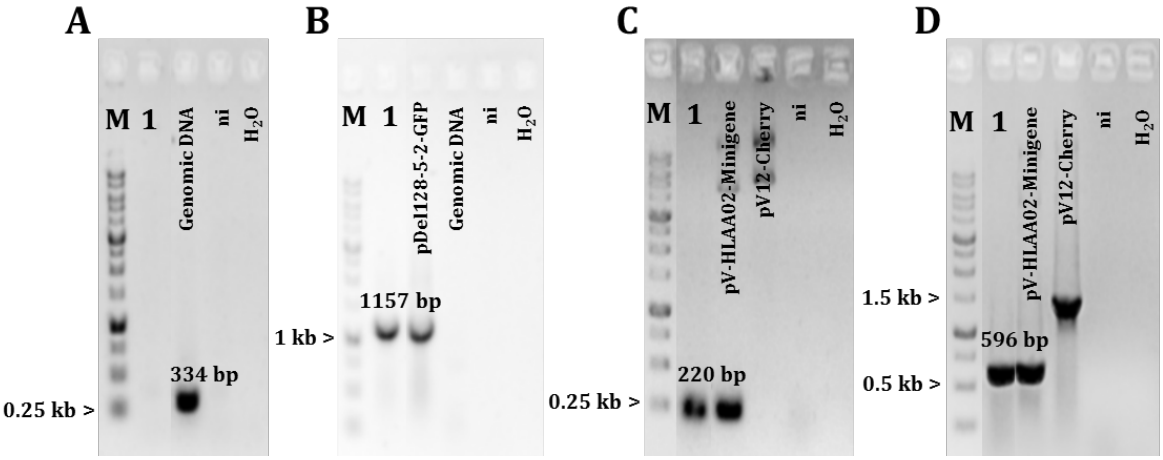


**Figure S65: PCR typing of purified Del-site recombinant VHLA128GFP. Genetic homogeneity of the Del128-locus was verified by PCRs 128 showing a loss of the ORF128 specific 334 bp fragment (A) and d128 showing the integration of GFP by detection of a specific 1157 bp fragment (B). Further, the Recall PCR detected the HLAA02 Minigene specific 220 bp fragment (C), while a *vegf*-locus PCR could confirm the Minigene integration by detection of a specific 596 bp fragment (D). 1% agarose gel; 1 = DNA from VHLA128GFP recombinant; ni = DNA from not infected Vero cells; M = Ready-To-Use 1 kb Ladder, Nippon Genetics.**

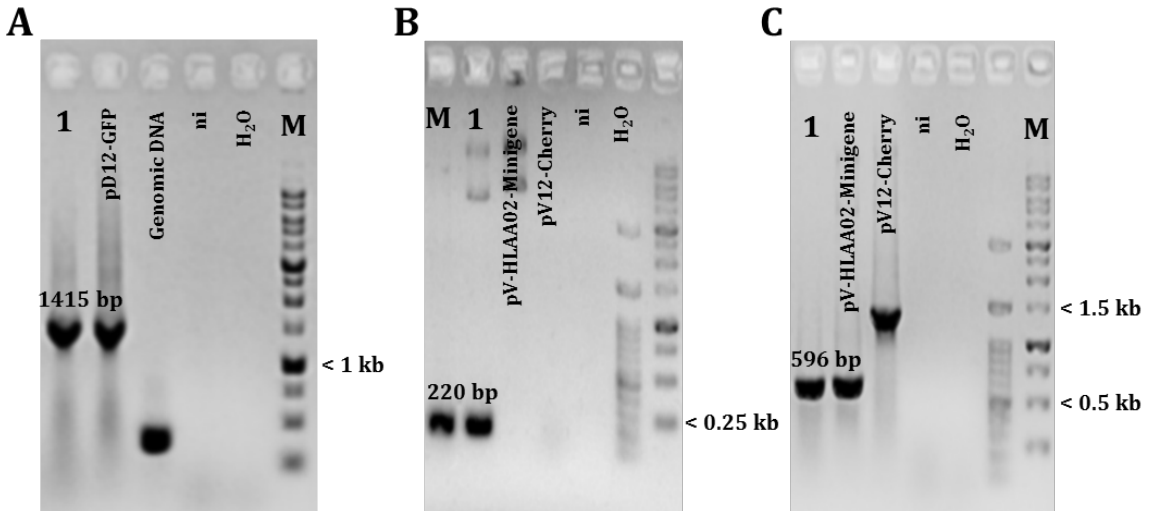


**Figure S66: PCR typing of purified Del-site recombinant VHLAD12GFP. Genetic homogeneity of the Del2-locus was verified by the Del2 PCR showing the integration of GFP by detection of a specific 1415 bp fragment (A). Further, the Recall PCR detected the HLAA02 Minigene specific 220 bp fragment (B), while a *vegf*-locus PCR could confirm the Minigene integration by detection of a specific 596 bp fragment (C). 1% agarose gel; 1 = DNA from VHLAD12GFP recombinant; ni = DNA from not infected Vero cells; M = Ready-To-Use 1 kb Ladder, Nippon Genetics.**

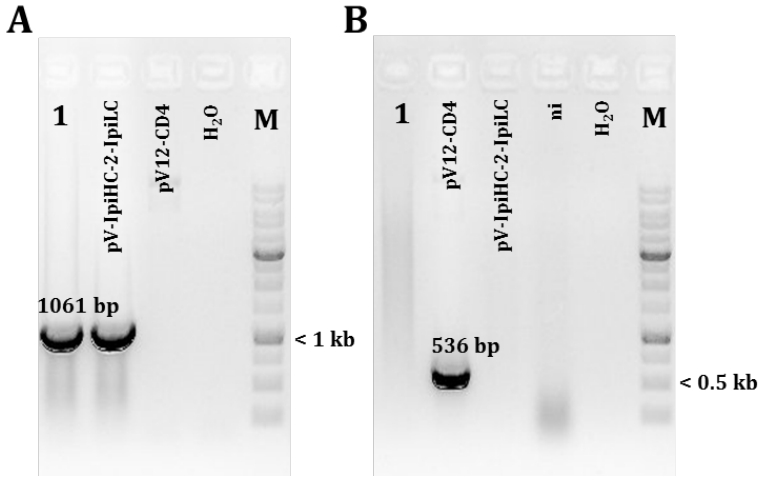


**Figure S67: PCR typing of purified ORFV recombinant Ipi-Ch. Genetic homogeneity of the *vegf*-locus was verified by the Ipilimumab PCR resulting in the detection of a specific 1061 bp fragment (A). Further, a CD4 PCR confirmed the loss of a specific 536 bp fragment as the result of successful homologous recombination (B). 1% agarose gel; 1 = DNA from Ipi-Ch recombinant; ni = DNA from not infected Vero cells; M = Ready-To-Use 1 kb Ladder, Nippon Genetics.**

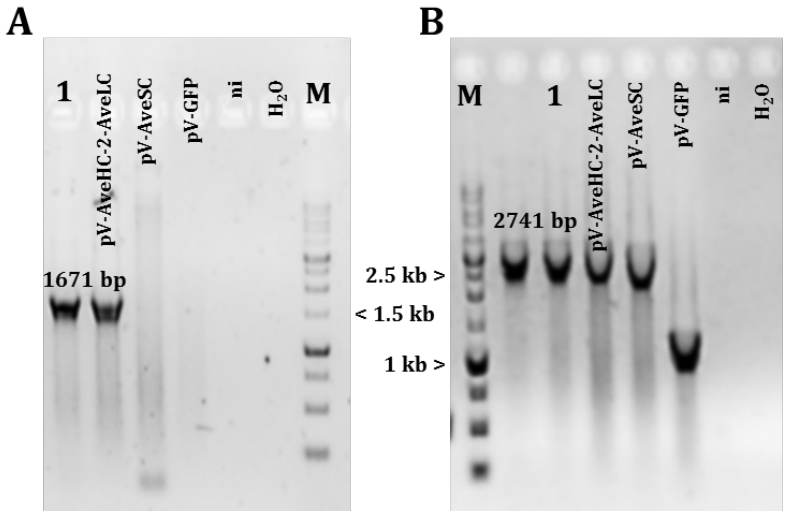


**Figure S68: PCR typing of purified ORFV recombinant Ave-Ch. Genetic homogeneity of the *vegf*-locus was verified by the Avelumab PCR resulting in the detection of a specific 1671 bp fragment (A). Further, a *vegf*-locus PCR confirmed the integration of Avelumab by detection of a specific 2741 bp fragment (B). 1% agarose gel; 1 = DNA from Ave-Ch recombinant; ni = DNA from not infected Vero cells; M = Ready-To-Use 1 kb Ladder, Nippon Genetics.**

## 5.3 Stable insertion of GFP into new Del-sites

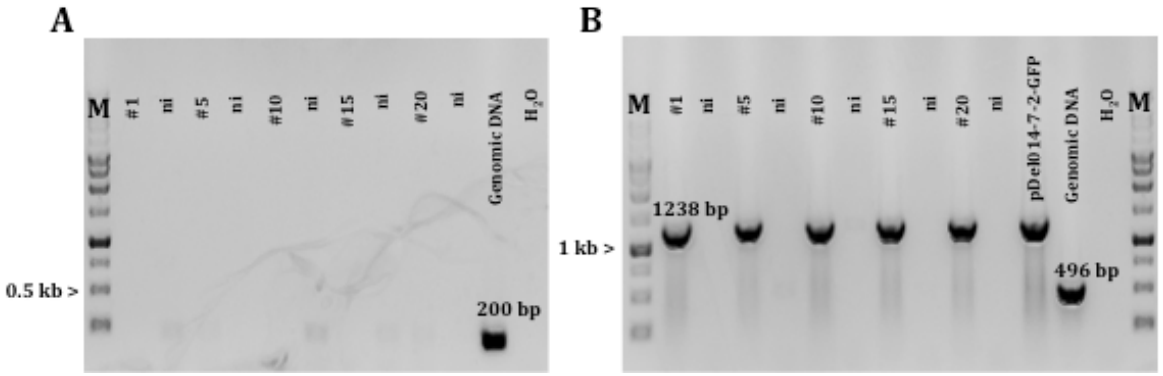


**Figure S69: GFP is stably integrated into Del014. 014 PCR after passage 1, 5, 10, 15 and 20 of VCh014GFP in Vero cells indicates a deletion of gene 014 (A), while d014 PCRs result in 1238 bp fragments specific for GFP inserted into the Del014 locus. 1% agarose gel; ni = DNA from not infected Vero cells; M = Ready-To-Use 1 kb Ladder, Nippon Genetics.**

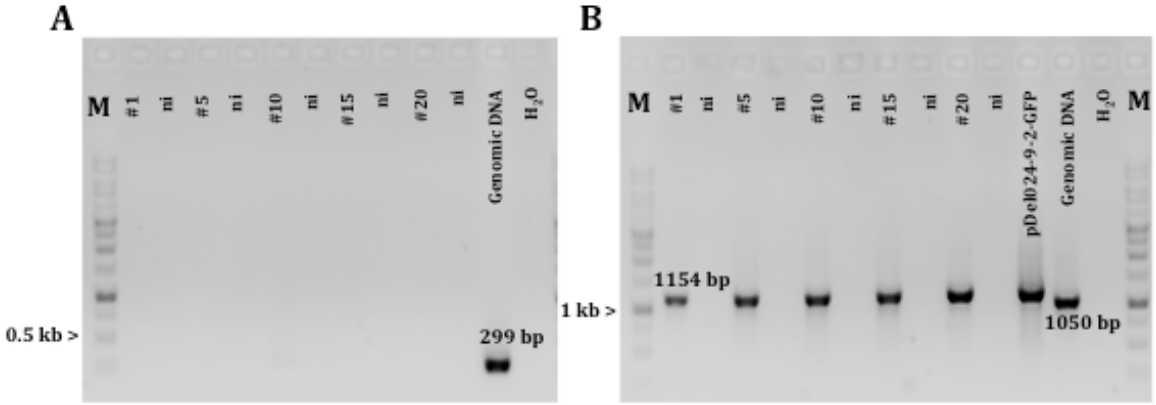


**Figure S70: GFP is stably integrated into Del024. 024 PCR after passage 1, 5, 10, 15 and 20 of VCh024GFP in Vero cells indicates a deletion of gene 024 (A), while d024 PCRs result in 1154 bp fragments specific for GFP inserted into the Del024 locus. 1% agarose gel; ni = DNA from not infected Vero cells; M = Ready-To-Use 1 kb Ladder, Nippon Genetics.**

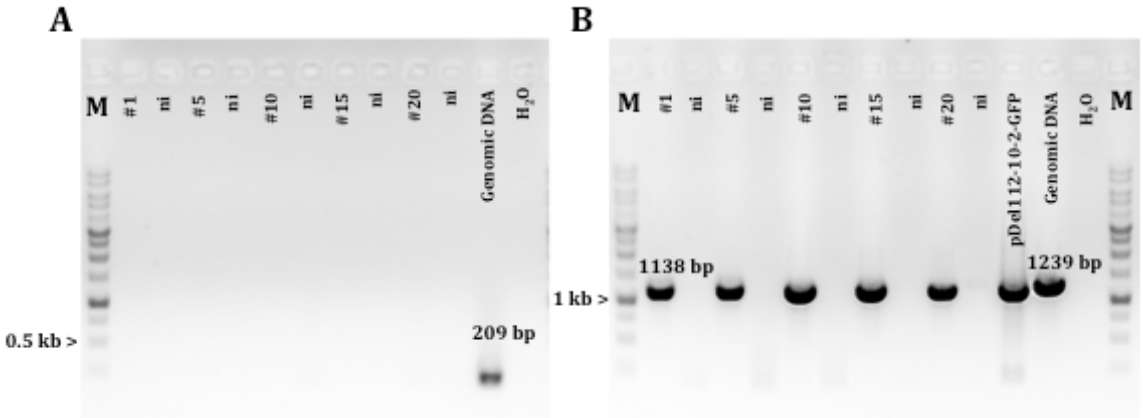


**Figure S71: GFP is stably integrated into Del112. 112 PCR after passage 1, 5, 10, 15 and 20 of VCh112GFP in Vero cells indicates a deletion of gene 112 (A), while d112 PCRs result in 1138 bp fragments specific for GFP inserted into the Del112 locus. 1% agarose gel; ni = DNA from not infected Vero cells; M = Ready-To-Use 1 kb Ladder, Nippon Genetics.**

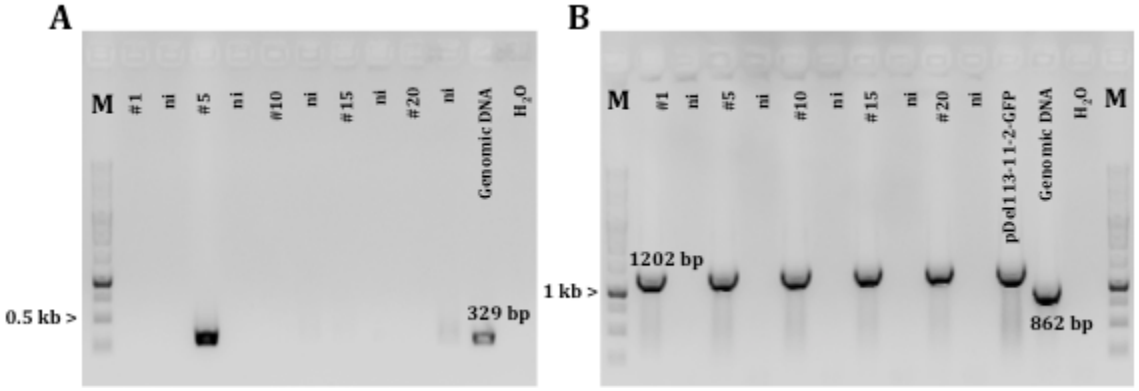


**Figure S72: GFP is stably integrated into Del113. 113 PCR after passage 1, 5, 10, 15 and 20 of VCh113GFP in Vero cells indicates a deletion of gene 113 (A), while d113 PCRs result in 1202 bp fragments specific for GFP inserted into the Del113 locus. 1% agarose gel; ni = DNA from not infected Vero cells; M = Ready-To-Use 1 kb Ladder, Nippon Genetics.**

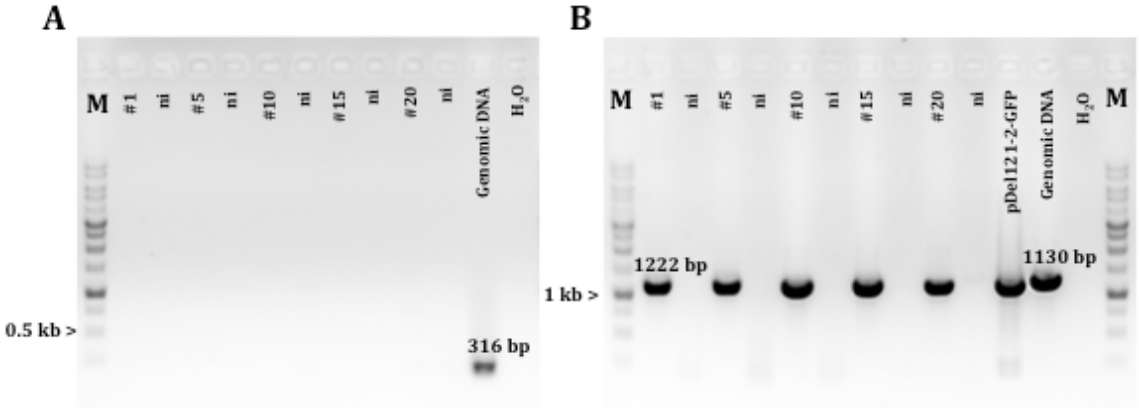


**Figure S73: GFP is stably integrated into Del121. 121 PCR after passage 1, 5, 10, 15 and 20 of VCh121GFP in Vero cells indicates a deletion of gene 121 (A), while d121 PCRs result in 1222 bp fragments specific for GFP inserted into the Del121 locus. 1% agarose gel; ni = DNA from not infected Vero cells; M = Ready-To-Use 1 kb Ladder, Nippon Genetics.**

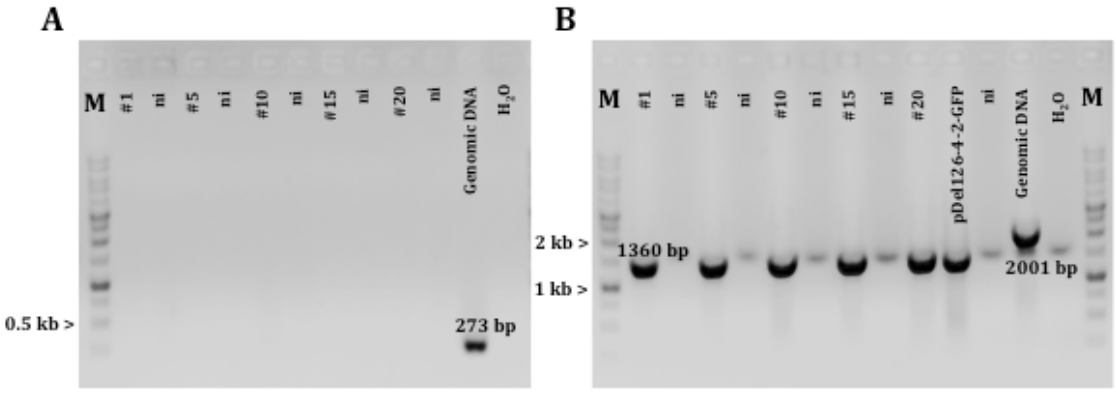


**Figure S74: GFP is stably integrated into Del126. 126 PCR after passage 1, 5, 10, 15 and 20 of VCh126GFP in Vero cells indicates a deletion of gene 126 (A), while d126 PCRs result in 1360 bp fragments specific for GFP inserted into the Del126 locus. 1% agarose gel; ni = DNA from not infected Vero cells; M = Ready-To-Use 1 kb Ladder, Nippon Genetics.**

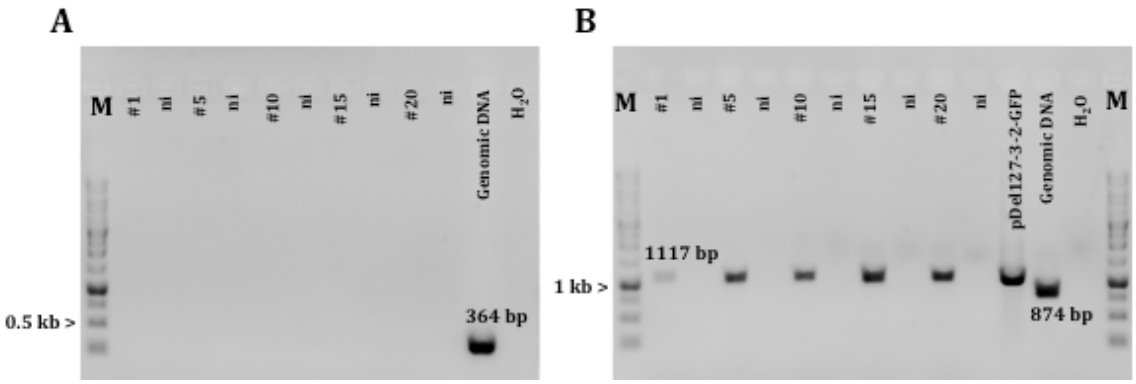


**Figure S75: GFP is stably integrated into Del127. 127 PCR after passage 1, 5, 10, 15 and 20 of VCh127GFP in Vero cells indicates a deletion of gene 127 (A), while d127 PCRs result in 1117 bp fragments specific for GFP inserted into the Del127 locus. 1% agarose gel; ni = DNA from not infected Vero cells; M = Ready-To-Use 1 kb Ladder, Nippon Genetics.**

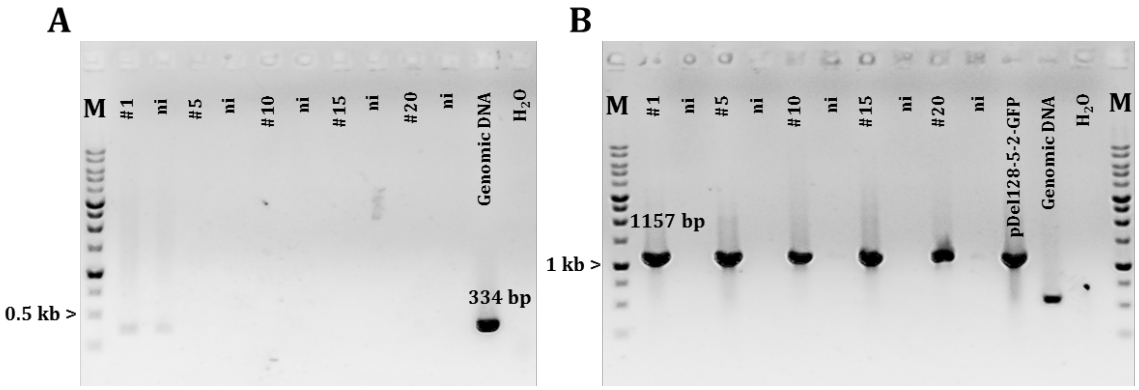


**Figure S76: GFP is stably integrated into Del128. 128 PCR after passage 1, 5, 10, 15 and 20 of VCh128GFP in Vero cells indicates a deletion of gene 128 (A), while d128 PCRs result in 1157 bp fragments specific for GFP inserted into the Del128 locus. 1% agarose gel; ni = DNA from not infected Vero cells; M = Ready-To-Use 1 kb Ladder, Nippon Genetics.**

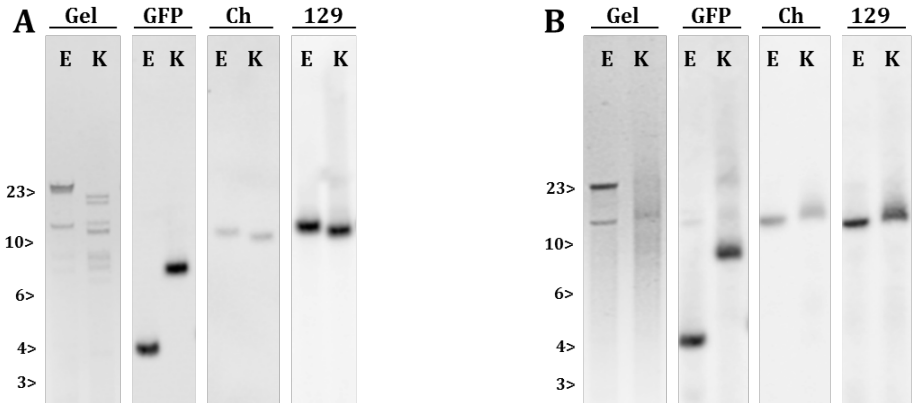


**Figure S77: Detection of GFP, mCherry and ORF129 in VCh112GFP DNA obtained after passage 1 (A) and 20 (B). Genomic viral DNA was digested with EcoR*I* (E) and Kpn*I* (K) prior to separation in a horizontal 0.8% agarose gel for 8 h. After alkaline blotting of the viral DNA onto nylon membranes, the digested DNAs (Gel) were hybridized using digoxigenin labelled GFP, mCherry and ORF129 probes to determine the corresponding genomic location.**

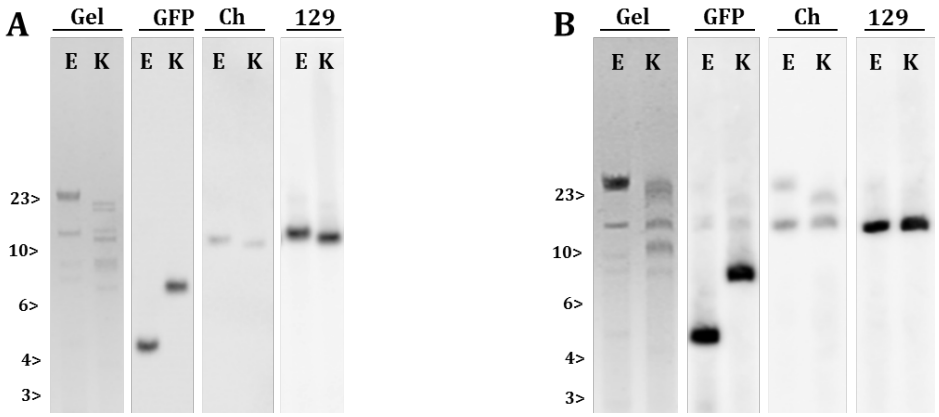


**Figure S78: Detection of GFP, mCherry and ORF129 in VCh113GFP DNA obtained after passage 1 (A) and 20 (B). Genomic viral DNA was digested with EcoR*I* (E) and Kpn*I* (K) prior to separation in a horizontal 0.8% agarose gel for 8 h. After alkaline blotting of the viral DNA onto nylon membranes, the digested DNAs (Gel) were hybridized using digoxigenin labelled GFP, mCherry and ORF129 probes to determine the corresponding genomic location.**

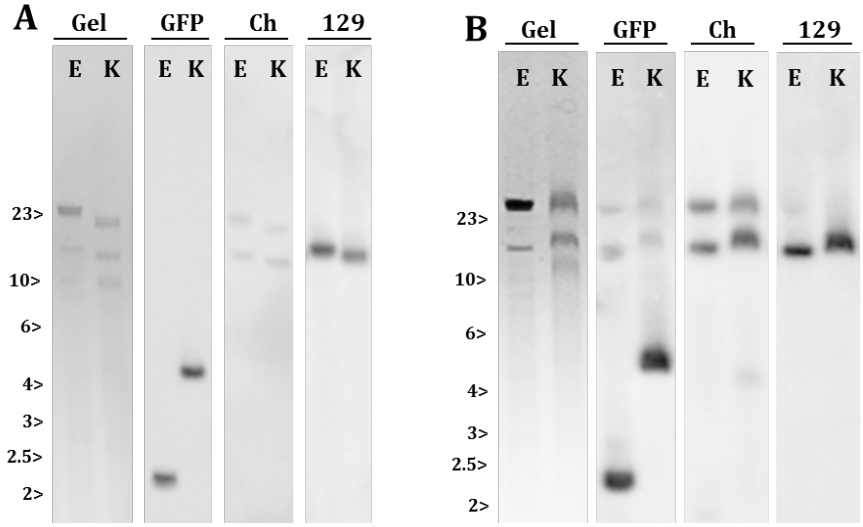


**Figure S79: Detection of GFP, mCherry and ORF129 in VCh119GFP DNA obtained after passage 1 (A) and 20 (B). Genomic viral DNA was digested with EcoR*I* (E) and Kpn*I* (K) prior to separation in a horizontal 0.8% agarose gel for 8 h. After alkaline blotting of the viral DNA onto nylon membranes, the digested DNAs (Gel) were hybridized using digoxigenin labelled GFP, mCherry and ORF129 probes to determine the corresponding genomic location.**

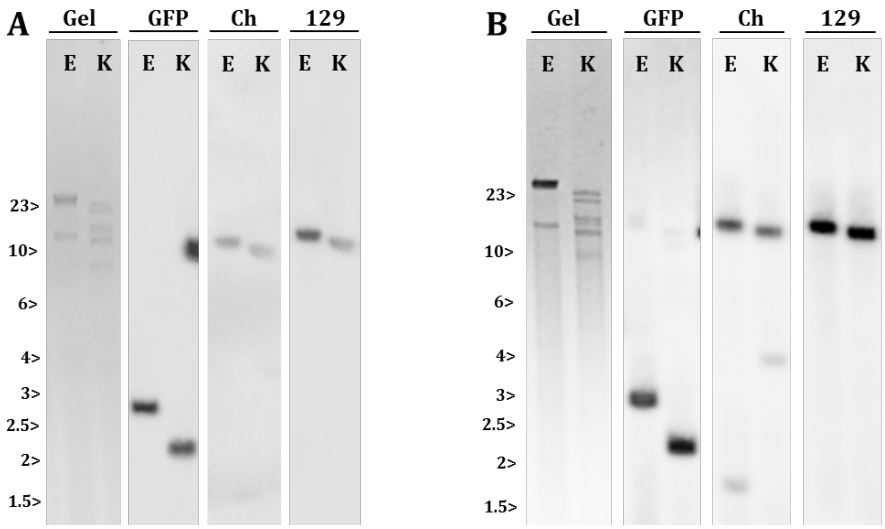


**Figure S80: Detection of GFP, mCherry and ORF129 in VCh121GFP DNA obtained after passage 1 (A) and 20 (B). Genomic viral DNA was digested with EcoR*I* (E) and Kpn*I* (K) prior to separation in a horizontal 0.8% agarose gel for 8 h. After alkaline blotting of the viral DNA onto nylon membranes, the digested DNAs (Gel) were hybridized using digoxigenin labelled GFP, mCherry and ORF129 probes to determine the corresponding genomic location.**

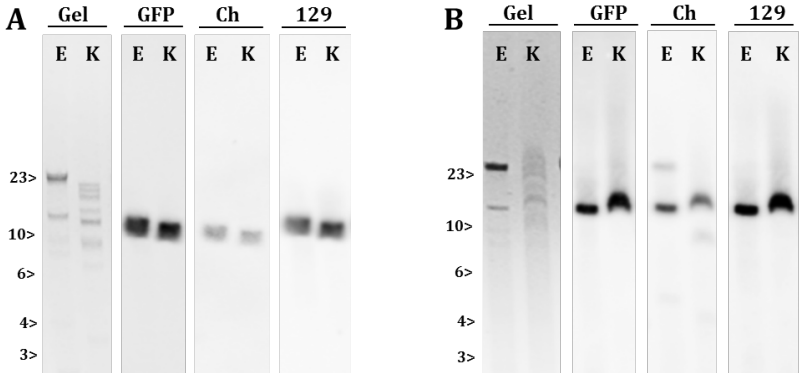


**Figure S81: Detection of GFP, mCherry and ORF129 in VCh126GFP DNA obtained after passage 1 (A) and 20 (B). Genomic viral DNA was digested with EcoR*I* (E) and Kpn*I* (K) prior to separation in a horizontal 0.8% agarose gel for 8 h. After alkaline blotting of the viral DNA onto nylon membranes, the digested DNAs (Gel) were hybridized using digoxigenin labelled GFP, mCherry and ORF129 probes to determine the corresponding genomic location.**

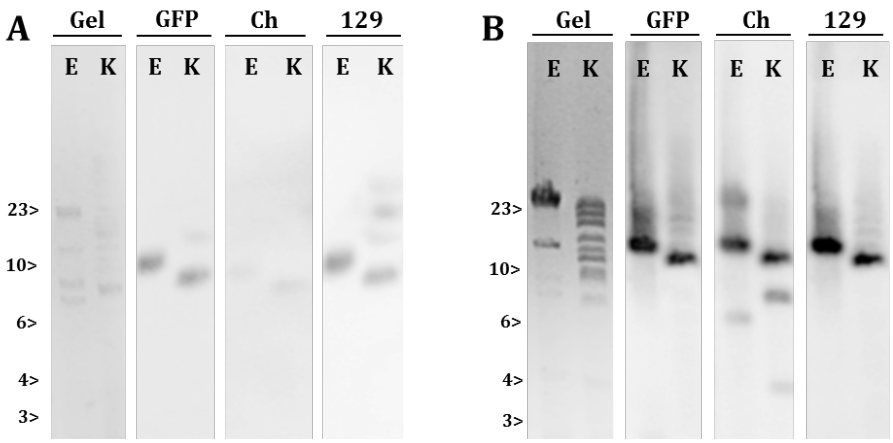


**Figure S82: Detection of GFP, mCherry and ORF129 in VCh127GFP DNA obtained after passage 1 (A) and 20 (B). Genomic viral DNA was digested with EcoR*I* (E) and Kpn*I* (K) prior to separation in a horizontal 0.8% agarose gel for 8 h. After alkaline blotting of the viral DNA onto nylon membranes, the digested DNAs (Gel) were hybridized using digoxigenin labelled GFP, mCherry and ORF129 probes to determine the corresponding genomic location.**

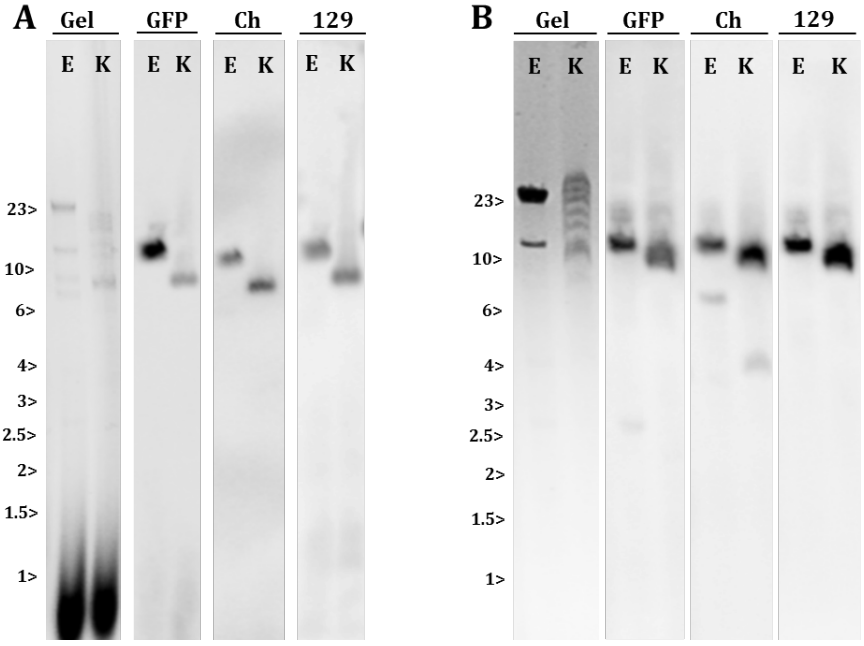


**Figure S83: Detection of GFP, mCherry and ORF129 in VCh128GFP DNA obtained after passage 1 (A) and 20 (B). Genomic viral DNA was digested with EcoR*I* (E) and Kpn*I* (K) prior to separation in a horizontal 0.8% agarose gel for 8 h. After alkaline blotting of the viral DNA onto nylon membranes, the digested DNAs (Gel) were hybridized using digoxigenin labelled GFP, mCherry and ORF129 probes to determine the corresponding genomic location.**

## 5.4 Infection rates of THP-1 Dual cells for the analysis of IRF- and NF-κB-pathway activation *in vitro*

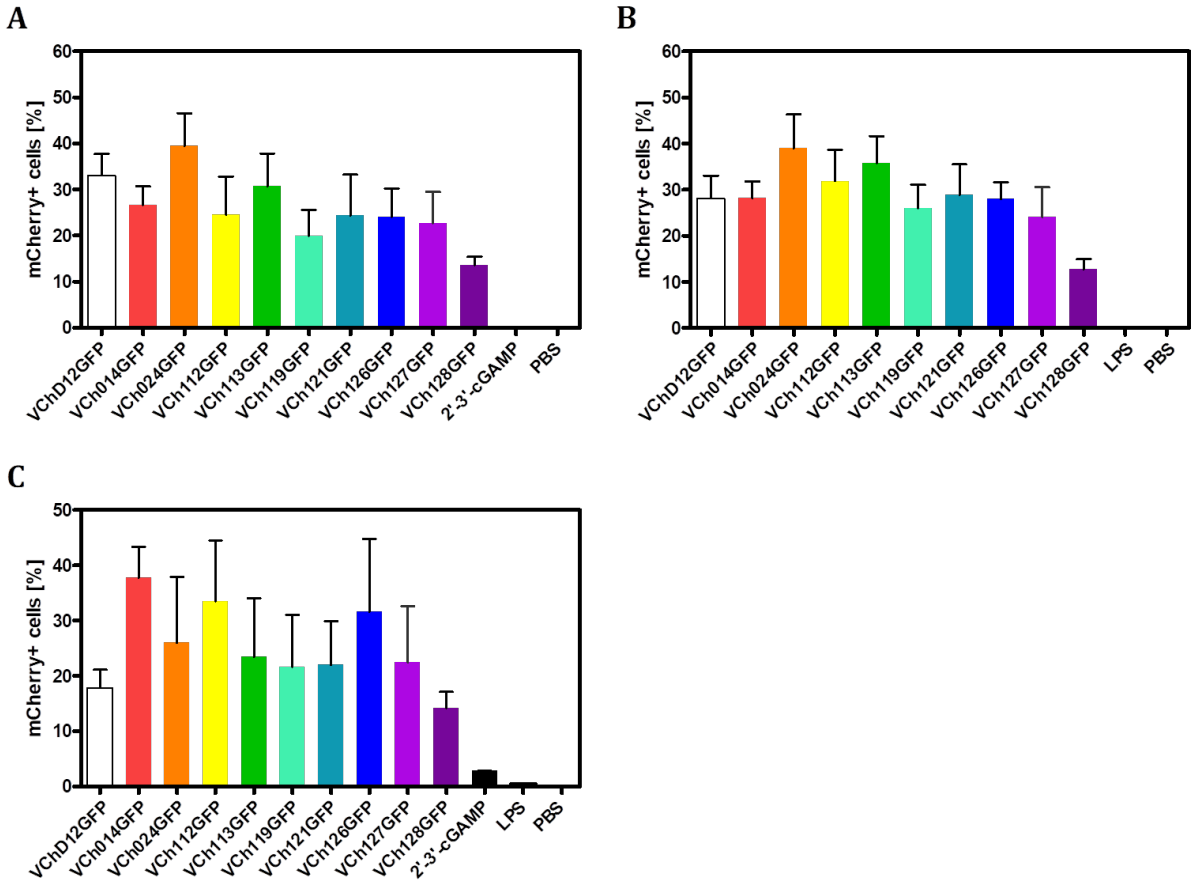


**Figure S84: Infection rates of THP-1 Dual cells for the analysis of IRF- and NF-κB-pathway activation. THP-1 Dual cells were infected with new Del-site recombinants for 24 h (A and B) and 48 h (C) and the percentage of mCherry expressing cells was determined by FACS analysis. Shown are the mean values and standard error of the mean from three independent experiments including three technical replicates for each group.**

## 5.5 Crosstabulation of relative mCherry and GFP expression strengths in Vero cells, THP-1 cells and moDCs

### Table S16: Relative mCherry expression 24 hpi in Vero cells.

| mCherry | VChD12GFP | VCh014GFP | VCh024GFP | VCh112GFP | VCh113GFP | VCh119GFP | VCh121GFP | VCh126GFP | VCh127GFP | VCh128GFP |
|---|---|---|---|---|---|---|---|---|---|---|
| VChD12GFP | 1 | 0,4 | 0,5 | 0,7 | 0,6 | 1,0 | 0,5 | 0,5 | 0,2 | 0,9 |
| VCh014GFP | 2,2 | 1 | 1,2 | 1,5 | 1,4 | 2,3 | 1,1 | 1,2 | 0,5 | 2,0 |
| VCh024GFP | 1,9 | 0,8 | 1 | 1,3 | 1,1 | 1,9 | 1,0 | 1,0 | 0,4 | 1,7 |
| VCh112GFP | 1,5 | 0,7 | 0,8 | 1 | 0,9 | 1,5 | 0,8 | 0,8 | 0,3 | 1,3 |
| VCh113GFP | 1,6 | 0,7 | 0,9 | 1,1 | 1 | 1,7 | 0,8 | 0,9 | 0,4 | 1,5 |
| VCh119GFP | 1,0 | 0,4 | 0,5 | 0,6 | 0,6 | 1 | 0,5 | 0,5 | 0,2 | 0,9 |
| VCh121GFP | 1,9 | 0,9 | 1,0 | 1,3 | 1,2 | 2,0 | 1 | 1,0 | 0,5 | 1,7 |
| VCh126GFP | 1,9 | 0,8 | 1,0 | 1,3 | 1,2 | 2,0 | 1,0 | 1 | 0,4 | 1,7 |
| VCh127GFP | 4,3 | 1,9 | 2,3 | 2,9 | 2,6 | 4,5 | 2,2 | 2,3 | 1 | 3,8 |
| VCh128GFP | 1,1 | 0,5 | 0,6 | 0,8 | 0,7 | 1,2 | 0,6 | 0,6 | 0,3 | 1 |

### Table S17: Relative mCherry expression 48 hpi in Vero cells.

| mCherry | VChD12GFP | VCh014GFP | VCh024GFP | VCh112GFP | VCh113GFP | VCh119GFP | VCh121GFP | VCh126GFP | VCh127GFP | VCh128GFP |
|---|---|---|---|---|---|---|---|---|---|---|
| VChD12GFP | 1 | 0,8 | 1,1 | 0,7 | 0,5 | 1,0 | 0,5 | 0,5 | 0,4 | 0,6 |
| VCh014GFP | 1,3 | 1 | 1,4 | 0,8 | 0,7 | 1,2 | 0,7 | 0,6 | 0,6 | 0,8 |
| VCh024GFP | 0,9 | 0,7 | 1 | 0,6 | 0,5 | 0,9 | 0,5 | 0,5 | 0,4 | 0,5 |
| VCh112GFP | 1,5 | 1,2 | 1,7 | 1 | 0,8 | 1,5 | 0,8 | 0,8 | 0,7 | 0,9 |
| VCh113GFP | 1,9 | 1,5 | 2,1 | 1,2 | 1 | 1,8 | 1,0 | 0,9 | 0,8 | 1,1 |
| VCh119GFP | 1,0 | 0,8 | 1,1 | 0,7 | 0,5 | 1 | 0,5 | 0,5 | 0,5 | 0,6 |
| VCh121GFP | 1,9 | 1,5 | 2,1 | 1,2 | 1,0 | 1,8 | 1 | 1,0 | 0,9 | 1,1 |
| VCh126GFP | 2,0 | 1,5 | 2,2 | 1,3 | 1,1 | 1,9 | 1,0 | 1 | 0,9 | 1,2 |
| VCh127GFP | 2,2 | 1,7 | 2,5 | 1,5 | 1,2 | 2,1 | 1,2 | 1,1 | 1 | 1,3 |
| VCh128GFP | 1,7 | 1,3 | 1,9 | 1,1 | 0,9 | 1,6 | 0,9 | 0,8 | 0,8 | 1 |

### Table S18: Relative GFP expression 24 hpi in Vero cells.

| GFP | VChD12GFP | VCh014GFP | VCh024GFP | VCh112GFP | VCh113GFP | VCh119GFP | VCh121GFP | VCh126GFP | VCh127GFP | VCh128GFP |
|---|---|---|---|---|---|---|---|---|---|---|
| VChD12GFP | 1 | 0,5 | 0,7 | 0,9 | 0,7 | 1,1 | 1,0 | 1,1 | 0,4 | 1,6 |
| VCh014GFP | 1,8 | 1 | 1,3 | 1,6 | 1,3 | 2,1 | 1,9 | 2,1 | 0,8 | 3,0 |
| VCh024GFP | 1,4 | 0,8 | 1 | 1,2 | 1,0 | 1,6 | 1,5 | 1,6 | 0,6 | 2,3 |
| VCh112GFP | 1,2 | 0,6 | 0,8 | 1 | 0,8 | 1,3 | 1,2 | 1,3 | 0,5 | 1,9 |
| VCh113GFP | 1,4 | 0,8 | 1,0 | 1,2 | 1 | 1,6 | 1,4 | 1,6 | 0,6 | 2,3 |
| VCh119GFP | 0,9 | 0,5 | 0,6 | 0,8 | 0,6 | 1 | 0,9 | 1,0 | 0,4 | 1,5 |
| VCh121GFP | 1,0 | 0,5 | 0,7 | 0,8 | 0,7 | 1,1 | 1 | 1,1 | 0,4 | 1,6 |
| VCh126GFP | 0,9 | 0,5 | 0,6 | 0,8 | 0,6 | 1,0 | 0,9 | 1 | 0,4 | 1,5 |
| VCh127GFP | 2,2 | 1,2 | 1,6 | 1,9 | 1,6 | 2,5 | 2,3 | 2,5 | 1 | 3,7 |
| VCh128GFP | 0,6 | 0,3 | 0,4 | 0,5 | 0,4 | 0,7 | 0,6 | 0,7 | 0,3 | 1 |

### Table S19: Relative GFP expression 48 hpi in Vero cells.

| GFP | VChD12GFP | VCh014GFP | VCh024GFP | VCh112GFP | VCh113GFP | VCh119GFP | VCh121GFP | VCh126GFP | VCh127GFP | VCh128GFP |
|---|---|---|---|---|---|---|---|---|---|---|
| VChD12GFP | 1 | 0,8 | 0,9 | 0,7 | 0,6 | 1,5 | 0,8 | 0,9 | 0,7 | 1,5 |
| VCh014GFP | 1,3 | 1 | 1,1 | 0,9 | 0,8 | 1,9 | 1,1 | 1,1 | 0,9 | 1,9 |
| VCh024GFP | 1,2 | 0,9 | 1 | 0,8 | 0,7 | 1,7 | 1,0 | 1,0 | 0,8 | 1,7 |
| VCh112GFP | 1,4 | 1,1 | 1,2 | 1 | 0,9 | 2,1 | 1,2 | 1,2 | 1,0 | 2,1 |
| VCh113GFP | 1,6 | 1,2 | 1,3 | 1,1 | 1 | 2,3 | 1,3 | 1,4 | 1,1 | 2,3 |
| VCh119GFP | 0,7 | 0,5 | 0,6 | 0,5 | 0,4 | 1 | 0,6 | 0,6 | 0,5 | 1,0 |
| VCh121GFP | 1,2 | 1,0 | 1,0 | 0,9 | 0,8 | 1,8 | 1 | 1,1 | 0,9 | 1,8 |
| VCh126GFP | 1,1 | 0,9 | 1,0 | 0,8 | 0,7 | 1,7 | 0,9 | 1 | 0,8 | 1,7 |
| VCh127GFP | 1,4 | 1,1 | 1,2 | 1,0 | 0,9 | 2,0 | 1,1 | 1,2 | 1 | 2,0 |
| VCh128GFP | 0,7 | 0,5 | 0,6 | 0,5 | 0,4 | 1,0 | 0,6 | 0,6 | 0,5 | 1 |

## Table S20: Relative mCherry expression 24 hpi in THP-1 cells.

| mCherry | VChD12GFP | VCh014GFP | VCh024GFP | VCh112GFP | VCh113GFP | VCh119GFP | VCh121GFP | VCh126GFP | VCh127GFP | VCh128GFP |
|---|---|---|---|---|---|---|---|---|---|---|
| VChD12GFP | 1 | 0,9 | 1,4 | 1,0 | 1,3 | 1,4 | 0,9 | 1,1 | 0,8 | 1,0 |
| VCh014GFP | 1,2 | 1 | 1,6 | 1,2 | 1,5 | 1,6 | 1,0 | 1,3 | 0,9 | 1,2 |
| VCh024GFP | 0,7 | 0,6 | 1 | 0,8 | 0,9 | 1,0 | 0,7 | 0,8 | 0,6 | 0,7 |
| VCh112GFP | 1,0 | 0,8 | 1,3 | 1 | 1,2 | 1,3 | 0,9 | 1,1 | 0,7 | 1,0 |
| VCh113GFP | 0,8 | 0,7 | 1,1 | 0,8 | 1 | 1,1 | 0,7 | 0,9 | 0,6 | 0,8 |
| VCh119GFP | 0,7 | 0,6 | 1,0 | 0,8 | 0,9 | 1 | 0,7 | 0,8 | 0,6 | 0,7 |
| VCh121GFP | 1,1 | 1,0 | 1,5 | 1,2 | 1,4 | 1,5 | 1 | 1,2 | 0,9 | 1,1 |
| VCh126GFP | 0,9 | 0,8 | 1,2 | 0,9 | 1,2 | 1,2 | 0,8 | 1 | 0,7 | 0,9 |
| VCh127GFP | 1,3 | 1,1 | 1,8 | 1,4 | 1,7 | 1,8 | 1,2 | 1,4 | 1 | 1,3 |
| VCh128GFP | 1,0 | 0,9 | 1,4 | 1,0 | 1,3 | 1,4 | 0,9 | 1,1 | 0,8 | 1 |

## Table S21: Relative mCherry expression 48 hpi in THP-1 cells.

| mCherry | VChD12GFP | VCh014GFP | VCh024GFP | VCh112GFP | VCh113GFP | VCh119GFP | VCh121GFP | VCh126GFP | VCh127GFP | VCh128GFP |
|---|---|---|---|---|---|---|---|---|---|---|
| VChD12GFP | 1 | 1,6 | 1,6 | 1,7 | 1,5 | 1,2 | 1,5 | 1,6 | 0,9 | 0,9 |
| VCh014GFP | 0,6 | 1 | 1,0 | 1,1 | 0,9 | 0,8 | 0,9 | 1,0 | 0,5 | 0,6 |
| VCh024GFP | 0,6 | 1,0 | 1 | 1,0 | 0,9 | 0,7 | 0,9 | 1,0 | 0,5 | 0,5 |
| VCh112GFP | 0,6 | 0,9 | 1,0 | 1 | 0,9 | 0,7 | 0,9 | 1,0 | 0,5 | 0,5 |
| VCh113GFP | 0,7 | 1,1 | 1,1 | 1,1 | 1 | 0,8 | 1,0 | 1,1 | 0,6 | 0,6 |
| VCh119GFP | 0,8 | 1,3 | 1,4 | 1,4 | 1,2 | 1 | 1,2 | 1,4 | 0,7 | 0,7 |
| VCh121GFP | 0,7 | 1,1 | 1,1 | 1,1 | 1,0 | 0,8 | 1 | 1,1 | 0,6 | 0,6 |
| VCh126GFP | 0,6 | 1,0 | 1,0 | 1,0 | 0,9 | 0,7 | 0,9 | 1 | 0,5 | 0,5 |
| VCh127GFP | 1,1 | 1,8 | 1,9 | 1,9 | 1,7 | 1,4 | 1,7 | 1,9 | 1 | 1,0 |
| VCh128GFP | 1,1 | 1,8 | 1,9 | 1,9 | 1,7 | 1,4 | 1,7 | 1,9 | 1,0 | 1 |

## Table S22: Relative GFP expression 24 hpi in THP-1 cells.

| GFP | VChD12GFP | VCh014GFP | VCh024GFP | VCh112GFP | VCh113GFP | VCh119GFP | VCh121GFP | VCh126GFP | VCh127GFP | VCh128GFP |
|---|---|---|---|---|---|---|---|---|---|---|
| VChD12GFP | 1 | 0,9 | 0,8 | 1,1 | 1,4 | 1,3 | 1,6 | 2,3 | 1,5 | 1,8 |
| VCh014GFP | 1,1 | 1 | 0,9 | 1,2 | 1,5 | 1,4 | 1,8 | 2,5 | 1,6 | 1,9 |
| VCh024GFP | 1,2 | 1,1 | 1 | 1,3 | 1,6 | 1,5 | 2,0 | 2,8 | 1,8 | 2,1 |
| VCh112GFP | 0,9 | 0,8 | 0,8 | 1 | 1,2 | 1,2 | 1,5 | 2,1 | 1,3 | 1,6 |
| VCh113GFP | 0,7 | 0,7 | 0,6 | 0,8 | 1 | 0,9 | 1,2 | 1,7 | 1,1 | 1,3 |
| VCh119GFP | 0,8 | 0,7 | 0,7 | 0,9 | 1,1 | 1 | 1,3 | 1,8 | 1,1 | 1,4 |
| VCh121GFP | 0,6 | 0,6 | 0,5 | 0,7 | 0,8 | 0,8 | 1 | 1,4 | 0,9 | 1,1 |
| VCh126GFP | 0,4 | 0,4 | 0,4 | 0,5 | 0,6 | 0,6 | 0,7 | 1 | 0,6 | 0,8 |
| VCh127GFP | 0,7 | 0,6 | 0,6 | 0,8 | 0,9 | 0,9 | 1,1 | 1,6 | 1 | 1,2 |
| VCh128GFP | 0,6 | 0,5 | 0,5 | 0,6 | 0,8 | 0,7 | 0,9 | 1,3 | 0,8 | 1 |

## Table S23: Relative GFP expression 48 hpi in THP-1 cells.

| GFP | VChD12GFP | VCh014GFP | VCh024GFP | VCh112GFP | VCh113GFP | VCh119GFP | VCh121GFP | VCh126GFP | VCh127GFP | VCh128GFP |
|---|---|---|---|---|---|---|---|---|---|---|
| VChD12GFP | 1 | 2,1 | 1,3 | 2,1 | 1,8 | 1,9 | 3,3 | 4,4 | 2,3 | 2,2 |
| VCh014GFP | 0,5 | 1 | 0,6 | 1,0 | 0,9 | 0,9 | 1,5 | 2,1 | 1,1 | 1,0 |
| VCh024GFP | 0,8 | 1,6 | 1 | 1,6 | 1,4 | 1,5 | 2,5 | 3,4 | 1,8 | 1,7 |
| VCh112GFP | 0,5 | 1,0 | 0,6 | 1 | 0,9 | 0,9 | 1,5 | 2,1 | 1,1 | 1,0 |
| VCh113GFP | 0,5 | 1,2 | 0,7 | 1,2 | 1 | 1,0 | 1,8 | 2,4 | 1,3 | 1,2 |
| VCh119GFP | 0,5 | 1,1 | 0,7 | 1,1 | 1,0 | 1 | 1,7 | 2,3 | 1,2 | 1,1 |
| VCh121GFP | 0,3 | 0,7 | 0,4 | 0,7 | 0,6 | 0,6 | 1 | 1,4 | 0,7 | 0,7 |
| VCh126GFP | 0,2 | 0,5 | 0,3 | 0,5 | 0,4 | 0,4 | 0,7 | 1 | 0,5 | 0,5 |
| VCh127GFP | 0,4 | 0,9 | 0,6 | 0,9 | 0,8 | 0,8 | 1,4 | 1,9 | 1 | 0,9 |
| VCh128GFP | 0,5 | 1,0 | 0,6 | 1,0 | 0,8 | 0,9 | 1,5 | 2,0 | 1,1 | 1 |

## Table S24: Relative mCherry expression 24 hpi in moDCs.

| mCherry | VChD12GFP | VCh014GFP | VCh024GFP | VCh112GFP | VCh113GFP | VCh119GFP | VCh121GFP | VCh126GFP | VCh127GFP | VCh128GFP |
|---|---|---|---|---|---|---|---|---|---|---|
| Del2-Ch | 1 | 0,7 | 1,3 | 0,9 | 0,8 | 0,4 | 1,1 | 1,1 | 0,4 | 0,6 |
| 014-Ch | 1,3 | 1 | 1,7 | 1,2 | 1,1 | 0,6 | 1,5 | 1,5 | 0,6 | 0,8 |
| 024-Ch | 0,8 | 0,6 | 1 | 0,7 | 0,6 | 0,3 | 0,9 | 0,9 | 0,3 | 0,5 |
| 112-Ch | 1,1 | 0,8 | 1,4 | 1 | 0,9 | 0,4 | 1,2 | 1,2 | 0,5 | 0,7 |
| 113-Ch | 1,3 | 0,9 | 1,6 | 1,2 | 1 | 0,5 | 1,4 | 1,4 | 0,6 | 0,8 |
| 119-Ch | 2,4 | 1,8 | 3,1 | 2,2 | 1,9 | 1 | 2,7 | 2,7 | 1,1 | 1,5 |
| 121-Ch | 0,9 | 0,7 | 1,2 | 0,8 | 0,7 | 0,4 | 1 | 1,0 | 0,4 | 0,6 |
| 126-Ch | 0,9 | 0,7 | 1,1 | 0,8 | 0,7 | 0,4 | 1,0 | 1 | 0,4 | 0,6 |
| 127-Ch | 2,2 | 1,7 | 2,9 | 2,1 | 1,8 | 0,9 | 2,5 | 2,5 | 1 | 1,4 |
| 128-Ch | 1,6 | 1,2 | 2,1 | 1,5 | 1,3 | 0,7 | 1,8 | 1,8 | 0,7 | 1 |

## Table S25: Relative mCherry expression 48 hpi in moDCs.

| mCherry | VChD12GFP | VCh014GFP | VCh024GFP | VCh112GFP | VCh113GFP | VCh119GFP | VCh121GFP | VCh126GFP | VCh127GFP | VCh128GFP |
|---|---|---|---|---|---|---|---|---|---|---|
| VChD12GFP | 1 | 0,5 | 0,8 | 0,6 | 0,4 | 0,2 | 0,5 | 0,7 | 0,5 | 0,4 |
| VCh014GFP | 2,2 | 1 | 1,7 | 1,2 | 1,0 | 0,5 | 1,2 | 1,6 | 1,2 | 0,8 |
| VCh024GFP | 1,3 | 0,6 | 1 | 0,7 | 0,6 | 0,3 | 0,7 | 0,9 | 0,7 | 0,5 |
| VCh112GFP | 1,8 | 0,8 | 1,4 | 1 | 0,8 | 0,4 | 1,0 | 1,3 | 1,0 | 0,7 |
| VCh113GFP | 2,3 | 1,0 | 1,8 | 1,3 | 1 | 0,5 | 1,2 | 1,7 | 1,2 | 0,8 |
| VCh119GFP | 4,3 | 2,0 | 3,4 | 2,4 | 1,9 | 1 | 2,3 | 3,2 | 2,3 | 1,6 |
| VCh121GFP | 1,8 | 0,9 | 1,5 | 1,0 | 0,8 | 0,4 | 1 | 1,4 | 1,0 | 0,7 |
| VCh126GFP | 1,4 | 0,6 | 1,1 | 0,8 | 0,6 | 0,3 | 0,7 | 1 | 0,7 | 0,5 |
| VCh127GFP | 1,8 | 0,9 | 1,5 | 1,0 | 0,8 | 0,4 | 1,0 | 1,4 | 1 | 0,7 |
| VCh128GFP | 2,7 | 1,3 | 2,2 | 1,5 | 1,2 | 0,6 | 1,5 | 2,0 | 1,5 | 1 |

## Table S26: Relative GFP expression 24 hpi in moDCs.

| GFP | VChD12GFP | VCh014GFP | VCh024GFP | VCh112GFP | VCh113GFP | VCh119GFP | VCh121GFP | VCh126GFP | VCh127GFP | VCh128GFP |
|---|---|---|---|---|---|---|---|---|---|---|
| VChD12GFP | 1 | 0,9 | 1,0 | 1,2 | 1,0 | 0,5 | 2,6 | 2,9 | 1,0 | 1,3 |
| VCh014GFP | 1,1 | 1 | 1,1 | 1,3 | 1,1 | 0,6 | 2,8 | 3,1 | 1,0 | 1,4 |
| VCh024GFP | 1,0 | 0,9 | 1 | 1,2 | 1,0 | 0,5 | 2,5 | 2,8 | 0,9 | 1,3 |
| VCh112GFP | 0,8 | 0,7 | 0,8 | 1 | 0,8 | 0,4 | 2,1 | 2,3 | 0,8 | 1,1 |
| VCh113GFP | 1,0 | 0,9 | 1,0 | 1,2 | 1 | 0,5 | 2,6 | 2,9 | 1,0 | 1,3 |
| VCh119GFP | 1,9 | 1,8 | 2,0 | 2,4 | 1,9 | 1 | 5,0 | 5,6 | 1,9 | 2,5 |
| VCh121GFP | 0,4 | 0,4 | 0,4 | 0,5 | 0,4 | 0,2 | 1 | 1,1 | 0,4 | 0,5 |
| VCh126GFP | 0,3 | 0,3 | 0,4 | 0,4 | 0,3 | 0,2 | 0,9 | 1 | 0,3 | 0,5 |
| VCh127GFP | 1,0 | 1,0 | 1,1 | 1,3 | 1,0 | 0,5 | 2,7 | 3,0 | 1 | 1,4 |
| VCh128GFP | 0,8 | 0,7 | 0,8 | 0,9 | 0,8 | 0,4 | 1,9 | 2,2 | 0,7 | 1 |

## Table S27: Relative GFP expression 48 hpi in moDCs.

| GFP | VChD12GFP | VCh014GFP | VCh024GFP | VCh112GFP | VCh113GFP | VCh119GFP | VCh121GFP | VCh126GFP | VCh127GFP | VCh128GFP |
|---|---|---|---|---|---|---|---|---|---|---|
| VChD12GFP | 1 | 0,8 | 0,8 | 0,8 | 0,6 | 0,3 | 1,4 | 2,0 | 1,3 | 1,0 |
| VCh014GFP | 1,3 | 1 | 1,0 | 1,0 | 0,8 | 0,3 | 1,8 | 2,6 | 1,7 | 1,4 |
| VCh024GFP | 1,3 | 1,0 | 1 | 1,0 | 0,8 | 0,3 | 1,8 | 2,5 | 1,7 | 1,3 |
| VCh112GFP | 1,3 | 1,0 | 1,0 | 1 | 0,8 | 0,3 | 1,8 | 2,5 | 1,7 | 1,3 |
| VCh113GFP | 1,6 | 1,2 | 1,3 | 1,3 | 1 | 0,4 | 2,3 | 3,3 | 2,1 | 1,7 |
| VCh119GFP | 3,9 | 3,0 | 3,1 | 3,1 | 2,4 | 1 | 5,5 | 7,9 | 5,1 | 4,0 |
| VCh121GFP | 0,7 | 0,5 | 0,6 | 0,6 | 0,4 | 0,2 | 1 | 1,4 | 0,9 | 0,7 |
| VCh126GFP | 0,5 | 0,4 | 0,4 | 0,4 | 0,3 | 0,1 | 0,7 | 1 | 0,7 | 0,5 |
| VCh127GFP | 0,8 | 0,6 | 0,6 | 0,6 | 0,5 | 0,2 | 1,1 | 1,5 | 1 | 0,8 |
| VCh128GFP | 1,0 | 0,7 | 0,8 | 0,8 | 0,6 | 0,2 | 1,4 | 2,0 | 1,3 | 1 |

## 5.6 Proportions of peptide specificities in expanded CD8+ T cells

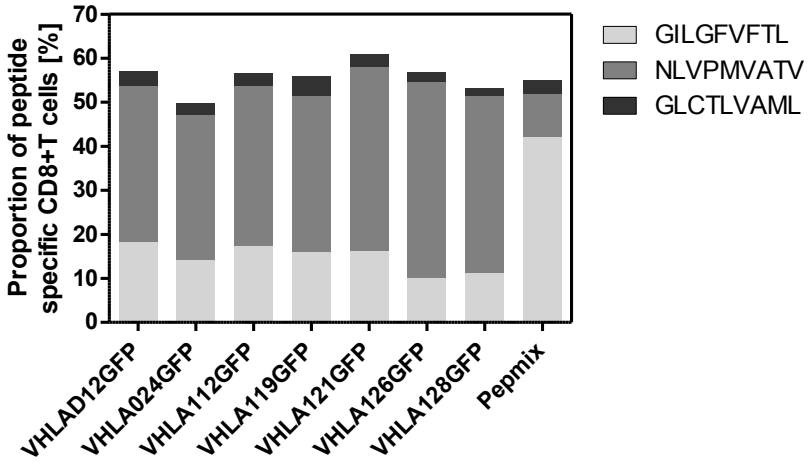


**Figure S85: Proportions of GILGFVFTL, NLVPMVATV and GLCTLVAML specific CD8+ T cells stimulated by different ORFV D1701-V recombinants or Pepmix for 12 days. Shown are the CD8+ T cell proportions of one experiment using PBMCs obtained from donor #186 possessing memory T cells against all three peptides.**

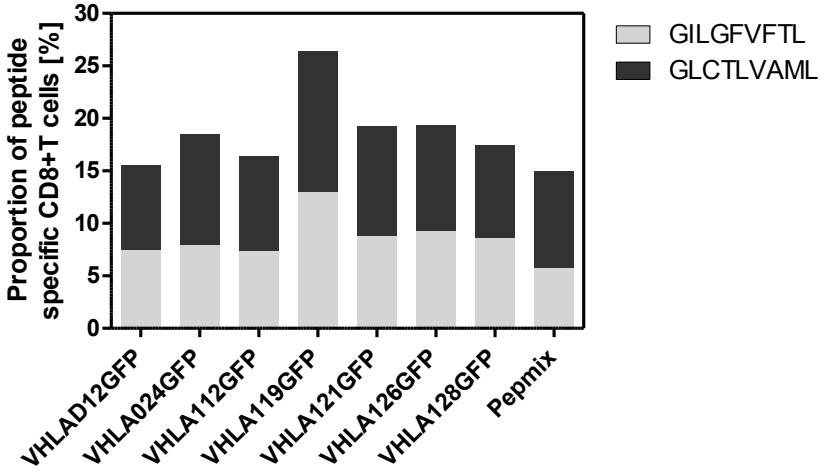


**Figure S86: Proportions of GILGFVFTL and GLCTLVAML specific CD8+ T cells stimulated by different ORFV D1701-V recombinants or Pepmix for 12 days. Shown are the mean CD8+ T cell proportions from 3 independent experiments using PBMCs obtained from donors #624, #013 and #016 possessing memory T cells against GILGFVFTL and GLCTLVAML.**

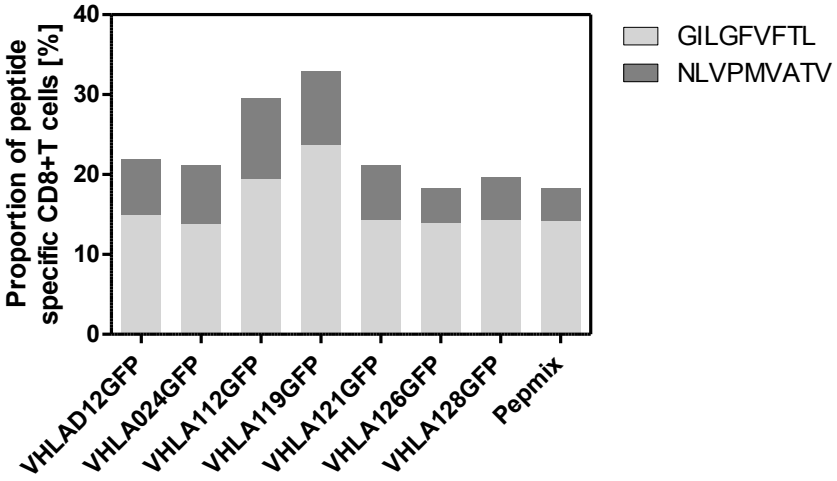


**Figure S87: Proportions of GILGFVFTL and NLVPMVATV specific CD8+ T cells stimulated by different ORFV D1701-V recombinants or Pepmix for 12 days. Shown are the mean CD8+ T cell proportions from 2 independent experiments using PBMCs obtained from donors #607 and #208 possessing memory T cells against GILGFVFTL and GLCTLVAML.**

# 6 Acknowledgement

First, I would like to thank Hans-Georg Rammensee for the opportunity to work at the department of immunology, as well as for supervision and assessment of my thesis. To me, one of his most important accomplishments as head of department is the establishment of a familiar working atmosphere in which science can flourish, while his immunological expertise and vision have always been encouraging and inspiring.

In this regard, I also want to thank Stefan Stevanović for supervision and assessment of my dissertation, and of course for the many social events that we could share a beer at.

I would like to express my sincere gratitude to Ralf Amann, not only for the opportunity to work on my thesis in his lab, the supervision, ideas and constructive discussions, but also for sharing his vision and enthusiasm about ORFV leading to collaboration beyond my PhD project. His commitment enabled financial security throughout my thesis and allowed scientific focus as well as professional trainings in various distinct areas.

I further want to thank Hanns-Joachim Rziha for his support and supervision of all projects in our group. His expertise, ideas and writing skill in the field of ORFV and viral vectors are exemplary and significantly contributed to my work.

Thank you Thomas Feger, Melanie Müller, Alena Reguzova, Felix Pagallies and Petra Schwarzmaier for a familiar working atmosphere, scientific discussions, technical assistance and friendship. In this regard, I also want to thank present and former students of the AG Amann such as Julian Senn, Anja Pohl, Yacine Maringer, Svenja Wöhrle, Alessa Voß and Pia Hüber for their scientific contributions to my work.

Sincere gratitude I owe to Timo Manz, Ana Marcu and Yamel Cardona Gloria for scientific support, fiendship and various good times apart from work, Latifa Zekri-Metref for antibody related advice, and all other elks for the great times and memories.

Furthermore, I want to thank my cooperation partners at Boehringer Ingelheim for the performance of animal experiments.

Last but not least, I want to express my deepest gratitude to my parents, family and Anne for love and infinite support in every possible manner.

# 7 Literature


1. Bonilla, F.A. and H.C. Oettgen, *Adaptive immunity.* J Allergy Clin Immunol, 2010. **125**(2 Suppl 2): p. S33-40.
2. Murphy, K., *Janeway's Immunobiology*. 8 ed. 2012, London & New York: Garland Science, Taylor & Francis Group, LLC.
3. Liu, Z.Z. and P.A. Roche, *Macropinocytosis in phagocytes: regulation of MHC class-II-restricted antigen presentation in dendritic cells.* Frontiers in Physiology, 2015. **6**.
4. Weninger, W., N. Manjunath, and U.H. von Andrian, *Migration and differentiation of CD8(+) T cells.* Immunological Reviews, 2002. **186**: p. 221-233.
5. Curtsinger, J.M. and M.F. Mescher, *Inflammatory cytokines as a third signal for T cell activation.* Current Opinion in Immunology, 2010. **22**(3): p. 333-340.
6. den Haan, J.M.M., R. Arens, and M.C. van Zelm, *The activation of the adaptive immune system: Cross-talk between antigen-presenting cells, T cells and B cells.* Immunology Letters, 2014. **162**(2): p. 103-112.
7. Greenwood, B., *The contribution of vaccination to global health: past, present and future.* Philos Trans R Soc Lond B Biol Sci, 2014. **369**(1645): p. 20130433.
8. *Measles*. 2018 [cited 2019 October 16]; Available from: https://www.who.int/immunization/diseases/measles/en/.
9. van Panhuis, W.G., J. Grefenstette, S.Y. Jung, N.S. Chok, A. Cross, H. Eng, B.Y. Lee, V. Zadorozhny, S. Brown, D. Cummings, and D.S. Burke, *Contagious diseases in the United States from 1888 to the present.* N Engl J Med, 2013. **369**(22): p. 2152-8.
10. García-Arriaza, J. and M. Esteban, *Enhancing poxvirus vectors vaccine immunogenicity.* Human vaccines & immunotherapeutics, 2014. **10**(8): p. 2235-2244.
11. Plotkin, S.A., Orenstein, W.A. & Offit, P.A., *Vaccines 5th edition*. 2008, Philadelphia: Saunders/Elsevier.
12. Pulendran, B. and R. Ahmed, *Immunological mechanisms of vaccination.* Nat Immunol, 2011. **12**(6): p. 509-17.
13. Del Giudice, G., R. Rappuoli, and A.M. Didierlaurent, *Correlates of adjuvanticity: A review on adjuvants in licensed vaccines.* Semin Immunol, 2018. **39**: p. 14-21.
14. Butler, N.S., J.C. Nolz, and J.T. Harty, *Immunologic considerations for generating memory CD8 T cells through vaccination.* Cell Microbiol, 2011. **13**(7): p. 925-33.
15. Mascola, J.R., A. Sambor, K. Beaudry, S. Santra, B. Welcher, M.K. Louder, T.C. Vancott, Y. Huang, B.K. Chakrabarti, W.P. Kong, Z.Y. Yang, L. Xu, D.C. Montefiori, G.J. Nabel, and N.L. Letvin, *Neutralizing antibodies elicited by immunization of monkeys with DNA plasmids and recombinant adenoviral vectors expressing human immunodeficiency virus type 1 proteins.* J Virol, 2005. **79**(2): p. 771-9.
16. van Rooij, E.M., F.A. Rijsewijk, H.W. Moonen-Leusen, A.T. Bianchi, and H.J. Rziha, *Comparison of different prime-boost regimes with DNA and recombinant Orf virus based vaccines expressing glycoprotein D of pseudorabies virus in pigs.* Vaccine, 2010. **28**(7): p. 1808-13.
17. *All cancers Fact Sheet*. 2018 [cited 2019 August 26]; Available from: http://gco.iarc.fr/today/data/factsheets/cancers/39-All-cancers-fact-sheet.pdf.
18. *Cancer statistics*. 2018 [cited 2019 August 26]; Available from: https://www.cancer.gov/about-cancer/understanding/statistics.

19. Arruebo, M., N. Vilaboa, B. Saez-Gutierrez, J. Lambea, A. Tres, M. Valladares, and A. Gonzalez-Fernandez, *Assessment of the evolution of cancer treatment therapies.* Cancers (Basel), 2011. **3**(3): p. 3279-330.
20. Gebhardt, U. *Mit Bakterien gegen Krebs*. 2010 [cited 2019 October 31]; Available from: https://www.zeit.de/wissen/2010-01/operation-lockvogel.
21. Coley, W.B., *The Treatment of Inoperable Sarcoma by Bacterial Toxins (the Mixed Toxins of the Streptococcus erysipelas and the Bacillus prodigiosus).* Proc R Soc Med, 1910. **3**(Surg Sect): p. 1-48.
22. Mellman, I., G. Coukos, and G. Dranoff, *Cancer immunotherapy comes of age.* Nature, 2011. **480**(7378): p. 480-9.
23. Kolb, H.J., *Donor leukocyte transfusions for treatment of leukemic relapse after bone marrow transplantation. EBMT Immunology and Chronic Leukemia Working Parties.* Vox Sang, 1998. **74 Suppl 2**: p. 321-9.
24. Hodi, F.S., S.J. O'Day, D.F. McDermott, R.W. Weber, J.A. Sosman, J.B. Haanen, R. Gonzalez, C. Robert, D. Schadendorf, J.C. Hassel, W. Akerley, A.J. van den Eertwegh, J. Lutzky, P. Lorigan, J.M. Vaubel, G.P. Linette, D. Hogg, C.H. Ottensmeier, C. Lebbe, C. Peschel, I. Quirt, J.I. Clark, J.D. Wolchok, J.S. Weber, J. Tian, M.J. Yellin, G.M. Nichol, A. Hoos, and W.J. Urba, *Improved survival with ipilimumab in patients with metastatic melanoma.* N Engl J Med, 2010. **363**(8): p. 711-23.
25. Kantoff, P.W., C.S. Higano, N.D. Shore, E.R. Berger, E.J. Small, D.F. Penson, C.H. Redfern, A.C. Ferrari, R. Dreicer, R.B. Sims, Y. Xu, M.W. Frohlich, P.F. Schellhammer, and I.S. Investigators, *Sipuleucel-T immunotherapy for castration-resistant prostate cancer.* N Engl J Med, 2010. **363**(5): p. 411-22.
26. Robert, C., G.V. Long, B. Brady, C. Dutriaux, M. Maio, L. Mortier, J.C. Hassel, P. Rutkowski, C. McNeil, E. Kalinka-Warzocha, K.J. Savage, M.M. Hernberg, C. Lebbe, J. Charles, C. Mihalcioiu, V. Chiarion-Sileni, C. Mauch, F. Cognetti, A. Arance, H. Schmidt, D. Schadendorf, H. Gogas, L. Lundgren-Eriksson, C. Horak, B. Sharkey, I.M. Waxman, V. Atkinson, and P.A. Ascierto, *Nivolumab in previously untreated melanoma without BRAF mutation.* N Engl J Med, 2015. **372**(4): p. 320-30.
27. Robert, C., J. Schachter, G.V. Long, A. Arance, J.J. Grob, L. Mortier, A. Daud, M.S. Carlino, C. McNeil, M. Lotem, J. Larkin, P. Lorigan, B. Neyns, C.U. Blank, O. Hamid, C. Mateus, R. Shapira-Frommer, M. Kosh, H. Zhou, N. Ibrahim, S. Ebbinghaus, A. Ribas, and K.-. investigators, *Pembrolizumab versus Ipilimumab in Advanced Melanoma.* N Engl J Med, 2015. **372**(26): p. 2521-32.
28. Burnet, M., *Cancer; a biological approach. I. The processes of control.* Br Med J, 1957. **1**(5022): p. 779-86.
29. Dunn, G.P., A.T. Bruce, H. Ikeda, L.J. Old, and R.D. Schreiber, *Cancer immunoediting: from immunosurveillance to tumor escape.* Nat Immunol, 2002. **3**(11): p. 991-8.
30. Dunn, G.P., C.M. Koebel, and R.D. Schreiber, *Interferons, immunity and cancer immunoediting.* Nat Rev Immunol, 2006. **6**(11): p. 836-48.
31. Shankaran, V., H. Ikeda, A.T. Bruce, J.M. White, P.E. Swanson, L.J. Old, and R.D. Schreiber, *IFNgamma and lymphocytes prevent primary tumour development and shape tumour immunogenicity.* Nature, 2001. **410**(6832): p. 1107-11.
32. Mittal, D., M.M. Gubin, R.D. Schreiber, and M.J. Smyth, *New insights into cancer immunoediting and its three component phases--elimination, equilibrium and escape.* Curr Opin Immunol, 2014. **27**: p. 16-25.

33. Schreiber, R.D., L.J. Old, and M.J. Smyth, *Cancer immunoediting: integrating immunity's roles in cancer suppression and promotion.* Science, 2011. **331**(6024): p. 1565-70.
34. Aguirre-Ghiso, J.A., *Models, mechanisms and clinical evidence for cancer dormancy.* Nat Rev Cancer, 2007. **7**(11): p. 834-46.
35. Riley, R.S., C.H. June, R. Langer, and M.J. Mitchell, *Delivery technologies for cancer immunotherapy.* Nat Rev Drug Discov, 2019. **18**(3): p. 175-196.
36. Quesada, J.R., E.M. Hersh, J. Manning, J. Reuben, M. Keating, E. Schnipper, L. Itri, and J.U. Gutterman, *Treatment of hairy cell leukemia with recombinant alpha-interferon.* Blood, 1986. **68**(2): p. 493-7.
37. Ahmed, S. and K.R. Rai, *Interferon in the treatment of hairy-cell leukemia.* Best Pract Res Clin Haematol, 2003. **16**(1): p. 69-81.
38. Croft, M., *Co-stimulatory members of the TNFR family: keys to effective T-cell immunity?* Nat Rev Immunol, 2003. **3**(8): p. 609-20.
39. Milling, L., Y. Zhang, and D.J. Irvine, *Delivering safer immunotherapies for cancer.* Adv Drug Deliv Rev, 2017. **114**: p. 79-101.
40. Chester, C., M.F. Sanmamed, J. Wang, and I. Melero, *Immunotherapy targeting 4-1BB: mechanistic rationale, clinical results, and future strategies.* Blood, 2018. **131**(1): p. 49-57.
41. Lim, W.A. and C.H. June, *The Principles of Engineering Immune Cells to Treat Cancer.* Cell, 2017. **168**(4): p. 724-740.
42. Schneble, E., G.T. Clifton, D.F. Hale, and G.E. Peoples, *Peptide-Based Cancer Vaccine Strategies and Clinical Results.* Methods Mol Biol, 2016. **1403**: p. 797-817.
43. Jackson, D.A., R.H. Symons, and P. Berg, *Biochemical method for inserting new genetic information into DNA of Simian Virus 40: circular SV40 DNA molecules containing lambda phage genes and the galactose operon of Escherichia coli.* Proc Natl Acad Sci U S A, 1972. **69**(10): p. 2904-9.
44. Smith, G.L., M. Mackett, and B. Moss, *Infectious vaccinia virus recombinants that express hepatitis B virus surface antigen.* Nature, 1983. **302**(5908): p. 490-5.
45. Moss, B., G.L. Smith, J.L. Gerin, and R.H. Purcell, *Live recombinant vaccinia virus protects chimpanzees against hepatitis B.* Nature, 1984. **311**(5981): p. 67-9.
46. Akira, S., S. Uematsu, and O. Takeuchi, *Pathogen recognition and innate immunity.* Cell, 2006. **124**(4): p. 783-801.
47. Ura, T., K. Okuda, and M. Shimada, *Developments in Viral Vector-Based Vaccines.* Vaccines (Basel), 2014. **2**(3): p. 624-41.
48. Park, K., W.J. Kim, Y.H. Cho, Y.I. Lee, H. Lee, S. Jeong, E.S. Cho, S.I. Chang, S.K. Moon, B.S. Kang, Y.J. Kim, and S.H. Cho, *Cancer gene therapy using adeno-associated virus vectors.* Front Biosci, 2008. **13**: p. 2653-9.
49. Lundstrom, K., *Viral Vectors in Gene Therapy.* Diseases (Basel, Switzerland), 2018. **6**(2): p. 42.
50. Beitelshees, M., A. Hill, P. Rostami, C.H. Jones, and B.A. Pfeifer, *Pressing diseases that represent promising targets for gene therapy.* Discov Med, 2017. **24**(134): p. 313-322.
51. Raty, J.K., J.T. Pikkarainen, T. Wirth, and S. Yla-Herttuala, *Gene therapy: the first approved gene-based medicines, molecular mechanisms and clinical indications.* Curr Mol Pharmacol, 2008. **1**(1): p. 13-23.
52. Zhang, W.W., L. Li, D. Li, J. Liu, X. Li, W. Li, X. Xu, M.J. Zhang, L.A. Chandler, H. Lin, A. Hu, W. Xu, and D.M. Lam, *The First Approved Gene Therapy Product for Cancer Ad-p53 (Gendicine): 12 Years in the Clinic.* Hum Gene Ther, 2018. **29**(2): p. 160-179.

53. Liu, T.C. and D. Kirn, *Gene therapy progress and prospects cancer: oncolytic viruses.* Gene Ther, 2008. **15**(12): p. 877-84.
54. Fukuhara, H., Y. Ino, and T. Todo, *Oncolytic virus therapy: A new era of cancer treatment at dawn.* Cancer Sci, 2016. **107**(10): p. 1373-1379.
55. Heo, J., T. Reid, L. Ruo, C.J. Breitbach, S. Rose, M. Bloomston, M. Cho, H.Y. Lim, H.C. Chung, C.W. Kim, J. Burke, R. Lencioni, T. Hickman, A. Moon, Y.S. Lee, M.K. Kim, M. Daneshmand, K. Dubois, L. Longpre, M. Ngo, C. Rooney, J.C. Bell, B.G. Rhee, R. Patt, T.H. Hwang, and D.H. Kirn, *Randomized dose-finding clinical trial of oncolytic immunotherapeutic vaccinia JX-594 in liver cancer.* Nat Med, 2013. **19**(3): p. 329-36.
56. Ramesh, N., Y. Ge, D.L. Ennist, M. Zhu, M. Mina, S. Ganesh, P.S. Reddy, and D.C. Yu, *CG0070, a conditionally replicating granulocyte macrophage colony-stimulating factor--armed oncolytic adenovirus for the treatment of bladder cancer.* Clin Cancer Res, 2006. **12**(1): p. 305-13.
57. Galanis, E., S.N. Markovic, V.J. Suman, G.J. Nuovo, R.G. Vile, T.J. Kottke, W.K. Nevala, M.A. Thompson, J.E. Lewis, K.M. Rumilla, V. Roulstone, K. Harrington, G.P. Linette, W.J. Maples, M. Coffey, J. Zwiebel, and K. Kendra, *Phase II trial of intravenous administration of Reolysin((R)) (Reovirus Serotype-3-dearing Strain) in patients with metastatic melanoma.* Mol Ther, 2012. **20**(10): p. 1998-2003.
58. Gollamudi, R., M.H. Ghalib, K.K. Desai, I. Chaudhary, B. Wong, M. Einstein, M. Coffey, G.M. Gill, K. Mettinger, J.M. Mariadason, S. Mani, and S. Goel, *Intravenous administration of Reolysin, a live replication competent RNA virus is safe in patients with advanced solid tumors.* Invest New Drugs, 2010. **28**(5): p. 641-9.
59. Oliveira, G.P., R.A.L. Rodrigues, M.T. Lima, B.P. Drumond, and J.S. Abrahao, *Poxvirus Host Range Genes and Virus-Host Spectrum: A Critical Review.* Viruses, 2017. **9**(11).
60. *Taxonomy*. [cited 2019 August 30]; Available from: https://talk.ictvonline.org/taxonomy/.
61. Moss, B., *Poxvirus DNA replication.* Cold Spring Harb Perspect Biol, 2013. **5**(9).
62. Price, P.J., L.E. Torres-Dominguez, C. Brandmuller, G. Sutter, and M.H. Lehmann, *Modified Vaccinia virus Ankara: innate immune activation and induction of cellular signalling.* Vaccine, 2013. **31**(39): p. 4231-4.
63. Zhu, J., J. Martinez, X. Huang, and Y. Yang, *Innate immunity against vaccinia virus is mediated by TLR2 and requires TLR-independent production of IFN-beta.* Blood, 2007. **109**(2): p. 619-25.
64. Kaufman, H.L., S. Kim-Schulze, K. Manson, G. DeRaffele, J. Mitcham, K.S. Seo, D.W. Kim, and J. Marshall, *Poxvirus-based vaccine therapy for patients with advanced pancreatic cancer.* J Transl Med, 2007. **5**: p. 60.
65. Petrulio, C.A. and H.L. Kaufman, *Development of the PANVAC-VF vaccine for pancreatic cancer.* Expert Rev Vaccines, 2006. **5**(1): p. 9-19.
66. Al Yaghchi, C., Z. Zhang, G. Alusi, N.R. Lemoine, and Y. Wang, *Vaccinia virus, a promising new therapeutic agent for pancreatic cancer.* Immunotherapy, 2015. **7**(12): p. 1249-58.
67. *Therion Biologics Corporation Reports Results Of Phase 3 PANVAC-VF Trial And Announces Plans For Company Sale*. 2006 [cited 2019 August 29]; Available from: https://www.biospace.com/article/releases/therion-biologics-corporation-reports-results-of-phase-3-panvac-vf-trial-and-announces-plans-for-company-sale-/.
68. Hanna, M., Jr., *Human vaccines & immunotherapeutics: news.* Hum Vaccin Immunother, 2014. **10**(7): p. 1773-7.

69. Rerks-Ngarm, S., P. Pitisuttithum, S. Nitayaphan, J. Kaewkungwal, J. Chiu, R. Paris, N. Premsri, C. Namwat, M. de Souza, E. Adams, M. Benenson, S. Gurunathan, J. Tartaglia, J.G. McNeil, D.P. Francis, D. Stablein, D.L. Birx, S. Chunsuttiwat, C. Khamboonruang, P. Thongcharoen, M.L. Robb, N.L. Michael, P. Kunasol, J.H. Kim, and M.-T. Investigators, *Vaccination with ALVAC and AIDSVAX to prevent HIV-1 infection in Thailand.* N Engl J Med, 2009. **361**(23): p. 2209-20.
70. Stickl, H., V. Hochstein-Mintzel, A. Mayr, H.C. Huber, H. Schafer, and A. Holzner, *[MVA vaccination against smallpox: clinical tests with an attenuated live vaccinia virus strain (MVA) (author's transl)].* Dtsch Med Wochenschr, 1974. **99**(47): p. 2386-92.
71. Nagington, J. and R.W. Horne, *Morphological studies of orf and vaccinia viruses.* Virology, 1962. **16**: p. 248-60.
72. Spehner, D., S. De Carlo, R. Drillien, F. Weiland, K. Mildner, D. Hanau, and H.J. Rziha, *Appearance of the bona fide spiral tubule of Orf virus is dependent on an intact 10-kilodalton viral protein.* Journal of Virology, 2004. **78**(15): p. 8085-8093.
73. Tan, J.L., N. Ueda, A.A. Mercer, and S.B. Fleming, *Investigation of orf virus structure and morphogenesis using recombinants expressing FLAG-tagged envelope structural proteins: evidence for wrapped virus particles and egress from infected cells.* J Gen Virol, 2009. **90**(Pt 3): p. 614-25.
74. Moss, B., *Poxvirus cell entry: how many proteins does it take?* Viruses, 2012. **4**(5): p. 688-707.
75. Wittek, R., C.C. Kuenzle, and R. Wyler, *High C + G content in parapoxvirus DNA.* J Gen Virol, 1979. **43**(1): p. 231-4.
76. Garon, C.F., E. Barbosa, and B. Moss, *Visualization of an inverted terminal repetition in vaccinia virus DNA.* Proc Natl Acad Sci U S A, 1978. **75**(10): p. 4863-7.
77. Wittek, R., A. Menna, H.K. Muller, D. Schumperli, P.G. Boseley, and R. Wyler, *Inverted terminal repeats in rabbit poxvirus and vaccinia virus DNA.* J Virol, 1978. **28**(1): p. 171-81.
78. Baroudy, B.M., S. Venkatesan, and B. Moss, *Incompletely base-paired flip-flop terminal loops link the two DNA strands of the vaccinia virus genome into one uninterrupted polynucleotide chain.* Cell, 1982. **28**(2): p. 315-24.
79. Wang, R., Y. Wang, F. Liu, and S. Luo, *Orf virus: A promising new therapeutic agent.* Rev Med Virol, 2019. **29**(1): p. e2013.
80. Delhon, G., E.R. Tulman, C.L. Afonso, Z. Lu, A. de la Concha-Bermejillo, H.D. Lehmkuhl, M.E. Piccone, G.F. Kutish, and D.L. Rock, *Genomes of the parapoxviruses ORF virus and bovine papular stomatitis virus.* J Virol, 2004. **78**(1): p. 168-77.
81. Mercer, A.A., N. Ueda, S.M. Friederichs, K. Hofmann, K.M. Fraser, T. Bateman, and S.B. Fleming, *Comparative analysis of genome sequences of three isolates of Orf virus reveals unexpected sequence variation.* Virus Res, 2006. **116**(1-2): p. 146-58.
82. Fleming, S.B., D.J. Lyttle, J.T. Sullivan, A.A. Mercer, and A.J. Robinson, *Genomic analysis of a transposition-deletion variant of orf virus reveals a 3.3 kbp region of non-essential DNA.* J Gen Virol, 1995. **76 ( Pt 12)**: p. 2969-78.
83. McInnes, C.J., A.R. Wood, P.E. Nettleton, and J.A. Gilray, *Genomic comparison of an avirulent strain of Orf virus with that of a virulent wild type isolate reveals that the Orf virus G2L gene is non-essential for replication.* Virus Genes, 2001. **22**(2): p. 141-50.
84. Rziha, H.-J., M. Büttner, M. Müller, F. Salomon, A. Reguzova, D. Laible, and R. Amann, *Genomic Characterization of Orf Virus Strain D1701-V (Parapoxvirus) and Development of Novel Sites for Multiple Transgene Expression.* Viruses, 2019. **11**(2): p. 127.

85. Meyer, H., G. Sutter, and A. Mayr, *Mapping of deletions in the genome of the highly attenuated vaccinia virus MVA and their influence on virulence.* J Gen Virol, 1991. **72 ( Pt 5)**: p. 1031-8.
86. White, J.M., S.E. Delos, M. Brecher, and K. Schornberg, *Structures and mechanisms of viral membrane fusion proteins: multiple variations on a common theme.* Crit Rev Biochem Mol Biol, 2008. **43**(3): p. 189-219.
87. Yang, Z., S.E. Reynolds, C.A. Martens, D.P. Bruno, S.F. Porcella, and B. Moss, *Expression profiling of the intermediate and late stages of poxvirus replication.* J Virol, 2011. **85**(19): p. 9899-908.
88. Fleming, S.B. and A.A. Mercer, *Genus Parapoxvirus*, in *Poxviruses*, A.A. Mercer, A. Schmidt, and O. Weber, Editors. 2007, Birkhäuser Basel: Basel. p. 127-165.
89. Haig, D.M. and C.J. McInnes, *Immunity and counter-immunity during infection with the parapoxvirus orf virus.* Virus Research, 2002. **88**(1): p. 3-16.
90. McKeever, D.J., D.M. Jenkinson, G. Hutchison, and H.W. Reid, *Studies of the pathogenesis of orf virus infection in sheep.* J Comp Pathol, 1988. **99**(3): p. 317-28.
91. Buttner, M. and H.J. Rziha, *Parapoxviruses: from the lesion to the viral genome.* J Vet Med B Infect Dis Vet Public Health, 2002. **49**(1): p. 7-16.
92. Hussain, K.A. and D. Burger, *In vivo and in vitro characteristics of contagious ecthyma virus isolates: host response mechanism.* Vet Microbiol, 1989. **19**(1): p. 23-36.
93. Rziha, H., M. Henkel, R. Cottone, B. Bauer, U. Auge, F. Gotz, E. Pfaff, M. Rottgen, C. Dehio, and M. Buttner, *Generation of recombinant parapoxviruses: non-essential genes suitable for insertion and expression of foreign genes.* J Biotechnol, 2000. **83**(1-2): p. 137-45.
94. Haig, D.M. and A.A. Mercer, *Ovine diseases. Orf.* Vet Res, 1998. **29**(3-4): p. 311-26.
95. Fairley, R.A., E.M. Whelan, P.A. Pesavento, and A.A. Mercer, *Recurrent localised cutaneous parapoxvirus infection in three cats.* N Z Vet J, 2008. **56**(4): p. 196-201.
96. Inoshima, Y., K. Murakami, D. Wu, and H. Sentsui, *Characterization of parapoxviruses circulating among wild Japanese serows (Capricornis crispus).* Microbiol Immunol, 2002. **46**(8): p. 583-7.
97. Azwai, S.M., S.D. Carter, and Z. Woldehiwet, *Immune responses of the camel (Camelus dromedarius) to contagious ecthyma (Orf) virus infection.* Vet Microbiol, 1995. **47**(1-2): p. 119-31.
98. Fleming, S.B., L.M. Wise, and A.A. Mercer, *Molecular genetic analysis of orf virus: a poxvirus that has adapted to skin.* Viruses, 2015. **7**(3): p. 1505-39.
99. Savage, J. and M.M. Black, *'Giant' orf of finger in a patient with a lymphoma.* Proc R Soc Med, 1972. **65**(9): p. 766-8.
100. Tan, S.T., G.B. Blake, and S. Chambers, *Recurrent orf in an immunocompromised host.* Br J Plast Surg, 1991. **44**(6): p. 465-7.
101. Anderson, I.E., H.W. Reid, P.F. Nettleton, C.J. McInnes, and D.M. Haig, *Detection of cellular cytokine mRNA expression during orf virus infection in sheep: differential interferon-gamma mRNA expression by cells in primary versus reinfection skin lesions.* Vet Immunol Immunopathol, 2001. **83**(3-4): p. 161-76.
102. Buddle, B.M. and H.D. Pulford, *Effect of passively-acquired antibodies and vaccination on the immune response to contagious ecthyma virus.* Vet Microbiol, 1984. **9**(6): p. 515-22.
103. Mayr, A., M. Herlyn, H. Mahnel, A. Danco, A. Zach, and H. Bostedt, *[Control of ecthyma contagiosum (pustular dermatitis) of sheep with a new parenteral cell culture live vaccine].* Zentralbl Veterinarmed B, 1981. **28**(7): p. 535-52.

104. Pye, D., *Vaccination of sheep with cell culture grown orf virus.* Aust Vet J, 1990. **67**(5): p. 182-6.
105. Nettleton, P.F., J. Brebner, I. Pow, J.A. Gilray, G.D. Bell, and H.W. Reid, *Tissue culture-propagated orf virus vaccine protects lambs from orf virus challenge.* Vet Rec, 1996. **138**(8): p. 184-6.
106. Weber, O., P. Knolle, and H.-D. Volk, *Immunomodulation by inactivated Orf virus (ORFV) - therapeutic potential*, in *Poxviruses*, A.A. Mercer, A. Schmidt, and O. Weber, Editors. 2007, Birkhäuser Basel: Basel. p. 297-310.
107. Weber, O., A.A. Mercer, A. Friebe, P. Knolle, and H.D. Volk, *Therapeutic immunomodulation using a virus--the potential of inactivated orf virus.* Eur J Clin Microbiol Infect Dis, 2013. **32**(4): p. 451-60.
108. Pohlscheidt, M., U. Langer, T. Minuth, B. Bodeker, H. Apeler, H.D. Horlein, D. Paulsen, H. Rubsamen-Waigmann, H.J. Henzler, and U. Reichl, *Development and optimisation of a procedure for the production of Parapoxvirus ovis by large-scale microcarrier cell culture in a non-animal, non-human and non-plant-derived medium.* Vaccine, 2008. **26**(12): p. 1552-65.
109. Chen, D.Y., J.A. Fabrizio, S.E. Wilkins, K.A. Dave, J.J. Gorman, J.M. Gleadle, S.B. Fleming, D.J. Peet, and A.A. Mercer, *Ankyrin Repeat Proteins of Orf Virus Influence the Cellular Hypoxia Response Pathway.* J Virol, 2017. **91**(1).
110. Cuninghame, S., R. Jackson, and I. Zehbe, *Hypoxia-inducible factor 1 and its role in viral carcinogenesis.* Virology, 2014. **456-457**: p. 370-83.
111. Deane, D., C.J. McInnes, A. Percival, A. Wood, J. Thomson, A. Lear, J. Gilray, S. Fleming, A. Mercer, and D. Haig, *Orf virus encodes a novel secreted protein inhibitor of granulocyte-macrophage colony-stimulating factor and interleukin-2.* J Virol, 2000. **74**(3): p. 1313-20.
112. Meyer, M., M. Clauss, A. Lepple-Wienhues, J. Waltenberger, H.G. Augustin, M. Ziche, C. Lanz, M. Buttner, H.J. Rziha, and C. Dehio, *A novel vascular endothelial growth factor encoded by Orf virus, VEGF-E, mediates angiogenesis via signalling through VEGFR-2 (KDR) but not VEGFR-1 (Flt-1) receptor tyrosine kinases.* EMBO J, 1999. **18**(2): p. 363-74.
113. Savory, L.J., S.A. Stacker, S.B. Fleming, B.E. Niven, and A.A. Mercer, *Viral vascular endothelial growth factor plays a critical role in orf virus infection.* J Virol, 2000. **74**(22): p. 10699-706.
114. Wise, L.M., T. Veikkola, A.A. Mercer, L.J. Savory, S.B. Fleming, C. Caesar, A. Vitali, T. Makinen, K. Alitalo, and S.A. Stacker, *Vascular endothelial growth factor (VEGF)-like protein from orf virus NZ2 binds to VEGFR2 and neuropilin-1.* Proc Natl Acad Sci U S A, 1999. **96**(6): p. 3071-6.
115. Rziha, H.J., M. Henkel, R. Cottone, M. Meyer, C. Dehio, and M. Buttner, *Parapoxviruses: potential alternative vectors for directing the immune response in permissive and non-permissive hosts.* J Biotechnol, 1999. **73**(2-3): p. 235-42.
116. Haig, D.M., C. McInnes, D. Deane, H. Reid, and A. Mercer, *The immune and inflammatory response to orf virus.* Comp Immunol Microbiol Infect Dis, 1997. **20**(3): p. 197-204.
117. Fischer, T., O. Planz, L. Stitz, and H.J. Rziha, *Novel recombinant parapoxvirus vectors induce protective humoral and cellular immunity against lethal herpesvirus challenge infection in mice.* J Virol, 2003. **77**(17): p. 9312-23.
118. Henkel, M., O. Planz, T. Fischer, L. Stitz, and H.J. Rziha, *Prevention of virus persistence and protection against immunopathology after Borna disease virus infection of the brain by a novel Orf virus recombinant.* J Virol, 2005. **79**(1): p. 314-25.

119. Dory, D., T. Fischer, V. Beven, R. Cariolet, H.J. Rziha, and A. Jestin, *Prime-boost immunization using DNA vaccine and recombinant Orf virus protects pigs against Pseudorabies virus (Herpes suid 1).* Vaccine, 2006. **24**(37-39): p. 6256-63.
120. Voigt, H., C. Merant, D. Wienhold, A. Braun, E. Hutet, M.F. Le Potier, A. Saalmuller, E. Pfaff, and M. Buttner, *Efficient priming against classical swine fever with a safe glycoprotein E2 expressing Orf virus recombinant (ORFV VrV-E2).* Vaccine, 2007. **25**(31): p. 5915-26.
121. Rohde, J., H. Schirrmeier, H. Granzow, and H.J. Rziha, *A new recombinant Orf virus (ORFV, Parapoxvirus) protects rabbits against lethal infection with rabbit hemorrhagic disease virus (RHDV).* Vaccine, 2011. **29**(49): p. 9256-64.
122. Amann, R., J. Rohde, U. Wulle, D. Conlee, R. Raue, O. Martinon, and H.J. Rziha, *A new rabies vaccine based on a recombinant ORF virus (parapoxvirus) expressing the rabies virus glycoprotein.* J Virol, 2013. **87**(3): p. 1618-30.
123. Rohde, J., R. Amann, and H.J. Rziha, *New Orf virus (Parapoxvirus) recombinant expressing H5 hemagglutinin protects mice against H5N1 and H1N1 influenza A virus.* PLoS One, 2013. **8**(12): p. e83802.
124. Müller, M., *Weiterentwicklung des Orf-Virus Stamms D1701-V zur Verwendung als therapeutische Vektor-Vakzine*, in *Interfaculty Institute of Cell Biology, Department of Immunology*. 2019, Dissertation Eberhard Karls Universität Tübingen: Tübingen.
125. Brun, A., E. Albina, T. Barret, D.A. Chapman, M. Czub, L.K. Dixon, G.M. Keil, B. Klonjkowski, M.F. Le Potier, G. Libeau, J. Ortego, J. Richardson, and H.H. Takamatsu, *Antigen delivery systems for veterinary vaccine development. Viral-vector based delivery systems.* Vaccine, 2008. **26**(51): p. 6508-28.
126. Buddle, B.M., R.W. Dellers, and G.G. Schurig, *Contagious ecthyma virus-vaccination failures.* Am J Vet Res, 1984. **45**(2): p. 263-6.
127. Kruse, N. and O. Weber, *Selective induction of apoptosis in antigen-presenting cells in mice by Parapoxvirus ovis.* J Virol, 2001. **75**(10): p. 4699-704.
128. Drexler, I., C. Staib, and G. Sutter, *Modified vaccinia virus Ankara as antigen delivery system: how can we best use its potential?* Current Opinion in Biotechnology, 2004. **15**(6): p. 506-512.
129. Gomez, C.E., J.L. Najera, M. Krupa, B. Perdiguero, and M. Esteban, *MVA and NYVAC as vaccines against emergent infectious diseases and cancer.* Curr Gene Ther, 2011. **11**(3): p. 189-217.
130. Draper, S.J., M.G. Cottingham, and S.C. Gilbert, *Utilizing poxviral vectored vaccines for antibody induction-progress and prospects.* Vaccine, 2013. **31**(39): p. 4223-30.
131. Edelstein, M. *Gene Therapy Clinical Trials Worldwide*. 2019 [cited 2019 July 30]; Available from: http://www.abedia.com/wiley/vectors.php.
132. Fleming, S.B., D.J. Lyttle, J.T. Sullivan, A.A. Mercer, and A.J. Robinson, *Genomic analysis of a transposition-deletion variant of orf virus reveals a 3.3 kbp region of non-essential DNA.* Journal of General Virology, 1995. **76**(12): p. 2969-2978.
133. Jacobs, B.L., J.O. Langland, K.V. Kibler, K.L. Denzler, S.D. White, S.A. Holechek, S. Wong, T. Huynh, and C.R. Baskin, *Vaccinia virus vaccines: past, present and future.* Antiviral Res, 2009. **84**(1): p. 1-13.
134. Wingren, A.G., E. Parra, M. Varga, T. Kalland, H.O. Sjogren, G. Hedlund, and M. Dohlsten, *T cell activation pathways: B7, LFA-3, and ICAM-1 shape unique T cell profiles.* Crit Rev Immunol, 1995. **15**(3-4): p. 235-53.
135. Shankar, P., J. Schlom, and J.W. Hodge, *Enhanced activation of rhesus T cells by vectors encoding a triad of costimulatory molecules (B7-1, ICAM-1, LFA-3).* Vaccine, 2001. **20**(5-6): p. 744-55.

136. Zhu, M., H. Terasawa, J. Gulley, D. Panicali, P. Arlen, J. Schlom, and K.Y. Tsang, *Enhanced activation of human T cells via avipox vector-mediated hyperexpression of a triad of costimulatory molecules in human dendritic cells.* Cancer Res, 2001. **61**(9): p. 3725-34.
137. Grosenbach, D.W., J. Schlom, L. Gritz, A. Gomez Yafal, and J.W. Hodge, *A recombinant vector expressing transgenes for four T-cell costimulatory molecules (OX40L, B7-1, ICAM-1, LFA-3) induces sustained CD4+ and CD8+ T-cell activation, protection from apoptosis, and enhanced cytokine production.* Cell Immunol, 2003. **222**(1): p. 45-57.
138. Kudo-Saito, C., J. Schlom, and J.W. Hodge, *Intratumoral vaccination and diversified subcutaneous/ intratumoral vaccination with recombinant poxviruses encoding a tumor antigen and multiple costimulatory molecules.* Clin Cancer Res, 2004. **10**(3): p. 1090-9.
139. Palena, C., M. Zhu, J. Schlom, and K.Y. Tsang, *Human B cells that hyperexpress a triad of costimulatory molecules via avipox-vector infection: an alternative source of efficient antigen-presenting cells.* Blood, 2004. **104**(1): p. 192-9.
140. Morse, M.A., T.M. Clay, A.C. Hobeika, T. Osada, S. Khan, S. Chui, D. Niedzwiecki, D. Panicali, J. Schlom, and H.K. Lyerly, *Phase I study of immunization with dendritic cells modified with fowlpox encoding carcinoembryonic antigen and costimulatory molecules.* Clin Cancer Res, 2005. **11**(8): p. 3017-24.
141. Gulley, J.L., P.M. Arlen, K.Y. Tsang, J. Yokokawa, C. Palena, D.J. Poole, C. Remondo, V. Cereda, J.L. Jones, M.P. Pazdur, J.P. Higgins, J.W. Hodge, S.M. Steinberg, H. Kotz, W.L. Dahut, and J. Schlom, *Pilot study of vaccination with recombinant CEA-MUC-1-TRICOM poxviral-based vaccines in patients with metastatic carcinoma.* Clin Cancer Res, 2008. **14**(10): p. 3060-9.
142. Madan, R.A., P.M. Arlen, M. Mohebtash, J.W. Hodge, and J.L. Gulley, *Prostvac-VF: a vector-based vaccine targeting PSA in prostate cancer.* Expert Opin Investig Drugs, 2009. **18**(7): p. 1001-11.
143. Abaitua, F., J.R. Rodriguez, A. Garzon, D. Rodriguez, and M. Esteban, *Improving recombinant MVA immune responses: potentiation of the immune responses to HIV-1 with MVA and DNA vectors expressing Env and the cytokines IL-12 and IFN-gamma.* Virus Res, 2006. **116**(1-2): p. 11-20.
144. Gherardi, M.M., J.C. Ramirez, and M. Esteban, *Interleukin-12 (IL-12) enhancement of the cellular immune response against human immunodeficiency virus type 1 env antigen in a DNA prime/vaccinia virus boost vaccine regimen is time and dose dependent: suppressive effects of IL-12 boost are mediated by nitric oxide.* J Virol, 2000. **74**(14): p. 6278-86.
145. Gherardi, M.M., J.C. Ramirez, D. Rodriguez, J.R. Rodriguez, G. Sano, F. Zavala, and M. Esteban, *IL-12 delivery from recombinant vaccinia virus attenuates the vector and enhances the cellular immune response against HIV-1 Env in a dose-dependent manner.* J Immunol, 1999. **162**(11): p. 6724-33.
146. Gonzalo, R.M., J.R. Rodriguez, D. Rodriguez, G. Gonzalez-Aseguinolaza, V. Larraga, and M. Esteban, *Protective immune response against cutaneous leishmaniasis by prime/booster immunization regimens with vaccinia virus recombinants expressing Leishmania infantum p36/LACK and IL-12 in combination with purified p36.* Microbes Infect, 2001. **3**(9): p. 701-11.
147. Nemeckova, S., V. Sroller, P. Hainz, J. Krystofova, M. Smahel, and L. Kutinova, *Experimental therapy of HPV16 induced tumors with IL12 expressed by recombinant vaccinia virus in mice.* Int J Mol Med, 2003. **12**(5): p. 789-96.

148. Rodriguez, A.M., M.F. Pascutti, C. Maeto, J. Falivene, M.P. Holgado, G. Turk, and M.M. Gherardi, *IL-12 and GM-CSF in DNA/MVA immunizations against HIV-1 CRF12_BF Nef induced T-cell responses with an enhanced magnitude, breadth and quality.* PLoS One, 2012. **7**(5): p. e37801.
149. Tapia, E., E. Perez-Jimenez, L. Lopez-Fuertes, R. Gonzalo, M.M. Gherardi, and M. Esteban, *The combination of DNA vectors expressing IL-12 + IL-18 elicits high protective immune response against cutaneous leishmaniasis after priming with DNA-p36/LACK and the cytokines, followed by a booster with a vaccinia virus recombinant expressing p36/LACK.* Microbes Infect, 2003. **5**(2): p. 73-84.
150. Goulding, J., V. Tahiliani, and S. Salek-Ardakani, *OX40:OX40L axis: emerging targets for improving poxvirus-based CD8(+) T-cell vaccines against respiratory viruses.* Immunol Rev, 2011. **244**(1): p. 149-68.
151. Liu, J., N. Ngai, G.W. Stone, F.Y. Yue, and M.A. Ostrowski, *The adjuvancy of OX40 ligand (CD252) on an HIV-1 canarypox vaccine.* Vaccine, 2009. **27**(37): p. 5077-84.
152. Vasir, B., C. Zarwan, R. Ahmad, K.D. Crawford, H. Rajabi, K. Matsuoka, J. Rosenblatt, Z. Wu, H. Mills, D. Kufe, and D. Avigan, *Induction of antitumor immunity ex vivo using dendritic cells transduced with fowl pox vector expressing MUC1, CEA, and a triad of costimulatory molecules (rF-PANVAC).* J Immunother, 2012. **35**(7): p. 555-69.
153. Bertley, F.M., P.A. Kozlowski, S.W. Wang, J. Chappelle, J. Patel, O. Sonuyi, G. Mazzara, D. Montefiori, A. Carville, K.G. Mansfield, and A. Aldovini, *Control of simian/human immunodeficiency virus viremia and disease progression after IL-2-augmented DNA-modified vaccinia virus Ankara nasal vaccination in nonhuman primates.* J Immunol, 2004. **172**(6): p. 3745-57.
154. Dreicer, R., W.M. Stadler, F.R. Ahmann, T. Whiteside, N. Bizouarne, B. Acres, J.M. Limacher, P. Squiban, and A. Pantuck, *MVA-MUC1-IL2 vaccine immunotherapy (TG4010) improves PSA doubling time in patients with prostate cancer with biochemical failure.* Invest New Drugs, 2009. **27**(4): p. 379-86.
155. Kaufman, H.L., B. Taback, W. Sherman, D.W. Kim, W.H. Shingler, D. Moroziewicz, G. DeRaffele, J. Mitcham, M.W. Carroll, R. Harrop, S. Naylor, and S. Kim-Schulze, *Phase II trial of Modified Vaccinia Ankara (MVA) virus expressing 5T4 and high dose Interleukin-2 (IL-2) in patients with metastatic renal cell carcinoma.* J Transl Med, 2009. **7**: p. 2.
156. Gomez, C.E., F. Abaitua, D. Rodriguez, and M. Esteban, *Efficient CD8+ T cell response to the HIV-env V3 loop epitope from multiple virus isolates by a DNA prime/vaccinia virus boost (rWR and rMVA strains) immunization regime and enhancement by the cytokine IFN-gamma.* Virus Res, 2004. **105**(1): p. 11-22.
157. Kolibab, K., A. Yang, S.C. Derrick, T.A. Waldmann, L.P. Perera, and S.L. Morris, *Highly persistent and effective prime/boost regimens against tuberculosis that use a multivalent modified vaccine virus Ankara-based tuberculosis vaccine with interleukin-15 as a molecular adjuvant.* Clin Vaccine Immunol, 2010. **17**(5): p. 793-801.
158. Li, S., X. Qi, Y. Gao, Y. Hao, L. Cui, L. Ruan, and W. He, *IL-15 increases the frequency of effector memory CD8+ T cells in rhesus monkeys immunized with HIV vaccine.* Cell Mol Immunol, 2010. **7**(6): p. 491-4.
159. Oh, S., J.A. Berzofsky, D.S. Burke, T.A. Waldmann, and L.P. Perera, *Coadministration of HIV vaccine vectors with vaccinia viruses expressing IL-15 but not IL-2 induces long-lasting cellular immunity.* Proc Natl Acad Sci U S A, 2003. **100**(6): p. 3392-7.

160. Perera, L.P., T.A. Waldmann, J.D. Mosca, N. Baldwin, J.A. Berzofsky, and S. Oh, *Development of smallpox vaccine candidates with integrated interleukin-15 that demonstrate superior immunogenicity, efficacy, and safety in mice.* J Virol, 2007. **81**(16): p. 8774-83.
161. Perera, P.Y., S.C. Derrick, K. Kolibab, F. Momoi, M. Yamamoto, S.L. Morris, T.A. Waldmann, and L.P. Perera, *A multi-valent vaccinia virus-based tuberculosis vaccine molecularly adjuvanted with interleukin-15 induces robust immune responses in mice.* Vaccine, 2009. **27**(15): p. 2121-7.
162. Poon, L.L., Y.H. Leung, J.M. Nicholls, P.Y. Perera, J.H. Lichy, M. Yamamoto, T.A. Waldmann, J.S. Peiris, and L.P. Perera, *Vaccinia virus-based multivalent H5N1 avian influenza vaccines adjuvanted with IL-15 confer sterile cross-clade protection in mice.* J Immunol, 2009. **182**(5): p. 3063-71.
163. Lai, L., S. Kwa, P.A. Kozlowski, D.C. Montefiori, G. Ferrari, W.E. Johnson, V. Hirsch, F. Villinger, L. Chennareddi, P.L. Earl, B. Moss, R.R. Amara, and H.L. Robinson, *Prevention of infection by a granulocyte-macrophage colony-stimulating factor co-expressing DNA/modified vaccinia Ankara simian immunodeficiency virus vaccine.* J Infect Dis, 2011. **204**(1): p. 164-73.
164. Lee, J.H., M.S. Roh, Y.K. Lee, M.K. Kim, J.Y. Han, B.H. Park, P. Trown, D.H. Kirn, and T.H. Hwang, *Oncolytic and immunostimulatory efficacy of a targeted oncolytic poxvirus expressing human GM-CSF following intravenous administration in a rabbit tumor model.* Cancer Gene Ther, 2010. **17**(2): p. 73-9.
165. Morse, M.A., D. Niedzwiecki, J.L. Marshall, C. Garrett, D.Z. Chang, M. Aklilu, T.S. Crocenzi, D.J. Cole, S. Dessureault, A.C. Hobeika, T. Osada, M. Onaitis, B.M. Clary, D. Hsu, G.R. Devi, A. Bulusu, R.P. Annechiarico, V. Chadaram, T.M. Clay, and H.K. Lyerly, *A randomized phase II study of immunization with dendritic cells modified with poxvectors encoding CEA and MUC1 compared with the same poxvectors plus GM-CSF for resected metastatic colorectal cancer.* Ann Surg, 2013. **258**(6): p. 879-86.
166. Nemeckova, S., M. Smahel, P. Hainz, J. Mackova, K. Zurkova, P. Gabriel, M. Indrova, and L. Kutinova, *Combination of intratumoral injections of vaccinia virus MVA expressing GM-CSF and immunization with DNA vaccine prolongs the survival of mice bearing HPV16 induced tumors with downregulated expression of MHC class I molecules.* Neoplasma, 2007. **54**(4): p. 326-33.
167. Gomez, C.E., J.L. Najera, R. Sanchez, V. Jimenez, and M. Esteban, *Multimeric soluble CD40 ligand (sCD40L) efficiently enhances HIV specific cellular immune responses during DNA prime and boost with attenuated poxvirus vectors MVA and NYVAC expressing HIV antigens.* Vaccine, 2009. **27**(24): p. 3165-74.
168. Lauterbach, H., J. Patzold, R. Kassub, B. Bathke, K. Brinkmann, P. Chaplin, M. Suter, and H. Hochrein, *Genetic Adjuvantation of Recombinant MVA with CD40L Potentiates CD8 T Cell Mediated Immunity.* Front Immunol, 2013. **4**: p. 251.
169. Liu, J., Q. Yu, G.W. Stone, F.Y. Yue, N. Ngai, R.B. Jones, R.S. Kornbluth, and M.A. Ostrowski, *CD40L expressed from the canarypox vector, ALVAC, can boost immunogenicity of HIV-1 canarypox vaccine in mice and enhance the in vitro expansion of viral specific CD8+ T cell memory responses from HIV-1-infected and HIV-1-uninfected individuals.* Vaccine, 2008. **26**(32): p. 4062-72.
170. Wyatt, L.S., P.L. Earl, J. Vogt, L.A. Eller, D. Chandran, J. Liu, H.L. Robinson, and B. Moss, *Correlation of immunogenicities and in vitro expression levels of recombinant modified vaccinia virus Ankara HIV vaccines.* Vaccine, 2008. **26**(4): p. 486-93.
171. Baur, K., K. Brinkmann, M. Schweneker, J. Patzold, C. Meisinger-Henschel, J. Hermann, R. Steigerwald, P. Chaplin, M. Suter, and J. Hausmann, *Immediate-early*

*expression of a recombinant antigen by modified vaccinia virus ankara breaks the immunodominance of strong vector-specific B8R antigen in acute and memory CD8 T-cell responses.* J Virol, 2010. **84**(17): p. 8743-52.
172. Moutaftsi, M., H.H. Bui, B. Peters, J. Sidney, S. Salek-Ardakani, C. Oseroff, V. Pasquetto, S. Crotty, M. Croft, E.J. Lefkowitz, H. Grey, and A. Sette, *Vaccinia virus-specific CD4+ T cell responses target a set of antigens largely distinct from those targeted by CD8+ T cell responses.* J Immunol, 2007. **178**(11): p. 6814-20.
173. Moutaftsi, M., D.C. Tscharke, K. Vaughan, D.M. Koelle, L. Stern, M. Calvo-Calle, F. Ennis, M. Terajima, G. Sutter, S. Crotty, I. Drexler, G. Franchini, J.W. Yewdell, S.R. Head, J. Blum, B. Peters, and A. Sette, *Uncovering the interplay between CD8, CD4 and antibody responses to complex pathogens.* Future Microbiol, 2010. **5**(2): p. 221-39.
174. Chakrabarti, S., J.R. Sisler, and B. Moss, *Compact, synthetic, vaccinia virus early/late promoter for protein expression.* Biotechniques, 1997. **23**(6): p. 1094-7.
175. Di Pilato, M., E. Mejías-Pérez, C.E. Gómez, B. Perdiguero, C.O.S. Sorzano, and M. Esteban, *New vaccinia virus promoter as a potential candidate for future vaccines.* Journal of General Virology, 2013. **94**(12): p. 2771-2776.
176. Barouch, D.H., K.E. Stephenson, E.N. Borducchi, K. Smith, K. Stanley, A.G. McNally, J. Liu, P. Abbink, L.F. Maxfield, M.S. Seaman, A.S. Dugast, G. Alter, M. Ferguson, W. Li, P.L. Earl, B. Moss, E.E. Giorgi, J.J. Szinger, L.A. Eller, E.A. Billings, M. Rao, S. Tovanabutra, E. Sanders-Buell, M. Weijtens, M.G. Pau, H. Schuitemaker, M.L. Robb, J.H. Kim, B.T. Korber, and N.L. Michael, *Protective efficacy of a global HIV-1 mosaic vaccine against heterologous SHIV challenges in rhesus monkeys.* Cell, 2013. **155**(3): p. 531-9.
177. Santra, S., H.-X. Liao, R. Zhang, M. Muldoon, S. Watson, W. Fischer, J. Theiler, J. Szinger, H. Balachandran, A. Buzby, D. Quinn, R.J. Parks, C.-Y. Tsao, A. Carville, K.G. Mansfield, G.N. Pavlakis, B.K. Felber, B.F. Haynes, B.T. Korber, and N.L. Letvin, *Mosaic vaccines elicit CD8+ T lymphocyte responses that confer enhanced immune coverage of diverse HIV strains in monkeys.* Nature Medicine, 2010. **16**: p. 324.
178. Schubert, B. and O. Kohlbacher, *Designing string-of-beads vaccines with optimal spacers.* Genome Med, 2016. **8**(1): p. 9.
179. Wyatt, L.S., P.L. Earl, W. Xiao, J.L. Americo, C.A. Cotter, J. Vogt, and B. Moss, *Elucidating and minimizing the loss by recombinant vaccinia virus of human immunodeficiency virus gene expression resulting from spontaneous mutations and positive selection.* J Virol, 2009. **83**(14): p. 7176-84.
180. Cottone, R., M. Büttner, B. Bauer, M. Henkel, E. Hettich, and H.-J. Rziha, *Analysis of genomic rearrangement and subsequent gene deletion of the attenuated Orf virus strain D1701.* Virus Research, 1998. **56**(1): p. 53-67.
181. Rziha, H.J., M. Henkel, R. Cottone, B. Bauer, U. Auge, F. Götz, E. Pfaff, M. Röttgen, C. Dehio, and M. Büttner, *Generation of recombinant parapoxviruses: non-essential genes suitable for insertion and expression of foreign genes.* Journal of Biotechnology, 2000. **83**(1): p. 137-145.
182. Fischer, T., O. Planz, L. Stitz, and H.-J. Rziha, *Novel recombinant parapoxvirus vectors induce protective humoral and cellular immunity against lethal herpesvirus challenge infection in mice.* Journal of virology, 2003. **77**(17): p. 9312-9323.
183. Henkel, M., O. Planz, T. Fischer, L. Stitz, and H.-J. Rziha, *Prevention of virus persistence and protection against immunopathology after Borna disease virus infection of the brain by a novel Orf virus recombinant.* Journal of virology, 2005. **79**(1): p. 314-325.

184. Dory, D., T. Fischer, V. Béven, R. Cariolet, H.-J. Rziha, and A. Jestin, *Prime-boost immunization using DNA vaccine and recombinant Orf virus protects pigs against Pseudorabies virus (Herpes suid 1).* Vaccine, 2006. **24**(37): p. 6256-6263.
185. Voigt, H., C. Merant, D. Wienhold, A. Braun, E. Hutet, M.-F. Le Potier, A. Saalmüller, E. Pfaff, and M. Büttner, *Efficient priming against classical swine fever with a safe glycoprotein E2 expressing Orf virus recombinant (ORFV VrV-E2).* Vaccine, 2007. **25**(31): p. 5915-5926.
186. van Rooij, E.M.A., F.A.M. Rijsewijk, H.W. Moonen-Leusen, A.T.J. Bianchi, and H.J. Rziha, *Comparison of different prime-boost regimes with DNA and recombinant Orf virus based vaccines expressing glycoprotein D of pseudorabies virus in pigs.* Vaccine, 2010. **28**(7): p. 1808-1813.
187. Rohde, J., H. Schirrmeier, H. Granzow, and H.-J. Rziha, *A new recombinant Orf virus (ORFV, Parapoxvirus) protects rabbits against lethal infection with rabbit hemorrhagic disease virus (RHDV).* Vaccine, 2011. **29**(49): p. 9256-9264.
188. Amann, R., J. Rohde, U. Wulle, D. Conlee, R. Raue, O. Martinon, and H.-J. Rziha, *A new rabies vaccine based on a recombinant ORF virus (parapoxvirus) expressing the rabies virus glycoprotein.* Journal of virology, 2013. **87**(3): p. 1618-1630.
189. Rohde, J., R. Amann, and H.-J. Rziha, *New Orf virus (Parapoxvirus) recombinant expressing H5 hemagglutinin protects mice against H5N1 and H1N1 influenza A virus.* PloS one, 2013. **8**(12): p. e83802-e83802.
190. Fleming, S.B., J. Blok, K.M. Fraser, A.A. Mercer, and A.J. Robinson, *Conservation of Gene Structure and Arrangement between Vaccinia Virus and Orf Virus.* Virology, 1993. **195**(1): p. 175-184.
191. Mercer, A.A., D.J. Lyttle, E.M. Whelan, S.B. Fleming, and J.T. Sullivan, *The establishment of a genetic map of orf virus reveals a pattern of genomic organization that is highly conserved among divergent poxviruses.* Virology, 1995. **212**(2): p. 698-704.
192. Mercer, A.A., K.M. Fraser, and J.J. Esposito, *Gene homology between orf virus and smallpox variola virus.* Virus Genes, 1996. **13**(2): p. 175-8.
193. Peart, M.J., M.V. Poyurovsky, E.M. Kass, M. Urist, E.W. Verschuren, M.K. Summers, P.K. Jackson, and C. Prives, *APC/C(Cdc20) targets E2F1 for degradation in prometaphase.* Cell Cycle, 2010. **9**(19): p. 3956-64.
194. McLean, J.R., D. Chaix, M.D. Ohi, and K.L. Gould, *State of the APC/C: organization, function, and structure.* Crit Rev Biochem Mol Biol, 2011. **46**(2): p. 118-36.
195. Mo, M., S. Shahar, S.B. Fleming, and A.A. Mercer, *How viruses affect the cell cycle through manipulation of the APC/C.* Trends Microbiol, 2012. **20**(9): p. 440-8.
196. Mo, M., S.B. Fleming, and A.A. Mercer, *Orf virus cell cycle regulator, PACR, competes with subunit 11 of the anaphase promoting complex for incorporation into the complex.* J Gen Virol, 2010. **91**(Pt 12): p. 3010-5.
197. Vallabhapurapu, S. and M. Karin, *Regulation and function of NF-kappaB transcription factors in the immune system.* Annu Rev Immunol, 2009. **27**: p. 693-733.
198. Sun, S.C. and Z.G. Liu, *A special issue on NF-kappaB signaling and function.* Cell Res, 2011. **21**(1): p. 1-2.
199. Liu, T., L. Zhang, D. Joo, and S.C. Sun, *NF-kappaB signaling in inflammation.* Signal Transduct Target Ther, 2017. **2**.
200. Karin, M. and M. Delhase, *The I kappa B kinase (IKK) and NF-kappa B: key elements of proinflammatory signalling.* Semin Immunol, 2000. **12**(1): p. 85-98.
201. Sun, S.C., *Non-canonical NF-kappaB signaling pathway.* Cell Res, 2011. **21**(1): p. 71-85.

202. Brady, G. and A.G. Bowie, *Innate immune activation of NFkappaB and its antagonism by poxviruses.* Cytokine Growth Factor Rev, 2014. **25**(5): p. 611-20.
203. Diel, D.G., S. Luo, G. Delhon, Y. Peng, E.F. Flores, and D.L. Rock, *A nuclear inhibitor of NF-kappaB encoded by a poxvirus.* J Virol, 2011. **85**(1): p. 264-75.
204. Diel, D.G., G. Delhon, S. Luo, E.F. Flores, and D.L. Rock, *A novel inhibitor of the NF-{kappa}B signaling pathway encoded by the parapoxvirus orf virus.* J Virol, 2010. **84**(8): p. 3962-73.
205. Khatiwada, S., G. Delhon, P. Nagendraprabhu, S. Chaulagain, S. Luo, D.G. Diel, E.F. Flores, and D.L. Rock, *A parapoxviral virion protein inhibits NF-kappaB signaling early in infection.* PLoS Pathog, 2017. **13**(8): p. e1006561.
206. Nagendraprabhu, P., S. Khatiwada, S. Chaulagain, G. Delhon, and D.L. Rock, *A parapoxviral virion protein targets the retinoblastoma protein to inhibit NF-kappaB signaling.* PLoS Pathog, 2017. **13**(12): p. e1006779.
207. Li, W., H. Chen, H. Deng, Z. Kuang, M. Long, D. Chen, X. Liao, M. Li, D.L. Rock, S. Luo, and W. Hao, *Orf Virus Encoded Protein ORFV119 Induces Cell Apoptosis Through the Extrinsic and Intrinsic Pathways.* Front Microbiol, 2018. **9**: p. 1056.
208. Baggiolini, M., *Chemokines and leukocyte traffic.* Nature, 1998. **392**(6676): p. 565-8.
209. Cyster, J.G., *Chemokines and cell migration in secondary lymphoid organs.* Science, 1999. **286**(5447): p. 2098-102.
210. Uguccioni, M., M. D'Apuzzo, M. Loetscher, B. Dewald, and M. Baggiolini, *Actions of the chemotactic cytokines MCP-1, MCP-2, MCP-3, RANTES, MIP-1 alpha and MIP-1 beta on human monocytes.* Eur J Immunol, 1995. **25**(1): p. 64-8.
211. Huang, H., F. Li, C.M. Cairns, J.R. Gordon, and J. Xiang, *Neutrophils and B cells express XCR1 receptor and chemotactically respond to lymphotactin.* Biochem Biophys Res Commun, 2001. **281**(2): p. 378-82.
212. Counago, R.M., K.M. Knapp, Y. Nakatani, S.B. Fleming, M. Corbett, L.M. Wise, A.A. Mercer, and K.L. Krause, *Structures of Orf Virus Chemokine Binding Protein in Complex with Host Chemokines Reveal Clues to Broad Binding Specificity.* Structure, 2015. **23**(7): p. 1199-213.
213. Lateef, Z., M.A. Baird, L.M. Wise, S. Young, A.A. Mercer, and S.B. Fleming, *The chemokine-binding protein encoded by the poxvirus orf virus inhibits recruitment of dendritic cells to sites of skin inflammation and migration to peripheral lymph nodes.* Cell Microbiol, 2010. **12**(5): p. 665-76.
214. Seet, B.T., C.A. McCaughan, T.M. Handel, A. Mercer, C. Brunetti, G. McFadden, and S.B. Fleming, *Analysis of an orf virus chemokine-binding protein: Shifting ligand specificities among a family of poxvirus viroceptors.* Proc Natl Acad Sci U S A, 2003. **100**(25): p. 15137-42.
215. Fleming, S.B., C. McCaughan, Z. Lateef, A. Dunn, L.M. Wise, N.C. Real, and A.A. Mercer, *Deletion of the Chemokine Binding Protein Gene from the Parapoxvirus Orf Virus Reduces Virulence and Pathogenesis in Sheep.* Front Microbiol, 2017. **8**: p. 46.
216. Ning, Z., Y. Peng, W. Hao, C. Duan, D.L. Rock, and S. Luo, *Generation of recombinant Orf virus using an enhanced green fluorescent protein reporter gene as a selectable marker.* BMC Vet Res, 2011. **7**: p. 80.
217. Herbert, M.H., C.J. Squire, and A.A. Mercer, *Poxviral ankyrin proteins.* Viruses, 2015. **7**(2): p. 709-38.
218. Rziha, H.J., B. Bauer, K.H. Adam, M. Rottgen, R. Cottone, M. Henkel, C. Dehio, and M. Buttner, *Relatedness and heterogeneity at the near-terminal end of the genome of a parapoxvirus bovis 1 strain (B177) compared with parapoxvirus ovis (Orf virus).* J Gen Virol, 2003. **84**(Pt 5): p. 1111-6.

219. Mosavi, L.K., T.J. Cammett, D.C. Desrosiers, and Z.Y. Peng, *The ankyrin repeat as molecular architecture for protein recognition.* Protein Sci, 2004. **13**(6): p. 1435-48.
220. Sonnberg, S., B.T. Seet, T. Pawson, S.B. Fleming, and A.A. Mercer, *Poxvirus ankyrin repeat proteins are a unique class of F-box proteins that associate with cellular SCF1 ubiquitin ligase complexes.* Proc Natl Acad Sci U S A, 2008. **105**(31): p. 10955-60.
221. Lacek, K., B. Bauer, K. Bienkowska-Szewczyk, and H.J. Rziha, *Orf virus (ORFV) ANK-1 protein mitochondrial localization is mediated by ankyrin repeat motifs.* Virus Genes, 2014. **49**(1): p. 68-79.
222. Fleming, S.B., C.A. McCaughan, A.E. Andrews, A.D. Nash, and A.A. Mercer, *A homolog of interleukin-10 is encoded by the poxvirus orf virus.* Journal of Virology, 1997. **71**(6): p. 4857.
223. Fleming, S.B., D.M. Haig, P. Nettleton, H.W. Reid, C.A. McCaughan, L.M. Wise, and A. Mercer, *Sequence and functional analysis of a homolog of interleukin-10 encoded by the parapoxvirus orf virus.* Virus Genes, 2000. **21**(1-2): p. 85-95.
224. Imlach, W., C.A. McCaughan, A.A. Mercer, D. Haig, and S.B. Fleming, *Orf virus-encoded interleukin-10 stimulates the proliferation of murine mast cells and inhibits cytokine synthesis in murine peritoneal macrophages.* J Gen Virol, 2002. **83**(Pt 5): p. 1049-58.
225. Chan, A., M. Baird, A.A. Mercer, and S.B. Fleming, *Maturation and function of human dendritic cells are inhibited by orf virus-encoded interleukin-10.* J Gen Virol, 2006. **87**(Pt 11): p. 3177-81.
226. Lateef, Z., S. Fleming, G. Halliday, L. Faulkner, A. Mercer, and M. Baird, *Orf virus-encoded interleukin-10 inhibits maturation, antigen presentation and migration of murine dendritic cells.* J Gen Virol, 2003. **84**(Pt 5): p. 1101-9.
227. Bennett, J.R., Z. Lateef, S.B. Fleming, A.A. Mercer, and L.M. Wise, *Orf virus IL-10 reduces monocyte, dendritic cell and mast cell recruitment to inflamed skin.* Virus Res, 2016. **213**: p. 230-237.
228. Fleming, S.B., I.E. Anderson, J. Thomson, D.L. Deane, C.J. McInnes, C.A. McCaughan, A.A. Mercer, and D.M. Haig, *Infection with recombinant orf viruses demonstrates that the viral interleukin-10 is a virulence factor.* J Gen Virol, 2007. **88**(Pt 7): p. 1922-7.
229. Pardoll, D.M., *The blockade of immune checkpoints in cancer immunotherapy.* Nat Rev Cancer, 2012. **12**(4): p. 252-64.
230. Darvin, P., S.M. Toor, V. Sasidharan Nair, and E. Elkord, *Immune checkpoint inhibitors: recent progress and potential biomarkers.* Exp Mol Med, 2018. **50**(12): p. 165.
231. Brunet, J.F., F. Denizot, M.F. Luciani, M. Roux-Dosseto, M. Suzan, M.G. Mattei, and P. Golstein, *A new member of the immunoglobulin superfamily--CTLA-4.* Nature, 1987. **328**(6127): p. 267-70.
232. Harper, K., C. Balzano, E. Rouvier, M.G. Mattei, M.F. Luciani, and P. Golstein, *CTLA-4 and CD28 activated lymphocyte molecules are closely related in both mouse and human as to sequence, message expression, gene structure, and chromosomal location.* J Immunol, 1991. **147**(3): p. 1037-44.
233. Linsley, P.S., W. Brady, M. Urnes, L.S. Grosmaire, N.K. Damle, and J.A. Ledbetter, *CTLA-4 is a second receptor for the B cell activation antigen B7.* J Exp Med, 1991. **174**(3): p. 561-9.

234. Linsley, P.S., J.L. Greene, W. Brady, J. Bajorath, J.A. Ledbetter, and R. Peach, *Human B7-1 (CD80) and B7-2 (CD86) bind with similar avidities but distinct kinetics to CD28 and CTLA-4 receptors.* Immunity, 1994. **1**(9): p. 793-801.
235. Peggs, K.S., S.A. Quezada, C.A. Chambers, A.J. Korman, and J.P. Allison, *Blockade of CTLA-4 on both effector and regulatory T cell compartments contributes to the antitumor activity of anti-CTLA-4 antibodies.* J Exp Med, 2009. **206**(8): p. 1717-25.
236. Wing, K., Y. Onishi, P. Prieto-Martin, T. Yamaguchi, M. Miyara, Z. Fehervari, T. Nomura, and S. Sakaguchi, *CTLA-4 control over Foxp3+ regulatory T cell function.* Science, 2008. **322**(5899): p. 271-5.
237. Leach, D.R., M.F. Krummel, and J.P. Allison, *Enhancement of antitumor immunity by CTLA-4 blockade.* Science, 1996. **271**(5256): p. 1734-6.
238. Tivol, E.A., F. Borriello, A.N. Schweitzer, W.P. Lynch, J.A. Bluestone, and A.H. Sharpe, *Loss of CTLA-4 leads to massive lymphoproliferation and fatal multiorgan tissue destruction, revealing a critical negative regulatory role of CTLA-4.* Immunity, 1995. **3**(5): p. 541-7.
239. Waterhouse, P., J.M. Penninger, E. Timms, A. Wakeham, A. Shahinian, K.P. Lee, C.B. Thompson, H. Griesser, and T.W. Mak, *Lymphoproliferative disorders with early lethality in mice deficient in Ctla-4.* Science, 1995. **270**(5238): p. 985-8.
240. Hodi , F.S., S.J. O'Day , D.F. McDermott , R.W. Weber , J.A. Sosman , J.B. Haanen , R. Gonzalez , C. Robert , D. Schadendorf , J.C. Hassel , W. Akerley , A.J.M. van den Eertwegh , J. Lutzky , P. Lorigan , J.M. Vaubel , G.P. Linette , D. Hogg , C.H. Ottensmeier , C. Lebbé , C. Peschel , I. Quirt , J.I. Clark , J.D. Wolchok , J.S. Weber , J. Tian , M.J. Yellin , G.M. Nichol , A. Hoos , and W.J. Urba *Improved Survival with Ipilimumab in Patients with Metastatic Melanoma.* New England Journal of Medicine, 2010. **363**(8): p. 711-723.
241. Fanoni, D., S. Tavecchio, S. Recalcati, Y. Balice, L. Venegoni, R. Fiorani, C. Crosti, and E. Berti, *New monoclonal antibodies against B-cell antigens: possible new strategies for diagnosis of primary cutaneous B-cell lymphomas.* Immunol Lett, 2011. **134**(2): p. 157-60.
242. Terme, M., E. Ullrich, L. Aymeric, K. Meinhardt, M. Desbois, N. Delahaye, S. Viaud, B. Ryffel, H. Yagita, G. Kaplanski, A. Prevost-Blondel, M. Kato, J.L. Schultze, E. Tartour, G. Kroemer, N. Chaput, and L. Zitvogel, *IL-18 induces PD-1-dependent immunosuppression in cancer.* Cancer Res, 2011. **71**(16): p. 5393-9.
243. Francisco, L.M., V.H. Salinas, K.E. Brown, V.K. Vanguri, G.J. Freeman, V.K. Kuchroo, and A.H. Sharpe, *PD-L1 regulates the development, maintenance, and function of induced regulatory T cells.* J Exp Med, 2009. **206**(13): p. 3015-29.
244. Freeman, G.J., A.J. Long, Y. Iwai, K. Bourque, T. Chernova, H. Nishimura, L.J. Fitz, N. Malenkovich, T. Okazaki, M.C. Byrne, H.F. Horton, L. Fouser, L. Carter, V. Ling, M.R. Bowman, B.M. Carreno, M. Collins, C.R. Wood, and T. Honjo, *Engagement of the PD-1 immunoinhibitory receptor by a novel B7 family member leads to negative regulation of lymphocyte activation.* J Exp Med, 2000. **192**(7): p. 1027-34.
245. Keir, M.E., S.C. Liang, I. Guleria, Y.E. Latchman, A. Qipo, L.A. Albacker, M. Koulmanda, G.J. Freeman, M.H. Sayegh, and A.H. Sharpe, *Tissue expression of PD-L1 mediates peripheral T cell tolerance.* J Exp Med, 2006. **203**(4): p. 883-95.
246. Nishimura, H., M. Nose, H. Hiai, N. Minato, and T. Honjo, *Development of lupus-like autoimmune diseases by disruption of the PD-1 gene encoding an ITIM motif-carrying immunoreceptor.* Immunity, 1999. **11**(2): p. 141-51.
247. Ahmadzadeh, M., L.A. Johnson, B. Heemskerk, J.R. Wunderlich, M.E. Dudley, D.E. White, and S.A. Rosenberg, *Tumor antigen-specific CD8 T cells infiltrating the*

*tumor express high levels of PD-1 and are functionally impaired.* Blood, 2009. **114**(8): p. 1537-44.
248. Sfanos, K.S., T.C. Bruno, A.K. Meeker, A.M. De Marzo, W.B. Isaacs, and C.G. Drake, *Human prostate-infiltrating CD8+ T lymphocytes are oligoclonal and PD-1+.* Prostate, 2009. **69**(15): p. 1694-703.
249. Dong, H., S.E. Strome, D.R. Salomao, H. Tamura, F. Hirano, D.B. Flies, P.C. Roche, J. Lu, G. Zhu, K. Tamada, V.A. Lennon, E. Celis, and L. Chen, *Tumor-associated B7-H1 promotes T-cell apoptosis: a potential mechanism of immune evasion.* Nat Med, 2002. **8**(8): p. 793-800.
250. Iwai, Y., M. Ishida, Y. Tanaka, T. Okazaki, T. Honjo, and N. Minato, *Involvement of PD-L1 on tumor cells in the escape from host immune system and tumor immunotherapy by PD-L1 blockade.* Proc Natl Acad Sci U S A, 2002. **99**(19): p. 12293-7.
251. Blank, C., I. Brown, A.C. Peterson, M. Spiotto, Y. Iwai, T. Honjo, and T.F. Gajewski, *PD-L1/B7H-1 inhibits the effector phase of tumor rejection by T cell receptor (TCR) transgenic CD8+ T cells.* Cancer Res, 2004. **64**(3): p. 1140-5.
252. Borghaei, H., L. Paz-Ares, L. Horn, D.R. Spigel, M. Steins, N.E. Ready, L.Q. Chow, E.E. Vokes, E. Felip, E. Holgado, F. Barlesi, M. Kohlhaufl, O. Arrieta, M.A. Burgio, J. Fayette, H. Lena, E. Poddubskaya, D.E. Gerber, S.N. Gettinger, C.M. Rudin, N. Rizvi, L. Crino, G.R. Blumenschein, Jr., S.J. Antonia, C. Dorange, C.T. Harbison, F. Graf Finckenstein, and J.R. Brahmer, *Nivolumab versus Docetaxel in Advanced Nonsquamous Non-Small-Cell Lung Cancer.* N Engl J Med, 2015. **373**(17): p. 1627-39.
253. Garon, E.B., N.A. Rizvi, R. Hui, N. Leighl, A.S. Balmanoukian, J.P. Eder, A. Patnaik, C. Aggarwal, M. Gubens, L. Horn, E. Carcereny, M.J. Ahn, E. Felip, J.S. Lee, M.D. Hellmann, O. Hamid, J.W. Goldman, J.C. Soria, M. Dolled-Filhart, R.Z. Rutledge, J. Zhang, J.K. Lunceford, R. Rangwala, G.M. Lubiniecki, C. Roach, K. Emancipator, L. Gandhi, and K.-. Investigators, *Pembrolizumab for the treatment of non-small-cell lung cancer.* N Engl J Med, 2015. **372**(21): p. 2018-28.
254. Larkin, J., V. Chiarion-Sileni, R. Gonzalez, J.J. Grob, C.L. Cowey, C.D. Lao, D. Schadendorf, R. Dummer, M. Smylie, P. Rutkowski, P.F. Ferrucci, A. Hill, J. Wagstaff, M.S. Carlino, J.B. Haanen, M. Maio, I. Marquez-Rodas, G.A. McArthur, P.A. Ascierto, G.V. Long, M.K. Callahan, M.A. Postow, K. Grossmann, M. Sznol, B. Dreno, L. Bastholt, A. Yang, L.M. Rollin, C. Horak, F.S. Hodi, and J.D. Wolchok, *Combined Nivolumab and Ipilimumab or Monotherapy in Untreated Melanoma.* N Engl J Med, 2015. **373**(1): p. 23-34.
255. Ribas, A., D.C. Hanson, D.A. Noe, R. Millham, D.J. Guyot, S.H. Bernstein, P.C. Canniff, A. Sharma, and J. Gomez-Navarro, *Tremelimumab (CP-675,206), a cytotoxic T lymphocyte associated antigen 4 blocking monoclonal antibody in clinical development for patients with cancer.* Oncologist, 2007. **12**(7): p. 873-83.
256. Kirkwood, J.M., P. Lorigan, P. Hersey, A. Hauschild, C. Robert, D. McDermott, M.A. Marshall, J. Gomez-Navarro, J.Q. Liang, and C.A. Bulanhagui, *Phase II trial of tremelimumab (CP-675,206) in patients with advanced refractory or relapsed melanoma.* Clin Cancer Res, 2010. **16**(3): p. 1042-8.
257. Simmons, A.D., M. Moskalenko, J. Creson, J. Fang, S. Yi, M.J. VanRoey, J.P. Allison, and K. Jooss, *Local secretion of anti-CTLA-4 enhances the therapeutic efficacy of a cancer immunotherapy with reduced evidence of systemic autoimmunity.* Cancer Immunol Immunother, 2008. **57**(8): p. 1263-70.
258. Dias, J.D., O. Hemminki, I. Diaconu, M. Hirvinen, A. Bonetti, K. Guse, S. Escutenaire, A. Kanerva, S. Pesonen, A. Löskog, V. Cerullo, and A. Hemminki, *Targeted cancer*

*immunotherapy with oncolytic adenovirus coding for a fully human monoclonal antibody specific for CTLA-4.* Gene Therapy, 2011. **19**: p. 988.
259. Engeland, C.E., C. Grossardt, R. Veinalde, S. Bossow, D. Lutz, J.K. Kaufmann, I. Shevchenko, V. Umansky, D.M. Nettelbeck, W. Weichert, D. Jager, C. von Kalle, and G. Ungerechts, *CTLA-4 and PD-L1 checkpoint blockade enhances oncolytic measles virus therapy.* Mol Ther, 2014. **22**(11): p. 1949-59.
260. Kleinpeter, P., L. Fend, C. Thioudellet, M. Geist, N. Sfrontato, V. Koerper, C. Fahrner, D. Schmitt, M. Gantzer, C. Remy-Ziller, R. Brandely, D. Villeval, K. Rittner, N. Silvestre, P. Erbs, L. Zitvogel, E. Quemeneur, X. Preville, and J.B. Marchand, *Vectorization in an oncolytic vaccinia virus of an antibody, a Fab and a scFv against programmed cell death -1 (PD-1) allows their intratumoral delivery and an improved tumor-growth inhibition.* Oncoimmunology, 2016. **5**(10): p. e1220467.
261. Stadler, C.R., H. Bahr-Mahmud, L. Celik, B. Hebich, A.S. Roth, R.P. Roth, K. Kariko, O. Tureci, and U. Sahin, *Elimination of large tumors in mice by mRNA-encoded bispecific antibodies.* Nat Med, 2017. **23**(7): p. 815-817.
262. Thran, M., J. Mukherjee, M. Pönisch, K. Fiedler, A. Thess, B.L. Mui, M.J. Hope, Y.K. Tam, N. Horscroft, R. Heidenreich, M. Fotin-Mleczek, C.B. Shoemaker, and T. Schlake, *mRNA mediates passive vaccination against infectious agents, toxins, and tumors.* EMBO molecular medicine, 2017. **9**(10): p. 1434-1447.
263. Chan, W.M. and G. McFadden, *Oncolytic Poxviruses.* Annu Rev Virol, 2014. **1**(1): p. 119-141.
264. Walsh, S.R. and R. Dolin, *Vaccinia viruses: vaccines against smallpox and vectors against infectious diseases and tumors.* Expert Rev Vaccines, 2011. **10**(8): p. 1221-40.
265. Turner, P.C. and R.W. Moyer, *The molecular pathogenesis of poxviruses.* Curr Top Microbiol Immunol, 1990. **163**: p. 125-51.
266. Buller, R.M. and G.J. Palumbo, *Poxvirus pathogenesis.* Microbiol Rev, 1991. **55**(1): p. 80-122.
267. McInnes, C.J., A.R. Wood, and A.A. Mercer, *Orf virus encodes a homolog of the vaccinia virus interferon resistance gene E3L.* Virus Genes, 1998. **17**(2): p. 107-115.
268. Diel, D.G., S. Luo, G. Delhon, Y. Peng, E.F. Flores, and D.L. Rock, *Orf virus ORFV121 encodes a novel inhibitor of NF-kappaB that contributes to virus virulence.* J Virol, 2011. **85**(5): p. 2037-49.
269. Westphal, D., E.C. Ledgerwood, M.H. Hibma, S.B. Fleming, E.M. Whelan, and A.A. Mercer, *A novel Bcl-2-like inhibitor of apoptosis is encoded by the parapoxvirus Orf virus.* Journal of Virology, 2007. **81**(13): p. 7178-7188.
270. Hautaniemi, M., N. Ueda, J. Tuimala, A.A. Mercer, J. Landenpera, and C.J. McInnes, *The genome of pseudocowpoxvirus: comparison of a reindeer isolate and a reference strain.* Journal of General Virology, 2010. **91**: p. 1560-1576.
271. Huang, T., E.R. Tulman, D.G. Diel, S. Khatiwada, W. Sims, J.F. Edwards, X. Wen, G.F. Kutish, D.L. Rock, and G. Delhon, *Coinfection with multiple strains of bovine papular stomatitis virus.* Archives of Virology, 2015. **160**(6): p. 1527-1532.
272. Antoine, G., F. Scheiflinger, F. Dorner, and F.G. Falkner, *The complete genomic sequence of the modified vaccinia Ankara (MVA) strain: Comparison with other orthopoxviruses (vol 244, pg 365, 1998).* Virology, 2006. **350**(2): p. 501-502.
273. Stittelaar, K.J., L.S. Wyatt, R.L. de Swart, H.W. Vos, J. Groen, G. van Amerongen, R.S. van Binnendijk, S. Rozenblatt, B. Moss, and A.D.M.E. Osterhaus, *Protective immunity in macaques vaccinated with a modified vaccinia virus Ankara-based*

*measles virus vaccine in the presence of passively acquired antibodies.* Journal of Virology, 2000. **74**(9): p. 4236-4243.
274. Wyatt, L.S., I.M. Belyakov, P.L. Earl, J.A. Berzofsky, and B. Moss, *Enhanced cell surface expression, immunogenicity and genetic stability resulting from a spontaneous truncation of HIV Env expressed by a recombinant MVA.* Virology, 2008. **372**(2): p. 260-272.
275. Wyatt, L.S., S.T. Shors, B.R. Murphy, and B. Moss, *Development of a replication-deficient recombinant vaccinia virus vaccine effective against parainfluenza virus 3 infection in an animal model.* Vaccine, 1996. **14**(15): p. 1451-1458.
276. Qiao, J., H.B. Yang, Y.L. Peng, Q.L. Meng, C. Chen, Y. Ma, K. Xie, T.L. Liu, X.P. Cai, and C.F. Chen, *Effect of ORF119 gene deletion on the replication and virulence of orf virus.* Acta Virologica, 2015. **59**(3): p. 257-264.
277. Mo, M., S.B. Fleming, and A.A. Mercer, *Cell cycle deregulation by a poxvirus partial mimic of anaphase-promoting complex subunit 11.* Proceedings of the National Academy of Sciences of the United States of America, 2009. **106**(46): p. 19527-19532.
278. Raup, A., V. Jérôme, R. Freitag, C.V. Synatschke, and A.H.E. Müller, *Promoter, transgene, and cell line effects in the transfection of mammalian cells using PDMAEMA-based nano-stars.* Biotechnology reports (Amsterdam, Netherlands), 2016. **11**: p. 53-61.
279. Liu, J.Y., M. Hellerstein, M. McDonnel, R.R. Amara, L.S. Wyatt, B. Moss, and H.L. Robinson, *Dose-response studies for the elicitation of CD8 T cells by a DNA vaccine, used alone or as the prime for a modified vaccinia Ankara boost.* Vaccine, 2007. **25**(15): p. 2951-2958.
280. zur Megede, J., M.C. Chen, B. Doe, M. Schaefer, C.E. Greer, M. Selby, G.R. Otten, and S.W. Barnett, *Increased expression and immunogenicity of sequence-modified human immunodeficiency virus type 1 gag gene.* Journal of Virology, 2000. **74**(6): p. 2628-2635.
281. Liu, J.Y., L.S. Wyatt, R.R. Amara, B. Moss, and H.L. Robinson, *Studies on in vitro expression and in vivo immunogenicity of a recombinant MVA HIV vaccine.* Vaccine, 2006. **24**(16): p. 3332-3339.
282. Sutter, G., L.S. Wyatt, P.L. Foley, J.R. Bennink, and B. Moss, *A Recombinant Vector Derived from the Host Range-Restricted and Highly Attenuated Mva Strain of Vaccinia Virus Stimulates Protective Immunity in Mice to Influenza-Virus.* Vaccine, 1994. **12**(11): p. 1032-1040.
283. Becker, P.D., M. Norder, S. Weissmann, R. Ljapoci, V. Erfle, I. Drexler, and C.A. Guzman, *Gene Expression Driven by a Strong Viral Promoter in MVA Increases Vaccination Efficiency by Enhancing Antibody Responses and Unmasking CD8(+) T Cell Epitopes.* Vaccines (Basel), 2014. **2**(3): p. 581-600.
284. Gasteiger, G., W. Kastenmuller, R. Ljapoci, G. Sutter, and I. Drexler, *Cross-priming of cytotoxic T cells dictates antigen requisites for modified vaccinia virus Ankara vector vaccines.* J Virol, 2007. **81**(21): p. 11925-36.
285. Kuwano, Y., C.M. Prazma, N. Yazawa, R. Watanabe, N. Ishiura, A. Kumanogoh, H. Okochi, K. Tamaki, M. Fujimoto, and T.F. Tedder, *CD83 influences cell-surface MHC class II expression on B cells and other antigen-presenting cells.* International Immunology, 2007. **19**(8): p. 977-992.
286. Mercer, A.A., S.B. Fleming, and N. Ueda, *F-box-like domains are present in most poxvirus ankyrin repeat proteins.* Virus Genes, 2005. **31**(2): p. 127-133.
287. Sonnberg, S., B.T. Seet, T. Pawson, S.B. Fleming, and A.A. Mercer, *Poxvirus ankyrin repeat proteins are a unique class of F-box proteins that associate with cellular*

*SCF1 ubiquitin ligase complexes.* Proceedings of the National Academy of Sciences of the United States of America, 2008. **105**(31): p. 10955-10960.
288. Sonnberg, S., S.B. Fleming, and A.A. Mercer, *A truncated two-alpha-helix F-box present in poxvirus ankyrin-repeat proteins is sufficient for binding the SCF1 ubiquitin ligase complex.* Journal of General Virology, 2009. **90**: p. 1224-1228.
289. Bai, C., P. Sen, K. Hofmann, L. Ma, M. Goebl, J.W. Harper, and S.J. Elledge, *SKP1 connects cell cycle regulators to the ubiquitin proteolysis machinery through a novel motif, the F-box.* Cell, 1996. **86**(2): p. 263-274.
290. Skowyra, D., K.L. Craig, M. Tyers, S.J. Elledge, and J.W. Harper, *F-box proteins are receptors that recruit phosphorylated substrates to the SCF ubiquitin-ligase complex.* Cell, 1997. **91**(2): p. 209-219.
291. Willems, A.R., M. Schwab, and M. Tyers, *A hitchhiker's guide to the cullin ubiquitin ligases: SCF and its kin.* Biochimica Et Biophysica Acta-Molecular Cell Research, 2004. **1695**(1-3): p. 133-170.
292. Biacchesi, S., M. LeBerre, A. Lamoureux, Y. Louise, E. Lauret, P. Boudinot, and M. Bremont, *Mitochondrial Antiviral Signaling Protein Plays a Major Role in Induction of the Fish Innate Immune Response against RNA and DNA Viruses.* Journal of Virology, 2009. **83**(16): p. 7815-7827.
293. Yoneyama, M. and T. Fujita, *RNA recognition and signal transduction by RIG-I-like receptors.* Immunological Reviews, 2009. **227**: p. 54-65.
294. Sancho, D., M. Gomez, and F. Sanchez-Madrid, *CD69 is an immunoregulatory molecule induced following activation.* Trends in Immunology, 2005. **26**(3): p. 136-140.
295. Freeman, B.E., E. Hammarlund, H.P. Raue, and M.K. Slifka, *Regulation of innate CD8(+) T-cell activation mediated by cytokines.* Proceedings of the National Academy of Sciences of the United States of America, 2012. **109**(25): p. 9971-9976.
296. Kleiveland, C.R., *Peripheral Blood Mononuclear Cells*, in *The Impact of Food Bioactives on Health: in vitro and ex vivo models*, K. Verhoeckx, et al., Editors. 2015, Springer International Publishing: Cham. p. 161-167.
297. Couzin-Frankel, J., *Breakthrough of the year 2013. Cancer immunotherapy.* Science, 2013. **342**(6165): p. 1432-3.
298. Graham, K.A., A.S. Lalani, J.L. Macen, T.L. Ness, M. Barry, L.Y. Liu, A. Lucas, A. ClarkLewis, R.W. Moyer, and G. McFadden, *The T1/35kDa family of poxvirus-secreted proteins bind chemokines and modulate leukocyte influx into virus-infected tissues.* Virology, 1997. **229**(1): p. 12-24.
299. Huang, H., F. Li, C.M. Cairns, J.R. Gordon, and J. Xiang, *Neutrophils and B cells express XCR1 receptor and chemotactically respond to lymphotactin.* Biochemical and Biophysical Research Communications, 2001. **281**(2): p. 378-382.
300. Kelner, G.S., J. Kennedy, K.B. Bacon, S. Kleyensteuber, D.A. Largaespada, N.A. Jenkins, N.G. Copeland, J.F. Bazan, K.W. Moore, T.J. Schall, and A. Zlotnik, *Lymphotactin - a Cytokine That Represents a New Class of Chemokine.* Science, 1994. **266**(5189): p. 1395-1399.
301. Yoshida, T., T. Imai, M. Kakizaki, M. Nishimura, S. Takagi, and O. Yoshie, *Identification of single C motif-1 lymphotactin receptor XCR1.* Journal of Biological Chemistry, 1998. **273**(26): p. 16551-16554.